DIVIDE AND PROSPER: MOLECULAR MECHANISMS AND CONSEQUENCES OF CYTOKINETIC RING REGULATION

By

Kenneth Adam Bohnert

Dissertation

Submitted to the Faculty of the

Graduate School of Vanderbilt University

in partial fulfillment of the requirements

for the degree of

DOCTOR OF PHILOSOPHY

in

Cell and Developmental Biology

August, 2013

Nashville, Tennessee

Approved:

Professor Kathleen L. Gould

Professor Stephen R. Hann

Professor Matthew J. Tyska

Professor Ellen H. Fanning

Professor Susan R. Wente

To my parents,

for demonstrating the power of hard work, loyalty, and integrity

ACKNOWLEDGEMENTS

First and foremost, I must thank my advisor, Kathy Gould. Working with Kathy has been a tremendous learning experience. Kathy's passion for science is infectious; a data-junkie at heart, she is always excited to discuss results and brainstorm new ideas. Kathy has allowed me the freedom to investigate the questions that I find most interesting, and she has been willing to explore research areas with which she is unfamiliar. I greatly appreciate her patience in letting me learn through my own mistakes and successes. I am also very thankful for the opportunities Kathy has provided for me to travel and present my research at conferences around the globe.

In addition to Kathy, many other researchers contributed much-needed expertise and advice during my graduate studies. Craig Vander Kooi at the University of Kentucky provided assistance with bioinformatics and structural analyses, which were useful for both the CPC and formin projects. David Kovar at the University of Chicago offered valuable instruction in actin and formin biochemistry, and his student, Agniezska Grzegorzewska, performed structure-function analysis critical to our formin project. My committee members, Susan Wente, Matt Tyska, Steve Hann, and Ellen Fanning, have given unique insight into my projects both inside and outside of committee meetings, and their guidance has kept me on track throughout my studies. Also, the Ohi labs, headed by Mel and Puck, have engaged in helpful and informative discussions at our joint lab meetings.

There have also been many members of the Gould laboratory with whom I have directly collaborated. During my rotation, Dawn Clifford Hart took me under her wings

and worked with me on the CPC story. Through Dawn's instruction, I learned how to ask the right questions and prioritize experiments. Jun-Song Chen also contributed experimental assistance to the CPC project, aiding in difficult biochemical assays. Malwina Huzarska, a previous technician in the lab, performed mass spectrometry of TAP samples, which enabled identification of *in vivo* Fic1 phosphosites. Recently, Alaina Willet joined me in studying cytokinetic formin Cdc12, and it has been exciting to shoot ideas back and forth with her as our projects have developed.

During the past five years, the Gould laboratory has been a fun and stimulating environment in which to study and learn. As a beginning graduate student in the lab, I was lucky to work under the tutelage of a senior graduate student, Rachel Roberts-Galbraith. Rachel's example inspired me to become a more critical thinker, and our discussions were instrumental in piquing my interest in the cytokinetic ring. In addition, two other graduate students, Matt Broadus and Alyssa Johnson, overlapped with much of my time in the lab. Matt was a valuable partner-in-crime in pranking lab members and organizing beer outings, and Alyssa has served a special role in my development both inside and outside of the lab. I will miss the experimental help and unintentional comic relief provided by the lab's technicians, Anna Feoktistova and Liping Ren. Anna also deserves a special thank-you for welcoming me into Disaster Bay and assuming the role of my adoptive Jewish mother. Our laboratory assistant, Magdalena Buchowski, made everyday life in the lab more manageable and stress-free through her hard work and no-nonsense attitude. I also thank other past and present members of the lab for all the work- and non-work-related memories.

I would like to acknowledge that these studies were generously supported by the

Integrated Biological Systems Training in Oncology training program (T32-CA119925), which also served as an important outlet for scientific discussion. This program broadened my perspective and helped me grasp the importance of my own fundamental science research.

Lastly, I would like to thank my friends and family for their unfailing love and support. These people are truly the rocks on which I have built my life, and I could not have accomplished anything without their advice or encouragement.

TABLE OF CONTENTS

Page

LIST OF FIGURES

LIST OF ABBREVIATIONS

BF	bright field
CB	Coomassie blue
CDK	cyclin-dependent kinase
CK2	casein kinase II
CPC	chromosomal passenger complex
CR	cytokinetic ring
EMM	Edinburgh minimal medium
ESCRT	endosomal sorting complex required for transport
GAP	GTPase-activating protein
GEF	guanine nucleotide exchange factor
FH	formin homology
Lat A	Latrunculin A
mCh	mCherry
NETO	new end take off
PKC ε	protein kinase C ε
SIN	septation initiation network
SPB	spindle pole body
TAP	tandem affinity purification
YE	yeast extract

CHAPTER I

INTRODUCTION

Overview of the eukaryotic cell cycle

Cells, the fundamental units of life, are not static entities. Indeed, in as little as a few days, a single cell can give rise to millions of other cells. For such propagation to occur, cells must undergo periods of growth and division. The cell cycle organizes these events into a coherent process. In a canonical cell cycle (Fig. 1-1), most cell growth occurs during two gap phases, G1 and G2. These gap phases flank S phase, during which the genome is replicated. Altogether, G1, S, and G2 phases comprise interphase, which precedes and sets the stage for mitosis. During mitosis, replicated genomes segregate to opposite poles of dividing cells. Once mitosis completes, the production of *bona fide* daughter cells demands physical separation of these two cell halves.

In a variety of organisms and cell types, cytokinesis follows nuclear division and directs the cleavage of the cellular cytoplasm (Fig. 1-1). Because failure to complete cytokinesis can result in cell death or aneuploidy, which has been linked to cancer (Gordon et al., 2012), relevant cytokinetic events (Fig. 1-2) must be fine-tuned both temporally and spatially. Cytokinesis initially requires selection of an appropriate division site. Following this, a contractile apparatus, termed the cytokinetic ring (CR) due to its shape, assembles at the division site and undergoes constriction. Daughter cells fully separate as cleavage completes during abscission, and each daughter cell then initiates its division cycle anew. Actin filaments combined with non-muscle myosin II

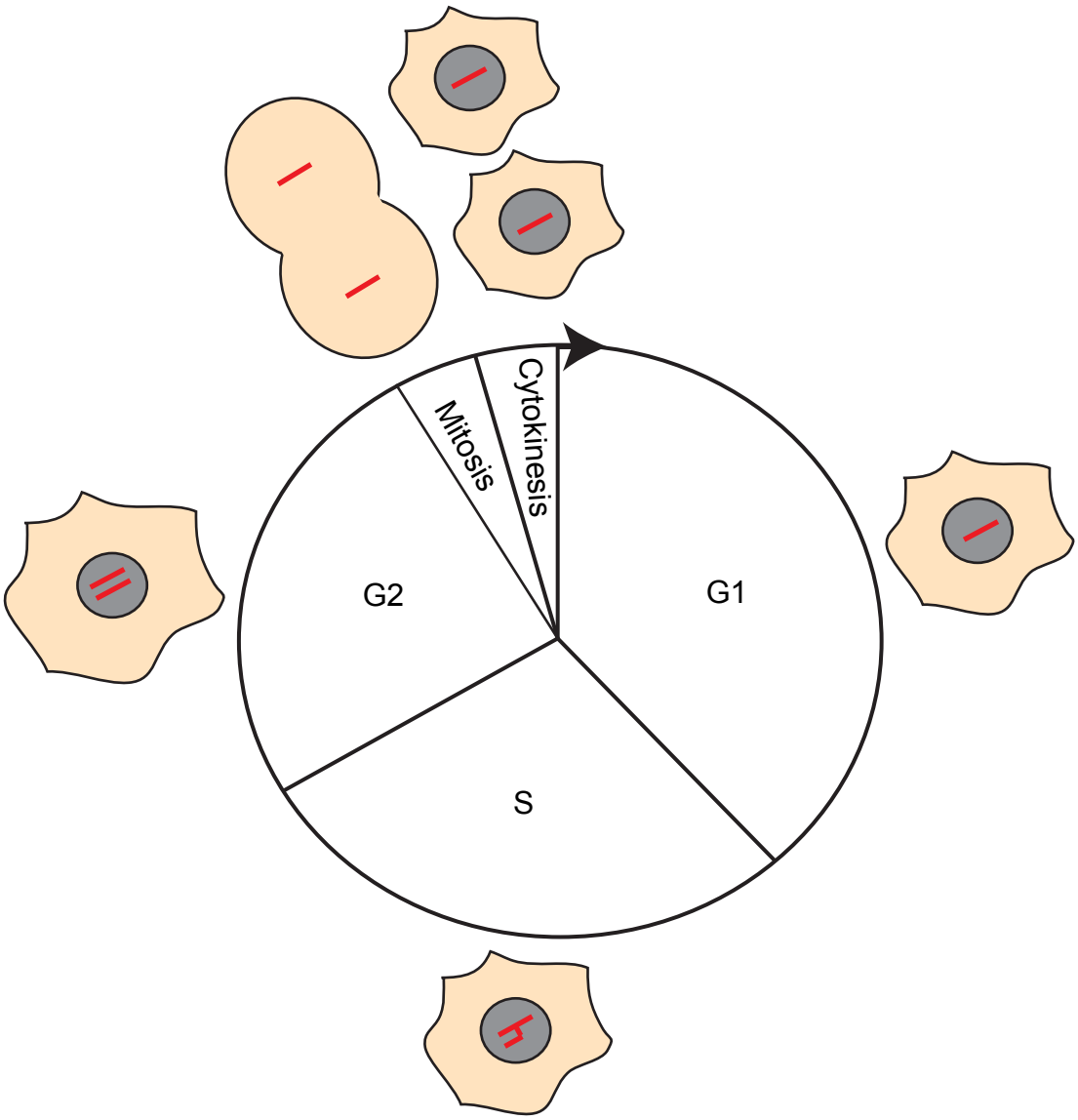

Figure 1-1

Schematic of the canonical cell cycle.
Interphase, which is comprised of G1, S, and G2 phases, occupies most of the cell cycle. Cell growth occurs in G1 and G2 phases, and the genome (red) is replicated during S phase. During mitosis, the replicated genome segregates to the two halves of the dividing cell. Then, the two daughter cells are physically separated from each other during cytokinesis, thereby completing the cell cycle. In animal cells (pictured), cell polarity and the nuclear envelope are lost during mitosis but re-established after cytokinesis.

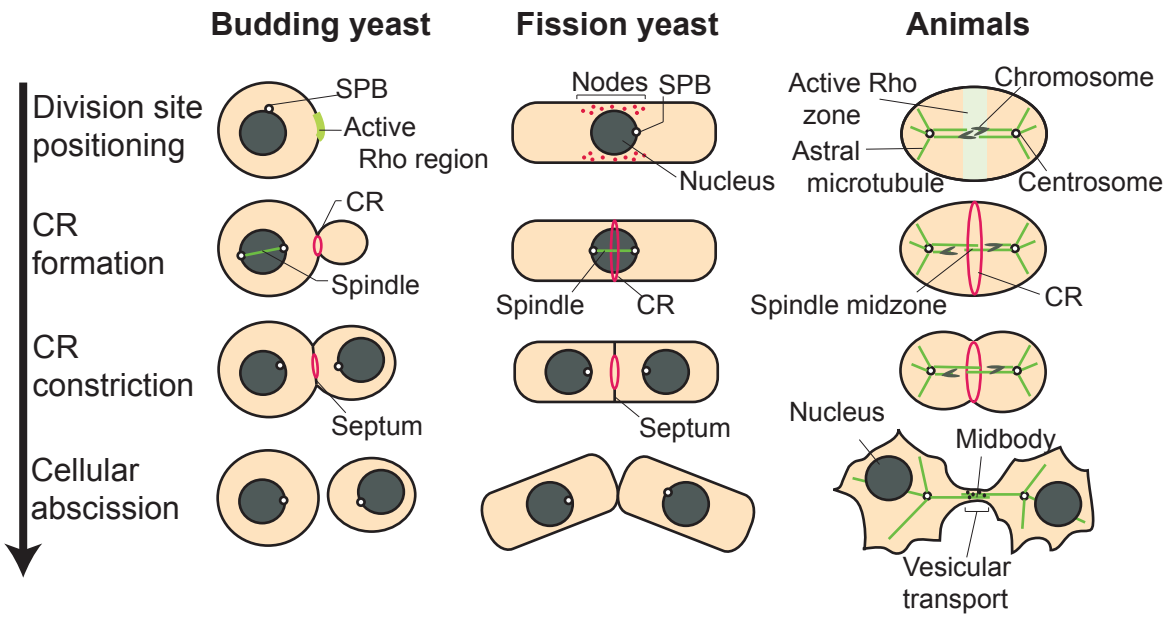

Figure 1-2

Stages of eukaryotic cytokinesis.
Schematics of the process of cytokinesis in budding yeast *Saccharomyces cerevisiae*, fission yeast *Schizosaccharomyces pombe*, and animal cells. Examples of cells at individual stages of cytokinesis are presented, with progression through the cell cycle oriented downward. In budding yeast and animal cells, the cytokinetic apparatus is positioned and assembled from an active Rho region. In wild-type fission yeast, CR assembly initates following spindle pole body (SPB) separation from node-like structures containing formin and myosin II, although initial ring assembly can also occur via node-independent mechanisms. Following constriction of the CR in budding and fission yeasts, new cell wall is deposited at the division site to form a septum, which is subsequently cleaved to allow for cell separation. In animal cells, vesicular transport to the midbody, the microtubule-based remnant of the anaphase spindle midzone, likewise promotes abscission via its effects on membrane composition at the division site as well as its delivery of important cleavage furrow factors.

provide the actomyosin core of the cytokinetic machinery in many organisms. Additionally, dozens of accessory proteins localize to the division site and dynamically impact cytokinesis. Given the conservation of many of these factors among eukaryotes (Fig. 1-3), regulatory mechanisms that mediate this process in one organism likely mirror those used by others [for review, see (Pollard, 2010)].

A primer on phosphoregulatory cues directing cytokinesis

The post-translational modification of proteins serves as one means by which protein activity, localization, and interactions acquire temporal and spatial specificity. Although roles for modifications in general cell cycle control have been known for some time [for reviews, see (Hunter, 1987; King et al., 1996)], their varied contributions to cytokinesis have only recently gained appreciation on a broader spectrum, most notably because of improved techniques in targeted and genome-wide proteomics. For one, the covalent attachment of phosphate groups to proteins by kinases is a widespread post-translational modification. This modification can exert positive, negative, and even cooperative effects depending on the context. The reversal of phosphorylation by phosphatases contributes an added level of control to this modification. In a variety of organisms, phosphorylation impacts multiple events during cytokinesis, as outlined below.

Positioning and assembly of the cytokinetic apparatus

In the fission yeast *Schizosaccharomyces pombe*, two separate but integrated mechanisms, both of which possess ties to upstream kinase regulation, are involved in

Functional description	General name	Budding yeast name	Fission yeast name	Mammalian name
Actomyosin core	Formin	Bni1, Bnr1	Cdc12	DIA2
	Myosin heavy chain	Myo1	Myo2	NMHC II
	Myosin light chain	Mlc1, Mlc2	Rlc1, Cdc4	MLC17, MLC20
Division site positioning	Anillin-like protein	Bud4	Mid1	ANLN
Accessory ring proteins	F-BAR/SH3 protein	Hof1	Cdc15	PSTPIP1
	IQGAP	Iqg1	Rng2	IQGAP1
	C2 domain protein	Inn1	Fic1	-
Regulatory enzymes	Polo-like kinase	Cdc5	Plo1	PLK1
	Terminal SIN/MEN kinase	Dbf2	Sid2	LATS1
	Cdc14-family phosphatase	Cdc14	Clp1/Flp1	CDC14A, CDC14B
	Aurora B kinase	Ipl1	Ark1	AURKB

Figure 1-3

Conservation of eukaryotic cytokinesis proteins.
Homologs of interest are noted. The only protein not described in mammalian cells is the C2 domain protein (budding yeast Inn1/ fission yeast Fic1).

CR assembly (Roberts-Galbraith and Gould, 2008). The first mechanism, known as the search-capture-pull-release model (Fig. 1-4A), is based on the observation that formin Cdc12 and type II myosin Myo2 localize to a broad series of medial nodes at the onset of mitosis, where they respectively mediate F-actin nucleation and actin filament condensation into a ring structure (Coffman et al., 2009; Vavylonis et al., 2008). Recruitment of both Cdc12 and Myo2 into nodes depends on anillin-related Mid1. Nuclear export via phosphorylation by the polo-like kinase concentrates Mid1 medially in early mitosis, thereby coupling the nucleus to division plane positioning in this organism (Almonacid et al., 2009; Bahler et al., 1998). Cues from distal cell tips, including inhibitory phosphorylation of Mid1-binding protein kinase Cdr2 by DYRK-family kinase Pom1, meanwhile reinforce medial node distribution to promote assembly of the CR in the middle of the cell (Huang et al., 2007; Martin and Berthelot-Grosjean, 2009; Moseley et al., 2009). *De novo* ring assembly from node-like bands of myosin II has also been reported in animals cells (Werner et al., 2007; Zhou and Wang, 2008). Whether this represents a conserved assembly mechanism and whether phosphorylation plays a role in this process in animal cells have yet to be fully addressed.

Nonetheless, in the absence of detectable nodes and Mid1, formation of a CR still occurs in *S. pombe*, albeit with reduced speed and efficiency (Huang et al., 2008). The spot/leading cable mechanism of CR assembly (Fig. 1-4B) might account for this fact, as electron microscopy suggests that actin filaments arise from a single aster and spread around the circumference of the cell to form the CR (Kamasaki et al., 2007). A conserved signaling network, known as the septation initiation network (SIN) in fission yeast, has been implicated in Mid1-independent ring assembly (Hachet and Simanis,

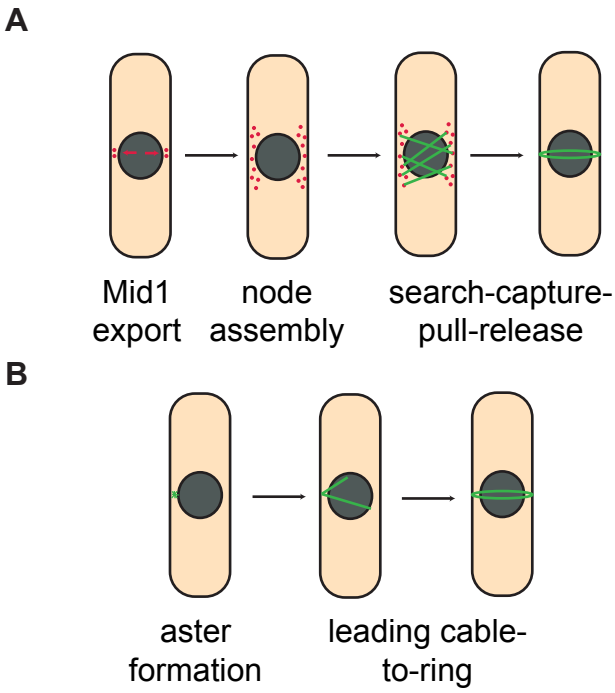

Figure 1-4

Two models for *S. pombe* CR assembly.
(A) In wild-type cells, nodes develop at cell middles upon polo-dependent Mid1 export. Mid1 then recruits multiple CR factors, including formin and myosin, to nodes. At these sites, formin nucleates and polymerizes F-actin. Then, myosin in distinct nodes "captures" F-actin, pulling it into a ring structure. Release of these interactions stabilizes mature CRs for the time being. (B) Upon loss of Mid1 and/or nodes, CRs still develop. Instead of forming from nodes, CRs form from asters. Presumably, formin activation at asters promotes extension of a leading actin cable, which subsequently encircles the cell to form a ring. SIN activation functions prominently in this Mid1-independent CR assembly. Currently, both models are thought to operate in *S. pombe* (Roberts-Galbraith and Gould, 2008).

2008). The SIN, which is orthologous to the mitotic exit network of budding yeast, consists of a GTPase-regulated kinase cascade that is initially triggered through polo-like kinase. The most downstream kinase, known as Dbf2 in budding yeast *Saccharomyces cerevisiae* and Sid2 in *S. pombe*, phosphorylates Cdc14-family phosphatases to control their cytoplasmic accumulation (Chen et al., 2008; Mohl et al., 2009), which is significant given the role of Cdc14 phosphatases in reversing phosphorylations catalyzed by M phase cyclin-dependent kinases (CDKs). While signaling through some kinases, including polo, advances cytokinesis, other kinases, such as M phase CDKs, instead inhibit cytokinesis. Indeed, global reduction of CDK activity in mitotically-arrested mammalian cells induces cytokinesis (Wolf et al., 2007). Just as SIN-activated dephosphorylation of F-BAR Cdc15 promotes CR assembly in *S. pombe* (Hachet and Simanis, 2008; Roberts-Galbraith et al., 2010), reversal of CDK phosphorylations on the *Candida albicans* cytokinetic IQGAP likewise promotes CR formation (Li et al., 2008). Still, it is unclear whether these events can be triggered via related signaling pathways.

In both models of *S. pombe* CR assembly, signaling begins through polo-like kinase. In budding yeast and animal cells, polo also influences small Rho GTPases, Rho1 and RhoA, respectively, to control early stages of cytokinesis and CR assembly. Rho proteins become activated through loading of GTP by guanine nucleotide exchange factors (GEFs) and inactivated following GTP hydrolysis mediated by GTPase-activating proteins (GAPs). In budding yeast, polo-like kinase phosphorylates Rho1 GEFs to target them to the bud neck (Yoshida et al., 2006). Rho1 GEFs subsequently bind and activate Rho1 at this site (Yoshida et al., 2009; Yoshida et al., 2006). In animal cells, polo signaling likewise controls RhoA function, with polo-like kinase phosphorylating a

RhoGAP, Cyk4/MgcRacGAP (Burkard et al., 2009; Wolfe et al., 2009). Cyk4 associates with kinesin MKLP1 to form centralspindlin, a microtubule-bundling complex that stably accumulates at the spindle midzone once CDK phosphosites on MKLP1 are reversed and Aurora B kinase phosphorylation of MKLP1 locally impedes 14-3-3 inhibition of centralspindlin in this region (Douglas et al., 2010; Mishima et al., 2004). Plk1-mediated phosphorylation of Cyk4 then primes centralspindlin for recruitment of RhoGEF Ect2 to the midzone and subsequent medial activation of RhoA (Burkard et al., 2009; Wolfe et al., 2009). Rho GTPase flux achieved through active RhoGAP meanwhile limits lateral spread of active Rho zones such that they are maintained medially (Miller and Bement, 2009). Rho GEF and GAP activities are themselves modulated through phosphorylation by diverse kinases such as Aurora B, CDKs, and polo-like kinases (Asiedu et al., 2008; Birkenfeld et al., 2007; Minoshima et al., 2003; Rosario et al., 2010; Toure et al., 2008). Protein phosphatase PP2A can reverse such phosphorylation (Toure et al., 2008), consistent with protein kinases and phosphatases operating in concert to dictate the timing of cytokinesis in various organisms.

Constriction of the cytokinetic apparatus

Though the exact mechanism guiding constriction of the CR has not been fully defined, the general assumption is that ring constriction proceeds similarly to constriction of muscle sarcomeres, with antiparallel F-actin sliding on myosin II (Pollard, 2010). Therefore, regulatory inputs impacting myosin II profoundly shape this step of cytokinesis. Like other type II myosins, those involved in cytokinesis possess both heavy and light chains. In animal cells, regulatory light chain phosphorylation at two sites,

threonine 18 and serine 19, enhances myosin II ATPase activity as well as myosin II filament formation in many organisms (Matsumura, 2005). Consistent with a role for light chain phosphorylation in cytokinesis, di-phosphorylated myosin II promotes total cellular contractility (Mizutani et al., 2006; Mizutani et al., 2009), and cancer cells that fail cytokinesis exhibit reduced myosin light chain phosphorylation (Wu et al., 2010). Though light chain phosphorylation was also previously thought to act as the predominant determinant of cortical localization of myosin II during cytokinesis (Matsumura, 2005), more recent research has suggested that factors independent of phosphorylation can control this targeting and thus impact initial ring assembly (Beach and Egelhoff, 2009; Uehara et al., 2010).

A variety of kinases, including two Rho-effector kinases, ROCK and citron kinase, as well as a calmodulin-effector kinase, myosin light chain kinase, contribute to myosin II di-phosphorylation (Matsumura, 2005). Scaffolding through septin SEPT2 is reported to enable many of these kinases to assemble together with myosin II for robust phosphorylation (Joo et al., 2007). Dissociation of ROCK and citron kinases from myosin II has been associated with cleavage furrow regression in Chinese hamster cells (Joo et al., 2007). Correspondingly, silencing of ROCK signaling has been posited to cause the late cytokinesis failure observed during polyploidization of human megakaryocytes (Lordier et al., 2008), and knockdown of citron kinase in HeLa cells blocks cytokinesis (Gruneberg et al., 2006). The effect of ROCK on myosin II function during cytokinesis is complicated by its phosphorylation of myosin light chain phosphatase. Such phosphorylation indirectly heightens myosin light chain phosphorylation by opposing the binding of myosin light chain phosphatase to myosin II

and by also inhibiting the phosphatase's activity (Matsumura, 2005). Unlike Rho-effector kinases, myosin light chain kinase becomes activated by calcium-calmodulin binding. In sea urchin eggs, forced release of calcium in early metaphase triggers premature cortical contraction, suggesting a prominent role for myosin light chain kinase in CR contractility in this organism (Lucero et al., 2006). Consistent with transient calcium-calmodulin-myosin light chain kinase interactions inducing localized cellular contraction, maximal equatorial binding of calcium-calmodulin to myosin light chain kinase occurs just prior to CR constriction during cytokinesis in rat kidney cells (Chew et al., 2002). Though all of these kinases can thus shape myosin activation during cytokinesis, more research is required to detail their relative timing and contribution in different organisms and cell types.

In addition to activating roles for myosin phosphorylation, some identified phosphorylation events instead confer inhibitory cues for cytokinesis. For example, an *S. pombe* PAK-related kinase, Pak1/Orb2, phosphorylates myosin II light chain Rlc1 to inhibit constriction of the CR (Loo and Balasubramanian, 2008), and phosphorylation of the myosin II heavy chain in the slime mold, *Dictyostelium*, actually prevents formation of myosin II filaments that are responsible for myosin II function in this organism (Bosgraaf and van Haastert, 2006). The involvement of heavy chain phosphorylation in myosin II regulation during cytokinesis has furthermore been documented in fission yeast, where such phosphorylation contrarily stimulates constriction through an unknown mechanism (Sladewski et al., 2009). Clearly, myosin II function in various organisms is controlled through a complicated array of phosphorylation events, though the exact locations and effects of these phosphosites may differ among species.

Separation of daughter cells

Just as initiation of CR assembly requires concentrated, medial RhoA activation in animal cells, completion of cytokinesis only occurs as active RhoA declines at the cleavage furrow. Protein kinase C ε (PKCε) promotes this local decrease in active RhoA following PKCε's priming phosphorylation, 14-3-3 binding, and full activation (Saurin et al., 2008). However, the relevant PKCε substrate mediating this effect has yet to be identified.

Concomitant with such Rho inhibition, the local lipid composition at the furrow must be dynamically refashioned for cytokinesis to complete (Echard, 2008). Lipid kinases perform crucial roles in this task and thus deserve recognition as key players in molecular modifications during cytokinesis. Despite being broadly distributed on the plasma membrane earlier in mitosis, the phosphoinositide phosphatidyl-4,5-bisphosphate [PtdIns(4,5)P_2] concentrates in the cytokinetic furrows of fission yeast and mammalian cells (Echard, 2008; Emoto et al., 2005; Field et al., 2005; Kouranti et al., 2006). The recruitment of relevant phosphoinositide kinases to the furrow is thought to be largely responsible for such accumulation (Echard, 2008; Emoto et al., 2005). Significantly, loss of PtdIns(4,5)P_2 from mammalian furrows results in late cytokinesis failure, most likely due to an inability to recruit post-furrowing factors such as septins and ezrin/radixin/moesin proteins and related defects in linking the cytokinetic apparatus to the plasma membrane (Echard, 2008; Emoto et al., 2005; Field et al., 2005). Unlike PtdIns(4,5)P_2, another phosphoinositide, phosphatidylinositol-3,4,5-trisphosphate [PtdIns(3,4,)P_3], is undetectable at the cleavage furrow but instead localizes to the poles

of dividing *Dictyostelium* cells. Experimental disruption of kinases controlling PtdIns(3,4,)P_3 destroys this localization pattern and prevents completion of cytokinesis following ingression (Janetopoulos et al., 2005), likewise underscoring the significance of spatial control in lipid kinase function.

During abscission, additional regulatory factors tied to phosphoinositide signaling are shuttled to the furrow. Indeed, disruption of cellular trafficking, especially of two Rab GTPases, Rab11 and Rab35, affects the final steps of cytokinesis in higher eukaryotes (Echard, 2008; Fielding et al., 2005; Kouranti et al., 2006; Wilson et al., 2005). In *Drosophila melanogaster*, the kinase Four wheel drive catalyzes formation of phosphatidylinositol-4-phosphate [PtdIns(4)P]. Subsequent incorporation of PtdIns(4)P into Golgi-derived vesicles promotes trafficking of Rab11 to the midbody, the microtubule remnant of the anaphase spindle midzone that links the two daughter cells (Polevoy et al., 2009). In the future, it will be interesting to examine whether lipid kinase function also directs Rab11 trafficking in mammals given Rab11's role in mammalian abscission (Fielding et al., 2005; Wilson et al., 2005). Disruption of Rab35-based cycling meanwhile perturbs the cellular distribution of PtdIns(4,5)P_2, most likely by affecting transport of relevant kinases to the furrow (Echard, 2008; Kouranti et al., 2006). Therefore, lipid kinases act both upstream and downstream of Rab GTPase-mediated endocytosis at the cleavage furrow. Moreover, phosphoinositides at the midbody can also directly bind factors needed for abscission. For example, phosphatidylinositol-3-phosphate [PtdIns(3)P] recruits a centrosomal protein, FYVE-CENT, to the midbody. Here, FYVE-CENT binds CHMP4B (Sagona et al., 2010), which is an ESCRT ('endosomal sorting complex required for transport')-III component, and this interaction

is significant given the proposed function of ESCRT-III in membrane bending and scission (Hanson et al., 2008). As lipid kinase activity directs secretory machinery and transport in yeasts as well (Yakir-Tamang and Gerst, 2009), these enzymes could potentially affect cell separation in multiple organisms through similar pathways.

In addition to cues that trigger abscission, chromatin persisting in the plane of division has been reported to delay completion of cytokinesis. In both budding yeast (Mendoza et al., 2009b; Norden et al., 2006) and human cells (Steigemann et al., 2009), Aurora B kinase activity safeguards cells from dividing through unsegregated chromosomes. In these organisms, Aurora B transfers with the rest of the chromosomal passenger complex (CPC) to the spindle midzone in anaphase following reversal of CDK-mediated phosphorylation of INCENP, another CPC subunit (Hummer and Mayer, 2009; Pereira and Schiebel, 2003). Thus, Aurora B is nicely positioned at this stage of the cell cycle to detect chromatin in the cleavage plane. Indeed, acetylated chromatin stalled in vicinity of the central spindle activates Aurora B in budding yeast (Mendoza et al., 2009b). Active Aurora B then initiates a NoCut checkpoint by targeting two abscission inhibitors, Boi1 and Boi2, to the bud neck, where they prevent chromosome cutting by the cytokinetic apparatus (Norden et al., 2006). In human cells, chromosome bridges likewise prolong Aurora B activity at the midbody, and this stabilizes ingressed furrows and protects against tetraplodization caused by furrow regression (Steigemann et al., 2009). Though the mechanism by which such stabilization occurs is currently unclear, it has been suggested that Aurora B phosphorylation of centralspindlin could be involved (Steigemann et al., 2009). Nonetheless, the generality of these mechanisms awaits further examples.

Detailed introductions to key signaling molecules and networks

Broadly, my dissertation research has aimed to improve our understanding of how cytokinesis accomplishes the faithful production of two daughter cells, both of which are viable and behave appropriately. Given the diverse roles that phosphorylation serves at the division site, much of this research has addressed molecular mechanisms and consequences of kinase and phosphatase signaling during cytokinesis, using fission yeast *S. pombe* as a model. Below, I introduce in more detail the pathways and proteins on which my dissertation research has been primarily focused.

Coordination of mitosis and cytokinesis by the CPC and Cdc14-family phosphatases

To ensure successful cell division, sister chromatids must segregate to opposite poles of dividing cells in mitosis and be partitioned into two new daughter cells during cytokinesis (Pines and Rieder, 2001). Highly intricate mechanisms control these processes, with various macromolecular complexes coordinating their activities such that the integrity of cell division is maintained. The CPC, which is composed of a catalytic subunit, Aurora B kinase, and three non-enzymatic subunits, INCENP, Survivin, and Borealin, functions as one of these critical regulatory complexes. As its name implies, this complex travels on chromosomes to various sites during cell division such that it can execute specific tasks at distinct locations and times (Fig. 1-5) (Earnshaw and Bernat, 1991). These functions include, but are not limited to, chromosome condensation, stabilization of the mitotic spindle, correction of improper kinetochore-microtubule

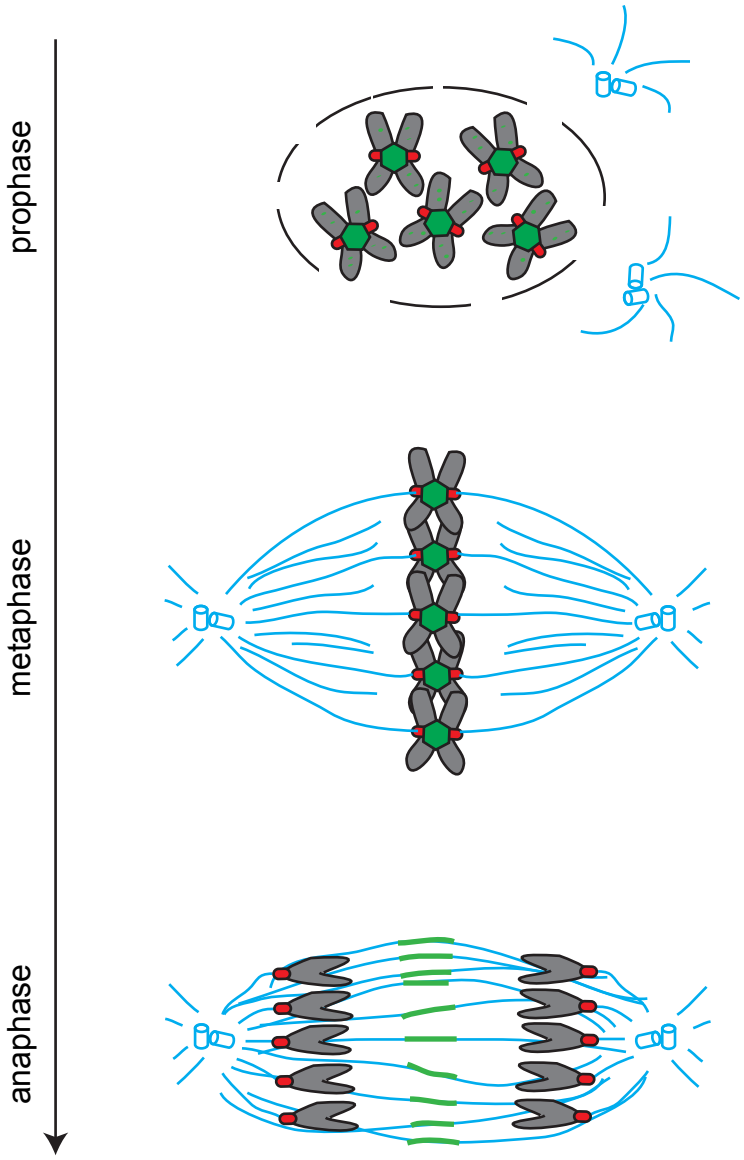

Figure 1-5

The CPC exhibits dynamic localization during the cell cycle.
During mitosis, the CPC (green) localizes to different cellular sites, where it aids in diverse events. In animal cells, as the nuclear envelope breaks down in prophase, the CPC localizes diffusely on chromosome arms (gray), where it aids in chromosome condensation. At this stage, the CPC begins to accumulate at inner centromeres between kinetochores (red), and remains at these sites through metaphase. Here, it mediates regulation of microtubule (blue) attachments to kinetochores. Once chromosomes segregate in anaphase, the CPC relocates to the spindle, where it ultimately accumulates at the spindle midzone. At this site, the CPC stabilizes the spindle and coordinates signaling relevant to cytokinesis in mutliple organisms. [schematics adapted from (Ruchaud et al., 2007)]

attachments, and regulation of cytokinesis [for reviews, see (Ruchaud et al., 2007; Vader et al., 2006; Vagnarelli and Earnshaw, 2004)].

The four CPC subunits are highly interdependent for proper localization, activity, and stability (Ruchaud et al., 2007). Consistent with such interdependency, these subunits are widely conserved among eukaryotes (Ruchaud et al., 2007). However, it has proven difficult to identify Borealin homologs in yeasts. Though some have speculated that yeast Borealin homologs might not exist due to fusion of the Borealin and Survivin subunits into a single yeast Survivin homolog (Vader et al., 2006), recent evidence suggests that there are in fact yeast Borealin homologs (Nakajima et al., 2009). Nonetheless, a Borealin homolog in fission yeast *S. pombe* had not been characterized.

Similar to the CPC, Cdc14-family phosphatases are also significant regulators of cell division. Named for Cdc14, the founding member identified in budding yeast, these phosphatases reverse CDK-mediated phosphorylation events to promote mitotic exit and cytokinesis (Queralt and Uhlmann, 2008). Like other Cdc14 family members, Clp1/Flp1, the *S. pombe* Cdc14 homolog, also functions in these processes. Specifically, Clp1 reverses CDK-mediated phosphorylation of the mitotic inducer Cdc25, allowing degradation of Cdc25 by the anaphase-promoting complex/cyclosome at the end of mitosis and ending the CDK auto-amplification loop (Esteban et al., 2004; Wolfe and Gould, 2004). Furthermore, Clp1 associates with the CR scaffold protein Mid1, and, through this interaction, Clp1 enhances CR stability and the precision of cytokinesis (Clifford et al., 2008).

In addition to these crucial functions during the concluding stages of the cell cycle, Cdc14-family phosphatases regulate chromosome segregation and CPC function

during mitosis. In *S. pombe*, Clp1 associates with *S. pombe* Aurora B kinase Ark1 and deletion of *clp1* results in increased co-segregation of sister chromatids (Trautmann et al., 2004). In *S. cerevisiae*, Cdc14 regulates localization of the CPC to the spindle during anaphase (Pereira and Schiebel, 2003; Stoepel et al., 2005). This Cdc14-mediated targeting of the CPC is crucial to its subsequent recruitment of the separase Esp1 and the chromosomal passenger Slk19 (Khmelinskii et al., 2007; Pereira and Schiebel, 2003), which influence the formation and stabilization of the mitotic spindle and the spindle midzone (Jensen et al., 2001; Zeng et al., 1999). Yet, while it is clear that Cdc14-family phosphatases regulate CPC localization and function, a reciprocal relationship has not been described.

Though effects of the CPC on Cdc14-family phosphatases are unclear, the CPC is known to play a critical role in cytokinesis in many organisms (Carmena, 2008). For example, in *S. cerevisiae*, CPC subunits regulate septin dynamics (Gillis et al., 2005; Thomas and Kaplan, 2007), and, as mentioned previously, *S. cerevisiae* and human Aurora B kinases mediate a NoCut checkpoint that delays cytokinesis when chromatin is stalled in the cleavage plane (Mendoza et al., 2009a; Norden et al., 2006; Steigemann et al., 2009). However, in *S. pombe*, the contribution of the CPC to cytokinesis was thought to be negligible. Overexpression of kinase-dead Ark1 does not affect cytokinesis but instead results in cut phenotypes in which septa form through unsegregated DNA (Petersen and Hagan, 2003), and *ark1* temperature-sensitive mutants similarly exhibit cut phenotypes. Because the division machinery appears intact in cut cells, these data suggest that Ark1 does not play a critical role in *S. pombe* cytokinesis (Petersen and

Hagan, 2003). As a result, connections between the CPC and the *S. pombe* cytokinetic apparatus had not been further explored.

SIN-mediated regulation of the actin cytoskeleton during cytokinesis

As noted previously, two distinct but synergistic pathways control fission yeast cytokinesis. The first originates at medial precursor nodes, where anillin-like Mid1 recruits multiple early CR proteins (Laporte et al., 2011), which guide F-actin coalescence into a ring structure (Vavylonis et al., 2008). Despite this early cytokinesis function, Mid1 is non-essential, and cells defective in Mid1 function undergo cytokinesis (Huang et al., 2008; Sohrmann et al., 1996), due to partial redundancy with the SIN (Hachet and Simanis, 2008; Huang et al., 2008). SIN proteins assemble at spindle pole bodies (SPBs), though the terminal SIN kinase Sid2 translocates to the CR during cytokinesis (Fig 1-6) (Johnson et al., 2012). The Sid2 homolog in human cells also localizes to the CR (Bothos et al., 2005), suggesting signaling outputs may be conserved in other species. Consistent with the SIN conferring sufficient cues for CR organization in *S. pombe*, precocious SIN activation drives multiple rounds of septation in interphase and permits orthogonal CR formation in *mid1*Δ cells (Huang et al., 2008; Krapp and Simanis, 2008; Minet et al., 1979). Importantly, the SIN also governs CR maintenance following node-initiated cytokinesis in *S. pombe*, and CRs collapse between segregated daughter nuclei when SIN signaling is selectively abolished (Hachet and Simanis, 2008; Le Goff et al., 1999; Liu et al., 1999; Mishra et al., 2004).

As SIN signaling culminates with the activation of three protein kinases, one of which translocates to the CR (Krapp and Simanis, 2008), protein phosphorylation likely directs the major functional outputs of this network (Fig 1-6). Though accumulation of

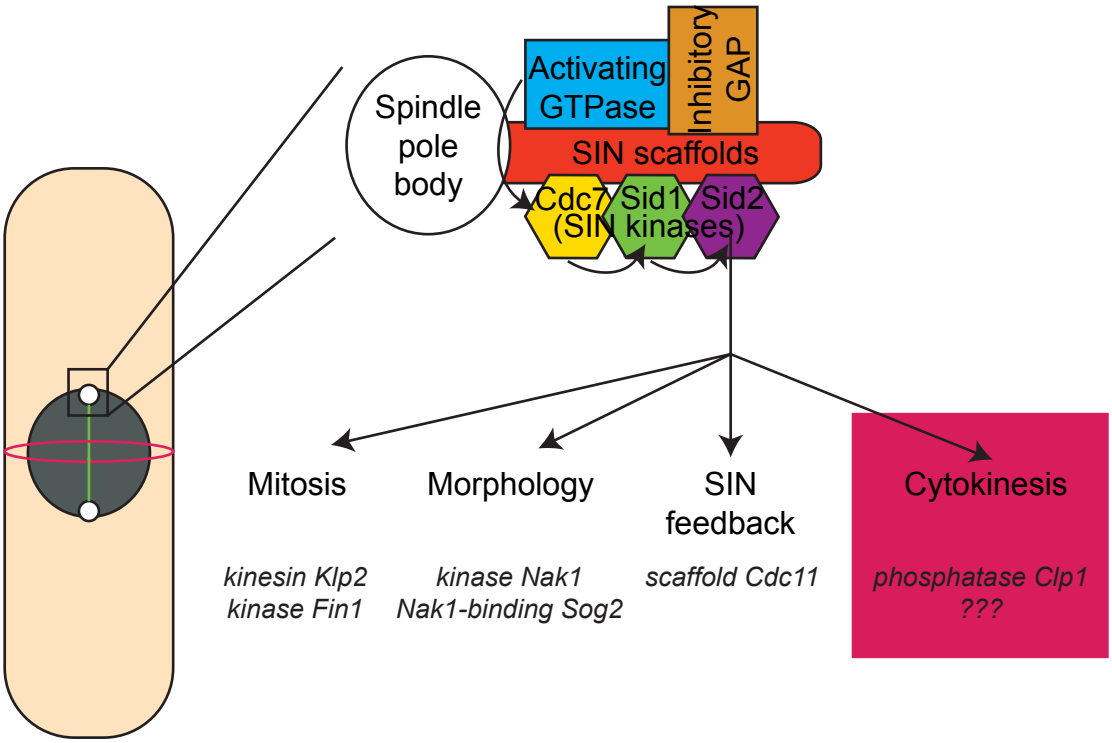

Figure 1-6

The SIN is an SPB-associated kinase cascade, whose essential cytokinetic substrates were unknown.

SIN signaling is anchored at SPBs through multiple scaffold proteins. Typically, an inhibitory GAP keeps the SIN off during interphase. Once this inhibition is relieved during mitosis, the activating GTPase initiates a kinase cascade, which terminates with kinase Sid2. Sid2 phosphorylates proteins involved in a variety of processes, including mitosis, cell morphology, SIN feedback regulation, and cytokinesis. Though SIN activity is required for cytokinesis in *S. pombe*, the only identified Sid2 substrate involved in cytokinesis was non-essential phosphatase Clp1. The identities of core, essential CR proteins targeted by Sid2 had been unknown.

F-BAR Cdc15 within a ring structure ultimately requires SIN activation (Hachet and Simanis, 2008), there is no evidence that Cdc15 is a direct SIN target. While some SIN substrates, including Cdc14-family phosphatase Clp1, have been identified (Feoktistova et al., 2012; Grallert et al., 2012; Gupta et al., 2013; Mana-Capelli et al., 2012), essential CR proteins directly targeted by Sid2 were unknown (Fig. 1-6).

Because cytokinesis in fission yeast, as in most eukaryotes, is actomyosin-based, the formin Cdc12, which localizes to the CR (Chang et al., 1997) and nucleates and polymerizes F-actin through its formin homology (FH) 1 and 2 domains (Fig. 1-7) (Kovar et al., 2003), is an essential component of the *S. pombe* cytokinetic machinery (Chang et al., 1997). Given that mechanisms regulating cytokinetic formin function were relatively unknown in any organism, it was unclear what cues sculpt the actin cytoskeleton during cell division. As hyperactivity of *S. pombe* Cdc12 is lethal (Kovar et al., 2003), it seemed likely that Cdc12 function is tightly regulated. Yet, Cdc12 domains homologous to autoinhibitory DID and DAD motifs (Fig. 1-7) have been reported to be inactive (Yonetani et al., 2008), and post-translational control of Cdc12 had not been demonstrated. Since SIN hyperactivation can induce formation of actin-based CRs even in interphase cells, it seemed reasonable that activation of this kinase cascade could influence Cdc12 formin activity. Nonetheless, it was uncertain whether this would be a direct or indirect mechanism.

Cytokinetic guidance of cellular morphogenesis

Many cells polarize in response to intrinsic and extrinsic signals. As cell polarization is generally multifaceted, cells must integrate both negative and positive cues

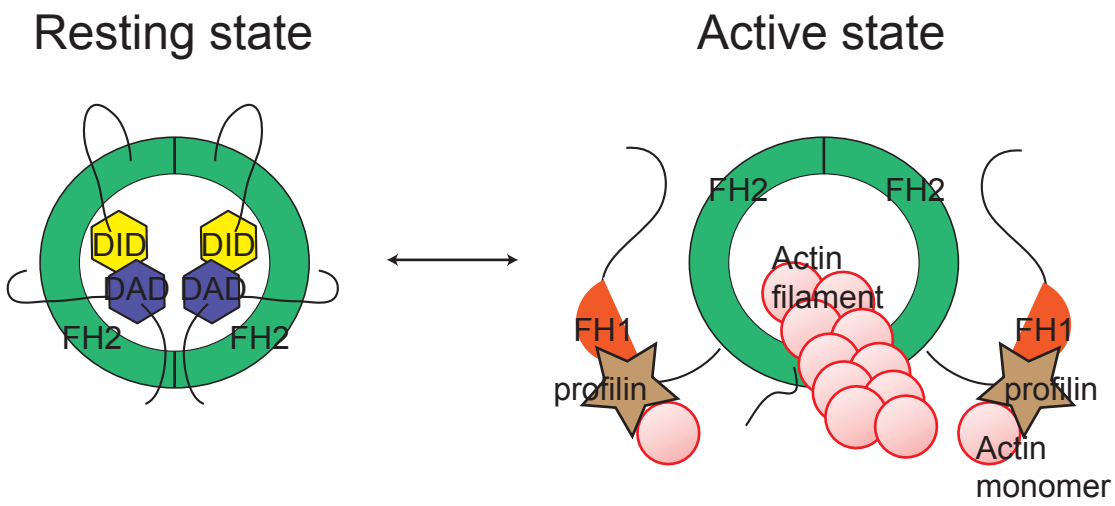

Figure 1-7

Diverse formin domains contribute to canonical autoregulation and F-actin assembly. Formins catalyze nucleation and polymerization of unbranched actin filaments. Canonically, formins achieve autoregulation via inhibitory interactions between N-terminal DID and C-terminal DAD motifs. This binding inhibits F-actin assembly. When autoinhibition is relieved, dimeric, doughnut-shaped FH2 domains, which bind F-actin, ride growing barbed ends. Meanwhile, the neighboring FH1 domain binds profilin, which recruits monomeric actin to support processive actin elongation. *S. pombe* Cdc12 possesses functional FH1 and FH2 domains, as well as DID and DAD motifs of unknown functionality. Thus, it had been uncertain how formin activity is regulated during cytokinesis.

for successful cellular morphogenesis. In various organisms, the cell cycle provides a platform on which these cues are organized [for reviews, see (Clark and Paluch, 2011; Howell and Lew, 2012)], thereby ensuring distinct polarization events occur at the appropriate location, time, and context.

S. pombe represents a genetically tractable organism for studying cell cycle regulation of growth polarity [for reviews, see (Huisman and Brunner, 2011; Martin and Chang, 2005)]. Wild-type *S. pombe* extend solely at their two cell tips, lengthening their rod-shaped bodies while retaining fairly constant widths. After cell division, *S. pombe* grow only at old ends, so-called because they served as ends of the dividing mother cell (Fig. 1-8A). Then, at a point in G2 known as new end take off (NETO), new ends, which arise from cell division, also initiate growth (Fig. 1-8A) (Mitchison and Nurse, 1985). NETO is not required for cell viability, and myriad mutants defective in this process have been identified (Huisman and Brunner, 2011; Martin and Chang, 2005). Intriguingly, protein kinases represent the broadest category of proteins affecting *S. pombe* NETO (Martin and Chang, 2005). This implies that several phosphorylation events participate in fission yeast morphogenesis. To date, all analyses of phosphorylation events involved in *S. pombe* morphogenesis have been limited to factors important at cell ends (Castagnetti et al., 2005; Kim et al., 2003; Martin and Chang, 2005). Whether polarity-relevant phosphorylations occur on proteins that localize to other cellular sites had not been previously demonstrated. Moreover, beyond requirements for S-phase completion and a minimal interphase cell size (Mitchison and Nurse, 1985), additional cell cycle controls on NETO had not been identified.

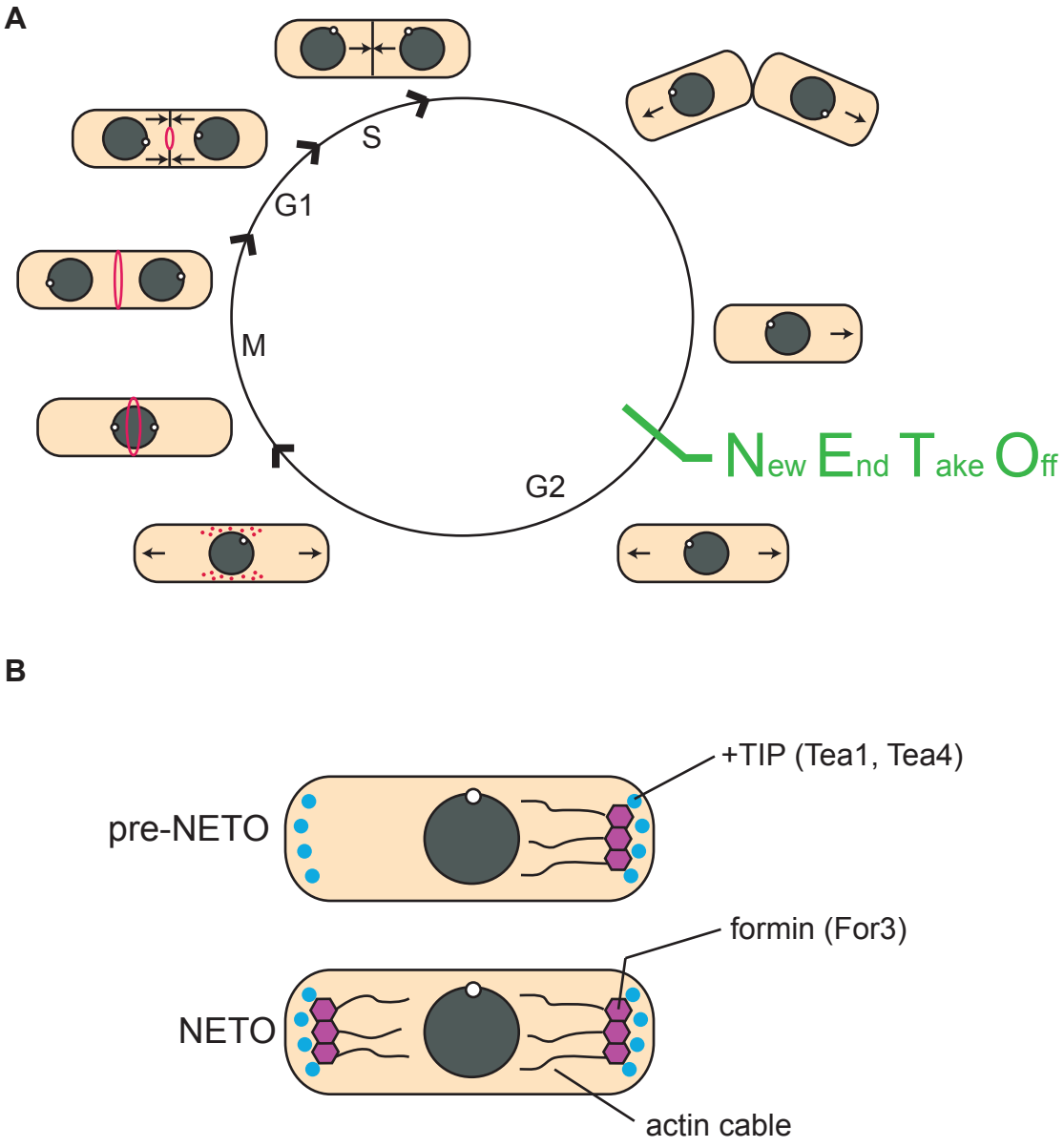

Figure 1-8

Upon NETO, *S. pombe* cells transition into bipolar growth.
(A) Schematic of the *S. pombe* cell cycle, with zones of cell growth indicated by arrows. (B) Microtubule plus-end associated factors (+TIPs) Tea1 and Tea4 constitutively associate with both cell ends. Before NETO, formin For3 only localizes to one end, the old end, where it polymerizes actin cables. Once NETO is activated, For3 is also recruited by +TIPs to the new end, establishing bipolar actin cables and activating bipolar growth.

As in other cell polarization events, cytoskeletal rearrangements accompany growth transitions in *S. pombe*. Prior to NETO, microtubule plus end-associated proteins Tea1 and Tea4 ride growing microtubule ends to both cell tip cortices (Fig. 1-8B) (Behrens and Nurse, 2002; Feierbach et al., 2004; Martin et al., 2005; Mata and Nurse, 1997), where they anchor based on their association with membrane proteins (Bicho et al., 2010; Snaith and Sawin, 2003). Upon NETO, Tea4 recruits formin For3, which had before only been tethered to old ends, into a complex with itself and Tea1 at new ends (Fig. 1-8B) (Martin et al., 2005). As over-expression of a Tea1-For3 fusion can drive NETO prematurely (Martin et al., 2005), this association likely brings For3 into the proximity of formin activators at new ends, stimulating For3 catalysis of F-actin cables that will deliver growth cargo to this tip. Not surprisingly, loss of Tea1, Tea4, and/or For3 impairs fission yeast polarization and elongation (Feierbach and Chang, 2001; Martin et al., 2005; Mata and Nurse, 1997; Nakano et al., 2002). Actin patches, which guide endocytic vesicle internalization and constitute a second F-actin structure, also re-polarize to both cell tips upon NETO (Gachet and Hyams, 2005). Disruption of proteins comprising these structures similarly jeopardizes growth polarity establishment (Cabrera et al., 2011; Castagnetti et al., 2005; Iwaki et al., 2004). Thus, alteration in protein composition at cell tips is coupled tightly to cytoskeletal rearrangements.

As mentioned previously, several tip-localized cell polarity factors, including Tea1 and Tea4, direct the cell division plane away from cell ends and towards the cell middle for cytokinesis (Huang et al., 2007), the process by which daughter cells undergo physical separation following nuclear division. However, whether the process of cytokinesis reciprocally modulates cell polarity is unclear. Some observations hint that

the cell division machinery may play a role in directing cell polarity. As was previously noted, new ends formed by cell division initiate growth well after old ends. In mutants in which cells remain physically connected at division sites for multiple cell divisions, internal cells can grow, though this occurs sub-apically adjacent to septa (Sipiczki et al., 1993; Sipiczki et al., 1998). Moreover, many polarity factors localize to the cell division site (Garcia et al., 2006; Glynn et al., 2001; Huisman and Brunner, 2011; Tatebe et al., 2005); nonetheless, only cell tip-localized populations of these polarity proteins have been demonstrated to contribute to growth polarity in *S. pombe*.

During *S. pombe* cytokinesis, several accessory proteins regulate the dynamics and organization of the CR. For one, Cdc15, which contains an N-terminal F-BAR domain and a C-terminal SH3 domain characteristic of the *pombe* Cdc15 homology protein family (Lippincott and Li, 2000), has been posited to link CR proteins to the cortical membrane at the division site (Roberts-Galbraith et al., 2010). Cdc15-binding proteins at the CR include formin, myosin, and the C2 domain protein Fic1 (Carnahan and Gould, 2003; Roberts-Galbraith et al., 2009). Fic1 localizes to both interphase cell tips and the cell division site (Roberts-Galbraith et al., 2009), though its specific functions at these sites had not been described. Fic1's budding yeast ortholog, Inn1, contributes to cytokinesis by linking the CR to the ingressing membrane and by participating in septum formation (Nishihama et al., 2009; Sanchez-Diaz et al., 2008). Together with the CR, septa provide mechanical force for membrane closure at the cell division site (Johnson et al., 2005), and subsequent septum degradation allows for abscission (Dekker et al., 2004; Martin-Cuadrado et al., 2003). Clearly, various remodeling events must occur at the cell division site for cytokinesis to complete

efficiently. Whether such remodeling events also influence daughter cell behavior has never been examined.

While wild-type *S. pombe* classically grow in a single-celled form, multiple fission yeasts, including *S. pombe*, possess the ability to assume an invasive, hyphal-like state (Amoah-Buahin et al., 2005; Sipiczki et al., 1998). The ability of pathogenic fungi to undergo such a morphogenetic switch contributes significantly to fungal infections (Brand, 2012). Though non-pathogenic, *S. pombe*, similar to the budding yeast (Gagiano et al., 2002), can transition into invasive growth as a foraging response to low nutrients (Amoah-Buahin et al., 2005). Invasive *S. pombe* form structures that technically qualify as pseudohyphae, for, unlike as in hyphal growth, cytokinetic constriction occurs (Dodgson et al., 2010; Pohlmann and Fleig, 2010). Pseudohyphae likely maintain their hyphal-like structure due to cellular adherence and preferential growth at old ends (Dodgson et al., 2010; Pohlmann and Fleig, 2010). Intriguingly, it has been postulated that single-celled fission yeast evolved from multicellular, filamentous fungi, with transcriptional networks that ensure efficient cell separation playing predominant roles in the evolution of a single-celled state (Bahler, 2005). Though *S. pombe* pseudohyphae do not commonly exhibit aborted cytokineses or multicellularity, it is an attractive hypothesis that inefficient, but not entirely defective, cytokinesis might somehow mark new ends to impair their growth and promote the dimorphic switch in *S. pombe*.

Summary

In this work, I have analyzed mechanisms by which different cytokinesis factors, many of which are involved in phosphosignaling, orchestrate the final stage of the cell

cycle, cytokinesis. In chapter I, I will describe the identification of a novel CPC component, which, along with Aurora kinase and the other CPC subunits, controls Cdc14/Clp1 localization to the CR. In chapter II, I will present evidence that the SIN directly targets formin Cdc12, and that this phosphorylation reverses a novel formin oligomerization event during late cytokinesis to prevent CR collapse. In chapter III, I will discuss how robust cytokinesis ensures proper polarized cell growth, and how cytokinesis-based growth defects facilitate an invasive morphological transition. In chapter IV, I will show that cytokinesis-based polarity controls, as well as the associated morphogenetic switch, are likewise subject to phosphoregulation, including by CDK. Collectively, these findings highlight new roles for well-studied kinases and phosphatases in cytokinesis regulation, and illustrate how such signaling allows for proper integration of multiple cell cycle events.

CHAPTER II

A LINK BETWEEN AURORA KINASE AND CLP1/CDC14 REGULATION UNCOVERED BY THE IDENTIFICATION OF A FISSION YEAST BOREALIN-LIKE PROTEIN

Introduction

The CPC regulates various events in cell division. This complex is composed of a catalytic subunit, Aurora B kinase, and three non-enzymatic subunits, INCENP, Survivin, and Borealin. Together, these four subunits interdependently regulate CPC function, and they are highly conserved among eukaryotes. However, a Borealin homolog had never been characterized in fission yeast *S. pombe*. Here, we isolate a previously uncharacterized *S. pombe* protein through association with Cdc14-family phosphatase Clp1/Flp1 and identify it as a Borealin-like member of the CPC. Nbl1 (novel Borealin-like 1) physically associates with known CPC components, affects the kinase activity and stability of *S. pombe* Aurora B, co-localizes with known CPC subunits during mitosis, and shows sequence similarity to human Borealin. Further analysis of the Clp1-Nbl1 interaction indicates that Clp1 requires CPC activity for its proper accumulation at the CR. Consistent with this, we describe negative genetic interactions between mutant alleles of CPC and CR components. Altogether, this work characterizes a fission yeast Borealin homolog and reveals a previously unrecognized connection between the CPC and the process of cytokinesis in *S. pombe*.

Results

Nbl1 is an essential protein that associates with and regulates the activity of the CPC

To identify Clp1-associated proteins in fission yeast *S. pombe*, we performed tandem affinity purification (TAP) of the phosphatase-dead Clp1-C286S mutant followed by mass spectrometry. One of the proteins identified through this approach was a sequence orphan, SPBC725.12 (Fig. 2-1A). SPBC725.12 had not been previously characterized except for its identification as an essential "meiotically upregulated gene" (mug) (Mata et al., 2002). For simplicity, we will subsequently refer to SPBC725.12 as Nbl1 (novel Borealin-like 1) based on the studies described in this work.

We confirmed that *nbl1* is an essential gene by analyzing tetrads from a diploid strain having one copy of *nbl1* disrupted with *ura4*$^+$. Tetrads showed a 2:2 ratio of *ura4*$^-$ viable to inviable spores or only one *ura4*$^-$ viable spore (Fig. 2-1B), indicating that Nbl1 is an essential protein. To examine the cause of inviability when *nbl1* is disrupted, we sporulated diploids heterozygous for the *nbl1* disruption and allowed only *ura4*$^+$ spores, containing the *nbl1* disruption, to germinate. DAPI staining indicated that 74% (148/200) of septated *nbl1*-disrupted cells exhibited a cut phenotype, with the septum slicing through the DNA (Fig. 2-1C). Cut phenotypes arise from defects in sister chromatid separation (Yanagida, 1998) and were not observed in wild-type cells (Fig. 2-1C). Thus, Nbl1 appears to affect chromosome segregation.

To verify that the observed cut phenotypes were in fact due to *nbl1* malfunction, we rescued the null mutation with a genomic clone containing *nbl1*$^+$ cDNA and also developed a *nbl1*-shutoff strain. The original open reading frame predicted for Nbl1 in the Pombe Genome Database was a truncated version, comprising only the first 95 amino

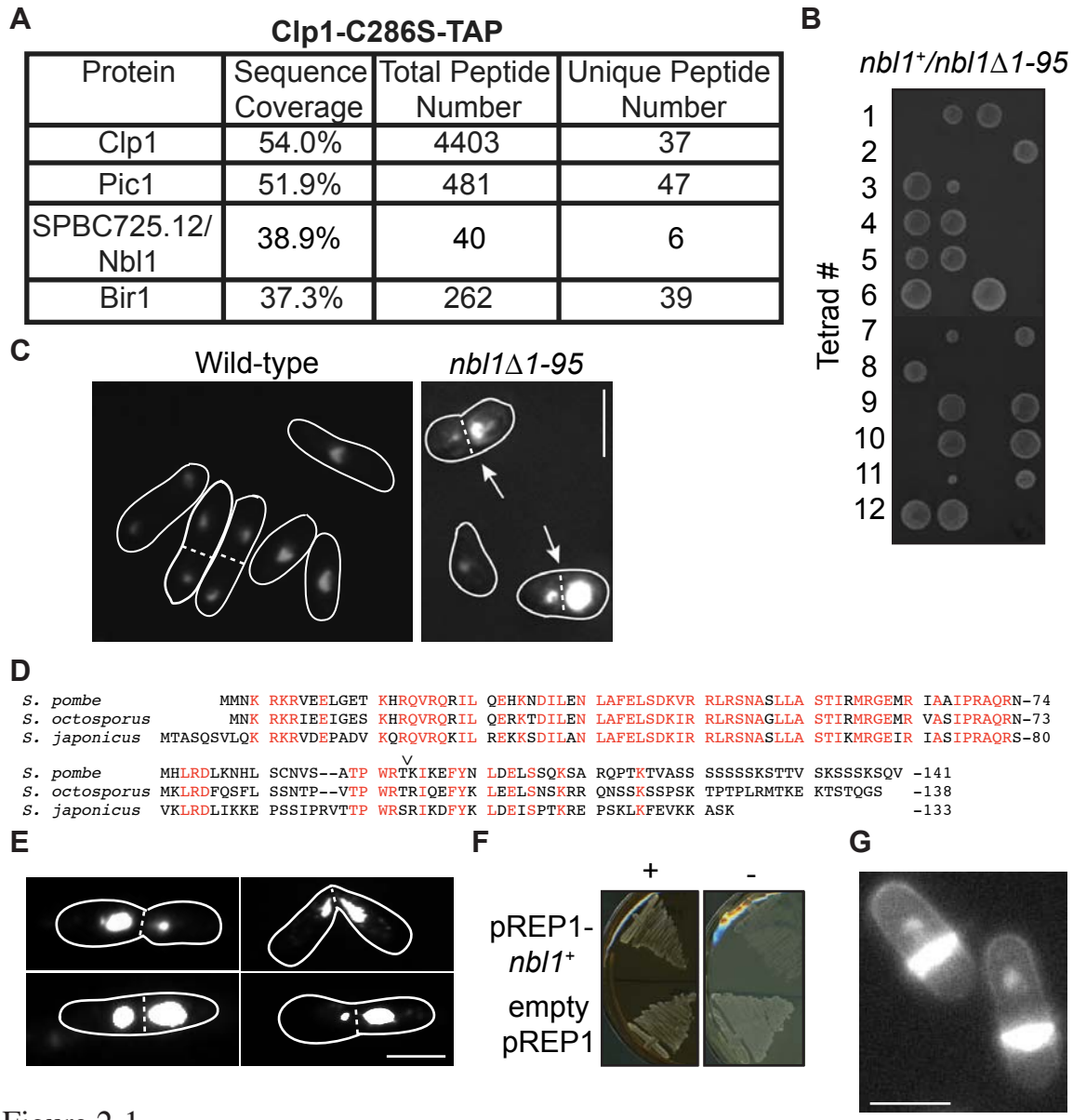

Figure 2-1

Clp1-associated Nbl1 is essential for chromosome segregation.
(A) Analysis of mass spectrometry data following TAP of *clp1-C286S*-TAP, with percent coverage, total peptide number, and unique peptide number for proteins of interest presented. (B) A diploid heterozygous for the *nbl1* disruption was sporulated, and tetrads were dissected. All viable colonies were *ura4*$^-$. (C) DAPI-stained wild-type or *ura4*$^+$ cells germinated following sporulation of a diploid heterozygous for the *nbl1* disruption. Cells are outlined in white, septa are represented by dashed white lines, and cut phenotypes are indicated by white arrows. (D) Alignment of sequences for *S. pombe* Nbl1 and homologs in *S. japonicus* and *S. octosporus*. Identical residues are in red, and the site of the Nbl1(1-95) truncation is indicated by an arrowhead. (E) DAPI-stained *nbl1*-shutoff cells. Cells are outlined in white, and septa are indicated by dashed white lines. (F) Wild-type cells were transformed with either empty pREP1 or pREP1-*nbl1*$^+$ and incubated on plates with (+) or without (-) thiamine. (G) DAPI- and methyl blue-stained *ark1*-GFP cells over-expressing *nbl1*$^+$. (Bars = 5 μm)

acids of Nbl1's 141 amino acids (Fig. 2-1D). Thus, we initially placed *nbl1(1-95)* cDNA under control of the thiamine repressible *nmt41* promoter (Basi et al., 1993) and integrated this fragment at the *leu1*$^+$ locus in a *nbl1*-disrupted strain. This truncated cDNA was sufficient to rescue the *nbl1* disruption, indicating that the C-terminus of Nbl1 is dispensable for proper Nbl1 function. Consistent with this, most sequence conservation between *S. pombe* Nbl1 and homologs in *S. octosporus* and *S. japonicus* lies in the N-terminus (Fig. 2-1D). Since Nbl1(1-95) was fully functional, we used this truncation interchangeably with full-length Nbl1 in our studies. Shutoff of *nbl1(1-95)* expression produced cut phenotypes (Fig. 2-1E) similar to those which were seen in *nbl1*-disrupted cells (Fig. 2-1C). Therefore, the previously described defects in chromosome segregation are due to disruption of *nbl1*.

To examine whether *nbl1* over-expression is tolerated by cells, *nbl1*$^+$ cDNA was placed under control of the *nmt1* promoter in pREP1 (Maundrell, 1990; Maundrell, 1993) and transformed into wild-type cells. Upon removal of thiamine, cells over-expressing *nbl1* failed to form colonies (Fig. 2-1F) and often showed unequal segregation of DNA (Fig. 2-1G). Thus, not only is *nbl1* an essential gene, but its protein levels must be regulated properly to ensure appropriate chromosome segregation.

To identify proteins with which Nbl1 interacts and functions, we performed a TAP of Nbl1(1-95) followed by mass spectrometry. Interestingly, Bir1/Cut17, the *S. pombe* Survivin homolog, and Pic1, the *S. pombe* INCENP homolog, which both had been previously identified along with Nbl1 in the Clp1-C286S-TAP (Fig. 2-1A), were identified along with Clp1 in a Nbl1(1-95)-TAP (Fig. 2-2A). We confirmed the association between Nbl1(1-95) and Bir1 by traditional co-immunoprecipitation (Fig. 2-

A

Nbl1(1-95)-TAP

Protein	Sequence Coverage	Total Peptide Number	Unique Peptide Number
Bir1	64.8%	423	65
Nbl1	64.2%	175	11
Pic1	33.9%	167	30
Clp1	25.5%	49	13

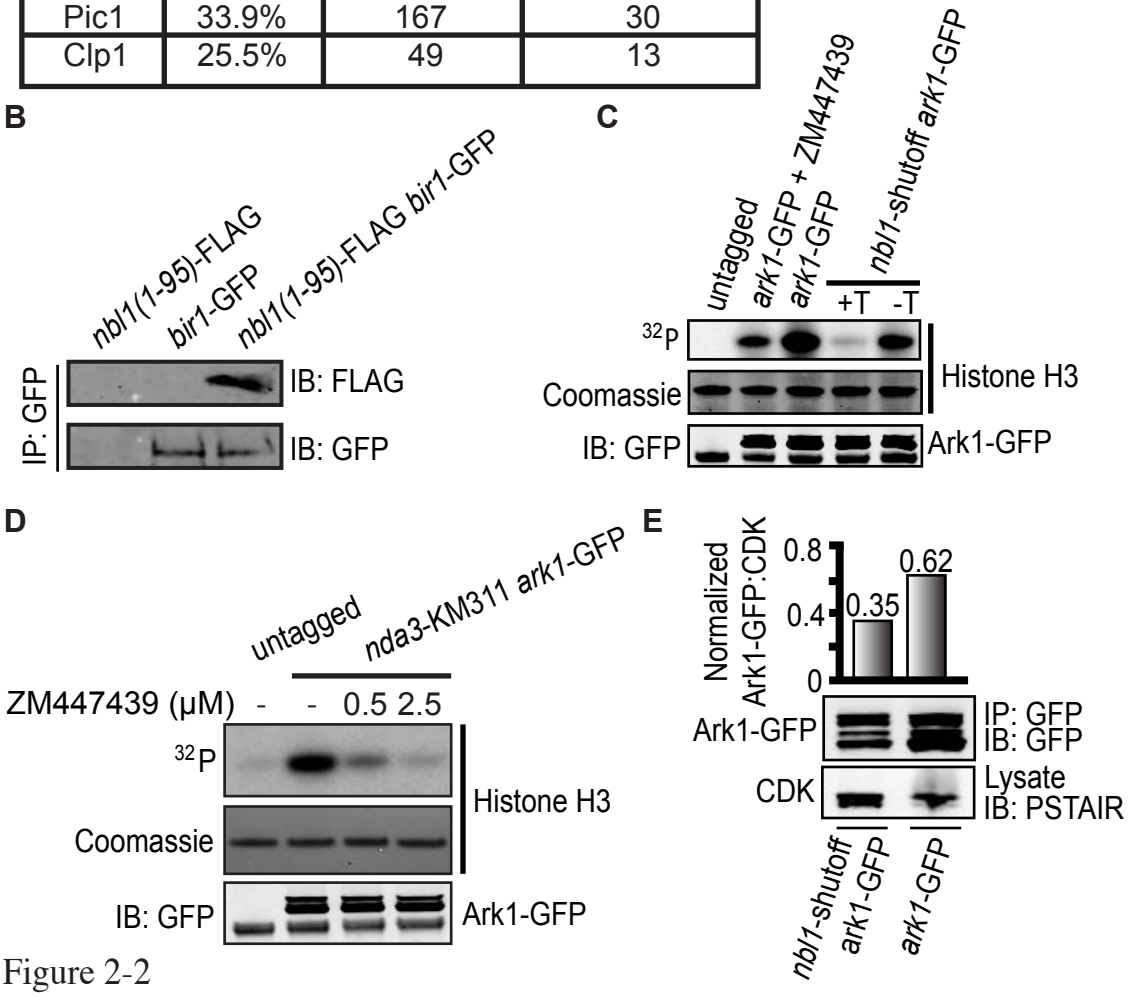

Figure 2-2

Nbl1 associates with the CPC and affects Aurora kinase stability and activity.
(A) Analysis of mass spectrometry data following TAP of *nbl1(1-95)*-TAP, with percent coverage, total peptide number, and unique peptide number for proteins of interest presented. (B) Anti-GFP immunoprecipitates from the indicated strains were blotted with anti-FLAG and anti-GFP antibodies. (C) Ark1-GFP was immunoprecipitated from the indicated strains and incubated with histone H3 in the presence of ^{32}P-ATP. Where appropriate, shutoff of *nbl1*-shutoff *ark1*-GFP was achieved prior to cell lysis via addition of thiamine (T). Kinase reactions using Ark1-GFP immunoprecipitated from *ark1*-GFP cells were carried out in either the presence or absence of an Aurora B inhibitor, ZM447439. (D) Ark1-GFP was immunoprecipitated from *nda3*-KM311 *ark1*-GFP during a prometaphase arrest and incubated with histone H3 in the presence of ^{32}P-ATP. Kinase reactions using immunoprecipitated Ark1-GFP were carried out in either the absence of an Aurora B inhibitor, ZM447439, or in the presence of this inhibitor in varying concentrations. (E) Anti-GFP immunoprecipitates were blotted with an anti-GFP antibody. Shutoff was achieved where appropriate by addition of thiamine. Ark1-GFP levels were normalized to CDK.

2B). In addition to Bir1 and Pic1, Ark1, which is the *S. pombe* Aurora B homolog, is a known member of the fission yeast CPC (Ruchaud et al., 2007). We did not detect Ark1 in the Nbl1(1-95)-TAP. However, TAPs of the Survivin homolog in *S. cerevisiae* also failed to recover the Aurora B homolog (Sandall et al., 2006; Widlund et al., 2006), suggesting that the kinase does not remain bound to its non-enzymatic subunits during a standard TAP procedure.

Given the association of Nbl1 with known CPC subunits, we tested the ability of Ark1, immunoprecipitated from wild-type and *nbl1*-shutoff strains, to phosphorylate histone H3 *in vitro*. Ark1-mediated phosphorylation of histone H3 is critical to establishment of condensed chromatin (Petersen and Hagan, 2003; Petersen et al., 2001), and thus histone H3 phosphorylation can be used as a readout of CPC activity. Not surprisingly, histone H3 was phosphorylated by Ark1-GFP from wild-type cells (Fig. 2-2C, lane 3), and such phosphorylation was decreased in the presence of an Aurora B kinase inhibitor, ZM447439 (Fig. 2-2C, lane 2). The specificity of this kinase assay for Ark1 was confirmed using higher concentrations of the Aurora B inhibitor (Fig. 2-2D). Interestingly, phosphorylation of histone H3 was nearly abolished when Ark1 was immunoprecipitated from cells in which *nbl1* expression had been repressed (Fig. 2-2C, lane 4). Although Nbl1 was required for the stability of Ark1 (Fig. 2-2E), we performed the kinase assay after Ark1 levels had been adjusted for equivalence (Fig. 2-2C, bottom panel). Thus, these results indicate that Nbl1 not only associates with CPC components but is required for proper activity and stability of the CPC.

Nbl1 and the CPC are interdependent for proper localization

Because Nbl1 and known CPC subunits exhibit physical and functional associations, we next examined whether Nbl1 localizes similarly to chromosomal passenger proteins. As shown by time-lapse microscopy of Nbl1(1-95)-GFP and Sid4-RFP, a marker for the *S. pombe* SPB (Chang and Gould, 2000), Nbl1(1-95)-GFP localized to dots consistent with centromeres in metaphase and relocated to the mitotic spindle and the spindle midzone during anaphase (Fig. 2-3A). This behavior was similar to that of Ark1, Pic1, and Bir1 (Fig. 2-3B) (Huang et al., 2005; Morishita et al., 2001; Petersen et al., 2001; Rajagopalan and Balasubramanian, 2002). In addition, Nbl1-GFP localized identically to the Nbl1(1-95)-GFP truncation (Fig. 2-3C), again demonstrating that Nbl1(1-95) is sufficient for proper localization and function of Nbl1.

During interphase and upon septation, Nbl1-GFP (Fig. 2-3C) and Nbl1(1-95)-GFP (Fig. 2-3A) accumulated within a distinct compartment of the nucleus. Previous studies have shown that the *S. pombe* CPC is nucleolar in interphase (Vanoosthuyse et al., 2007). Co-localization of Nbl1(1-95)-GFP and Nog1-RFP, a nucleolus marker (Matsuyama et al., 2006), confirmed that Nbl1 is also nucleolar in interphase (Fig. 2-4A). Additionally, imaging of Nbl1-GFP with Nuf2-RFP, a kinetochore marker (Nabetani et al., 2001), verified that the Nbl1-GFP dots seen during metaphase were consistent with Nbl1 localization to centromeres in metaphase (Fig. 2-4B). Though Nbl1-GFP and Nuf2-RFP did not completely overlap, their side-by-side orientation is similar to that which has previously been observed for other centromeric CPC proteins and kinetochore markers in metaphase (Vanoosthuyse et al., 2007). To furthermore validate that Nbl1 co-localizes with the CPC during mitosis, we imaged Nbl1(1-95)-GFP along with Pic1-mCherry. Nbl1(1-95)-GFP and Pic1-mCherry co-localized to centromeres in metaphase and to the

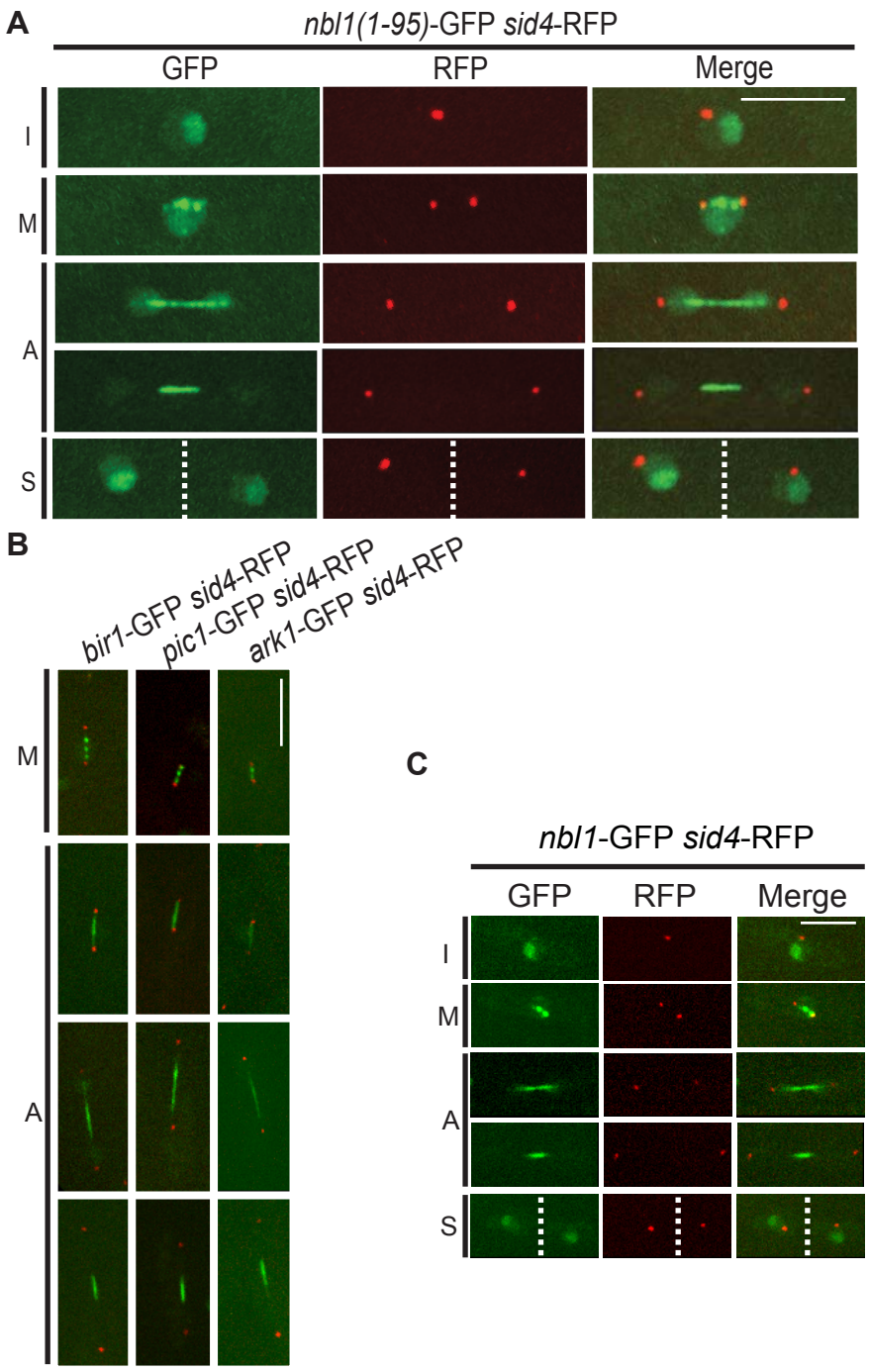

Figure 2-3

Like the CPC, Nbl1 localizes to kinetochores, the mitotic spindle, and the spindle midzone. I=interphase, M=metaphase, A=anaphase, and S=septation. (A) Live-cell GFP, RFP, and GFP/RFP merged images of *nbl1(1-95)*-GFP *sid4*-RFP cells at various stages of the cell cycle. The septum is indicated by a dashed white line. (B) Live-cell GFP, RFP, and GFP/RFP merged images of *bir1*-GFP *sid4*-RFP, *pic1*-GFP *sid4*-RFP, and *ark1*-GFP *sid4*-RFP cells in metaphase and anaphase. (C) Live-cell GFP, RFP, and GFP/RFP merged images of *nbl1*-GFP *sid4*-RFP cells at various stages of the cell cycle. The dashed white line indicates the location of the septum. (Bars = 5 μm)

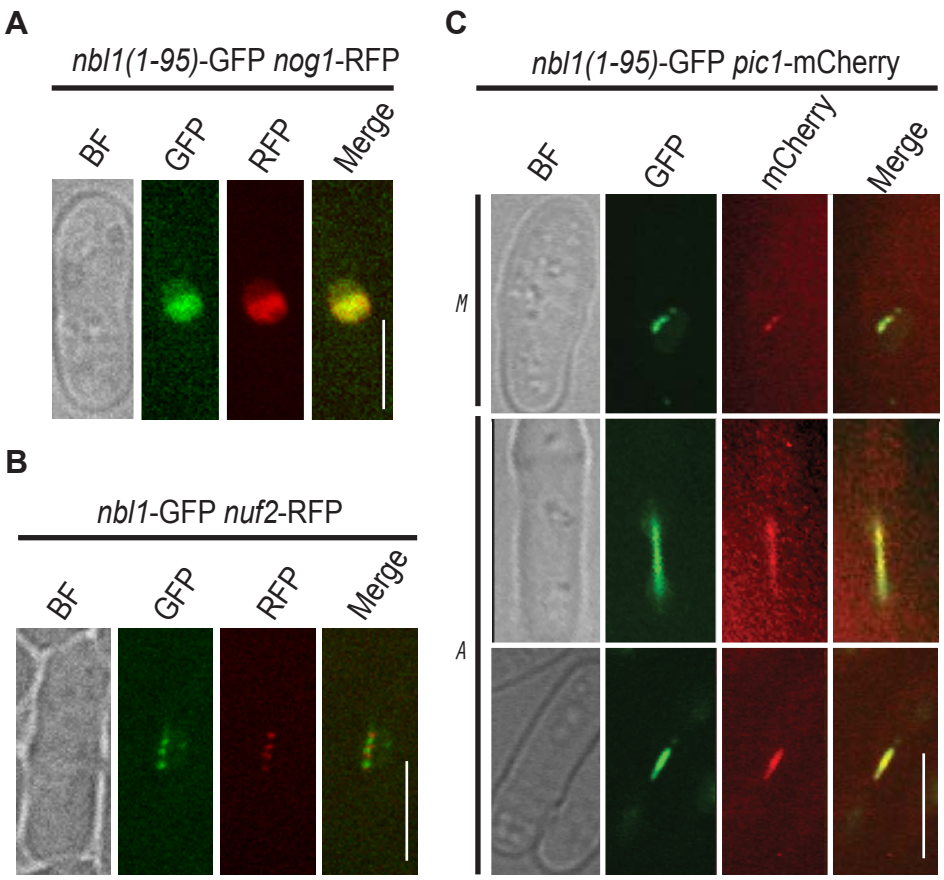

Figure 2-4

Nbl1 travels with the CPC during mitosis.
(A) Live-cell bright field (BF), GFP, RFP, and GFP/RFP merged images of a *nbl1(1-95)*-GFP *nog1*-RFP interphase cell. (B) Live-cell BF, GFP, RFP, and GFP/RFP merged images of a *nbl1*-GFP *nuf2*-RFP metaphase cell. (C) Live-cell BF, GFP, mCherry, and GFP/mCherry merged images of *nbl1(1-95)*-GFP *pic1*-mCherry cells in metaphase or anaphase. M=metaphase, and A=anaphase. (Bars = 5 μm)

mitotic spindle and the spindle midzone in anaphase (Figure 2-4C). Therefore, taken together with our evidence for a physical association between Nbl1 and the CPC, it seems evident that Nbl1 travels as a part of the CPC.

We next examined whether Nbl1 requires Bir1, Pic1, and/or Ark1 for proper mitotic localization. Nbl1-GFP localized normally in wild-type cells at 36°C (Fig. 2-5A). At this restrictive temperature in *cut17*-275 and *pic1*-T269 temperature-sensitive cells, Nbl1-GFP accumulated at centromeres as usual (16 out of 16 cells, 100%; and 38 out of 38 cells, 100%, respectively) but commonly failed to localize to the mitotic spindle or the spindle midzone correctly. Instead, Nbl1-GFP often localized diffusely in the nucleoplasm in *cut17*-275 and *pic1*-T269 cells (57 out of 72 cells, 79%; and 58 out of 88 cells, 66%, respectively) (Figs. 2-5B and 2-5C), indicating that Bir1 and Pic1 are necessary for its proper spindle localization. Additionally, Nbl1-GFP segregated unevenly at the completion of anaphase (Figs. 2-5B and 2-5C), consistent with unequal segregation of DNA in CPC mutants (Leverson et al., 2002; Samejima et al., 1993). At the restrictive temperature in *ark1*-T7 temperature-sensitive cells, however, Nbl1-GFP localized normally to both centromeres (53 out of 53 cells, 100%) and the mitotic spindle (71 out of 74 cells, 96%) (Fig. 2-5D). Yet, similar to Nbl1-GFP in *cut17*-275 and *pic1*-T269 septated cells, Nbl1-GFP segregated unevenly (Fig. 2-5D). In sum, although Nbl1-GFP localized independently of other CPC components to centromeres, it required the function of Bir1 and Pic1 for proper spindle localization.

Next, we investigated whether localization of known *S. pombe* CPC subunits requires Nbl1. As previously demonstrated (Huang et al., 2005; Morishita et al., 2001; Petersen et al., 2001; Rajagopalan and Balasubramanian, 2002), Bir1-GFP, Pic1-GFP,

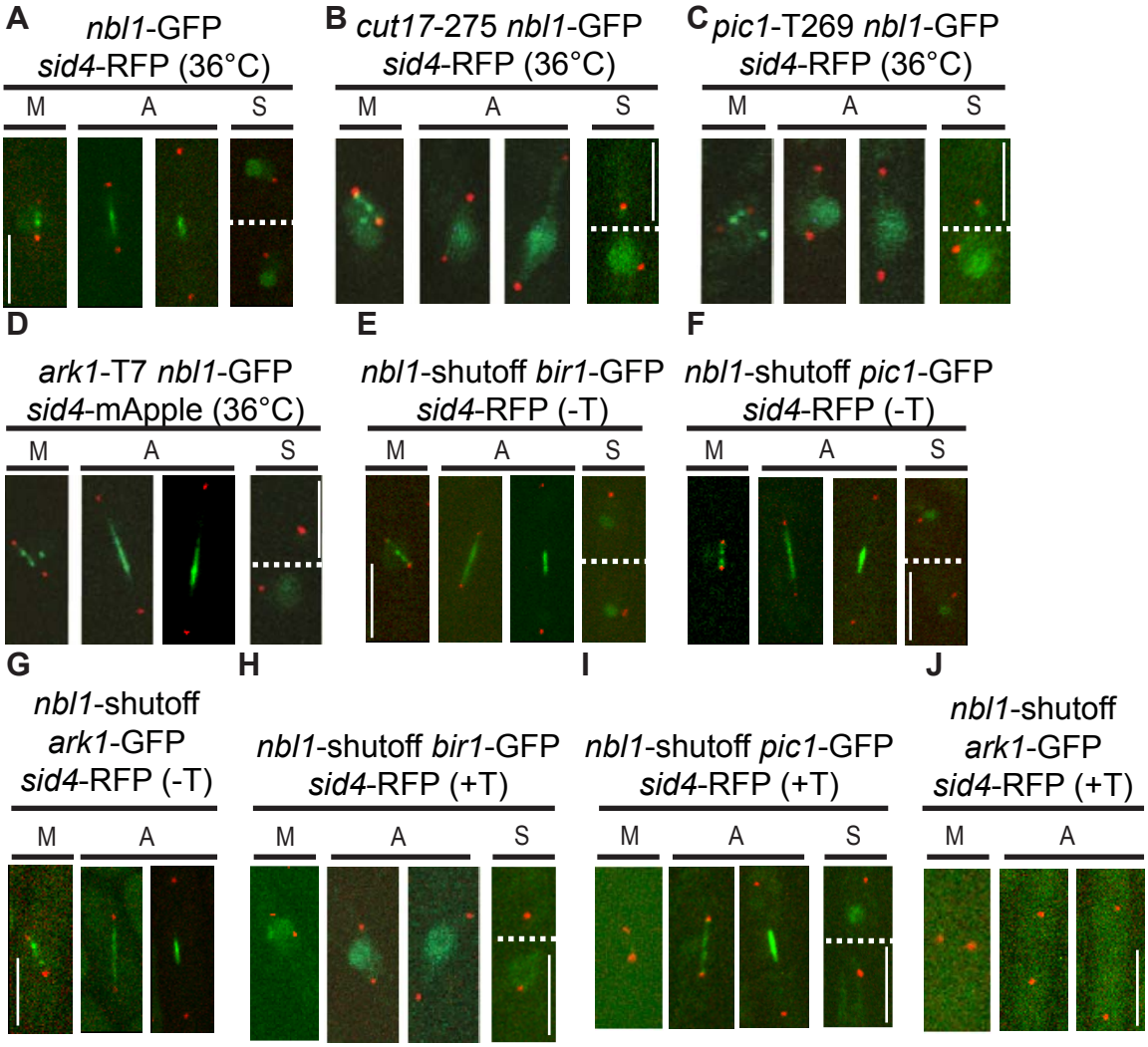

Figure 2-5

Nbl1 and the CPC are interdependent for mitotic localizations.
M=metaphase, A=anaphase, and S=septation. (A-D) Live-cell GFP/RFP or GFP/mApple merged images of *nbl1*-GFP *sid4*-RFP, *cut17*-275 *nbl1*-GFP *sid4*-RFP, *pic1*-T269 *nbl1*-GFP *sid4*-RFP, and *ark1*-T7 *nbl1*-GFP *sid4*-mApple cells progressing through mitosis after G2 synchronization and shift to 36°C. Septa are indicated by dashed white lines. (E-J) Live-cell GFP/RFP merged images of *nbl1*-shutoff *bir1*-GFP *sid4*-RFP , *nbl1*-shutoff *pic1*-GFP *sid4*-RFP, and *nbl1*-shutoff *ark1*-GFP *sid4*-RFP cells in the absence of thiamine (-T) or following 10 h of *nbl1* repression with thiamine (+T). Septa are indicated by dashed white lines. (Bars = 5 μm)

and Ark1-GFP localized to centromeres in metaphase and to the mitotic spindle and the spindle midzone in anaphase of wild-type cells (Fig. 2-3B). This localization was maintained in *nbl1*-shutoff cells in the absence of thiamine (Figs. 2-5E, 2-5F, and 2-5G). However, following repression with thiamine, Bir1-GFP, Pic1-GFP, and Ark1-GFP for the most part did not accumulate at centromeres in metaphase cells (Figs. 2-5H, 2-5I, and 2-5J), with 11 out of 12 (92%), 15 out of 20 (75%), and 19 out of 21 (90%) cells lacking clear Bir1-GFP, Pic1-GFP, and Ark1-GFP signals, respectively, at the centromeres. Additionally, during anaphase in *nbl1*-repressed cells, Bir1-GFP localized diffusely within the nucleoplasm instead of tightly on the spindle in 31 of 35 (89%) cells (Fig. 2-5H). In contrast, Pic1-GFP localized normally on the mitotic spindle and on the spindle midzone in 32 of 36 (89%) cells (Fig. 2-5I). We nonetheless observed unequal segregation following anaphase of both Bir1-GFP and Pic1-GFP (Figs. 2-5H and 2-5I). Due to the high background signal for Ark1-GFP, it was more difficult to ascertain the localization of Ark1-GFP in anaphase upon repression of *nbl1* expression. However, we observed separated SPBs in 52 out of 72 (72%) anaphase cells in the absence of any detectable Ark1-GFP signal on the spindle (Fig. 2-5J). This observation suggests that Ark1-GFP localization to the spindle and the midzone, similar to that of Bir1-GFP, was impaired by *nbl1* disruption.

Nbl1 sequence analysis reveals similarities to human Borealin

Given that Nbl1 associates with known CPC components and co-localizes with them in a dependent fashion, it seemed reasonable that Nbl1 might be a fourth subunit of the *S. pombe* CPC, related to Borealin. To pursue this possibility, we analyzed the

predicted secondary structure of Nbl1 using the Jpred3 server (Cole et al., 2008). The N-terminal region of Nbl1, from residues 14-85, is predicted to be highly α-helical (Fig. 2-6A). Additionally, Nbl1 exhibits coiled-coil oligomer potential from residues 22-56 of this helical region. Using BLAST to search for related proteins, we identified the helical region of Borealin as a sequence homolog. The central helical region of Nbl1, spanning residues 32-79, is 20% identical and 52% homologous to residues 25-72 of the Borealin N-terminus (Fig. 2-6B). We independently analyzed Nbl1 using the Phyre protein threading server to search for homologs with known structure (Bennett-Lovsey et al., 2008). The first match was the N-terminus of human Borealin, with an E-value of 0.35 and estimated precision of 85% [PDB=2RAX, (Bourhis et al., 2007)]. All other matches were unrelated helical proteins with significantly lower similarity (E-value >2.7, precision <55%).

The N-terminal region of Borealin encodes an extended helix, which interacts with both Survivin and INCENP to form a three-helix bundle (Fig. 2-6C) (Jeyaprakash et al., 2007). The Phyre-based model of Nbl1 (N29-H83) is consistent with core features of Borealin important for this interaction, containing both an extended coiled-coil followed by a helical region similar to the region of Borealin that binds to the dimerization arm of Survivin (Fig. 2-6C). Additionally, the specific residues conserved between Borealin and Nbl1 strongly cluster to those residues at the protein-protein interaction surface. 22 of the 25 conserved residues are predicted to be localized to the protein-protein interaction face of Nbl1 (Fig. 2-6D). The three residues positioned on the opposite helical face (E33, R44, R70) are charged residues. One of the strictly conserved residues is proline 69 (Figs. 2-6B and 2-6D). This proline serves to break the long helix of Borealin and

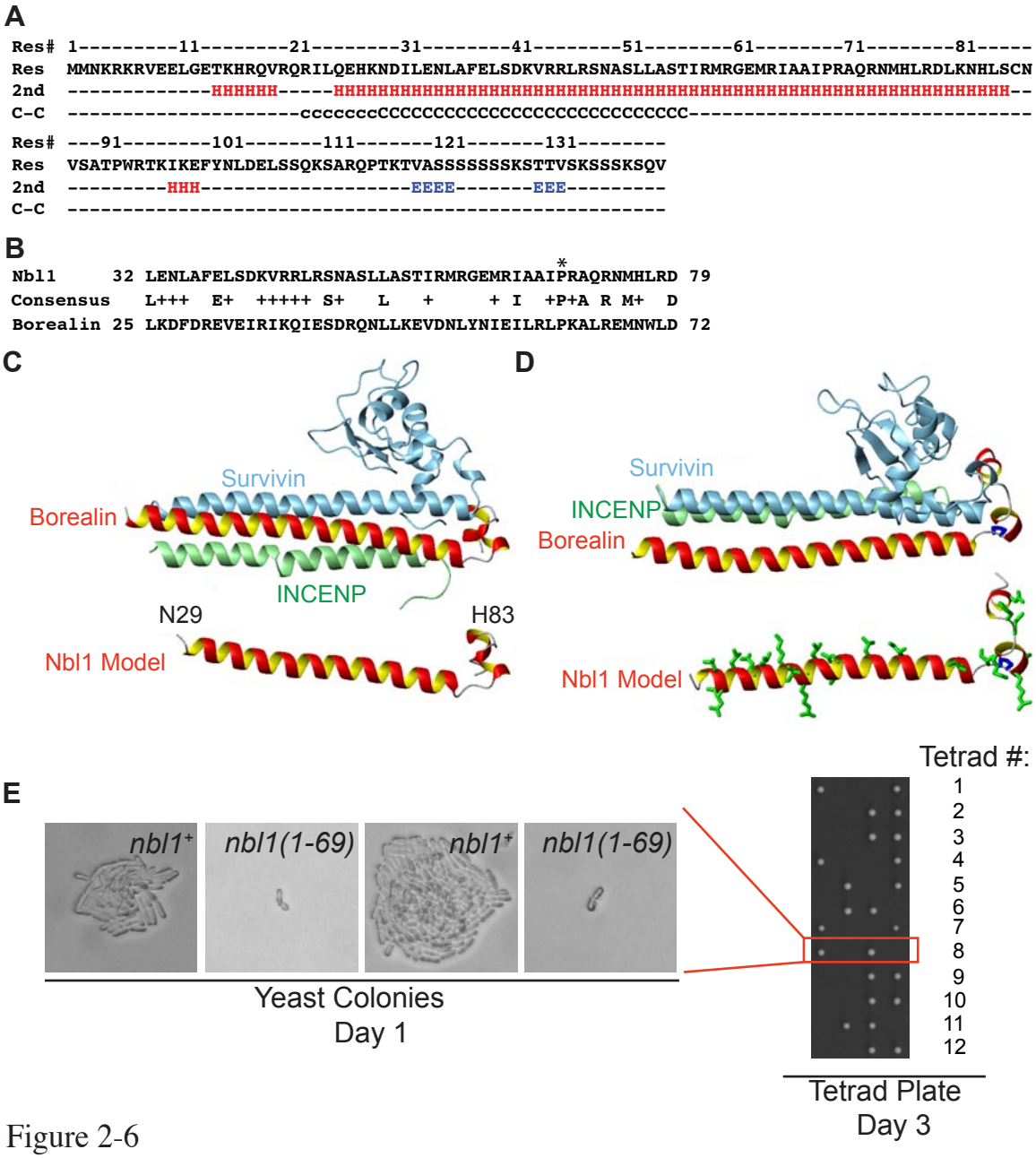

Figure 2-6

Nbl1 is similar to human Borealin.

(A) Secondary structure and coiled-coil predictions of Nbl1. H indicates α-helix, E indicates a β-strand, and C indicates a coiled-coil region. (B) Sequence alignment of the core region of Nbl1 and human Borealin. The conserved proline is indicated by an asterisk. (C) Comparison of the structure of Borealin in the trimeric complex of Survivin (blue), Borealin (red and yellow), and INCENP (green) (upper) with the model of Nbl1 (lower). (D) An alternate rotation of the structures viewing along the edge of the Borealin trimer interface. Conserved residues are mapped on the Nbl1 model in green sticks. The conserved proline in the dimerization arm of Borealin is represented in both Borealin and Nbl1 as blue sticks. (E) Diploids heterozygous for the *nbl1(1-69)* truncation were sporulated on glutamate plates, and tetrads were picked and allowed to germinate. Colony pictures (on the left) were taken after one day. A picture of the tetrad plate after three days is given on the right.

positions the helical segments which bind to the dimerization arm of Survivin (Fig. 2-6C). This interaction leads to the observed dimer to monomer transition of Survivin, which is important for Survivin function (Bourhis et al., 2007). Interestingly, although cells were viable when we truncated Nbl1 to its first 95 amino acids, truncation of Nbl1 after the conserved proline at residue 69 rendered cells inviable (Fig. 2-6E). Specifically, *nbl1(1-69)* cells cut in their first division (Fig. 2-6E). Thus, the additional short helical stretch following the conserved proline in Nbl1 appears to be likewise relevant for CPC function in *S. pombe*. Accordingly, Nbl1 and Borealin share a conserved N-terminal half that is both physically and functionally important. Together with the physical and functional associations of Nbl1 with the CPC, these similarities further support the identification of Nbl1 as the *S. pombe* Borealin homolog.

Clp1 and the CPC are also interdependent for proper localization

We next analyzed in more detail the association between CPC components and the Clp1/Cdc14 phosphatase, given that they had purified in our Clp1-TAP. Phosphatase-dead Clp1-C286S-GFP co-immunoprecipitated Nbl1(1-95)-FLAG during and following release from an *nda3-KM311* prometaphase arrest (Fig. 2-7A), suggesting that Clp1 and Nbl1 associate in both metaphase and anaphase. Consistent with this, Clp1-GFP and Nbl1(1-95)-mTomato co-localized to centromeres in metaphase and to the mitotic spindle and the spindle midzone in anaphase (Fig. 2-7B).

Because Clp1 reverses CDK-mediated phosphorylation events, we examined whether Nbl1 might be a CDK target that is regulated by its phosphorylation state. CDK can in fact phosphorylate Nbl1(1-95) *in vitro* (Fig. 2-8A), and T91 is the only S/T site

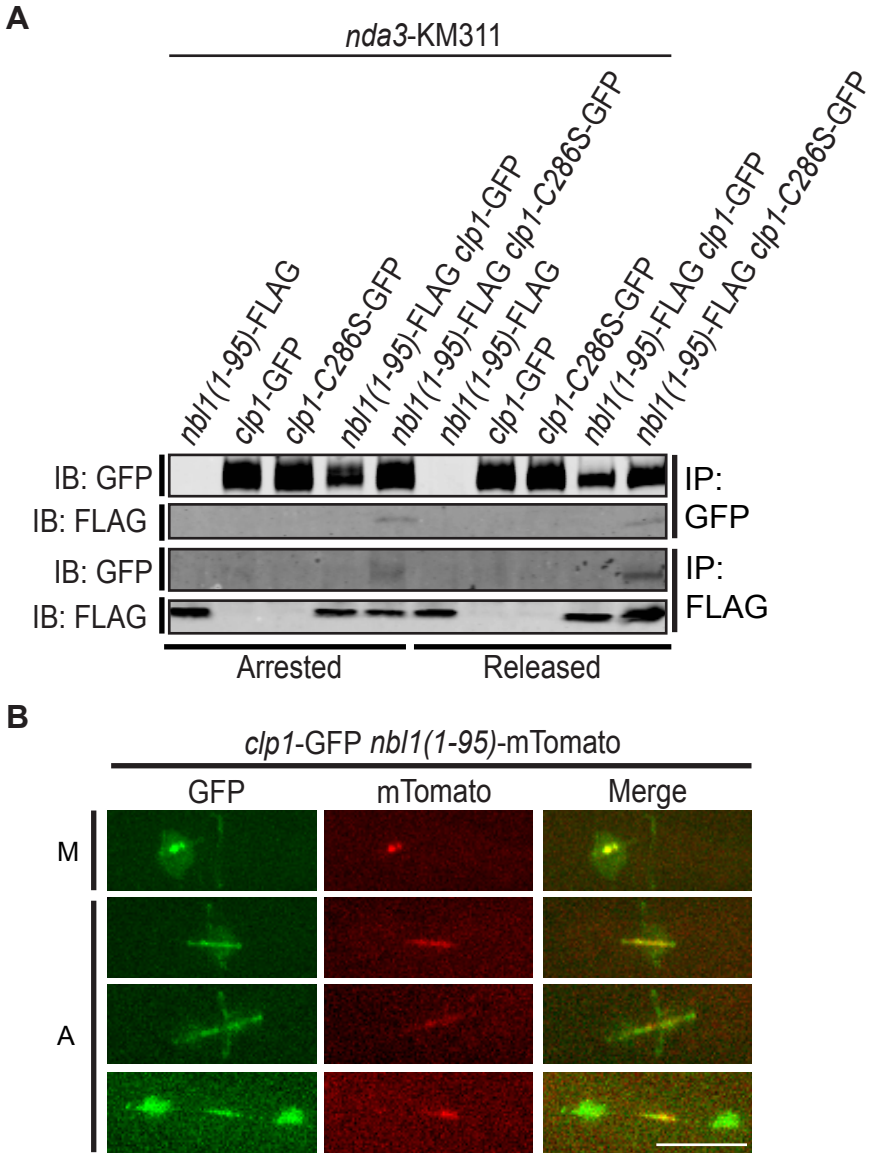

Figure 2-7

Nbl1 associates with Clp1.

(A) Indicated strains were lysed either during an *nda3*-KM311 prometaphase block or 30 min following release from this block. Anti-GFP and anti-FLAG immunoprecipitates were blotted with anti-GFP and anti-FLAG antibodies. (B) Live-cell GFP, mTomato, and GFP/mTomato merged images of *clp1*-GFP *nbl1(1-95)*-mTomato cells. M=metaphase, and A=anaphase. (Bar = 5 μm)

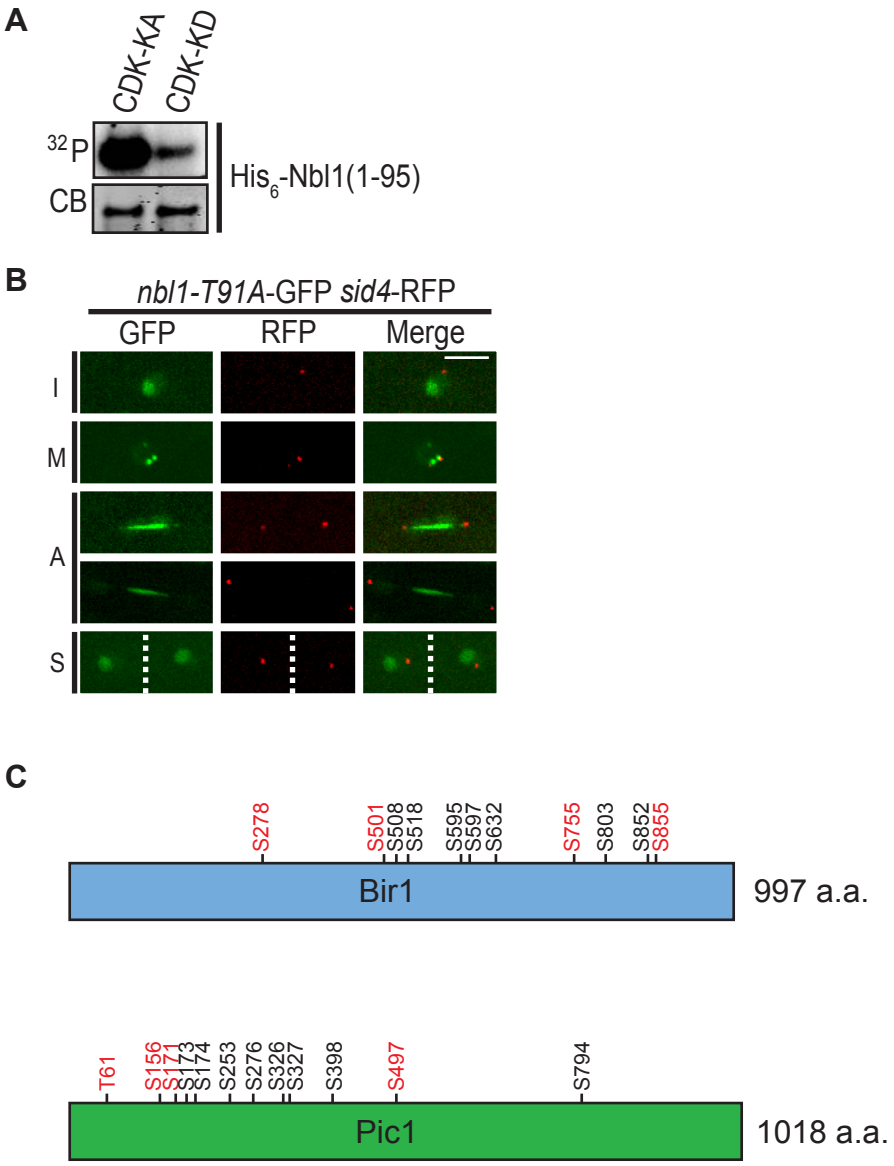

Figure 2-8

***S. pombe* CPC subunits are phosphoproteins.**
(A) Bacterially produced His_6-Nbl1(1-95) was incubated with kinase-active (KA) or kinase-dead (KD) CDK. Autoradiography and Coomassie blue (CB) staining of the reactions were performed. (B) Live-cell GFP, RFP, and GFP/RFP merged images of *nbl1-T91A*-GFP *sid4*-RFP cells. The dashed white line indicates the location of the septum. I=interphase, M=metaphase, A=anaphase, and S=septation. (C) Schematic of Bir1 and Pic1 phosphosites detected by mass spectrometry. Consensus CDK sites are in red. (Bar = 5 μm)

matching a CDK consensus within the protein. Replacing T91 with an alanine at the *nbl1* locus revealed that Nbl1 localization was unaffected by this mutation (Fig. 2-8B). Analysis of mass spectrometry data for Bir1 and Pic1 in the Clp1-TAPs indicated that these proteins are phosphorylated on many sites, and many of their phosphorylation sites match the CDK consensus (Fig. 2-8C). More recent data have demonstrated that CDK-mediated Bir1 phosphorylation is functionally most important in CPC-dependent chromosome biorientation (Tsukahara et al., 2010).

A previous report suggested that Clp1 is required for proper centromere targeting of Ark1 and Bir1 (Trautmann et al., 2004). We thus examined whether localization of Nbl1 is perturbed in *clp1Δ* cells. Centromere localization of Nbl1-GFP was intact in all 21 *clp1Δ* cells examined (Fig. 2-9A). Also, in contrast to the earlier report, we detected all other CPC proteins at centromeres in *clp1Δ* cells (n>=20) (Fig. 2-9A). Thus, we concluded that Clp1 does not affect CPC localization to centromeres. However, though Nbl1-GFP, like the rest of the CPC, initially localized to the mitotic spindle appropriately in *clp1Δ* cells (n>=20) (Fig. 2-9B), Nbl1-GFP did not localize to the midzone correctly in *clp1*Δ cells (Fig. 2-9C). Instead, it tailed off to one pole during anaphase (Fig. 2-9C). We noted that Nbl1-GFP mislocalized similarly in a strain with the phosphatase-dead *clp1-C286S* mutation (Fig. 2-9C), supporting the conclusion that Clp1 phosphatase activity is relevant to the midzone localization of the CPC.

Midzone localization of Ark1 in *S. pombe* has been linked previously to a requirement for Ase1, a microtubule-bundling protein that is necessary for midzone stability (Yamashita et al., 2005). In *clp1Δ* and *clp1-C286S* cells, Ase1-GFP also tailed off to one pole during anaphase (Fig. 2-9D). This suggests that the midzone itself was

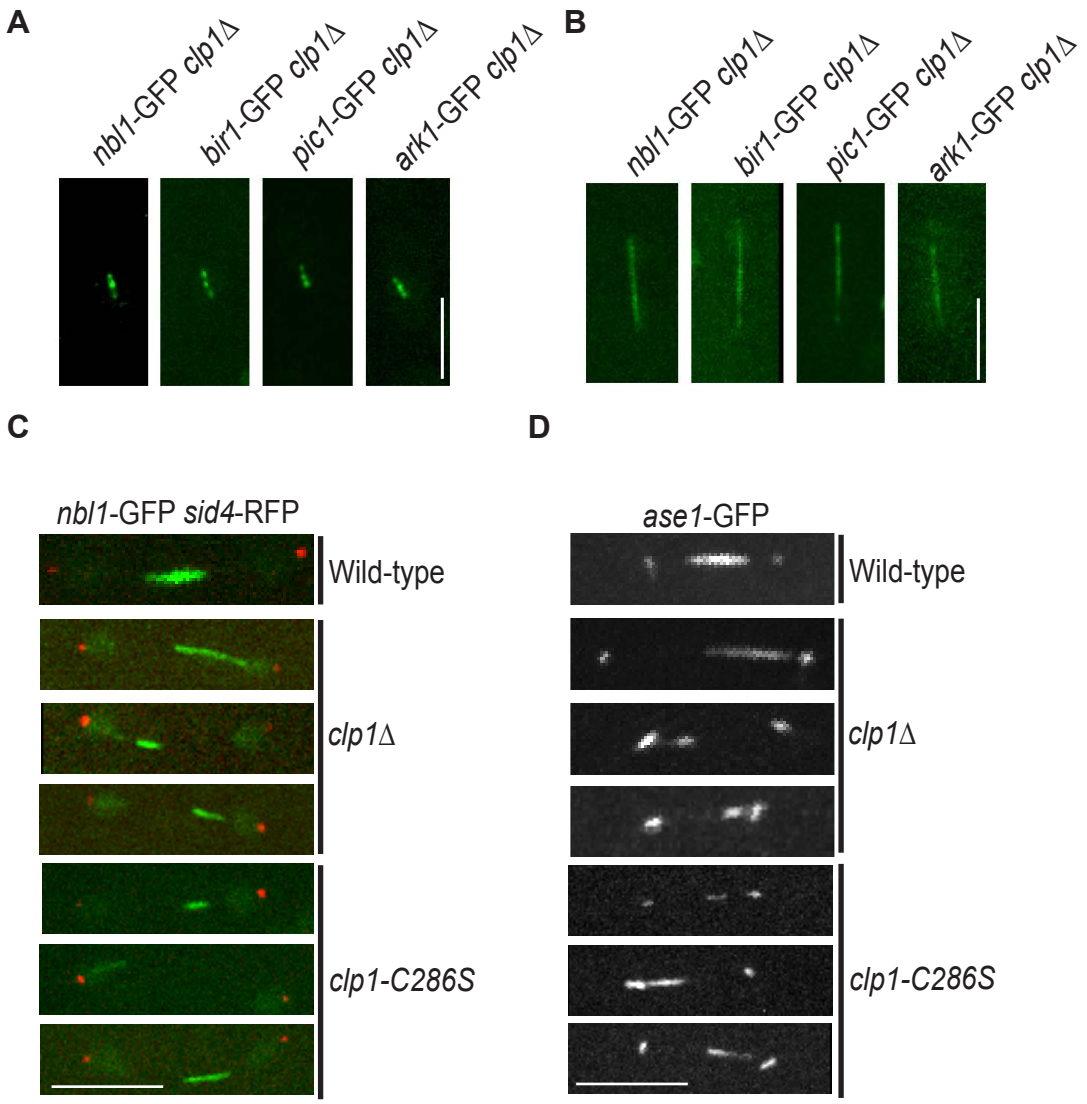

Figure 2-9

Clp1 only controls midzone targeting of the CPC.
(A) Live-cell GFP images of *nbl1*-GFP *clp1Δ*, *bir1*-GFP *clp1Δ*, *pic1*-GFP *clp1Δ*, and *ark1*-GFP *clp1Δ* cells in metaphase. (B) Live-cell GFP images of *nbl1*-GFP *clp1Δ*, *bir1*-GFP *clp1Δ*, *pic1*-GFP *clp1Δ*, and *ark1*-GFP *clp1Δ* cells in anaphase. (C) Live-cell GFP/RFP merged images of *nbl1*-GFP *sid4*-RFP, *nbl1*-GFP *sid4*-RFP *clp1Δ*, and *nbl1*-GFP *sid4*-RFP *clp1-C286S* cells. (D) Live-cell GFP/RFP merged images of *ase1*-GFP *sid4*-RFP, *ase1*-GFP *sid4*-RFP *clp1Δ*, and *ase1*-GFP *sid4*-RFP *clp1-C286S* cells. Ase1 localizes to SPBs in addition to the spindle midzone, and thus the two most outlying dots in each image are indicative of SPB localization. (Bars = 5 μm)

improperly formed in *clp1Δ* and *clp1-C286S* strains. Thus, mis-localization of Nbl1 and other CPC components in *clp1Δ* and *clp1-C286S* strains appears to be due to faulty midzone formation in the absence of Clp1 phosphatase activity, an idea that has since been validated by others (Fu et al., 2009).

We next tested whether disruption of *nbl1* affects Clp1 localization by monitoring Clp1-GFP and Sid4-RFP after repression of *nbl1* expression. In anaphase of wild-type cells, Clp1-GFP localizes to both the spindle and the CR (Cueille et al., 2001). However, in *nbl1*-shutoff cells, Clp1-GFP localized to the spindle but not the CR during anaphase in 23 out of 33 (70%) cells (Fig. 2-10A). In addition, Clp1-GFP often accumulated between separated SPBs in an unsegregated mass (Fig. 2-10A), consistent with the chromosome segregation defects seen in *nbl1*-disrupted cells. We then examined Clp1-GFP and Sid4-RFP in the CPC temperature strains *cut17-275*, *pic1-T269*, and *ark1-T7*. Though some *cut17-275, pic1-T269*, and *ark1-T7* cells showed localization of Clp1-GFP to the CR in early anaphase at the restrictive temperature (panel I of Figs. 2-10B, 2-10C, and 2-10D), most anaphase *cut17*-275 (27 of 35, 77%), *pic1*-T269 (24 of 31, 67%), and *ark1*-T7 (36 of 42, 86%) cells lacked any detectable Clp1-GFP signal at the CR (panels II-IV of Figs. 2-10B, 2-10C, and 2-10D). Instead, Clp1-GFP solely localized to the mitotic spindle and to an unsegregated mass between SPBs in these cells (panels II-IV of Figs. 2-10B, 2-10C, and 2-10D). Thus, Clp1-GFP accumulation at the CR was abnormal in all CPC mutations tested.

To study the defects of Clp1 localization in more detail, Clp1-GFP and Sid4-RFP were imaged by time-lapse microscopy in the *ark1-T7* strain. As suggested by the still images, Clp1-GFP never accumulated properly on the CR during anaphase. In some

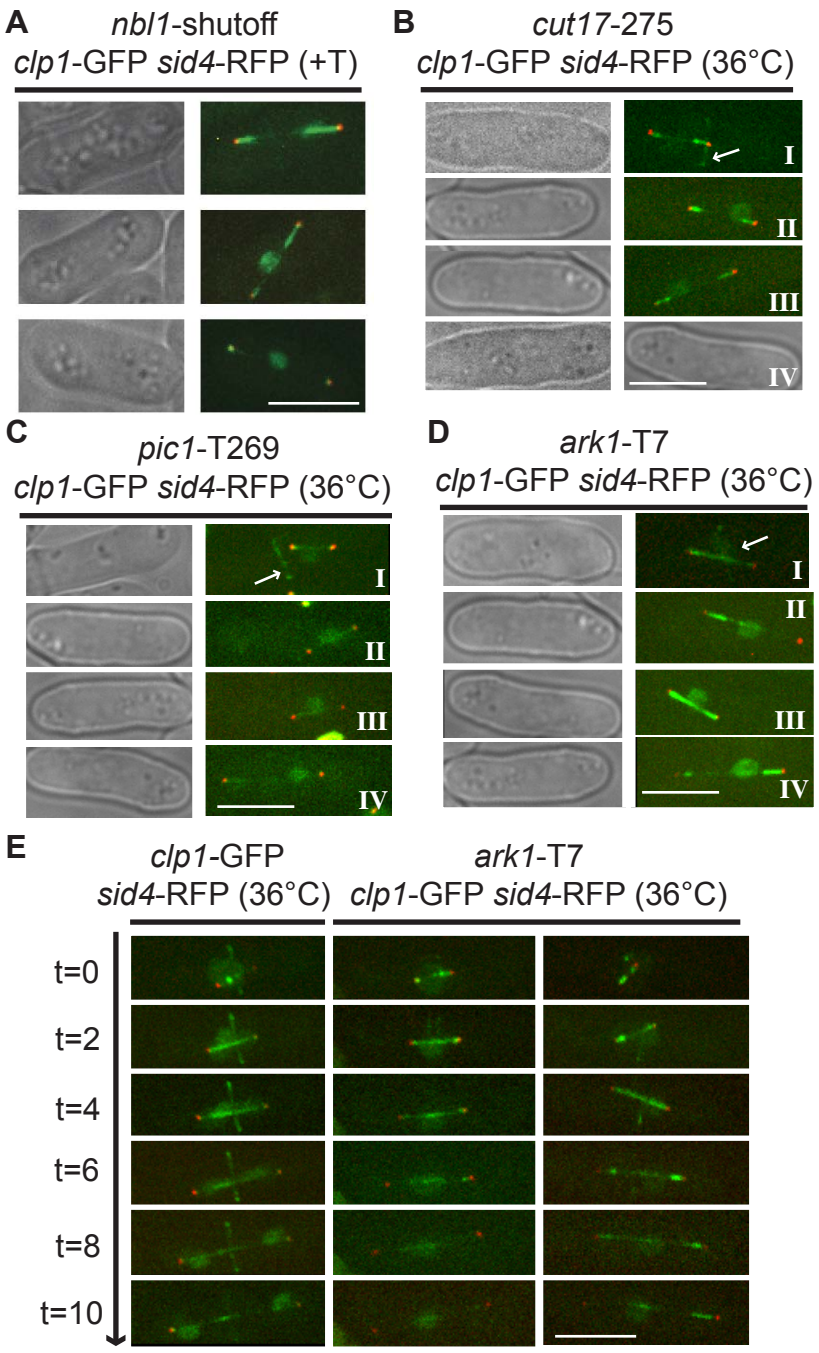

Figure 2-10

The CPC regulates accumulation of Clp1 at the CR.
(A) Live-cell bright field (BF) and GFP/RFP merged images of *nbl1*-shutoff *clp1*-GFP *sid4*-RFP cells after 10 h of *nbl1* repression with thiamine (+T). (B-D) Live-cell BF and GFP/RFP merged images of *cut17*-275 *clp1*-GFP *sid4*-RFP, *pic1*-T269 *clp1*-GFP *sid4*-RFP, and *ark1*-T7 *clp1*-GFP *sid4*-RFP cells progressing through mitosis after G2 synchronization and shift to 36°C. Clp1 localization at the CR is indicated by white arrows. (E) Time-lapse GFP/RFP merged images of *ark1*-T7 *clp1*-GFP *sid4*-RFP and *clp1*-GFP *sid4*-RFP cells progressing through mitosis after G2 synchronization and shift to 36°C. Initial images were taken at the metaphase-to-anaphase transition, and subsequent images were taken every two minutes. (Bars = 5 μm)

cases, Clp1 failed to localize to any degree on the CR (middle column of Fig. 2-10E). In other cases, we detected faint CR localization of Clp1-GFP, but this signal dissipated prematurely and never reached its normal intensity (right column of Fig. 2-10E). These observations are in striking contrast to what was seen in wild-type *clp1*-GFP *sid4*-RFP cells, in which Clp1-GFP localized strongly to the CR initially in metaphase and continued on the CR through anaphase (left column of Fig. 2-10E). Accordingly, disruption of CPC function severely affected Clp1 accumulation at the CR.

The CPC genetically interacts with the *S. pombe* cytokinetic apparatus

Clp1 accumulation at the CR is required for the fidelity of cytokinesis (Chen et al., 2008; Clifford et al., 2008; Trautmann and McCollum, 2005). Furthermore, temperature-sensitive alleles of CR components exhibit a strong genetic interaction with *mid1Δ431-481*, which encodes a Mid1 mutant that lacks the region necessary to recruit Clp1 to the CR (Clifford et al., 2008). Therefore, given the relevance of the CPC to Clp1 accumulation at the CR, we used a genetic approach to examine whether previously unrecognized connections between the *S. pombe* CPC and the cytokinetic apparatus exist. Interestingly, we observed negative genetic interactions (Fig. 2-11A) between *ark1*-T7 and temperature-sensitive alleles of the following genes: *cdc12*, which encodes a critical cytokinetic formin (Kovar et al., 2003; Pelham and Chang, 2002); *rng2*, which encodes an IQGAP-related protein required for CR formation (Eng et al., 1998); and *sid2*, which encodes a kinase that functions in septation initiation (Balasubramanian et al., 1998). The observed negative genetic interactions between *ark1*-T7 and CR mutant alleles specifically correlated with an exacerbation of cytokinesis and septation defects, because

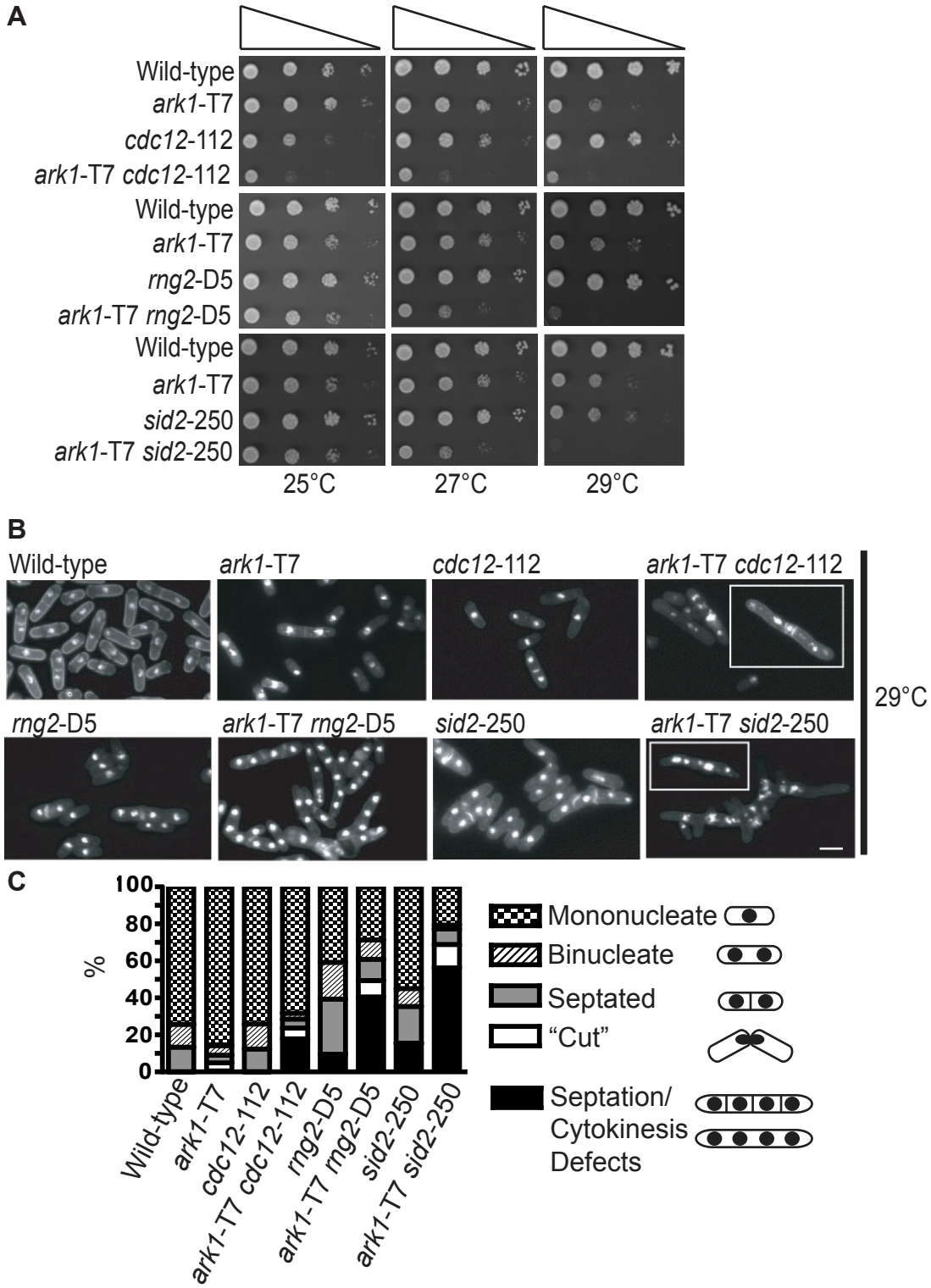

Figure 2-11

***ark1*-T7 exhibits negative genetic interactions with mutant CR alleles.**
(A) Serial 10-fold dilutions of cells of the indicated genotypes. (B) Fixed-cell images of DAPI- and methyl blue-stained cells. (C) Quantification of (B), with n>300 per genotype. (Bar = 5 μm)

double mutants showed a greater proportion of defective cells than either of the relevant single mutants (Figs. 2-11B and 2-11C). In addition, we noted that two temperature-sensitive alleles of *bir1*, *cut17*-275 and *bir1*-T1, also showed a negative genetic interaction with *cdc12*-112 (Figs. 2-12A and 2-12B) and that the relevant double mutants likewise exhibited an increased instance of cytokinesis and septation defects (Figs. 2-12C and 2-12D). We did not, however, detect genetic interactions between CPC temperature-sensitive alleles and the *mid1Δ431-481* mutant allele (Fig. 2-13), consistent with primary role of the CPC in cytokinesis being to mediate Clp1 accumulation at the CR.

We next examined whether *ark1*-T7 cells are sensitive to latrunculin A (Lat A), a drug which inhibits actin polymerization (Ayscough et al., 1997). Though high-dose Lat A treatment (>10μM) results in a complete loss of F-actin structures in wild-type cells (Pelham and Chang, 2001), low-dose Lat A treatment (0.2 μM) is not lethal (Mishra et al., 2004). However, low-dose Lat A treatment mildly perturbs the cytokinetic machinery, and cells defective in cytokinesis, such as those lacking *clp1*, are sensitive to these low-doses (Figs. 2-14A, 2-14B, and 2-14C) (Mishra et al., 2004). Though growth of *ark1*-T7 on control and low-dose Lat A-containing plates was similar at 25ºC, growth of *ark1*-T7 was slightly impaired at 27ºC and considerably impaired at 29ºC on low-dose Lat A-containing plates (Fig. 2-14A). Consistent with this observation, *ark1*-T7 cells showed significant cytokinesis and septation defects in the presence of low-dose Lat A in liquid culture (Figs. 2-14B and 2-14C). Therefore, *ark1*-T7 cells are sensitive to mild inhibition of actin polymerization at semi-permissive temperature. These data support the notion that the fission yeast CPC promotes the process of cytokinesis.

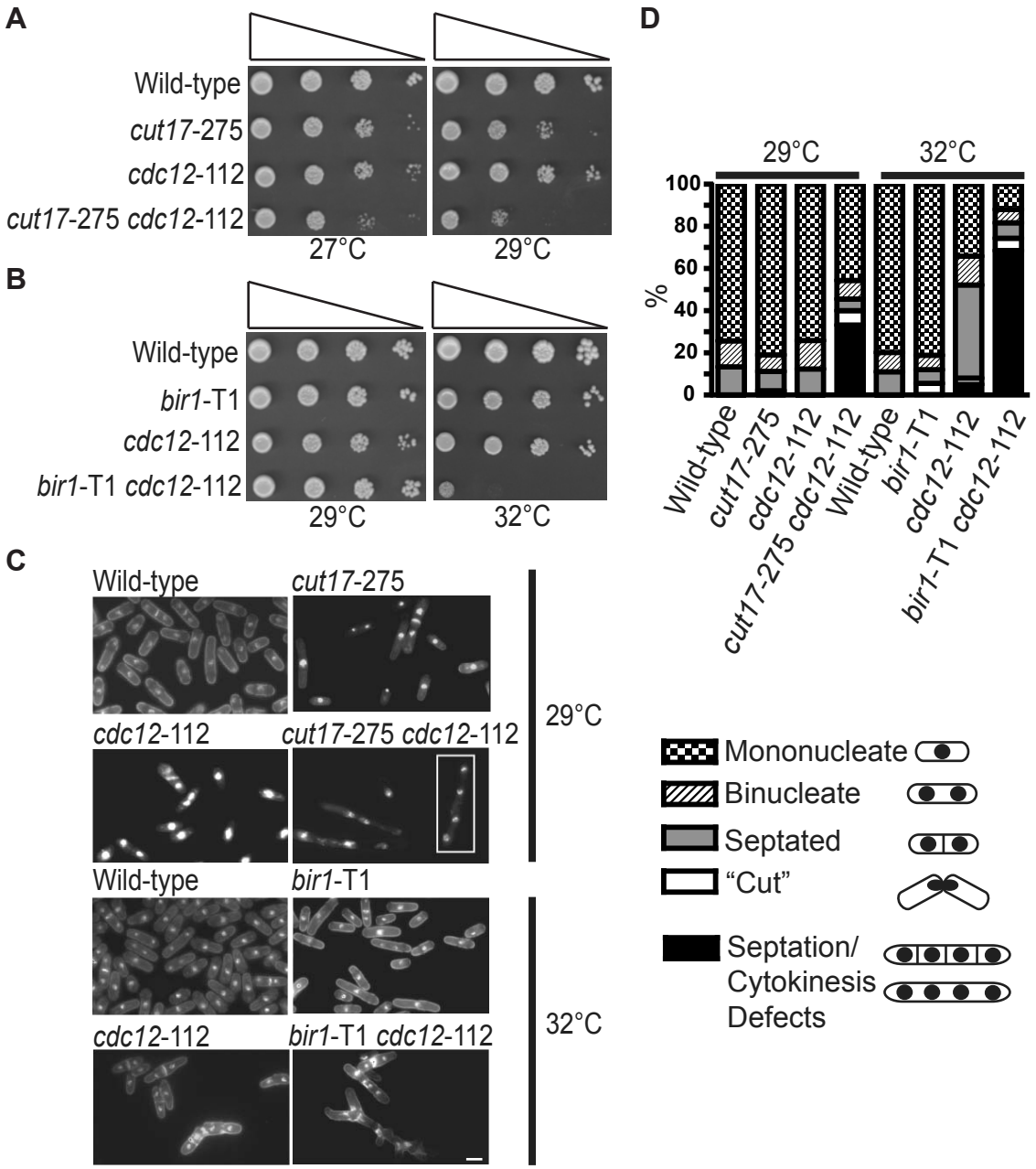

Figure 2-12

Additional negative genetic interactions between CPC and CR mutant alleles.
(A and B) Serial 10-fold dilutions of cells of the indicated genotypes. (C) Fixed-cell images of DAPI- and methyl blue-stained cells. (D) Quantification of (C), with n>300 per genotype. (Bar = 5 μm)

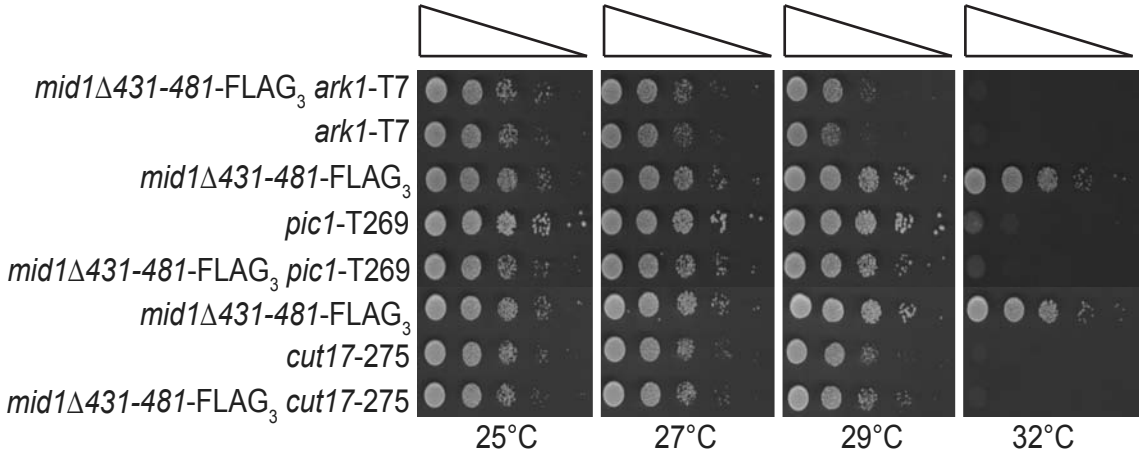

Figure 2-13

Mutant CPC alleles do not interact genetically with *mid1Δ431-481*.
Serial 10-fold dilutions of cells of the indicated genotypes.

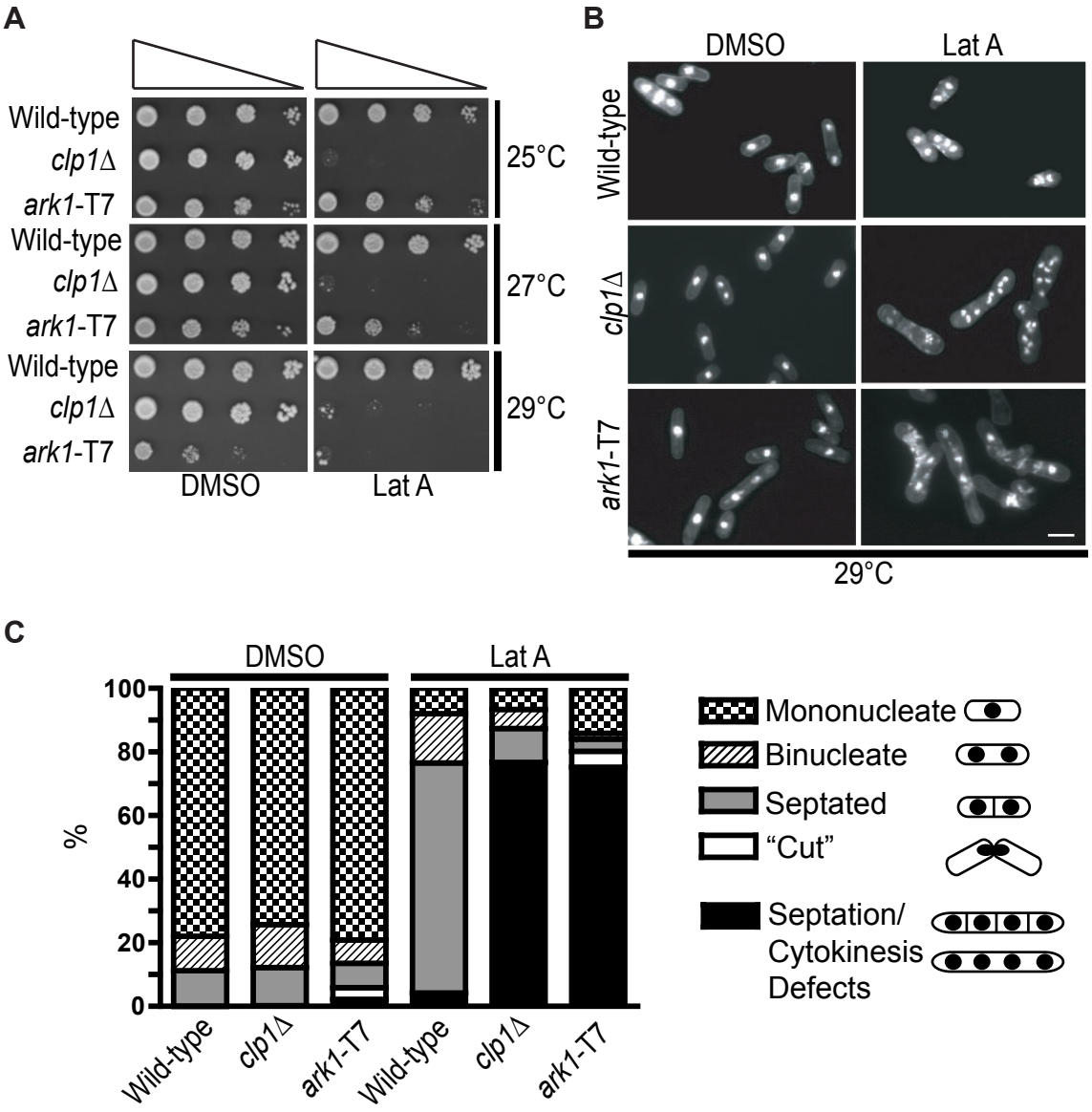

Figure 2-14

***ark1*-T7 cells are sensitive to low-dose Lat A.**

(A) Serial 10-fold dilutions of cells of the indicated genotypes. Cells were spotted on YE plates containing DMSO alone (control) or DMSO plus low-dose Lat A. (B) Fixed-cell images of DAPI- and methyl blue-stained cells, which had been treated with DMSO alone (control) or with DMSO plus low-dose Lat A. (C) Quantification of (B), with n>300 per genotype. (Bar = 5 μm)

Discussion

Similar to their orthologs in other organisms (Ruchaud et al., 2007; Vader et al., 2006; Vagnarelli and Earnshaw, 2004), the *S. pombe* proteins Ark1, Pic1, and Bir1 function within a chromosomal passenger complex that regulates critical mitotic events such as chromosome segregation and spindle elongation (Huang et al., 2005; Leverson et al., 2002; Morishita et al., 2001; Petersen et al., 2001; Rajagopalan and Balasubramanian, 2002; Widlund et al., 2006). However, whether these three proteins operate alone in this complex had been unclear, for a Borealin homolog had not been previously described in *S. pombe*. Here, we characterize Nbl1 as an *S. pombe* Borealin-like protein based on its association with known CPC components, its co-localization with other CPC subunits during mitosis, and its sequence and proposed structural similarity to human Borealin. Consistent with previous data directly linking Borealin to Aurora B activation (Jelluma et al., 2008), we additionally demonstrate that Nbl1 is required for Ark1 activity. Furthermore, we show that the *S. pombe* CPC influences the process of cytokinesis, at least partially by controlling the localization of *S. pombe* Cdc14-family phosphatase Clp1.

Conservation and structure-function relationship of Borealin

Identification of Borealin homologs in yeasts has previously been hampered by the fact that they do not possess open reading frames with significant primary sequence identity to human Borealin. Even the Nbl1(1-95) sequence, which was sufficient to rescue disruption of *nbl1* and to support proper localization and associations of the CPC during mitosis, possesses only a few residues which are identical to residues at the same

positions in Borealin. As we finished this study, another manuscript was published describing a budding yeast Borealin homolog (Nakajima et al., 2009). In this paper, the authors also identified putative Borealin homologs in almost 200 species through Hidden Markov Model-based searches. One of the putative homologs which they noted in this analysis (Nakajima et al., 2009) is the *S. pombe* protein described in our study. Thus, our work supports their findings and confirms that Nbl1 is in fact an *S. pombe* Borealin homolog.

We fortuitously discovered that a truncation of Nbl1 lacking the last 46 amino acids localizes correctly, interacts with other CPC components, and does not exhibit genetic interactions consistent with a loss of function. Though a recent study suggested that full-length Borealin is required for the formation of a competent Borealin-Survivin complex which can bind INCENP (Zhou et al., 2009), it has been posited that Borealin-like proteins in lower eukaryotes retain only structures involved in formation of the critical three-helix bundle of Borealin-Survivin-INCENP homologs (Nakajima et al., 2009). Proper function of Nbl1(1-95) supports this hypothesis since it maintains the core three-helix bundle region. Nbl1(1-95) also retains a second helical stretch that follows a conserved proline. Given that this helical stretch is additionally necessary for viability, this region represents another critical structural domain. It will be interesting to analyze whether this region, similar to the helical stretch following the conserved kink in human Borealin (Bourhis et al., 2007), blocks homodimerization of the Survivin homolog.

Interdependencies of Borealin-CPC localizations

A significant question in the CPC field concerns how CPC localization is regulated by its different subunits. In human cells, CPC proteins are strikingly interdependent, with knockdown or disruption of any of the CPC subunits impeding proper localization of the others (Gassmann et al., 2004; Honda et al., 2003). While mutation of Bir1 has been found to impede localization of Ark1 and Pic1 (Huang et al., 2005; Morishita et al., 2001; Rajagopalan and Balasubramanian, 2002), a comprehensive dissection of CPC interdependency in localization has been lacking in *S. pombe*. Here, we undertook a thorough analysis of Nbl1-CPC interdependency and noted additional associations relevant to CPC localization. An intriguing possibility suggested by our data is that Nbl1 contributes to centromeric targeting of the CPC. We found that Nbl1 localization to centromeres is independent of Bir1, Pic1, and Ark1, whereas centromere localization of Bir1, Pic1, and Ark1 requires Nbl1. Intriguingly, human Borealin binds DNA (Klein et al., 2006), and its interactions with the centromeric adaptor Shugoshin enhance CPC centromere targeting (Tsukahara et al., 2010). It will thus be intriguing to address a possible conserved function for Borealin homologs in CPC targeting to the centromere.

CPC phosphoregulation by CDK and Cdc14-family phosphatases

Our data furthermore highlight that Clp1, similar to Cdc14 in *S. cerevisiae* (Pereira and Schiebel, 2003; Stoepel et al., 2005), is a *bona fide* CPC-interacting protein. Ark1 has previously been shown to associate with Clp1 during mitosis (Trautmann et al., 2004), and we additionally identified Bir1, Pic1, and Nbl1 in our Clp1-C286S-TAP complexes. The fact that Clp1 and the CPC co-localize during mitosis furthermore

confirms their close association. An obvious question stemming from these observations is whether *S. pombe* CPC proteins are directly regulated by their phosphorylation state. While an in-depth analysis of CPC phosphoregulation in *S. pombe* was beyond the scope of this study, others have since found that CDK-mediated Survivin phosphorylation impacts CPC-Shugoshin interactions in multiple species, thereby affecting CPC centromere targeting and chromosome biorientation (Tsukahara et al., 2010).

On a related note, it is currently unclear whether dephosphorylation of *S. pombe* CPC proteins by Clp1 occurs and, if so, whether this is important for CPC function. The fact that Nbl1, Bir1, and Pic1 co-purified with the substrate-trapping Clp1-C286S mutant suggests, however, that at least one of the three is a direct target of Clp1. This possibility is supported by a previous report indicating that Clp1 phosphatase activity is required for Clp1 to affect chromosome segregation through the CPC (Trautmann et al., 2004). While this issue is unresolved, a few points regarding CPC localization in *clp1*Δ cells deserve noting. Though it was suggested that deletion of *clp1* affects localization of CPC subunits to centromeres (Trautmann et al., 2004), our data indicate that the CPC localizes normally to centromeres in the absence of Clp1. Also, unlike Cdc14 (Pereira and Schiebel, 2003), Clp1 is not required for the initial spindle recruitment of any CPC component in *S. pombe*. Therefore, it is most likely that if Clp1 affects the CPC directly, it would influence its localization dynamics or its specific activity. Although Nbl1 localization to the midzone is disrupted in both *clp1*Δ and *clp1-C286S* cells, we have found that the midzone itself is disrupted in the absence of Clp1 activity. In *S. cerevisiae*, Cdc14 controls midzone formation via de-phosphorylation of Ase1 (Khmelinskii et al.,

2007). Our data support a more recent study (Fu et al., 2009) indicating that Clp1-Ase1 interactions similarly control midzone assembly in *S. pombe*.

CPC-mediated control of Cdc14-family phosphatases and cytokinesis

It had not been examined previously whether the CPC in any organism affects Cdc14 family function. We found, unexpectedly, that Clp1 accumulation at the CR was defective in all tested CPC mutations. Clp1 contributes to CR stability and the fidelity of cytokinesis (Chen et al., 2008; Clifford et al., 2008; Trautmann and McCollum, 2005). Yet, because Clp1 is non-essential in *S. pombe*, its loss at the CR perturbs, but does not normally prevent, cytokinesis. Consistent with the CPC affecting this aspect of cytokinesis integrity, *ark1*-T7 cells are sensitive to low-dose Lat A treatment and temperature-sensitive alleles of genes encoding CPC and CR components display negative genetic interactions. Therefore, although Ark1 is not essential for *S. pombe* cytokinesis (Petersen and Hagan, 2003), our data indicate that Ark1 does play a role in this process.

The CPC has similarly been implicated in *S. cerevisiae* cytokinesis. In *S. cerevisiae*, distinct passenger complexes control septin organization in anaphase (Gillis et al., 2005; Thomas and Kaplan, 2007), and the Aurora B homolog mediates a NoCut cytokinesis checkpoint by recruiting abscission inhibitors when DNA fails to segregate out of the cleavage plane (Mendoza et al., 2009; Norden et al., 2006). Though the extent of the *S. pombe* CPC's contribution to cytokinesis is currently unclear, it is unlikely to monitor DNA remaining in the division plane. Cut mutations resulting from inhibition of a variety of mitotic factors are readily obtained in *S. pombe* (Yanagida, 1998), indicating

that there is no robust mechanism in this organism to delay or prevent cytokinesis when chromosomes remain in the division plane. Furthermore, the genetic interactions we have uncovered indicate that the CPC promotes, rather than inhibits, cytokinesis in *S. pombe*. In future studies, it will be important to determine whether the sole function of the CPC in *S. pombe* cytokinesis involves regulating Clp1 localization.

CHAPTER III

SIN-DEPENDENT PHOSPHOINHIBITION OF FORMIN MULTIMERIZATION CONTROLS FISSION YEAST CYTOKINESIS

Introduction

Many eukaryotes accomplish cell division by building and constricting a medial actomyosin-based CR. In *S. pombe*, a Hippo-related signaling pathway known as the SIN controls CR formation, maintenance, and constriction. However, how the SIN regulates integral CR components was unknown. Here, we identify the essential cytokinetic formin Cdc12 as the primary CR substrate of SIN kinase Sid2. Eliminating Sid2-mediated Cdc12 phosphorylation leads to persistent Cdc12 clustering, which prevents CR assembly in the absence of anillin-like Mid1 and causes CRs to collapse when cytokinesis is delayed. Molecularly, Sid2 phosphorylation of Cdc12 abrogates multimerization of a previously unrecognized Cdc12 domain that confers F-actin bundling activity. Taken together, our findings identify a SIN-triggered oligomeric switch that modulates cytokinetic formin function, revealing a novel mechanism of actin cytoskeleton regulation during cell division.

Results

The SIN kinase Sid2 phosphorylates cytokinetic formin Cdc12

To assess potential cell cycle regulation of formin Cdc12, we analyzed the SDS-PAGE mobility of Cdc12-HA_3 through the cell cycle. Intriguingly, Cdc12-HA_3 migrated

more slowly during nuclear division just prior to septation (Fig. 3-1A). Lambda phosphatase treatment of Cdc12-HA_3 immunoprecipitates from selected samples indicated that gel mobility shifts were due to phosphorylation, and that Cdc12-HA_3 was hyperphosphorylated immediately before septation (Fig. 3-1B). Similar gel mobility patterns were observed for Cdc12 tagged with a different epitope ($V5_3$) and released from an S phase arrest (Fig. 3-1C). Lambda phosphatase treatment of Cdc12-$V5_3$ immunoprecipitates from cytokinesis-arrested cells, which block after CR formation due to impaired septum deposition (Le Goff et al., 1999; Liu et al., 2000), or from G1-arrested cells confirmed that Cdc12 phosphorylation peaks during cell division (Fig. 3-1D).

Given this phosphorylation pattern, we asked whether the SIN, whose activity increases during mitosis and is maintained during a cytokinesis arrest (Liu et al., 1999; Sparks et al., 1999), directly targets Cdc12. We found that SIN induction, achieved via inactivation of the inhibitory GAP Cdc16 (Krapp and Simanis, 2008; Minet et al., 1979), resulted in Cdc12-$V5_3$ hyperphosphorylation (Fig. 3-2A). Moreover, the SIN kinase Sid2, which localizes to SPBs and the CR during a *cps1*-191 cytokinesis arrest (Fig. 3-2B), directly phosphorylated MBP-tagged Cdc12 fragments *in vitro* (Figs. 3-2C and 3-2D). In accord with Sid2 family kinases targeting RxxS motifs (Mah et al., 2005), Sid2 phosphorylated exclusively serines on Cdc12 fragments (Fig. 3-2E). Alanine mutation of Sid2-consensus serines identified residues S824, S1523, S1543, and S1811 as the major Sid2-targeted residues (Figs. 3-3A, 3-3B, and 3-3C). All four of these sites reside outside of well-characterized formin domains (Fig. 3-3A). Cells were viable when wild-type *cdc12*$^+$ was replaced with *cdc12-4A*, in which the four Sid2-targeted serines are mutated

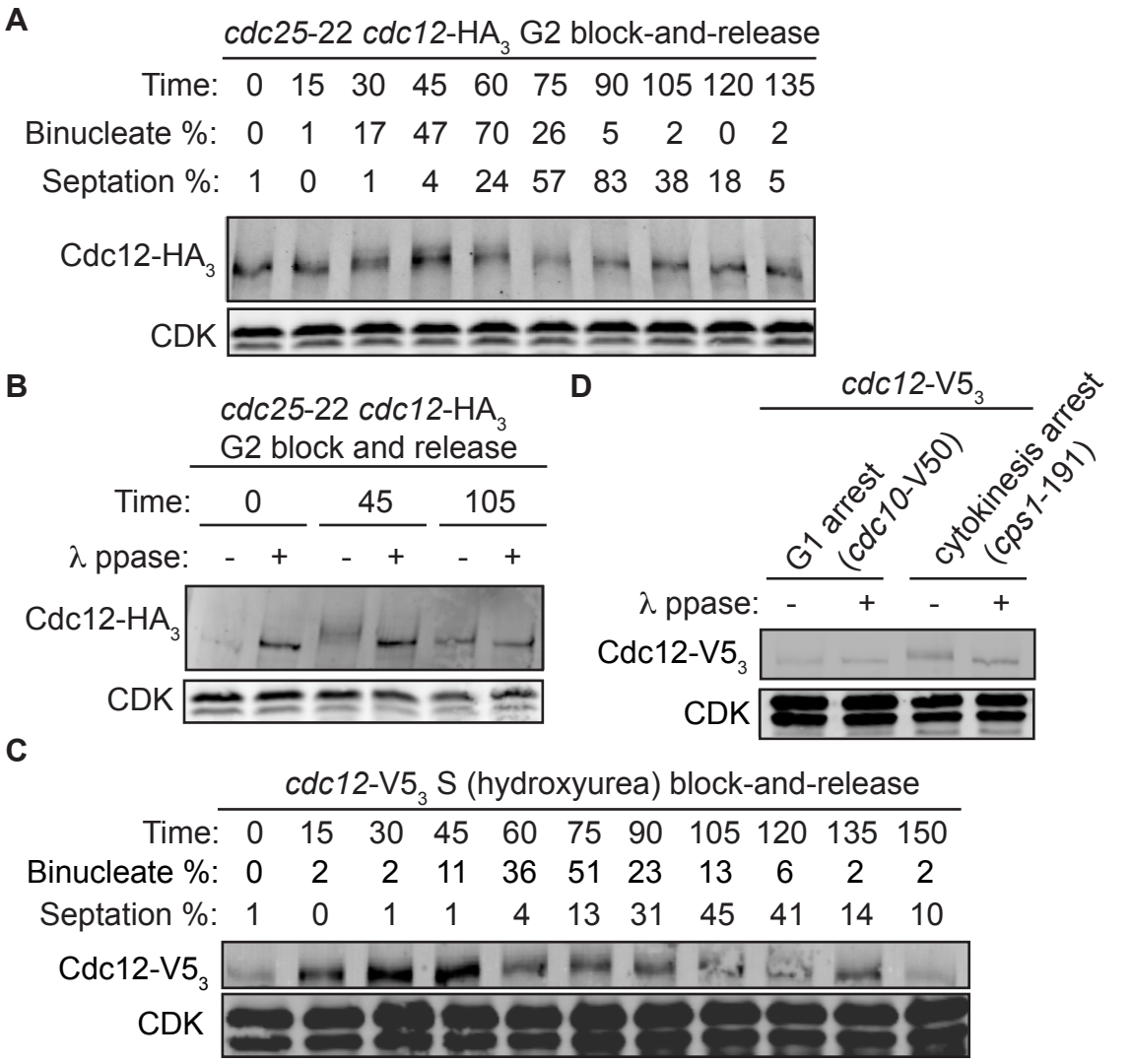

Figure 3-1

Formin Cdc12 is hyperphosphorylated during cytokinesis.
(A) Block-and-release of *cdc25*-22 *cdc12*-HA_3 cells. At the indicated time points, cell cycle progression was monitored by binucleate and septation percentages. Denatured cell lysates from the different time points were probed with an anti-HA antibody, and immunoprecipitates were resolved by SDS-PAGE and immunoblotted. CDK is a loading control. (B) For the *cdc25*-22 *cdc12*-HA_3 block-and-release experiment, denatured cell lysates were prepared for samples of the indicated time points and probed with an anti-HA antibody. Immunoprecipitates were subjected to either phosphatase treatment or a buffer control before being resolved by SDS-PAGE and immunoblotted. CDK is a loading control. (C) Block-and-release of *cdc12*-$V5_3$ cells from a hydroxyurea-induced S phase arrest. At the indicated time points, cell cycle progression was monitored by binucleate and septation percentages. Denatured cell lysates from the different time points were probed with an anti-V5 antibody, and immunoprecipitates were resolved by SDS-PAGE and immunoblotted. CDK is a loading control. (D) Denatured cell lysates of *cdc10*-V50 *cdc12*-$V5_3$ or *cps1*-191 *cdc12*-$V5_3$ cells arrested at the indicated stages were probed with an anti-V5 antibody. Immunoprecipitates were subjected to either phosphatase treatment or a buffer control before being resolved by SDS-PAGE and immunoblotted. CDK is a loading control.

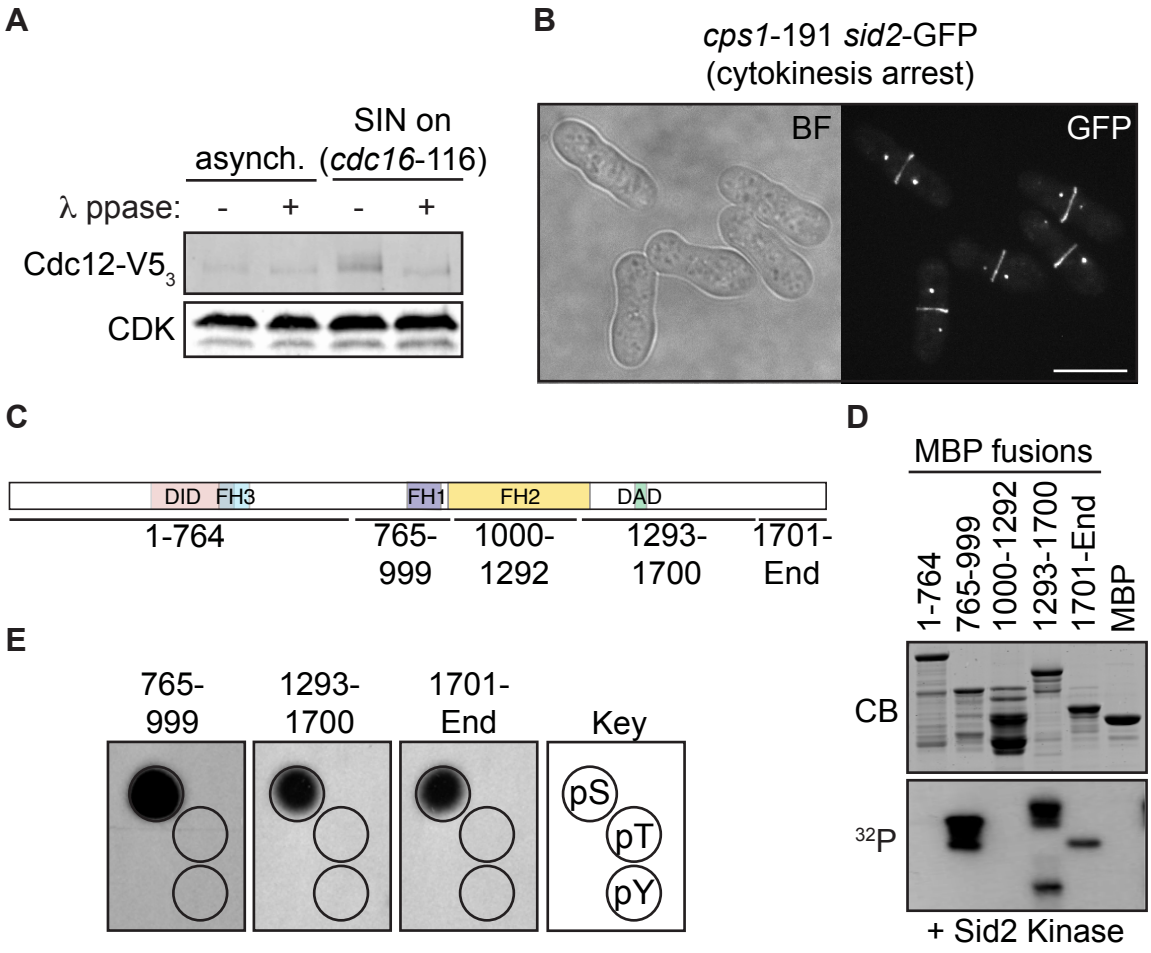

Figure 3-2

The SIN kinase Sid2 phosphorylates formin Cdc12.
(A) Denatured cell lysates of asynchronous *cdc12*-V5$_3$ or SIN-activated *cdc16*-116 *cdc12*-V5$_3$ cells were probed with an anti-V5 antibody. Immunoprecipitates were subjected to either phosphatase treatment or a buffer control before being resolved by SDS-PAGE and immunoblotted. CDK is a loading control. (B) Live-cell bright field (BF) and GFP images of *cps1*-191 *sid2*-GFP cells arrested in cytokinesis. (C) Schematic of Cdc12, with recombinant fragments used in *in vitro* kinase assays illustrated. (D) *In vitro* kinase assay using Sid2-Myc$_{13}$ immunoprecipitated from *cdc16*-116 *sid2*-Myc$_{13}$ cells and various recombinant MBP-Cdc12 fragments illustrated in (C). Proteins labeled by γ–^{32}P were detected by autoradiography, and the protein gel was stained with Coomassie blue (CB). (E) Phosphoamino acid analysis of MBP-Cdc12 fragments phosphorylated by Sid2-Myc$_{13}$. The positions of phospho-serine, phospho-threonine, and phospho-tyrosine standards are indicated in the key. (Bar = 5 μM)

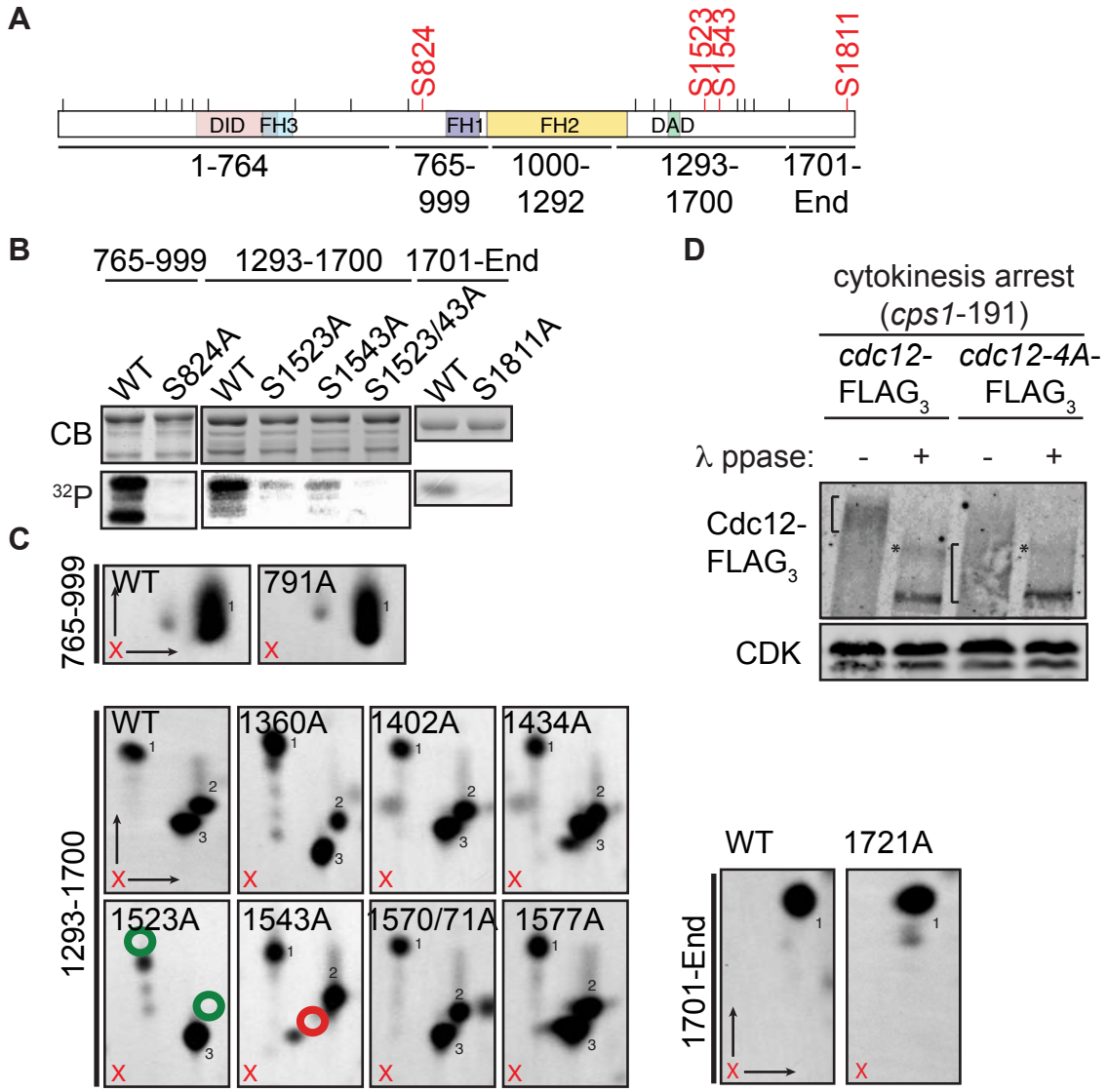

Figure 3-3

Sid2 phosphorylates Cdc12 on four RxxS consensus serines.
(A) Schematic of Cdc12, with Sid2-targeted residues labeled in red, additional Sid2 consensus motifs marked by black ticks, and recombinant protein fragments used in *in vitro* kinase assays illustrated. (B) *In vitro* kinase assays using Sid2-Myc$_{13}$ immunoprecipitated from *cdc16*-116 *sid2*-Myc$_{13}$ cells and various recombinant MBP-Cdc12 wild-type and mutant fragments. Proteins labeled by γ–^{32}P were detected by autoradiography, and the protein gel was stained with Coomassie blue (CB). (C) Phospho-tryptic peptide analysis of MBP-Cdc12 wild-type and mutant fragments phosphorylated by Sid2 kinase. The position of the origin is indicated by a red "x", and major spots are numbered. The anode is on the left. Loss of phosphorylated peptides for the S1523A and S1543A mutants of the MBP-Cdc12(1293-1700) fragment are indicated by green and red circles. (D) Denatured cell lysates of *cps1*-191 *cdc12*-FLAG$_3$ and *cps1*-191 *cdc12-4A*-FLAG$_3$ cells arrested in cytokinesis were probed with an anti-FLAG antibody. Immunoprecipitates were treated with phosphatase or a buffer control before being resolved by SDS-PAGE and immunoblotted. 10 μM Phos-tag was included in the protein gel. Brackets span phosphorylated smears, and asterisks denote a non-collapsible species. CDK is a loading control.

to alanines. However, Cdc12-4A-FLAG$_3$ was not hyperphosphorylated to the same extent as wild-type Cdc12-FLAG$_3$ during a *cps1*-191 cytokinesis arrest (Fig. 3-3D), signifying that Cdc12-4A cannot be fully phosphorylated *in vivo*. Therefore, we concluded that Sid2 phosphorylates formin Cdc12 during cytokinesis.

Cdc12-4A localizes to the CR but compromises actomyosin function

Mutant Cdc12-4A-GFP$_3$ localized normally to the CR (Fig. 3-4A). However, unlike wild-type Cdc12-GFP$_3$ (Coffman et al., 2009), Cdc12-4A-GFP$_3$ also localized to SPBs during CR constriction as detected by still and time-lapse imaging (Figs. 3-4A and 3-4B). This abnormal localization suggested that Cdc12-4A was deregulated. Consistent with this interpretation, combining the *cdc12-4A* allele with various loss-of-function alleles in the cytokinetic actomyosin machinery revealed severe negative genetic interactions (Figs. 3-5A and 3-5B). These alleles included mutations or deletions of genes encoding myosin Myo2, myosin regulatory light chain Rlc1, or actin Act1. *cdc12-4A* cells treated with low-dose (0.2 μM) Lat A, which impedes actin polymerization (Ayscough et al., 1997), also exhibited grossly amplified cytokinetic errors (Figs. 3-5C and 3-5D), similar to Lat A-treated cells lacking the SIN target Clp1 (Mishra et al., 2004). These data indicate that loss of Sid2-mediated Cdc12 phosphorylation impairs the cytokinetic actomyosin machinery without preventing Cdc12 localization to the CR.

Cdc12-4A is defective in SIN-dependent cytokinesis

We next tested whether SIN-dependent events during cytokinesis were impaired in the *cdc12-4A* mutant. Because the SIN is critical for Mid1/node-independent

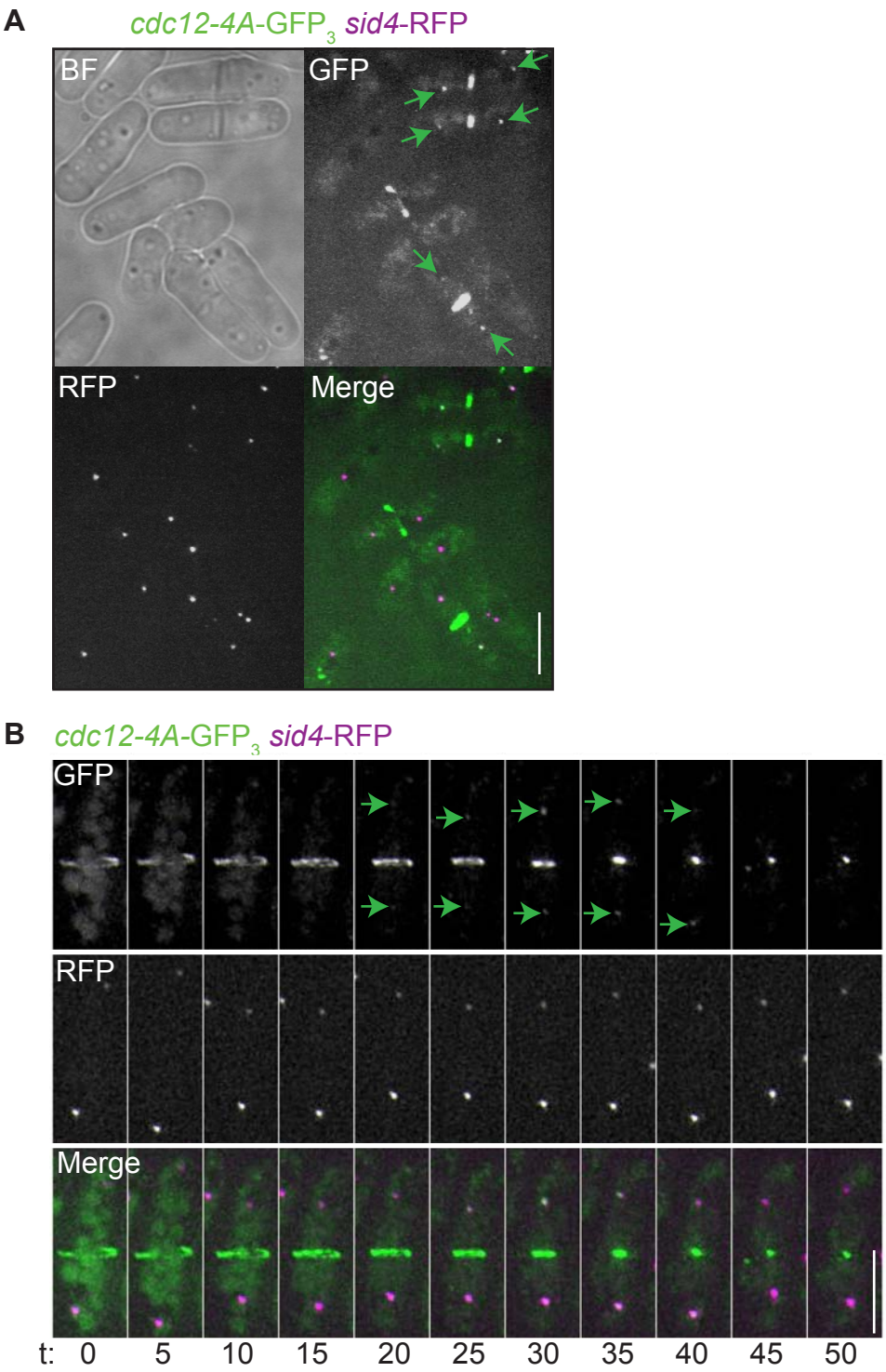

Figure 3-4

Cdc12-4A-GFP$_3$ localizes to the CR and SPBs during cytokinesis.
(A) Live-cell bright field (BF), GFP, RFP, and merged GFP/RFP images of *cdc12-4A*-GFP$_3$ *sid4*-RFP cells. Green arrows denote SPB localization. (B) Live-cell GFP/RFP movie of a *cdc12-4A*-GFP$_3$ *sid4*-RFP cell undergoing cytokinesis. Green arrows denote SPB localization during CR constriction. (Bars = 5 μm)

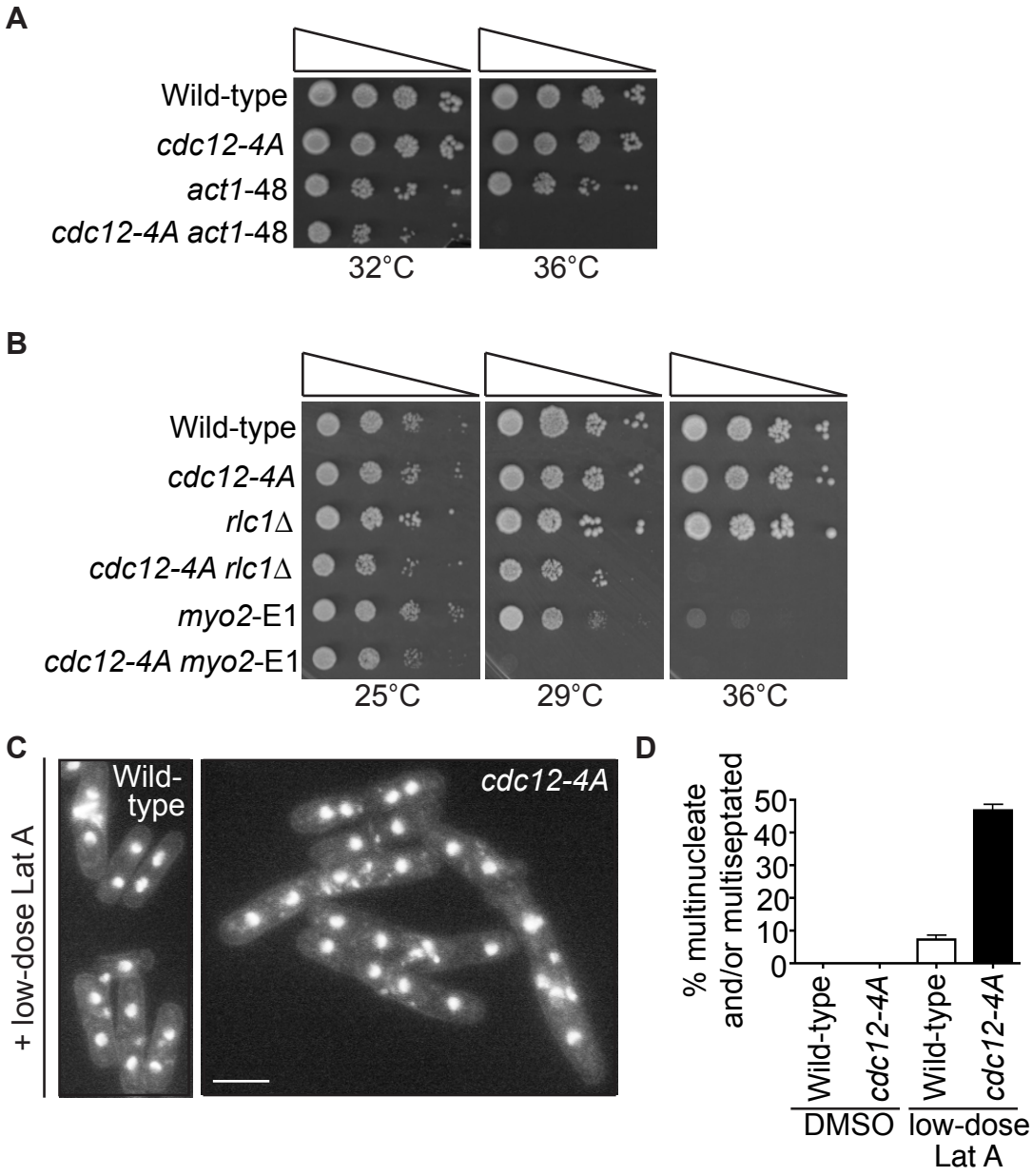

Figure 3-5

Cdc12-4A cannot support proper actomyosin function at the CR.
(A and B) Serial 10-fold dilutions of the indicated strains at various temperatures. (C) Fixed-cell images of DAPI- and methyl blue-stained wild-type and *cdc12-4A* cells treated with low-dose Lat A. (D) Quantification of cytokinesis defects of cells imaged in (C). DMSO treatments were administered as a control. n>200 for each. (Bar = 5 μm)

cytokinesis (Hachet and Simanis, 2008; Huang et al., 2008), we combined *mid1Δ* and *cdc12-4A* alleles. Importantly, *cdc12-4A mid1Δ* cells were significantly more defective in cytokinesis than either individual mutant (Figs. 3-6A and 3-6B) and died at elevated temperatures (Fig. 3-6C). F-BAR protein Cdc15 is also vital for Mid1-independent cytokinesis (Hachet and Simanis, 2008). Accordingly, *cdc12-4A* was synthetically sick with a *cdc15* temperature-sensitive allele (Fig. 3-6D). These results are consistent with Sid2-mediated Cdc12 phosphorylation representing an important facet of SIN-based CR regulation.

To further explore the contribution of Cdc12 phosphorylation to SIN signaling, we tested whether Cdc12-4A was capable of driving interphase CR assembly and septation upon SIN hyperactivation. We utilized a temperature-sensitive allele of the inhibitory GAP Cdc16, which when inactivated leads to multiple rounds of CR formation and septation (Fig. 3-7A) (Krapp and Simanis, 2008; Minet et al., 1979). Cells were synchronized in G2 phase (Fig. 3-7B) by centrifugal elutriation and then shifted to the restrictive temperature. Mononucleate *cdc12*-$V5_3$ cells septated almost immediately, and nearly all mononucleates developed multiple septa within four hours (Figs. 3-7A and 3-7B). However, a majority of *cdc12-4A*-$V5_3$ mononucleates failed to septate within this timeframe (Figs. 3-7A and 3-7B). Instead, these cells accumulated abnormal cell wall deposits near their cell middles (Fig. 3-7A). *cdc12-4A*-$V5_3$ mutants also contained medial spots, but not rings, of actin and CR proteins IQGAP YFP-Rng2 and Cdc15-GFP (Figs. 3-8A and 3-8B), which arose from earlier filament-like structures that fragmented and subsequently clustered into distinct foci (Fig. 3-8C). Like *cdc16*-116 *cdc12*-$V5_3$ cells, *cdc16*-116 *cdc12-4A*-$V5_3$ cells that slipped into mitosis completed medial septation

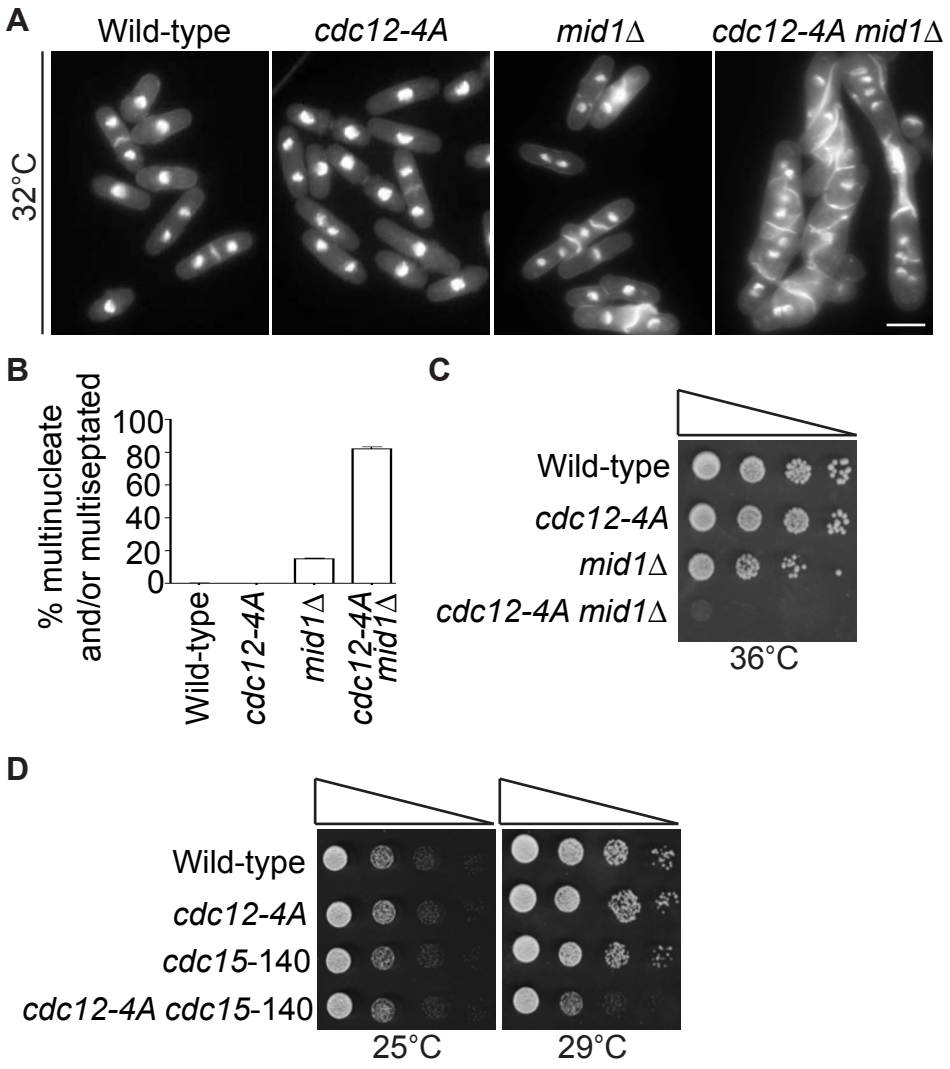

Figure 3-6

***cdc12-4A* impedes node/Mid1-independent cytokinesis.**
(A) Fixed-cell images of DAPI- and methyl blue-stained wild-type, *cdc12-4A*, *mid1Δ*, and *cdc12-4A mid1Δ* cells grown at 32°C. (B) Quantification of cytokinesis defects of cells imaged in (A). n>200 for each. (C and D) Serial 10-fold dilutions of the indicated strains at various temperatures.

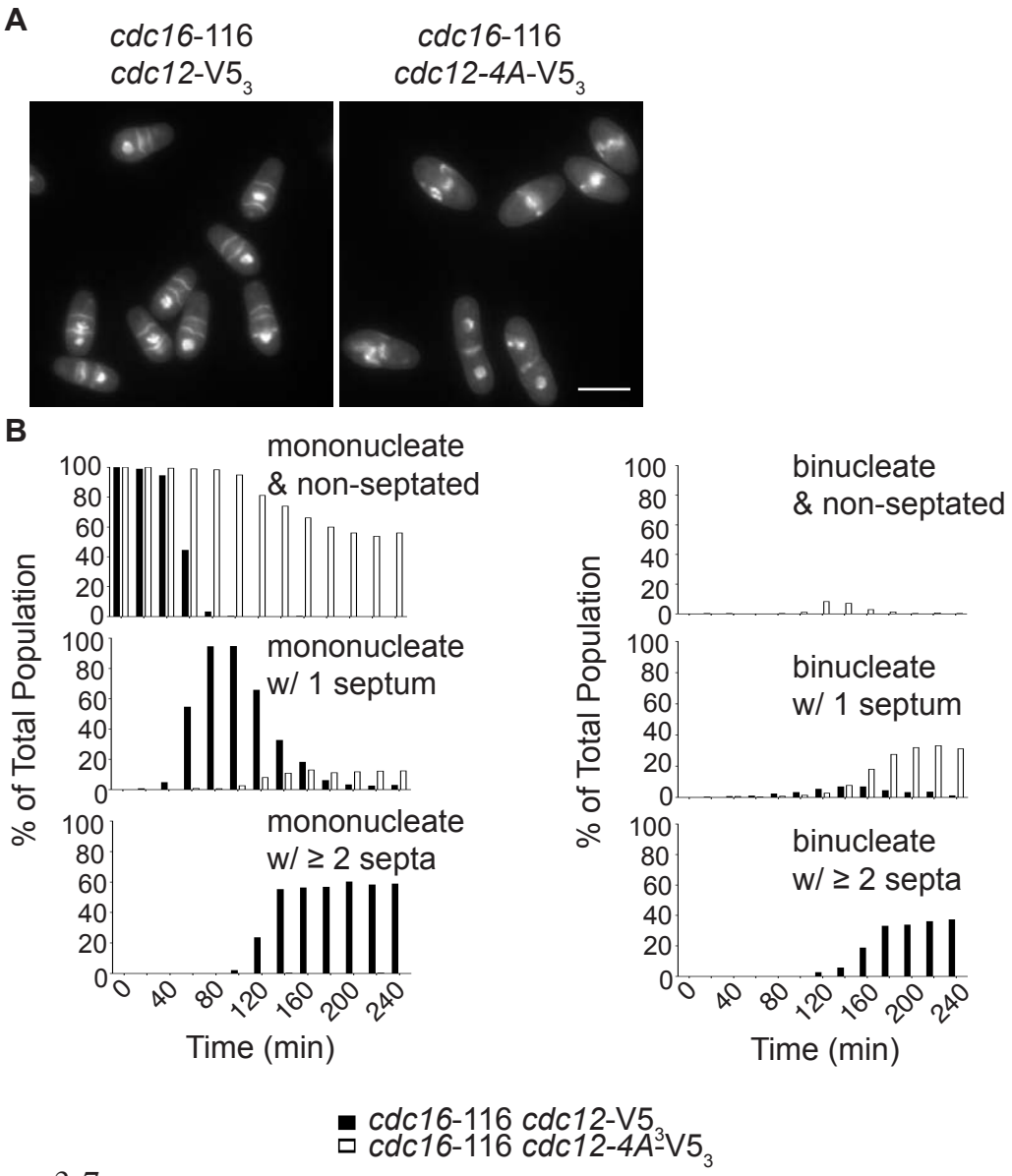

Figure 3-7

***cdc12-4A* impedes septation upon SIN hyperactivation.**
(A) Fixed-cell images of DAPI- and methyl blue-stained *cdc16*-116 *cdc12*-V5$_3$ and *cdc16*-116 *cdc12-4A*-V5$_3$ cells after 4 h at the restrictive temperature. (B) Quantification of septation upon SIN induction in *cdc16*-116 *cdc12*-V5$_3$ and *cdc16*-116 *cdc12-4A*-V5$_3$ cells. Cells were initially synchronized by centrifugal elutriation, and then shifted to the restrictive temperature for 4 h. n>300 for each time point. Data are separated for mononucleates and binucleates. (Bar = 5 μm)

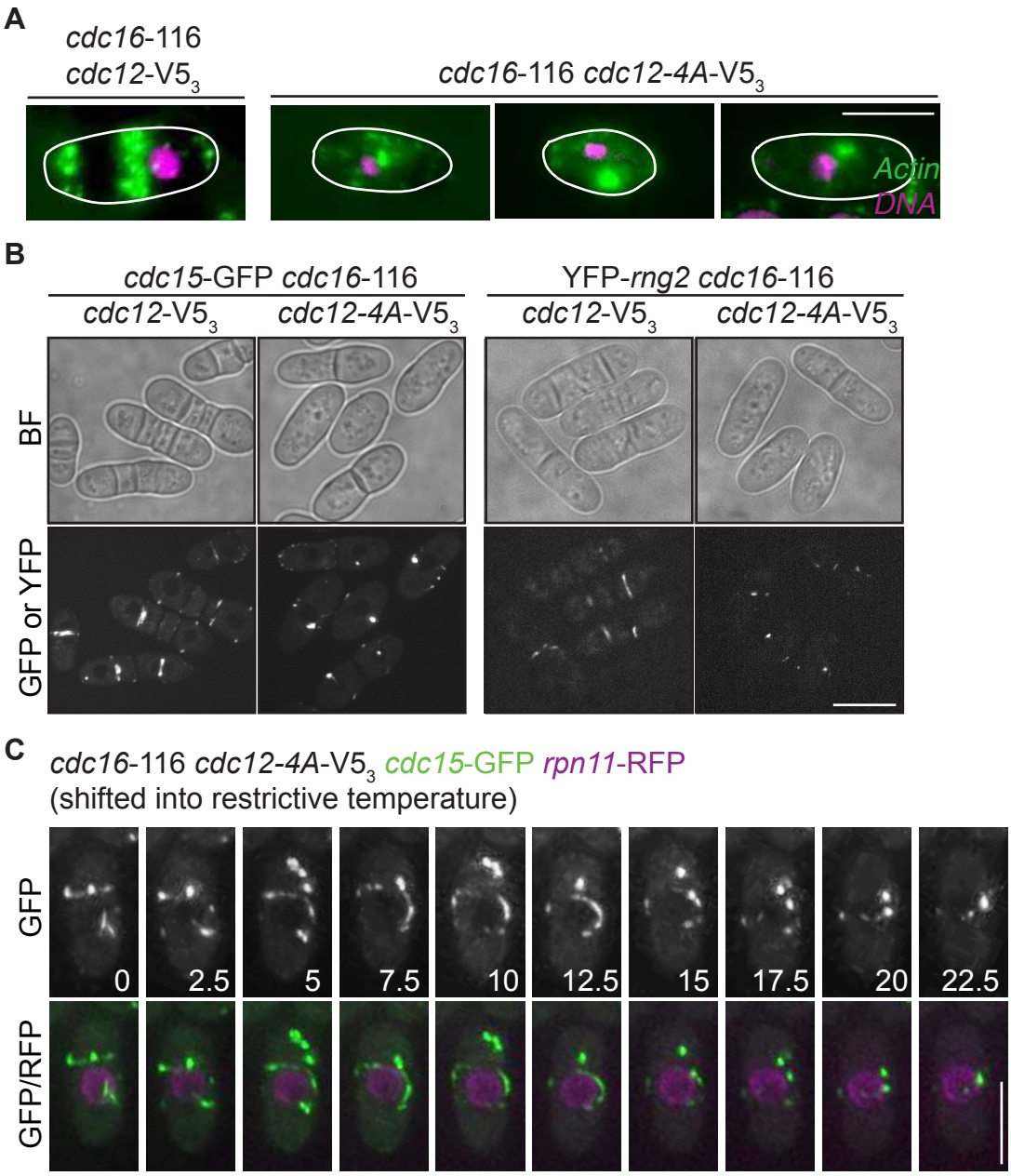

Figure 3-8

***cdc12-4A* impedes CR assembly upon SIN hyperactivation.**
(A) Fixed-cell images of phalloidin (green)- and DAPI (magenta)-stained *cdc16*-116 *cdc12*-V5$_3$ and *cdc16*-116 *cdc12-4A*-V5$_3$ cells after 4 h at the restrictive temperature. (B) Live-cell bright field (BF) and fluorescence images of *cdc16*-116 *cdc12*-V5$_3$ *cdc15*-GFP, *cdc16*-116 *cdc12-4A*-V5$_3$ *cdc15*-GFP, *cdc16*-116 *cdc12*-V5$_3$ YFP-*rng2*, and *cdc16*-116 *cdc12-4A*-V5$_3$ YFP-*rng2* cells after 4 h at the restrictive temperature. (C) Live-cell GFP/RFP movie of a *cdc16*-116 *cdc12-4A*-V5$_3$ *cdc15*-GFP *rpn11*-RFP interphase cell just after being shifted to the restrictive temperature. Images were acquired every 2.5 min. (Bars = 5 μm)

(Figs. 3-7A and 3-7B), illustrating that the *cdc12-4A* allele does not block node-based cytokinesis. Yet, additional non-medial septa never formed in *cdc16*-116 *cdc12-4A*-$V5_3$ binucleates (Figs. 3-7A and 3-7B), consistent with the *cdc12-4A* allele eliminating a key SIN signal.

Prolonged CR maintenance requires Sid2-mediated Cdc12 phosphorylation

Even when Mid1/node-based modules contribute to CR assembly at mitotic onset, sustained CR integrity demands SIN signaling. This is most evident in a *cps1*-191 β-glucan synthase mutant, which conditionally activates a cytokinetic checkpoint due to impaired septum deposition (Le Goff et al., 1999; Liu et al., 2000). Though *cps1*-191 cells form CRs, these mutants require SIN activity for CR maintenance during the arrest (Hachet and Simanis, 2008; Liu et al., 1999; Mishra et al., 2004). Consistent with Sid2-mediated Cdc12 phosphorylation constituting a critical SIN signal, intact F-actin rings were not observed in *cps1*-191 *cdc12-4A* arrested cells as they were in *cps1*-191 arrested cells (Fig. 3-9A). Similar to *cps1*-191 *sid2*-250 double mutants (Hachet and Simanis, 2008), *cps1*-191 *cdc12-4A* cells often contained medial F-actin clumps flanking 'kissing nuclei' that had returned to cell middles following failed cytokinesis (Fig. 3-9A). We found that these F-actin defects were associated with Cdc12 mislocalization. Whereas Cdc12-GFP_3 persisted in rings during a *cps1*-191 arrest (Fig. 3-9B), it accumulated in medial spots in *cps1*-191 *sid2*-250 arrested cells (Fig. 3-9B). Cdc12-4A-GFP_3 formed similar spot-like structures in a *cps1*-191 arrest (Fig. 3-9B), validating that Sid2 cannot target Cdc12-4A.

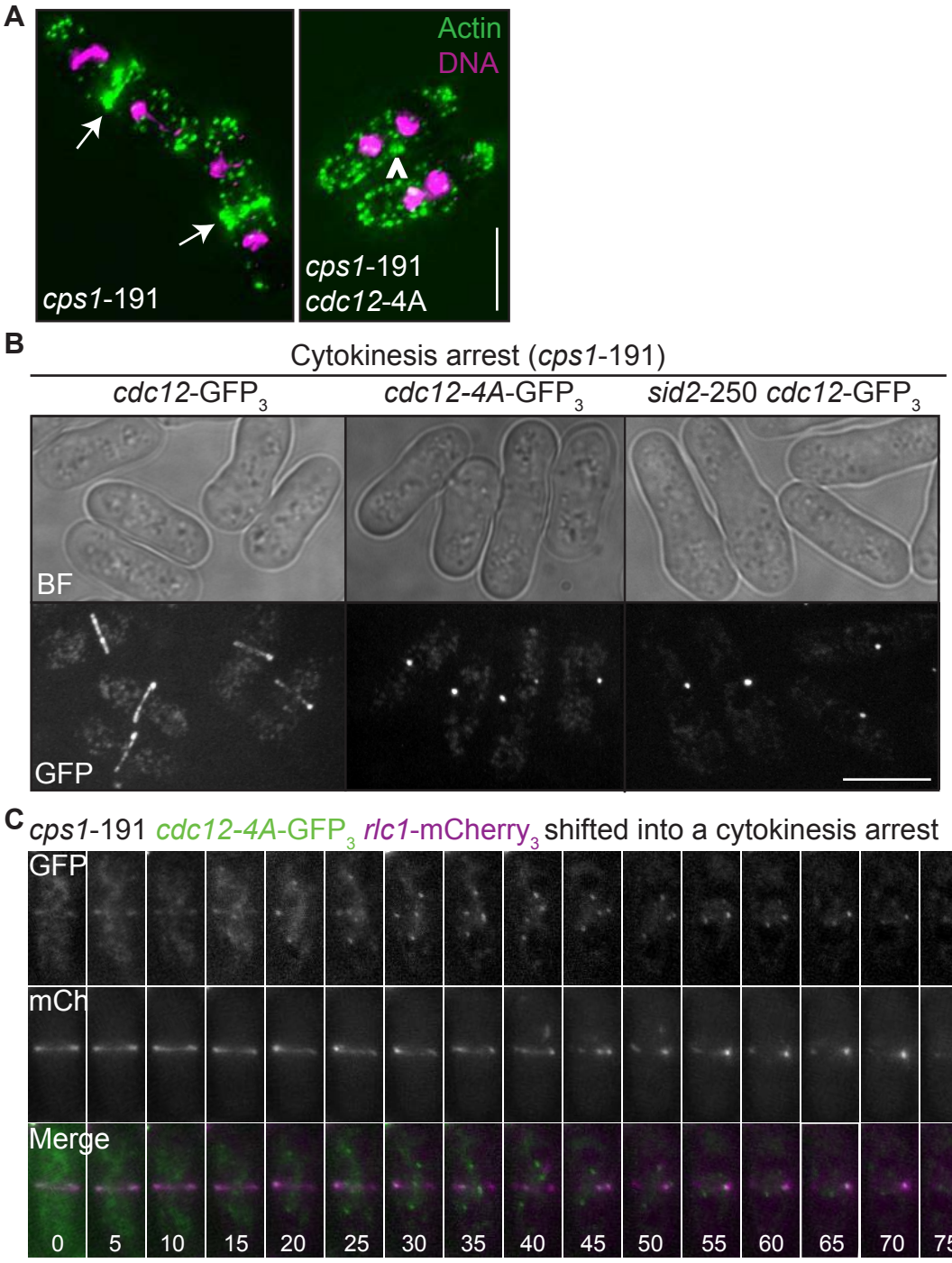

Figure 3-9

***cdc12-4A* cells fail at SIN-dependent CR maintenance.**
(A) Fixed-cell images of phalloidin (green)- and DAPI (magenta)-stained *cps1*-191 and *cps1*-191 *cdc12-4A* cells arrested in cytokinesis. Arrows indicate actin CRs, whereas an arrowhead points to a medial actin mass. (B) Live-cell bright field (BF) and GFP images of *cps1*-191 *cdc12*-GFP$_3$, *cps1*-191 *cdc12-4A*-GFP$_3$, and *cps1*-191 *sid2*-250 *cdc12*-GFP$_3$ cells arrested in cytokinesis. (C) Live-cell GFP/mCherry (mCh) movie of a *cps1*-191 *cdc12-4A*-GFP$_3$ *rlc1*-mCherry$_3$ cell just after being shifted to the restrictive temperature. Images were acquired every 5 min. (Bars = 5 μm)

We predicted these spot-like structures originated from collapsing CRs. Time-lapse imaging of Cdc12-4A-GFP_3 with the CR marker Rlc1-$mCherry_3$ confirmed that CRs formed as cells were shifted into the cytokinesis arrest but then collapsed (Fig. 3-9C). Ultimately, Cdc12-4A-GFP_3 clustered with Rlc1-$mCherry_3$ into a medial mass (Fig. 3-9C). Thus, Sid2-mediated Cdc12 phosphorylation is required for SIN-dependent CR maintenance.

Sid2-mediated phosphorylation inhibits Cdc12 C-terminal multimerization

Sid2 phosphorylates Cdc12 on residues located outside of characterized formin domains (Fig. 3-10A). Thus, we assessed whether Sid2-mediated phosphorylation disrupts the function of an uncharacterized Cdc12 domain. To identify such a domain, we introduced C-terminal tags at the endogenous *cdc12*$^+$ locus to produce serial 100-residue truncations (Fig. 3-10A). Though over-expression of similar C-terminal truncations is lethal (Yonetani and Chang, 2010), we found that endogenous *cdc12* truncations lacking residues C-terminal to Cdc12's FH2 domain were viable (Fig. 3-10B). Despite comparable viability, these mutants differed in CR phenotypes. Whereas Cdc12(1-1600)-GFP_3 formed complete ring structures, Cdc12(1-1400)-GFP_3 formed discontinuous CRs (Fig. 3-10C). Thus, we predicted that residues 1400-1600 contain a domain critical to Cdc12 regulation. In complementary experiments, we found that over-expressing the Cdc12 C-terminus strongly inhibited cytokinesis (Figs. 3-11A and 3-11B), and we defined a minimal C-terminal fragment (residues 1451-1538) that was sufficient for this activity (Figs. 3-11A, 3-11B, and 3-11C). Importantly, this fragment overlaps

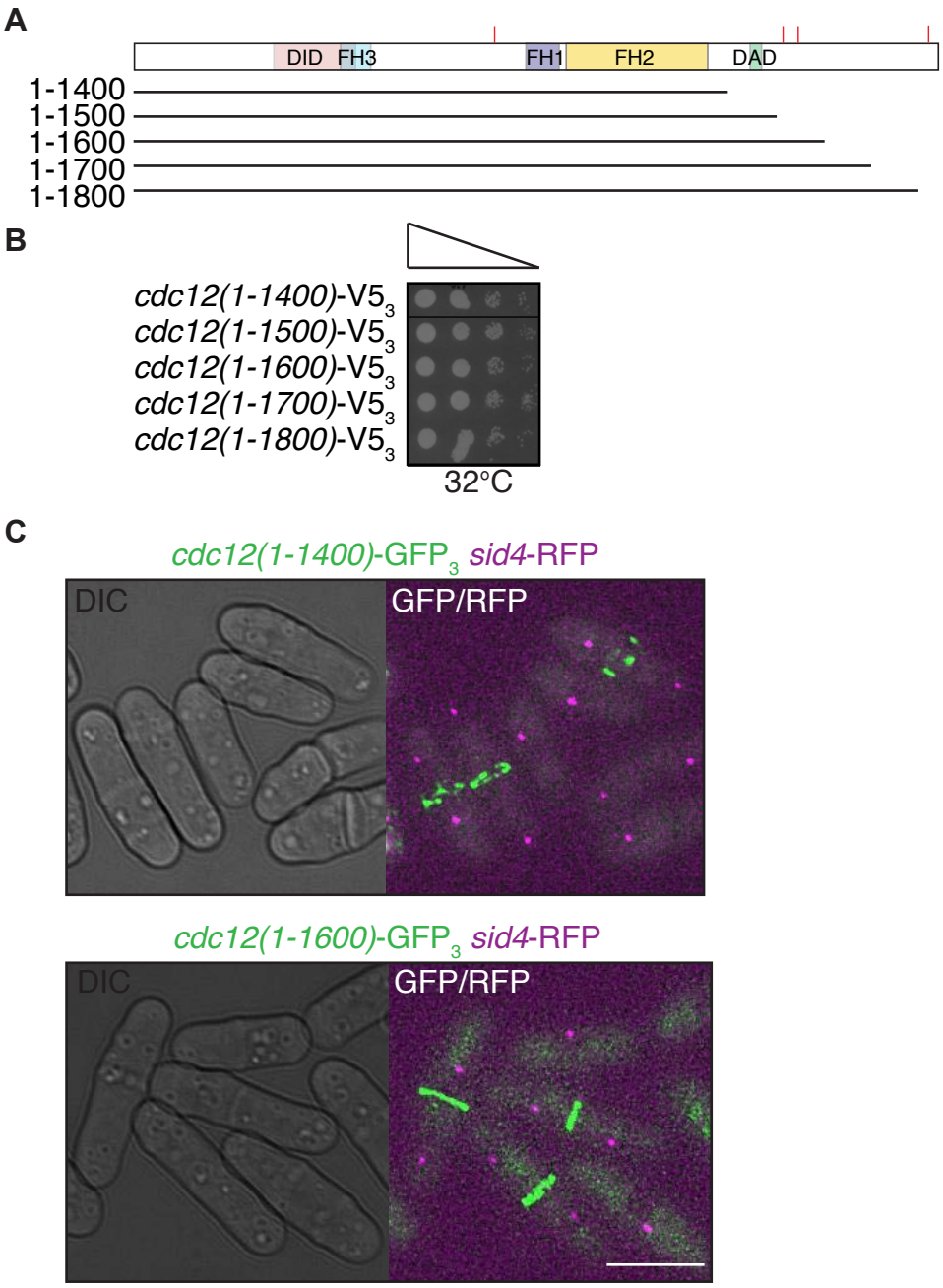

Figure 3-10

The Cdc12 C-terminus is important for CR formation.
(A) Schematic of Cdc12, with Sid2-targeted phosphosites indicated by red ticks and endogenous truncations illustrated. (B) Serial 10-fold dilutions of the indicated strains. (C) Live-cell DIC and merged GFP/RFP images of *cdc12(1-1400)*-GFP$_3$ *sid4*-RFP and *cdc12(1-1600)*-GFP$_3$ *sid4*-RFP cells. (Bar = 5 μm)

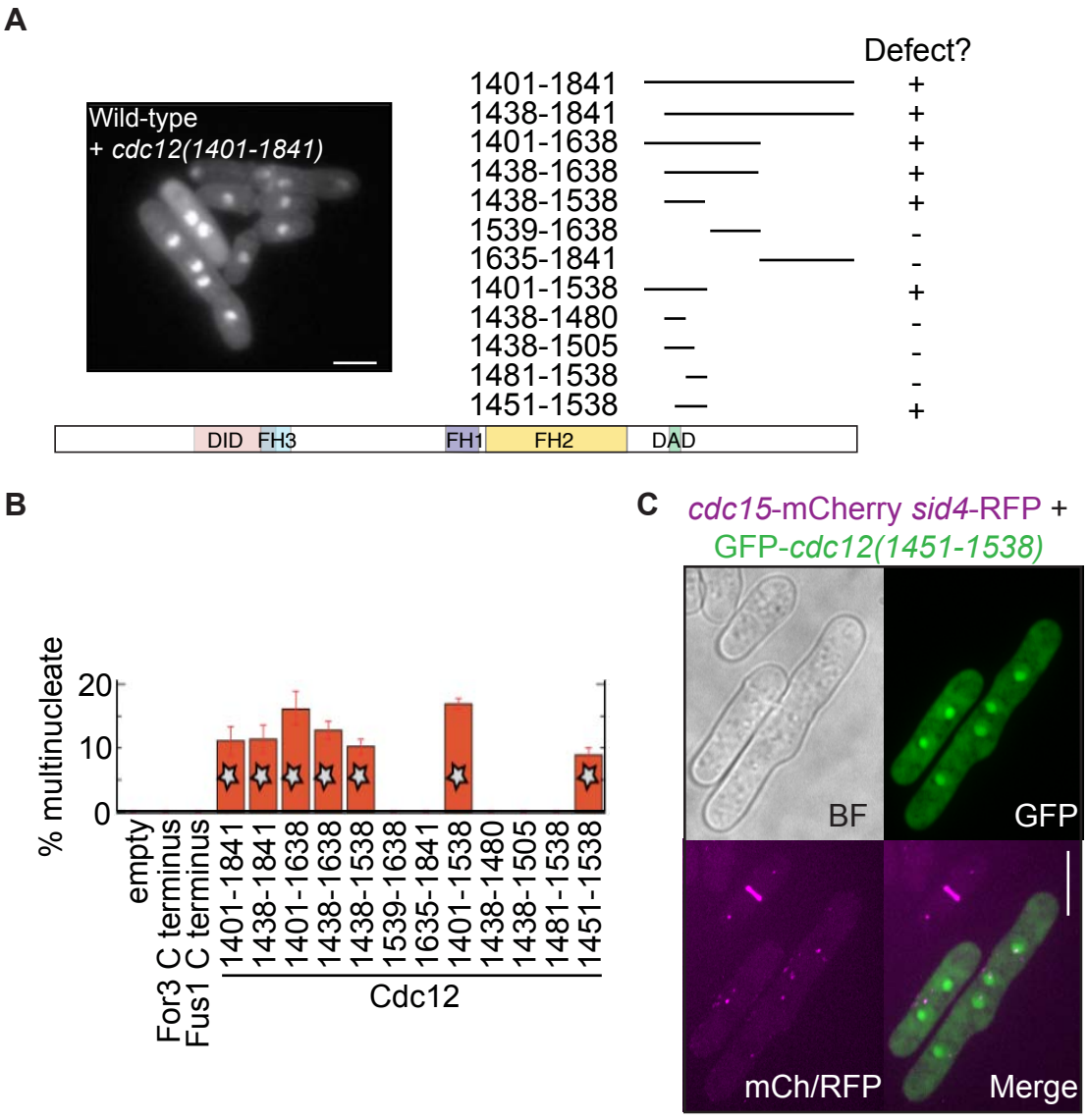

Figure 3-11

Over-expression of a minimal Cdc12 C-terminal fragment is lethal.
(A) Schematic representation of Cdc12, with over-expressed C-terminal fragments illustrated. Fragments were over-expressed from the pSGP527a plasmid. "+" indicates that the fragment caused cytokinesis defects upon over-expression, while "-" indicates that it did not. A fixed-cell image of a DAPI- and methyl blue-stained wild-type cell over-expressing *cdc12(1401-1841)* is given to show an example of cytokinesis defects caused by such over-expression. (B) Quantification of cells defective in cytokinesis upon over-expression of fragments illustrated in (A). Starred bars denote fragments that impaired cytokinesis. Over-expression of C-termini of other *S. pombe* formins, For3 and Fus1, served as controls. Two trials were performed per fragment, with n>100 for each trial. (C) Live-cell bright field (BF), GFP, mCherry (mCh)/RFP, and merged fluorescence images of *cdc15*-mCherry *sid4*-RFP cells, some of which over-express GFP-*cdc12(1451-1538)*. This fragment was over-expressed from the pSGP572a plasmid. (Bars = 5 μm)

with the region contributing to CR formation (Fig. 3-10C), suggesting that residues 1451-1538 comprise a functional domain.

Sequence analysis revealed a high percentage of basic and serine residues within this region (Fig. 3-12A), reminiscent of RS domains involved in oligomerization (Boucher et al., 2001). Accordingly, when resolved under native conditions, His_6-Cdc12(1451-1538) was detected in various multimeric forms (Fig. 3-12B), suggesting it oligomerized. Consistent with self-association, MBP-Cdc12(1451-1538) and His_6-Cdc12(1451-1538) interacted *in vitro* (Fig. 3-12C). Further, *cdc12(1451-1538)* over-expression in cells drove endogenous Cdc12-GFP_3 into spot-like structures (Fig. 3-12D), which resembled those observed upon loss of SIN function (Fig. 3-9B). We also found that Cdc12Δ1451-1538-GFP_3, unlike wild-type Cdc12-GFP_3 (Coffman et al., 2009), never formed interphase spots (Figs. 3-12E and 3-12F). Thus, residues 1451-1538 function as an oligomerization domain, which influences Cdc12 clustering.

RS domain-mediated oligomerizations can be reversed via phosphorylation (Nikolakaki et al., 2008; Peng et al., 2008). As two Sid2-directed phosphosites were within or near the Cdc12 oligomerization domain (Fig. 3-13A) and Cdc12 clustered during cytokinesis upon loss of this phosphorylation (Fig. 3-9B), we asked whether Sid2-mediated Cdc12 phosphorylation regulates this self-interaction. First, we immunoprecipitated wild-type Cdc12-$FLAG_3$ or phosphomutant Cdc12-4A-$FLAG_3$ from a *cps1*-191 arrest, in which wild-type Cdc12 is phosphorylated by Sid2 (Fig. 3-3D), and tested whether immunoprecipitates bound His_6-Cdc12(1451-1538). Only Cdc12-4A-$FLAG_3$ bound His_6-Cdc12(1451-1538) (Fig. 3-13B). Next, we repeated the *in vitro* binding experiments with recombinant proteins, but phosphorylated bead-bound MBP-

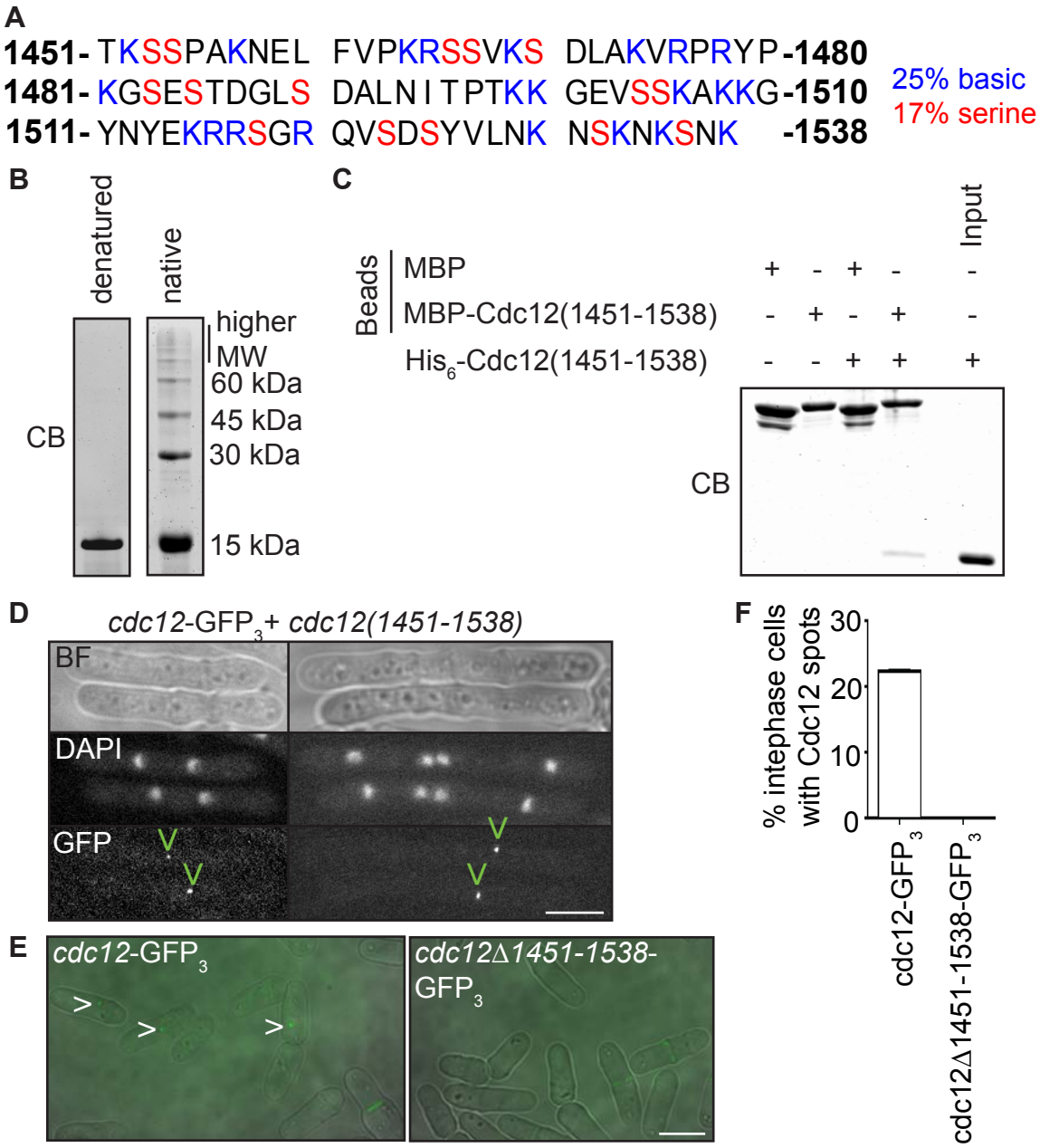

Figure 3-12

The Cdc12 C-terminus contains an oligomerization domain, which impacts clustering. (A) The C-terminal Cdc12 oligomerization domain, amino acids 1451-1538, is nearly half basic (blue) or serine (red). (B) Recombinant His_6-Cdc12(1451-1538) was resolved under native or denaturing conditions, and protein gels were Coomassie blue (CB)-stained. (C) *In vitro* binding of bead-bound recombinant MBP or MBP-Cdc12(1451-1538) with recombinant His_6-Cdc12(1451-1538). Samples were washed, resolved by SDS-PAGE, and CB-stained. The His_6-Cdc12(1451-1538) input is given as a control (D) Fixed-cell bright field (BF), GFP, and DAPI images of *cdc12*-GFP_3 cells defective in cytokinesis due to over-expression of *cdc12(1451-1538)*. This fragment was over-expressed from the pREP1 plasmid. (E) Live-cell BF/GFP overlay images of *cdc12*-GFP_3 and *cdc12Δ1451-1538*-GFP_3 cells. Arrowheads indicate interphase Cdc12 spots. (F) Quantification of interphase Cdc12 spots imaged in (E). Two trials were performed per genotype, with n>100 for each trial. (Bars = 5 μm)

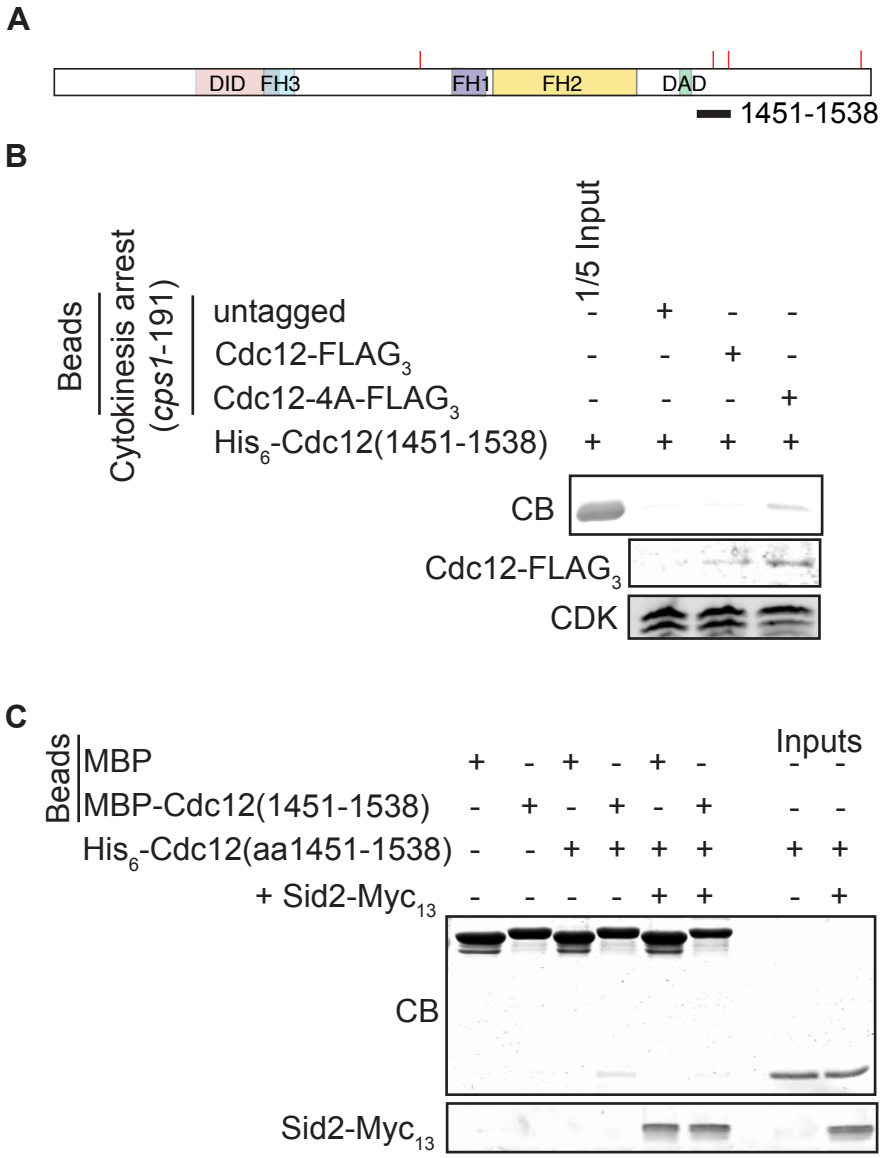

Figure 3-13

Cdc12 multimerization is inhibited by Sid2-mediated phosphorylation.
(A) Schematic of Cdc12, with phosphosites marked by red ticks and the 1451-1538 fragment illustrated. (B) *In vitro* binding of recombinant His_6-Cdc12(1451-1538) with bead-bound Cdc12-$FLAG_3$ or Cdc12-4A-$FLAG_3$ immunoprecipitated from a cytokinesis arrest. Samples were washed, resolved by SDS-PAGE, and gel halves were either immunoblotted with an anti-FLAG antibody or Coomassie blue (CB)-stained. (C) *In vitro* binding of bead-bound recombinant MBP or MBP-Cdc12(1451-1538), which had been phosphorylated by Sid2-Myc_{13}, with recombinant His_6-Cdc12(1451-1538). Sid2-Myc_{13} was immunoprecipitated from *cdc16*-116 *sid2*-Myc_{13} cells and incubated with ATP and bead-bound recombinant proteins. Following binding to His_6-Cdc12(1451-1538), samples were washed, resolved by SDS-PAGE, and CB-stained.

Cdc12(1451-1538) using Sid2-Myc_{13} prior to incubation. We found that phosphorylation by Sid2-Myc_{13} significantly abrogated the self-interaction (Fig. 3-13C). Collectively, these data indicate that Sid2-mediated Cdc12 phosphorylation counteracts C-terminal multimerization, and that abnormal Cdc12 clustering occurs when this self-interaction persists.

Cdc12 C-terminal multimerization directs linear F-actin bundling

Deletion of the Cdc12 C-terminus could preclude clustering even when CRs deteriorated during a *cps1*-191 arrest (Fig. 3-14A). However, loss of the Cdc12 C-terminus compromised CR formation (Fig. 3-10C), indicating that oligomerization must be important earlier during cytokinesis. Because the endogenous *cdc12Δ1451-1538* allele was synthetically sick with *fim1Δ* and *rng2*-D5 (Figs. 3-14B and 3-14C), mutant alleles of two demonstrated F-actin bundlers at the CR (Skau et al., 2011; Takaine et al., 2009), we investigated the possibility that Cdc12 multimerization contributes to F-actin bundling, an activity which Cdc12's FH1 and FH2 domains alone cannot perform (Scott et al., 2011).

We found that a C-terminal fragment ('Cdc12C', residues 1293-end), which contains the oligomerization domain but lacks the FH1FH2 region (Fig. 3-15A), co-pelleted with F-actin in high-speed (100,000g) sedimentation assays (Fig. 3-15B). Titration of this binding event revealed a K_D of 0.67 μM (Fig. 3-15C), which is similar to those described for other F-actin bundlers at the CR (Takaine et al., 2009). Notably, MBP-Cdc12C also co-pelleted with F-actin in low-speed (15,000g) sedimentation assays (Fig. 3-15D) and organized rhodamine-phalloidin-stained F-actin into long, linear

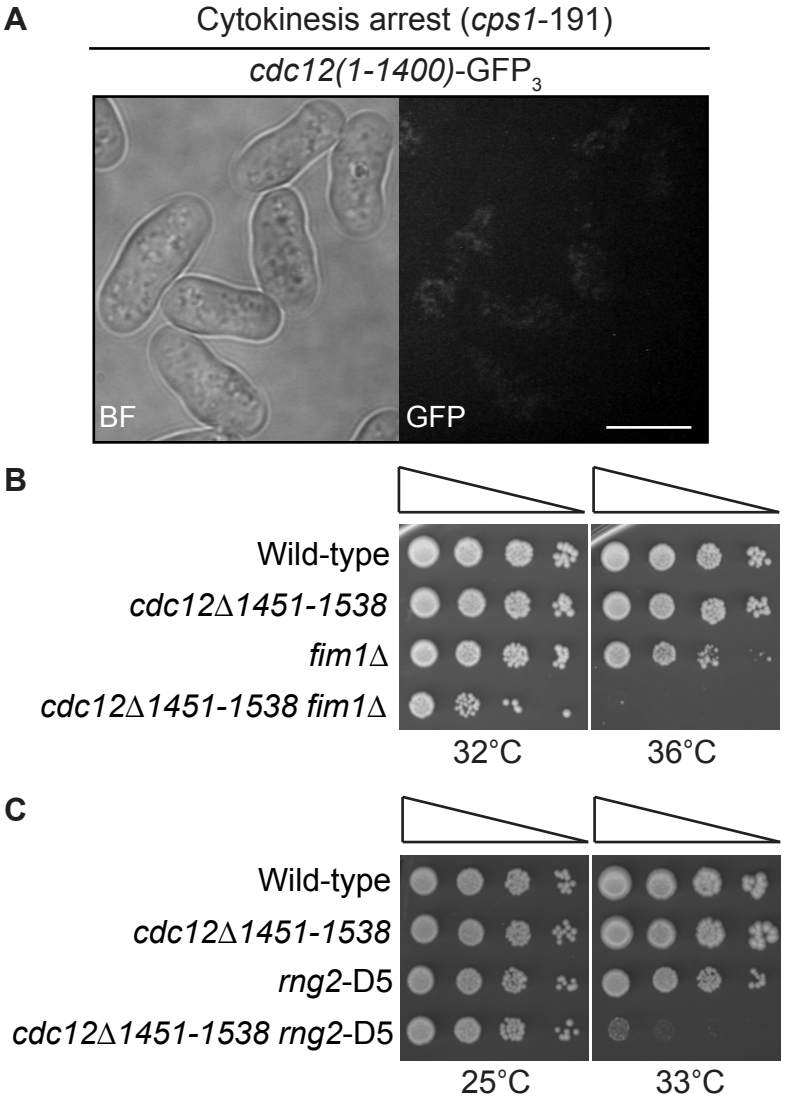

Figure 3-14

Additional characterization of C-terminal mutants.
(A) Live-cell bright field (BF) and GFP images of *cps1*-191 *cdc12(1-1400)*-GFP_3 cells arrested in cytokinesis. (B and C) Serial 10-fold dilutions of the indicated strains at various temperatures. (Bar = 5 μm)

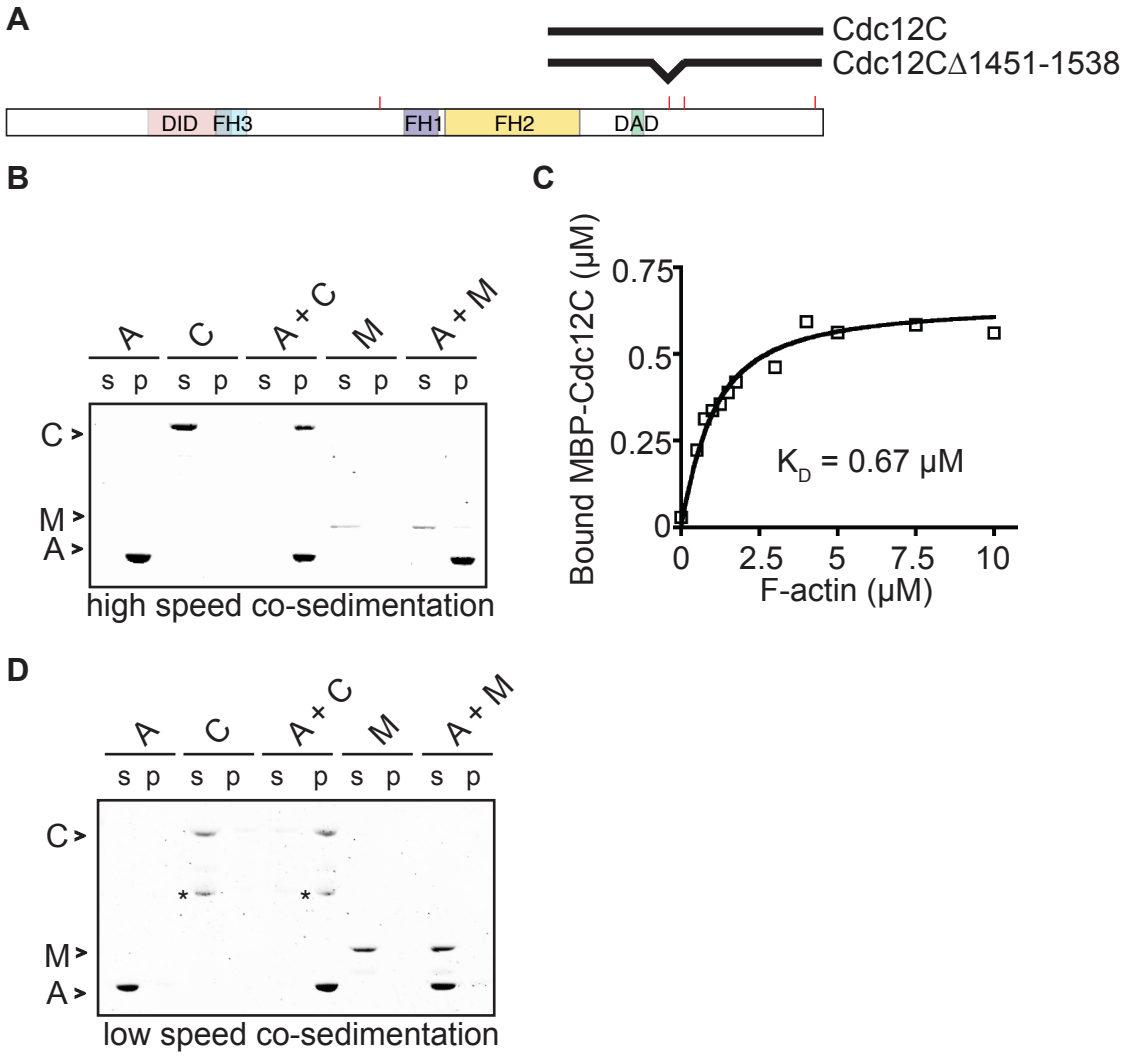

Figure 3-15

Cdc12's C-terminus binds and crosslinks F-actin.
(A) Schematic of Cdc12, with relevant recombinant fragments illustrated and Sid2-phosphorylated residues marked by red ticks. (B) High-speed (100,000g) sedimentation assay of MBP-Cdc12C (C) or MBP (M) with F-actin (A). Equal portions of supernatants (s) and pellets (p) were resolved by SDS-PAGE and then Coomassie blue-stained. (C) Titration of MBP-Cdc12C binding to F-actin. High-speed (100,000g) sedimentations were performed with varying F-actin concentrations, and the amount of co-pelleted MBP-Cdc12C was measured. The K_D was determined by fitting a quadratic equation to these data. (D) Low-speed (15,000g) sedimentation assay of MBP-Cdc12C (C) or MBP (M) with F-actin (A). Equal portions of supernatants (s) and pellets (p) were resolved by SDS-PAGE and then Coomassie blue-stained. Asterisks indicate degradation products.

bundles (Fig. 3-16A). Accordingly, the Cdc12 C-terminus can both bind and bundle F-actin. In contrast, a Cdc12CΔ1451-1538 mutant fragment, which lacks the oligomerization domain (Fig. 3-15A), did not bundle F-actin but instead formed disordered crosslinks (Fig. 3-16A). Thus, the Cdc12 oligomerization domain supports linear F-actin bundling *in vitro*, though this domain itself cannot efficiently bind F-actin (Fig. 3-16B).

If Cdc12 multimerization guides F-actin bundling *in vivo*, we expected that a *cdc12Δ1451-1538* mutant would be defective in CR assembly. Indeed, imaging actin marker LifeAct-GFP in a *cdc25*-22 mutant at permissive temperature, in which the longer cell length clarifies medial actin structures (Huang et al., 2012), gave the impression that deleting the multimerization domain compromised actin condensation into a discrete CR (Fig. 3-17A). To score this defect, we quantified condensed and non-condensed CRs in mitotic *cdc25*-22 cells at permissive temperature. We found that roughly a quarter of *cdc12Δ1451-1538* binucleates possessed medial actin that had yet to condense into a ring (Figs. 3-17B and 3-17C). In contrast, nearly all *cdc12*$^{+}$ binucleates showed a condensed CR (Figs. 3-17B and 3-17C). These data suggest that Cdc12 multimerization initially facilitates ordered F-actin bundling to promote early stages of CR formation, and that Sid2-based reversal of multimerization subsequently limits this activity.

Discussion

Though the SIN is a well-documented cytokinesis regulator, essential CR targets of this network had not been described. Here, we establish the essential cytokinetic formin Cdc12 as a direct Sid2 target that is key to SIN-driven cytokinesis.

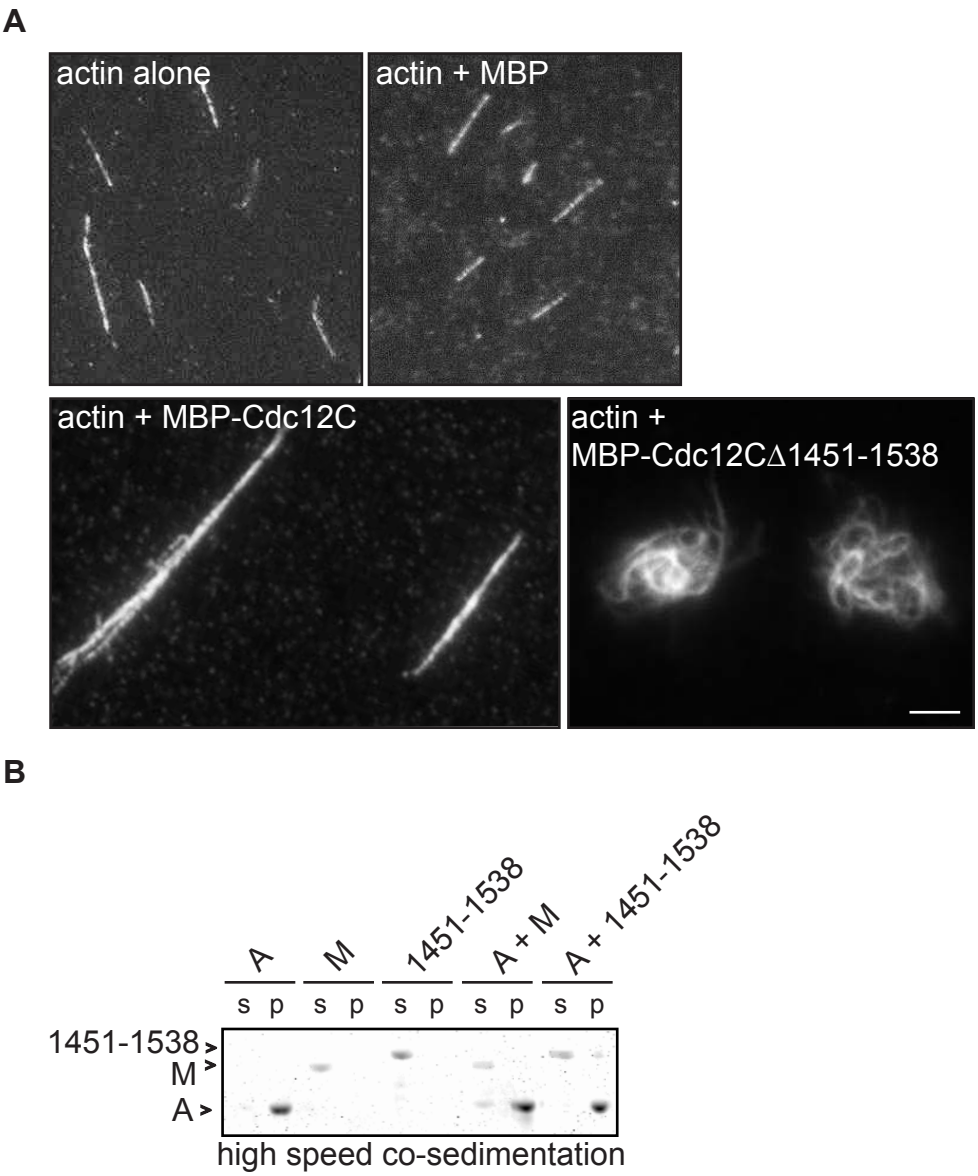

Figure 3-16

The Cdc12 C-terminus bundles F-actin partly through its oligomerization domain.
(A) Representative fluorescence images of rhodamine-phalloidin-stained actin filaments in the absence or presence of MBP, MBP-Cdc12C, or MBP-Cdc12CΔ1451-1538. (B) High-speed (100,000g) sedimentation assay of MBP-Cdc12(1451-1538) (marked as 1451-1538) or MBP (M) with F-actin (A). Equal portions of supernatants (s) and pellets (p) were resolved by SDS-PAGE and then Coomassie blue-stained. (Bar = 5 μm)

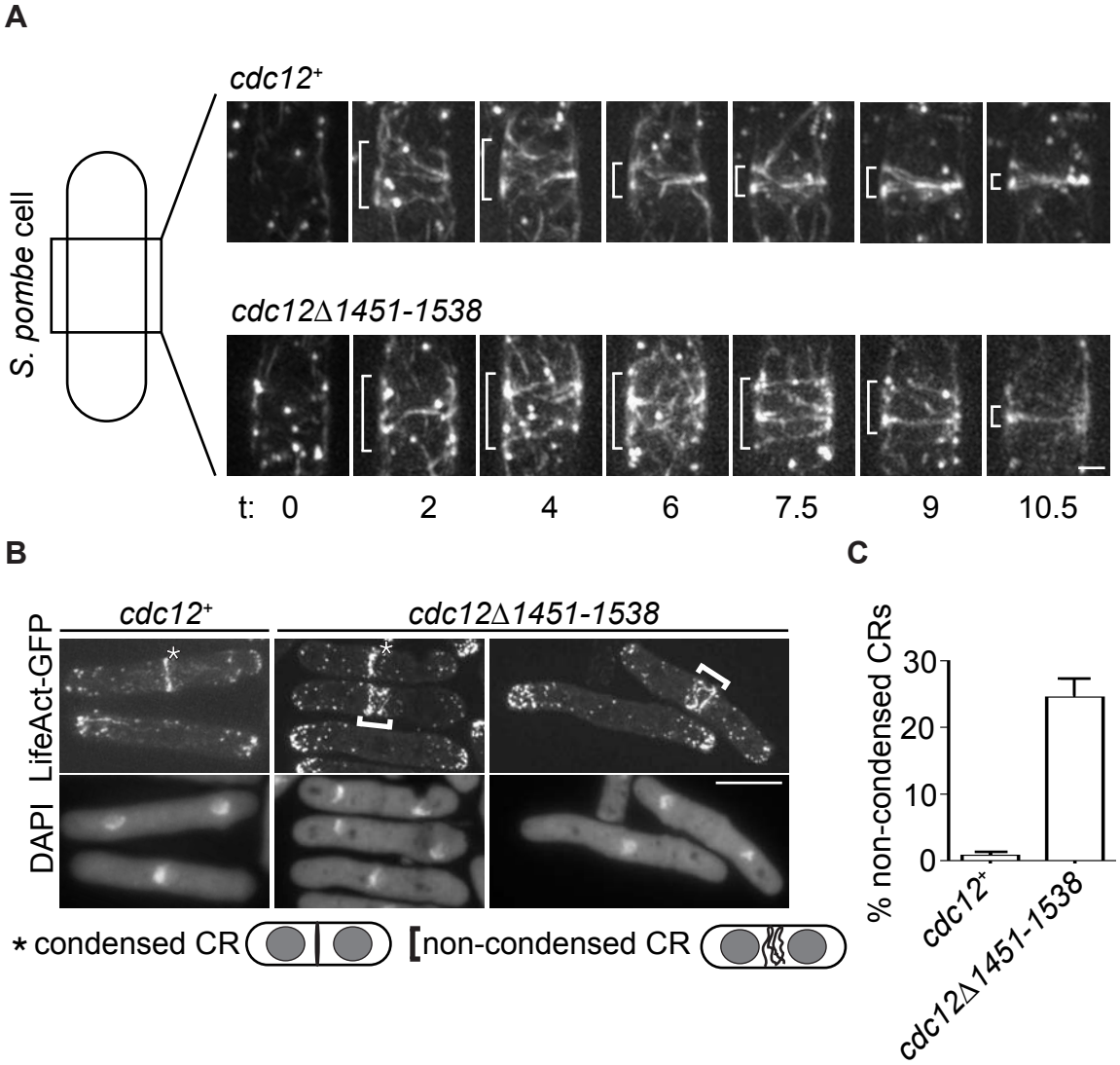

Figure 3-17

Deletion of the multimerization domain compromises CR condensation *in vivo*.
(A) Live-cell GFP movies of *cdc25*-22 LifeAct-GFP or *cdc25*-22 *cdc12Δ1451-1538* LifeAct-GFP cells assembling a CR. Cells were grown at 25°C. Frames show cell middles and start as actin accumulates medially. Brackets span the breadth of medial actin. (B) Fixed-cell GFP and DAPI images of *cdc25*-22 LifeAct-GFP or *cdc25*-22 *cdc12Δ1451-1538* LifeAct-GFP cells grown at 25°C. (C) Quantification of condensed and non-condensed CRs in binucleate *cdc25*-22 LifeAct-GFP or binucleate *cdc25*-22 *cdc12Δ1451-1538* LifeAct-GFP cells grown at 25°C. [Bars = 1 μm in (A) and 5 μm in (B)]

Phosphoregulation of Cdc12 during cytokinesis appears to function as an oligomeric switch, promoting Cdc12 multimer disassembly necessary for CR maintenance (Figs. 3-18A and 3-18B). When left unchecked during late cytokinesis, persistent Cdc12 multimerization results in abnormal formin clustering, which leads to CR disintegration and failure of cell cleavage (Fig. 3-18B).

Regulation of Cdc12 clustering and multimerization through the cell cycle

The intrinsic ability of Cdc12 to multimerize and cluster explains the origin of Cdc12-containing spots that have been detected in interphase cells (Fig. 3-18A) (Coffman et al., 2009; Yonetani et al., 2008), in cells over-expressing Cdc12 (Carnahan and Gould, 2003; Chang, 1999; Chang et al., 1997), and in mutants with impaired SIN function (Fig. 3-9B). Why spots form and how they relate to formin activity and CR formation have been topics of debate (Roberts-Galbraith and Gould, 2008). Though a previous study implicated Cdc12's N-terminal FH3 domain in spot formation, this same study demonstrated more dramatic clustering upon over-expression of Cdc12's C-terminus (Yonetani et al., 2008). Indeed, we have found that C-terminal multimerization facilitates spot formation during interphase or when the self-association domain is hyper-abundant (Figs. 3-9A and 3-9B). In both contexts, Cdc12 cannot induce cytokinesis, supporting the ideas that (1) spots serve as reservoirs that restrict formin function (Coffman et al., 2009; Yonetani et al., 2008); and (2) the Cdc12 C-terminus possesses a domain that inhibits formin function (Yonetani and Chang, 2010). When interphase is prolonged and CR proteins prematurely localize to the division site, even more pronounced Cdc12 spots

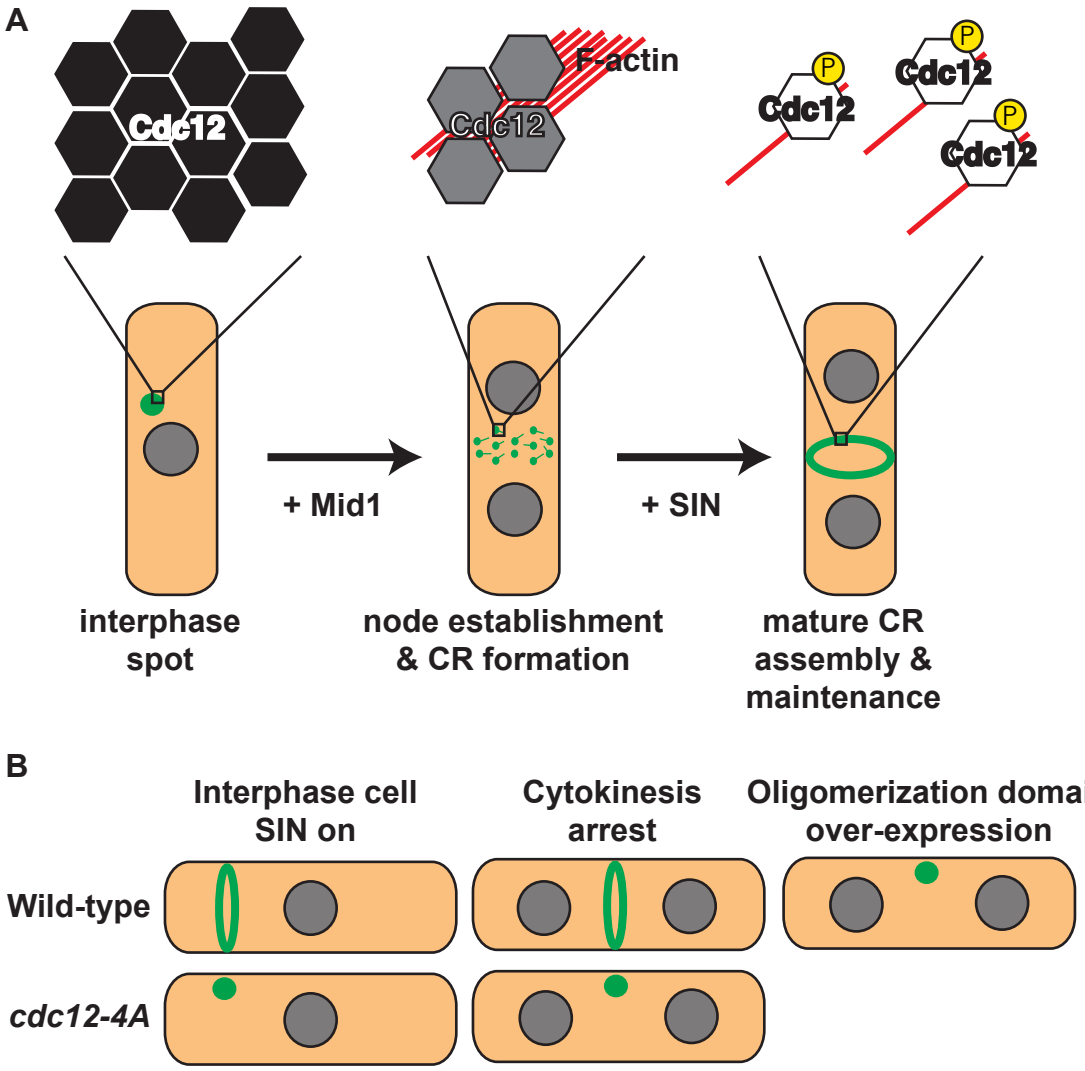

Figure 3-18

Model for Sid2-mediated Cdc12 phosphorylation during *S. pombe* cytokinesis.
(A) During interphase, Cdc12 exists in a spot-like structure, which serves as a reservoir. At mitotic onset, anillin-like Mid1 assembles medial nodes, to which Cdc12 and other CR factors are recruited. Nodes spatially restrict Cdc12 spot formation and aid in initial de-clustering. As CRs form from nodes, multimeric Cdc12 bundles F-actin, aiding in CR condensation. Upon full activation of the SIN, Sid2 phosphorylates Cdc12 to inhibit multimerization of Cdc12's C-terminal oligomerization domain. This oligomeric switch facilitates mature CR assembly and maintenance by blocking Cdc12 spot formation once Mid1 has exited the CR in late cytokinesis. (B) Typically, *cdc12*$^{+}$ cells maintain a CR during a cytokinesis arrest and undergo septation in interphase when the SIN is prematurely activated. In these contexts, CRs do not collapse, because Cdc12 clustering is inhibited by the SIN. But, when the SIN kinase Sid2 cannot phosphorylate Cdc12, Cdc12 and other CR proteins cluster abnormally, similar to when Cdc12's oligomerization domain is over-expressed. Persistent multimerization leads to the formation of spot-like structures during a cytokinesis arrest or in SIN-activated interphase cells. Thus, Sid2-mediated Cdc12 phosphorylation constitutes a critical SIN signal, which reverses Cdc12 multimerization at the appropriate time to enable proper CR performance.

develop (Roberts-Galbraith et al., 2010). Thus, Cdc12 clusters can expand with time if relevant disassembly cues are not triggered.

How is the Cdc12 clustering/de-clustering cycle regulated? For the CR to form, Cdc12 spots must disassemble and re-mobilize into a ring-like structure. During early mitosis, Mid1/node-dependent pathways may initially antagonize Cdc12 clustering (Fig. 3-18A), for in their absence CRs assemble from spot-like asters (Huang et al., 2008). Two separate Mid1-dependent modules, based on either myosin and IQGAP Rng2 or Cdc15, recruit Cdc12 medially (Laporte et al., 2011), where Cdc12 likely binds multiple node proteins capable of serving as cortical anchors (Guzman-Vendrell et al., 2013; Saha and Pollard, 2012). Presumably, these anchors spatially restrict Cdc12 clustering, but permit some degree of Cdc12 multimerization that facilitates F-actin bundling (Fig. 3-18A). In support of Mid1/node-dependent pathways contributing de-clustering signals during CR formation, *cdc12-4A* cells undergo cytokinesis when the cell cycle is otherwise unperturbed. Despite Mid1-based compensation at the CR, Cdc12-4A still accumulates at SPBs during CR constriction, consistent with a multimer disassembly defect and other data suggesting an SPB-Cdc12 binding interface (Petersen et al., 1998).

Mid1 remains at the CR through its assembly (Sohrmann et al., 1996), though Mid1 exits during a *cps1*-191 arrest (Pardo and Nurse, 2003). In Mid1's absence, other mechanisms must counteract formin clustering to prevent premature spot formation and CR collapse. Our data show that Sid2-mediated phosphoinhibition of Cdc12 multimerization provides a mechanism to inhibit formin clustering in late cytokinesis (Figs. 3-18A and 3-18B). Previous studies have demonstrated that phosphorylation can disrupt autoinhibitory formin interactions (Takeya et al., 2008; Wang et al., 2009). Our

results provide a striking parallel, revealing that formin *trans* interactions, which mediate oligomerization, can also be phosphoregulated. While our model (Fig. 3-18A) proposes that tandem Mid1/node- and SIN-dependent de-clustering signals ensure efficient CR assembly and maintenance, other mechanisms likely contribute to activation of formin nucleation and elongation activities, because rudimentary filament-like structures still form in the absence of Mid1 and Sid2-mediated Cdc12 phosphorylation (Fig. 3-8C).

Formin-mediated F-actin bundling during cytokinesis

Although it is well established that formin dimerization via FH2 domains allows efficient bard end binding and elongation (Otomo et al., 2005; Xu et al., 2004), it has been unclear whether formins can formed higher-ordered oligomers and, if so, what function these oligomerization events would serve. In this study, we have shown that C-terminal multimerization guides Cdc12-mediated F-actin bundling. It seems reasonable that Cdc12 would possess an F-actin bundling domain, because (1) node condensation and mature CR formation require F-actin bundling (Laporte et al., 2012); and (2) node-localized Cdc12 is ideally positioned for this task (Coffman et al., 2009). Our data indicate that Cdc12 may cooperate with myosin in pulling F-actin into a ring structure (Fig. 3-18A) (Vavylonis et al., 2008), and this activity may be particularly useful for incorporating non-medial F-actin cables into the CR (Huang et al., 2012). Because Cdc12 F-actin bundling activity correlates with its C-terminal oligomeric state, the Sid2-based phosphoregulatory switch must be precisely timed; whereas delayed reversal of multimerization during late cytokinesis precipitates CR collapse, premature loss of multimerization during early mitosis jeopardizes F-actin bundling and CR formation.

Consistent with formin-mediated F-actin bundling shaping the cytokinetic cytoskeleton in diverse species, the mammalian cytokinetic formin mDia2 (Watanabe et al., 2008) also bundles F-actin (Esue et al., 2008; Harris et al., 2006; Machaidze et al., 2010). Though F-actin bundling formins have been identified in yeasts (Moseley and Goode, 2005; Scott et al., 2011), plants (Michelot et al., 2005; Xue et al., 2011; Yang et al., 2011; Zhang et al., 2011), flies (Barko et al., 2010), mammals (Esue et al., 2008; Harris et al., 2006; Machaidze et al., 2010; Vaillant et al., 2008), and parasites (Skillman et al., 2012), of these only mammalian FRL3 requires its C-terminus for F-actin bundling (Vaillant et al., 2008). Still, the C-termini of other formins have been shown to confer additional activities, including actin nucleation and severing (Chhabra and Higgs, 2006; Gould et al., 2011; Heimsath and Higgs, 2012). Thus, our identification of a C-terminal bundling domain builds on the notion that regions downstream of FH1FH2 domains can directly contribute to formin-mediated actin assembly. The separation of Cdc12's F-actin bundling and FH1FH2 domains likely facilitates exquisite temporal control of nucleating and bundling activities, and precludes competition between them. In the future, it should prove fruitful to determine the relationship between the Cdc12 C-terminus and Cdc12's FH1 and/or FH2 activities.

CHAPTER IV

CYTOKINESIS-BASED CONSTRAINTS ON POLARIZED CELL GROWTH IN FISSION YEAST

Introduction

Rod-shaped *S. pombe*, which undergoes cycles of monopolar-to-bipolar tip growth, is an attractive organism for studying cell cycle regulation of polarity establishment. Previous research had described factors mediating this process from interphase cell tips. Here, we demonstrate that division site signaling also impacts the re-establishment of bipolar cell growth in the ensuing cell cycle. Complete loss or targeted disruption of the non-essential cytokinesis protein Fic1 at the division site, but not at interphase cell tips, resulted in many cells failing to grow at new ends created by cell division. This appeared due to faulty disassembly and abnormal persistence of the cell division machinery at new ends of *fic1*Δ cells. Moreover, additional mutants defective in the final stages of cytokinesis exhibited analogous growth polarity defects, supporting that robust completion of cell division contributes to new end growth competency. To test this model, we genetically manipulated *S. pombe* cells to undergo NETO immediately after cell division. Intriguingly, such cells elongated constitutively at new ends unless cytokinesis was perturbed. Thus, cell division imposes constraints that partially override positive controls on growth. We posit that such constraints facilitate invasive fungal growth, as cytokinesis mutants displaying bipolar growth defects formed numerous pseudohyphae. Collectively, these data highlight a role for previous cell cycles in defining a cell's capacity to polarize at specific sites, and they additionally provide

insight into how a unicellular yeast can transition into a quasi-multicellular state.

Results

The *S. pombe* cytokinesis factor Fic1 promotes the establishment of bipolar cell growth

Recently, our laboratory identified Fic1, which was implicated in cytokinesis based on its protein and genetic interactions and its localization to the CR (Roberts-Galbraith et al., 2009). In addition to defects in cytokinesis, deletion of *S. pombe fic1*$^{+}$, which is a non-essential gene, resulted in an abnormally high percentage of cells that grew only from one end (i.e., monopolar cells) (Figs. 4-1A, 4-1B, and 4-1C). Tip growth was judged using calcofluor staining, as birth scars formed at previous division sites do not stain well with calcofluor and growth can be assessed using the position of these scars relative to cell tips (Fig. 4-1D) (Mitchison and Nurse, 1985). The growth defects observed upon *fic1*$^{+}$ disruption suggested that Fic1 not only participates in cytokinesis but also in the establishment of bipolar cell growth.

Although the upstream NETO factors Tea1 and Tea4 localized normally to both cell tips in *fic1Δ* cells (Figs. 4-2A and 4-2B), other cell tip proteins implicated in growth polarity regulation exhibited unusual localization patterns in this mutant. Unlike wild-type cells with mostly bipolar actin patch distribution (Figs. 4-2C and 4-2D), a variety of mutants defective in bipolar cell growth exhibit monopolar actin patches (Garcia et al., 2006; Glynn et al., 2001; Martin et al., 2005; Tatebe et al., 2005). As in such mutants, the actin patch marker Crn1-GFP (Pelham and Chang, 2001) accumulated preferentially at one cell end in a high percentage of *fic1Δ* cells (Figs. 4-2C and 4-2D). Signaling

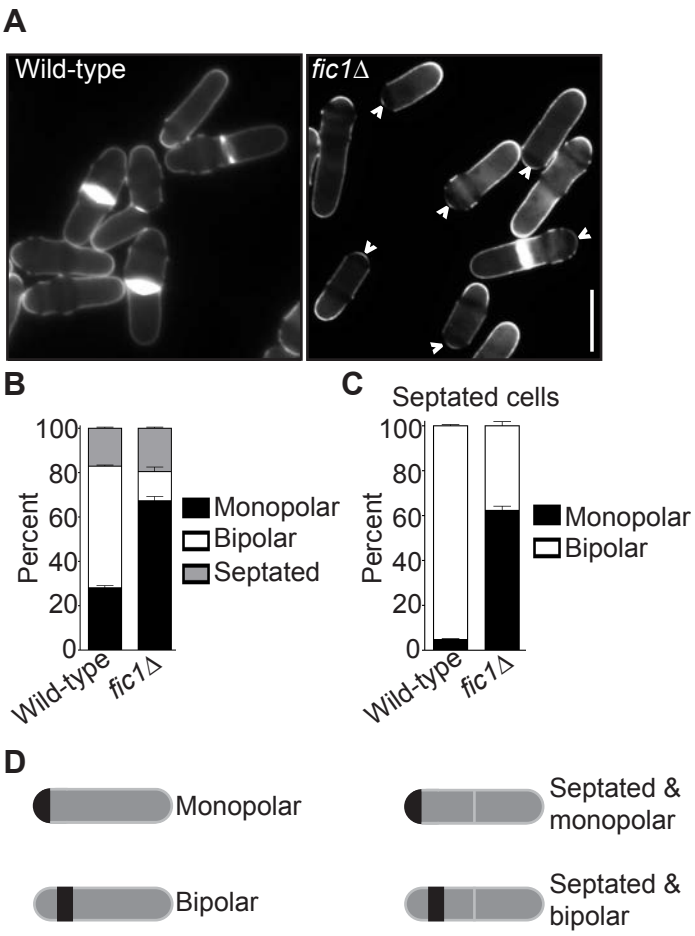

Figure 4-1

General growth polarity defects of *fic1Δ* cells.
(A) Live-cell images of calcofluor-stained wild-type and *fic1Δ* cells. Birth scars remain unstained and appear as dark bands across cells. Arrowheads indicate monopolar cells, i.e. cells that have only grown at one end, with birth scars abutting cell ends. (B) Quantification of (A), with three trials per genotype and n>300 for each trial. Data are presented as mean ± SEM for each category. (C) Quantification of septated cells in (A) and (B), with three trials per genotype and n>200 for each trial. Data are presented as mean ± SEM for each category. (D) Schematic of phenotypes scored by calcofluor staining. Black bands represent birth scars. (Bar = 5 μm)

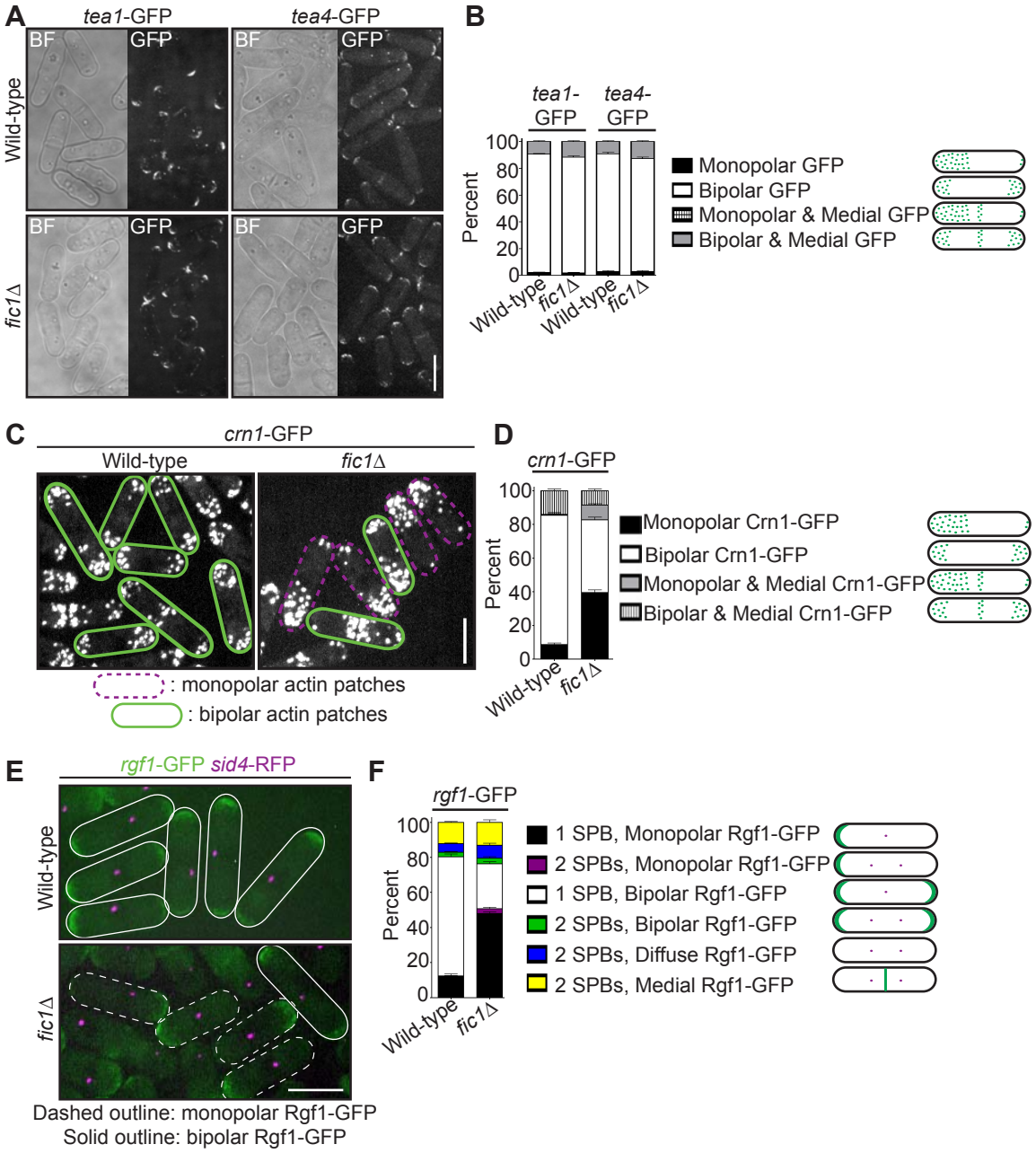

Figure 4-2

***fic1Δ* cells lack bipolarity of some cytoskeletal factors.**
(A) Live-cell bright field (BF) and GFP images of *tea1*-GFP, *tea4*-GFP, *fic1Δ tea1*-GFP, and *fic1Δ tea4*-GFP cells. (B) Quantification of (A), with three trials per genotype and n>200 for each trial. Data are presented as mean ± SEM for each category. (C) Live-cell GFP images of *crn1*-GFP and *fic1Δ crn1*-GFP cells. (D) Quantification of (C), with three trials per genotype and n>200 for each trial. Data are presented as mean ± SEM for each category. (E) Live-cell GFP (in green) and RFP (in magenta) merged images of *rgf1*-GFP *sid4*-RFP and *fic1Δ rgf1*-GFP *sid4*-RFP cells. (F) Quantification of (E), with three trials per genotype and n>200 for each trial. Data are presented as mean ± SEM for each category. (Bars = 5 μm)

through Rho GTPases controls actin patch organization in *S. pombe* (Arellano et al., 1997; Nakano et al., 2002), and the Rho1 activator Rgf1 (Garcia et al., 2006), which was GFP-tagged and imaged with the SPB marker Sid4-RFP (Chang and Gould, 2000), likewise predominated on one end of many *fic1Δ* cells (Figs. 4-2E and 4-2F). Not surprisingly, in both wild-type and *fic1Δ* cells, Rgf1-GFP and Crn1-RFP concentrated at the same ends (Fig. 4-3A), which were confirmed by calcofluor staining to be the growing ends of *fic1Δ* cells (Fig. 4-3B). Consistent with Fic1 affecting both actin and Rho networks, deletion of *fic1*$^{+}$ was synthetically sick with deletion of genes encoding factors involved in F-actin nucleation (WASp Wsp1) and Rho GTPase regulation (RhoGEF Rgf1 and RhoGAP Rga1) (Fig. 4-3C). Thus, we concluded that the absence of Fic1 upsets patterning of some but not all polarity factors.

To discern whether new and/or old ends were defective in resuming growth following cell division in *fic1Δ* cells, we performed time-lapse DIC imaging to trace birth scars in live cells. As expected, nearly all wild-type cells underwent NETO prior to subsequent septation (Figs. 4-4A and 4-4B). However, following roughly two-thirds of *fic1Δ* cell divisions, either one or both daughter cells failed to initiate new end growth prior to the next septation (Figs. 4-4A and 4-4C). The most predominant growth pattern in *fic1Δ* cells was that in which one daughter cell underwent NETO while the other did not (Figs. 4-4A and 4-4C), with nearly 70% of those daughter cells that did not exhibit NETO being the younger daughter cell. Unlike *tea1Δ* and *tea4*Δ cells, in which one daughter cell commonly fails at its new end and the other daughter cell fails at its old end (Fig. 4-4D) (Glynn et al., 2001; Martin et al., 2005; Tatebe et al., 2005), *fic1Δ* cells were specifically defective in the re-establishment of growth at new ends following cell

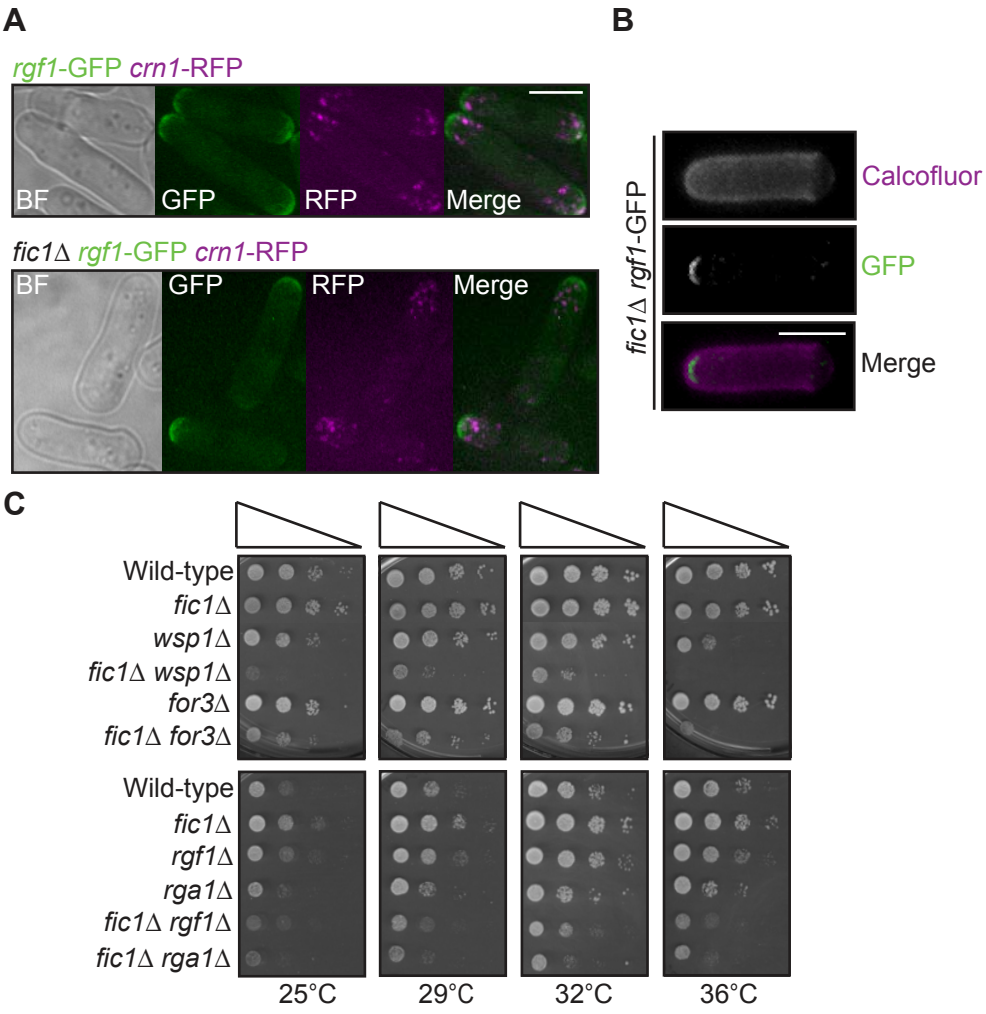

Figure 4-3

Actin and Rho signaling networks are simultaneously disrupted in *fic1Δ* cells.
(A) Live-cell bright field (BF), GFP (green), RFP (magenta), and GFP/RFP merged images of *rgf1*-GFP *crn1*-RFP and *fic1Δ rgf1*-GFP *crn1*-GFP cells. (B) Live cell calcofluor (magenta), GFP (green), and calcofluor/GFP merged images of a calcofluor-stained *fic1Δ rgf1*-GFP cell. (C) Serial 10-fold dilutions of cells of the indicated genotypes. (Bars = 5 μm)

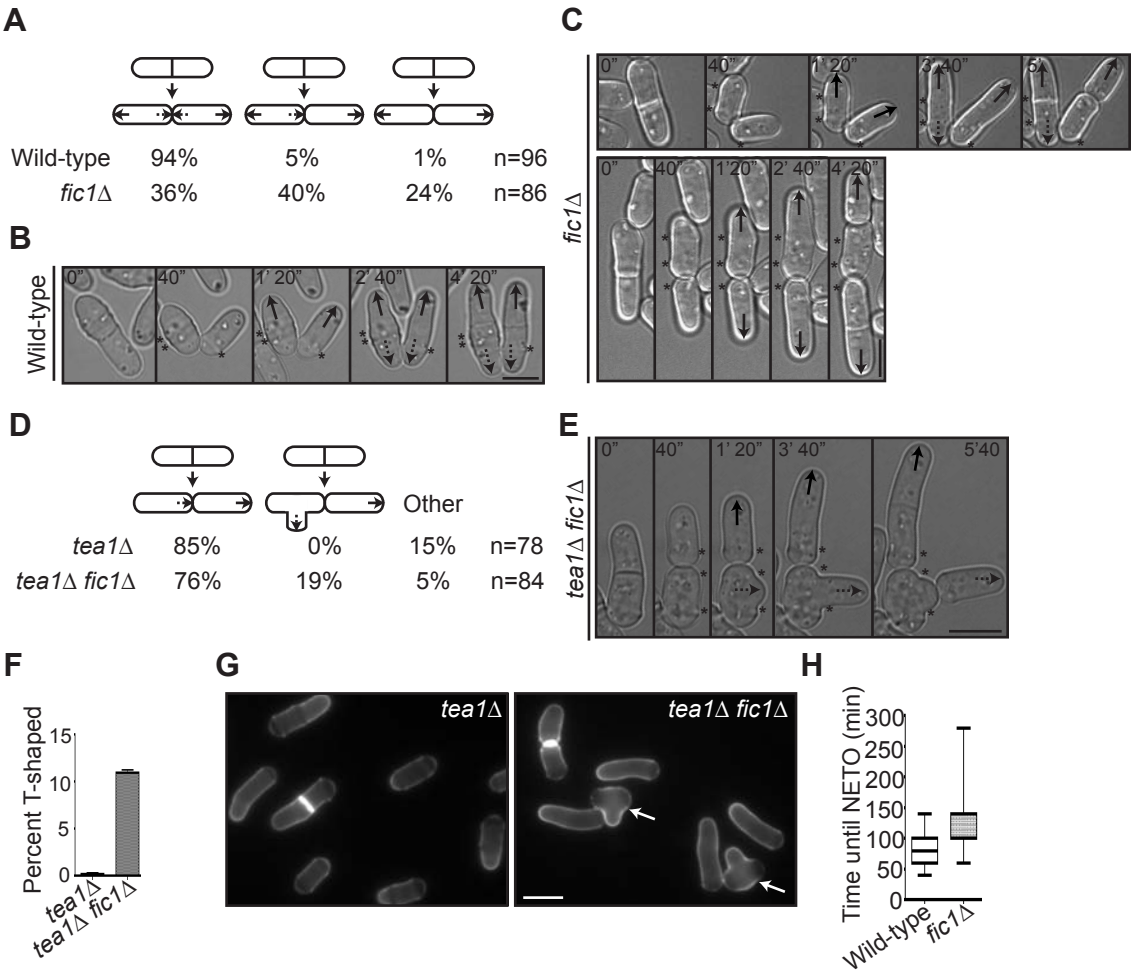

Figure 4-4

Growth polarity defects of *fic1Δ* cells are specific to new ends created by cytokinesis. (A) Quantification of growth patterns for wild-type and *fic1Δ* cells, with sample size (n) provided. (B-C) Live-cell DIC movies of wild-type or *fic1Δ* cells quantified in (A). Solid arrows denote old end growth, whereas dashed arrows indicate new end growth. Birth scars are marked by asterisks. Time points are noted. (D) Quantification of growth patterns for *tea1Δ* and *tea1Δ fic1Δ* cells, with sample size (n) provided. (E) Live-cell DIC movie of a *tea1Δ fic1Δ* cell that gives rise to a T-shaped daughter cell. The solid arrow denotes old end growth, whereas the dashed arrow indicates non-tip growth. Birth scars are marked by asterisks. Time points are noted. (F) Quantification of T-shaped cells in *tea1Δ* and *tea1Δ fic1Δ* strains grown at 25°C, with three trials per genotype and n>300 for each trial. Data are presented as mean ± SEM for each genotype. (G) Live-cell images of calcofluor-stained *tea1Δ* and *tea1Δ fic1Δ* cells grown at 25°C. Arrows indicate T-shaped cells. (H) Quantification of times from septum splitting to initiation of new end growth in cells that undergo NETO prior to the next septation in (A-C). Data are presented in box-and-whisker plots showing the median (line in the box), 25th-75th percentiles (box), and 5th-95th percentiles (whiskers) for each genotype. (Bars = 5 μm)

division (Figs. 4-4A and 4-4C). Intriguingly, *tea1Δ fic1Δ* double mutants grew mainly in a *tea1Δ* pattern, though nearly one-fifth of cell divisions produced a T-shaped daughter cell (Figs. 4-4D and 4-4E). Consistent with this, roughly 10% of *tea1Δ fic1Δ* cells were T-shaped at 25°C, while T-shaped *tea1Δ* cells were almost never observed at this temperature (Fig. 4-4F). T-shapes always arose in cells that the *tea1Δ* growth pattern dictated should grow at their new ends (Figs. 4-4D and 4-4E) but that actually grew at neither (Figs. 4-4E and 4-4G), suggesting these cells polarize at sites other than their tips because growth is inhibited at both ends. These data confirmed that the polarity defect caused by loss of Fic1 stochastically impacts new end growth in a variety of genetic backgrounds. Importantly, *fic1Δ* new ends that failed to extend in one cell cycle initiated growth as an old end in the next cell cycle, suggesting the defect in growth polarity caused by loss of Fic1 was not permanent. Consistent with a delay but not a block in growth, new ends that initiated growth prior to the next septation did so much later on average in *fic1Δ* cells than in wild-type cells (120 min vs 75 min) (Fig. 4-4H).

To test whether *fic1Δ*'s polarity defect was independent of S phase completion, we arrested *fic1Δ* cells in late G2 using *cdc25*-22, a temperature-sensitive allele of the phosphatase that activates cyclin-dependent kinase at the G2-M transition. As was previously observed (Mitchison and Nurse, 1985), otherwise wild-type cells blocked in G2 almost always underwent NETO (Figs. 4-5A and 4-5B). However, roughly half of *fic1Δ* cells remained monopolar (Figs. 4-5A and 4-5B), indicating that the *fic1Δ* polarity defect occurs irrespective of S phase completion. To test whether *fic1Δ* cells were too small to initiate NETO, we measured cell lengths at division. Though slightly shorter on average than wild-type cells (13.3 μm vs 15.3 μm), all *fic1Δ* cells were longer at division

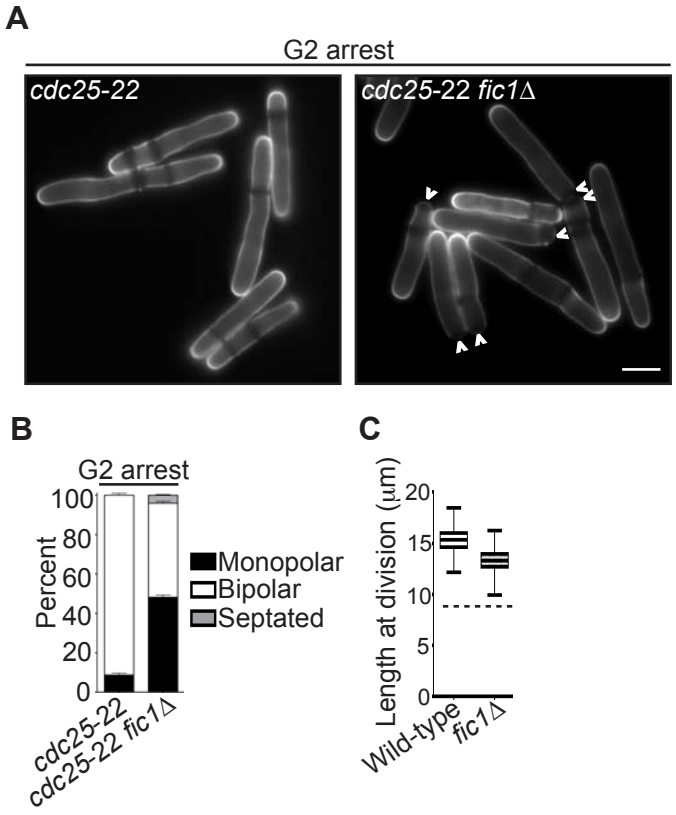

Figure 4-5

Growth polarity defects of *fic1Δ* cells occur irrespective of other NETO controls. (A) Live-cell images of calcofluor-stained *cdc25*-22 and *fic1Δ cdc25*-22 cells that had been arrested in G2. Arrowheads indicate monopolar cells. (B) Quantification of (A), with three trials per genotype and n>300 for each trial. Data are presented as mean ± SEM for each category. (C) Quantification of cell lengths at cell division, with n>200 for each genotype. Data are presented as box-and-whisker plots showing the median (line in the box), 25th-75th percentiles (box), and 5th-95th percentiles (whiskers) for each genotype. The dashed line represents the minimum length required for NETO. (Bar = 5 μm)

than the minimum length required for NETO (~9 μm) (Fig. 4-5C) (Mitchison and Nurse, 1985). Therefore, it is unlikely that the *fic1Δ* growth polarity defect is caused by reduced cell length. These data underscore that loss of Fic1 disrupts the establishment and timing of NETO independently of previously described cell cycle controls.

Fic1 protein-protein interactions at the CR support subsequent polarized cell growth at new ends

Though many cell polarity factors localize to the cell division site in addition to interphase cell tips, only the actions of these proteins at interphase cell tips have been demonstrated to be relevant to polarity regulation. As was observed previously (Roberts-Galbraith et al., 2009), cytoplasmic Fic1-GFP localizes to cell tips during interphase and later to the CR during cell division (Fig. 4-6A). We also detected another pool of Fic1-GFP lining the division site as the CR constricted (Fig. 4-6A). Given this localization pattern and the specific new end growth defect of *fic1Δ* cells, we asked whether Fic1 affected the timing of NETO via its functions at the cell division site.

Like *S. cerevisiae* Inn1 (Sanchez-Diaz et al., 2008), Fic1 is comprised of an N-terminal C2 domain and a C-terminal stretch of PxxP motifs (Fig. 4-6B). As was found for Inn1 (Nishihama et al., 2009; Sanchez-Diaz et al., 2008), the C-terminus of Fic1 ("Fic1C", amino acids 127-272), expressed from its endogenous locus and GFP-tagged, was sufficient for CR localization, as judged by co-localization with the CR protein Cdc15-mCherry (Fig. 4-6C). In contrast, a GFP-tagged N-terminal C2 domain fragment ("Fic1N", amino acids 1-126) was never observed at the CR (Fig. 4-6C) though it was produced *in vivo* (Fig. 4-6D). Importantly, medial-localizing Fic1C, unlike Fic1N, supported proper growth polarity establishment (Figs. 4-6E, 4-6F, and 4-6G), and, in

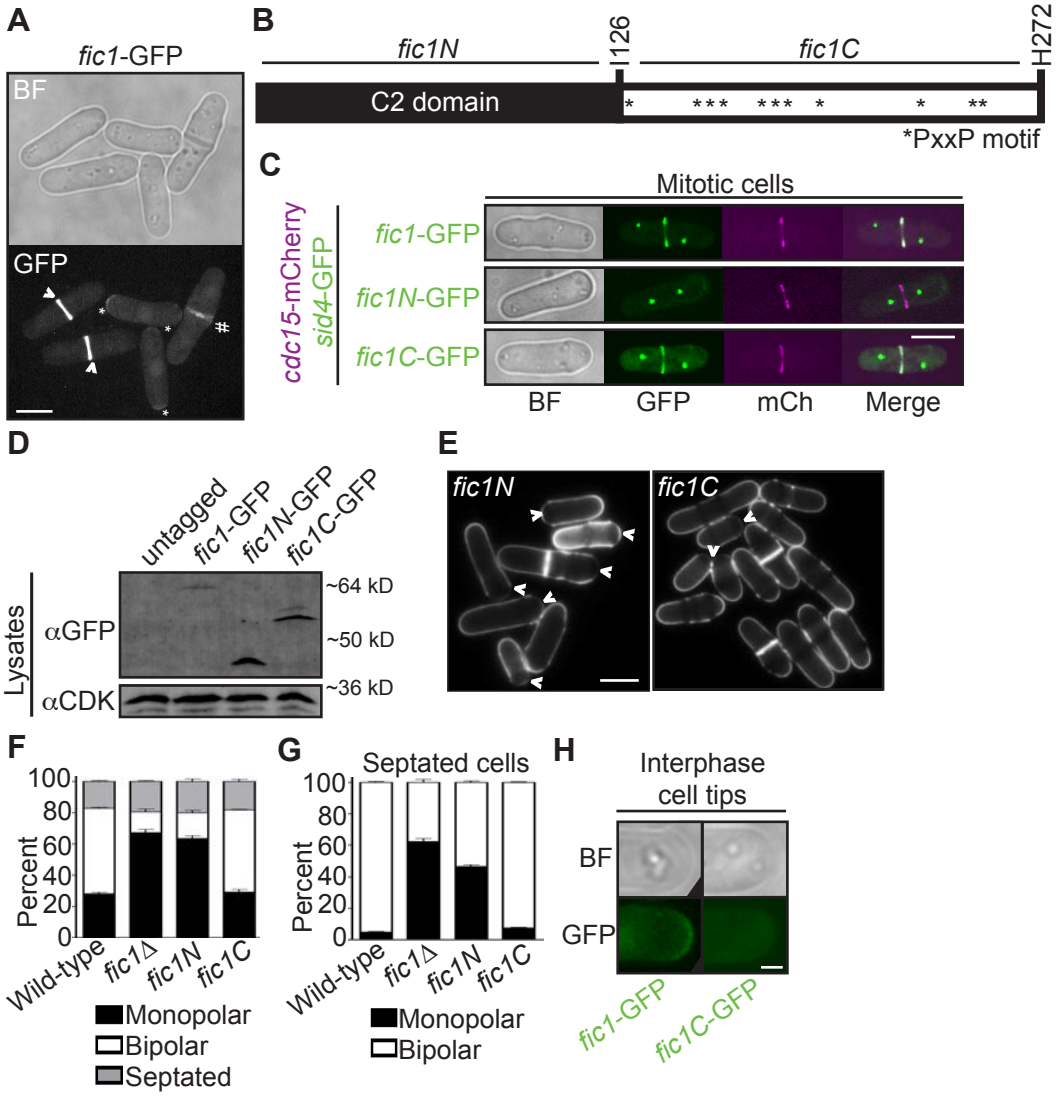

Figure 4-6

Fic1's C-terminus is necessary and sufficient for Fic1's polarity function at the division site.

(A) Live-cell bright field (BF) and GFP images of *fic1*-GFP cells. Localization to cell tips (*), the cytokinetic ring (>), and the division site (#) are marked. (B) Schematic of Fic1 protein domain organization. Residues and fragments of interest are marked. (C) Live-cell BF, GFP (green), mCherry (mCh) (magenta), and GFP/mCh merged images of *fic1*-GFP *sid4*-GFP *cdc15*-mCherry, *fic1N*-GFP *sid4*-GFP *cdc15*-mCherry, and *fic1C*-GFP *sid4*-GFP *cdc15*-mCherry cells. (D) Lysates from cells of the indicated genotypes were blotted with an anti-GFP antibody, as well as with anti-CDK as a loading control. (E) Live-cell images of calcofluor-stained *fic1N* and *fic1C* cells. Arrowheads indicate monopolar cells. (F) Quantification of (E), with three trials per genotype and n>300 for each trial. Data are presented as mean ± SEM for each category. (G) Quantification of septated cells in (E) and (F), with three trials per genotype and n>200 for each trial. Data are presented as mean ± SEM for each category. (H) Live-cell BF and GFP images of interphase cell tips of *fic1*-GFP and *fic1C*-GFP cells. [Bars = 5 μm, except for (H) where Bar = 1 μm]

contrast to full-length Fic1-GFP, Fic1C-GFP was not detected at tips of interphase cells (Fig. 4-6H). We thus concluded that Fic1, unlike other characterized growth polarity factors, does not exert its polarity function at cell tips during interphase, but instead does so at the cell division site during cytokinesis.

Because Fic1's C-terminus was necessary and sufficient for proper growth polarity, we examined whether protein-protein interactions at the CR mediated by Fic1's C-terminal PxxP motifs, which bind SH3 domains, govern Fic1's polarity function. Fic1 was originally identified based on its interaction with Cdc15's SH3 domain (Roberts-Galbraith et al., 2009). As would be expected if association of Cdc15 with Fic1's C-terminus is important in establishing the timing of NETO, calcofluor-stained *cdc15ΔSH3* cells, which are viable but lack Fic1-Cdc15 interaction (Roberts-Galbraith et al., 2009), exhibited growth polarity defects (Figs. 4-7A, 4-7B, and 4-7C).

To address the consequence of specifically disrupting Fic1-Cdc15 interaction, we determined which of Fic1's C-terminal PxxP motifs interact(s) with Cdc15's SH3 domain. Previous yeast-two hybrid data indicated Fic1 amino acids 190-269 mediate direct association with Cdc15's SH3 domain (Roberts-Galbraith et al., 2009). This region contains four of the eleven PxxP motifs within Fic1's C-terminus (Fig. 4-7D). To identify which are relevant for Cdc15 interaction, yeast two-hybrid assays using single and combinations of proline to alanine mutations were performed (Fig. 4-7E). Mutation of PxxPs 10 and 11 in combination, or P257 of PxxP 11 alone, abolished the two-hybrid interaction (Fig. 4-7E), and the P257A mutation eliminated co-immunoprecipitation of Fic1-$FLAG_3$ with Cdc15 *in vivo* (Fig. 4-7F). Supporting the idea that the Fic1-Cdc15 interaction is most relevant during cell division, co-immunoprecipitation of Fic1-$FLAG_3$

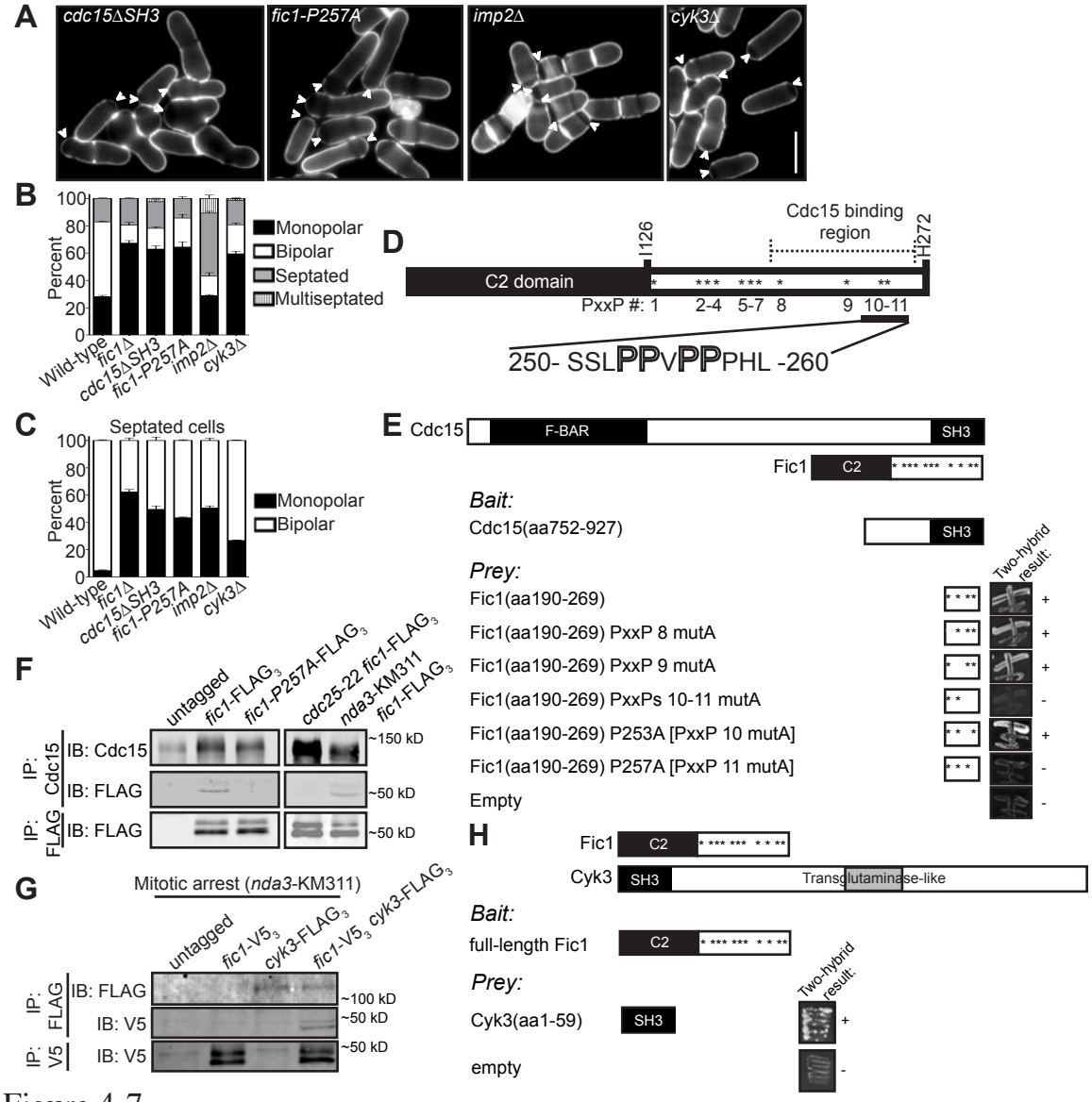

Figure 4-7

Fic1 protein-protein interactions at the CR guide growth polarity.
(A) Live-cell images of calcofluor-stained *cdc15ΔSH3*, *fic1-P257A*, *imp2Δ*, and *cyk3Δ* cells. Arrowheads indicate monopolar cells. (B) Quantification of (A), with three trials per genotype and n>300 for each trial. Data are presented as mean ± SEM for each category. (C) Quantification of septated cells in (A) and (B), with three trials per genotype and n>300 for each trial. Data are presented as mean ± SEM for each category. (D) Schematic of Fic1, with residues of interest marked, PxxP motifs (*) numbered, the Cdc15-binding region indicated, and the sequence spanning the terminal two PxxPs given. (E) Yeast two-hybrid identification of the Cdc15 binding site on Fic1. P253A and P257A mutations were used to distinguish between PxxPs 10 and 11 as the motif responsible for Cdc15 binding. (F) Anti-Cdc15 and anti-FLAG immunoprecipitates from cells of the indicated genotypes were blotted with anti-Cdc15 and/or anti-FLAG antibodies. *cdc25*-22 cells and *nda3*-KM311 cells were arrested in G2 and prometaphase, respectively, prior to pelleting and lysis. (G) Anti-FLAG and anti-V5 immunoprecipitates from prometaphase-arrested cells of the indicated genotypes were blotted with anti-FLAG and/or anti-V5 antibodies. (H) Yeast two-hybrid identification of the Fic1 binding to Cyk3's SH3 domain. (Bar = 5 μm)

with Cdc15 was considerably stronger in mitosis than in interphase (Fig. 4-7F). This is similar to other Cdc15 protein-protein interactions, which become enriched upon Cdc15 dephosphorylation at mitosis (Roberts-Galbraith et al., 2010). *fic1-P257A* cells exhibited monopolar growth defects similar to *fic1Δ* and *cdc15ΔSH3* cells (Figs. 4-7A, 4-7B, and 4-7C), confirming that binding of Fic1's C-terminus to Cdc15 is critical for Fic1's polarity function.

To corroborate that PxxP-mediated protein-protein interactions at the CR play a predominant role in Fic1's polarity function, we tested whether other interactors participate in *S. pombe* polarity regulation. The SH3 protein Imp2 has previously been shown to function redundantly with Cdc15 and bind Fic1 during cytokinesis (Roberts-Galbraith et al., 2009). Consistent with additional Fic1 interactions guiding growth polarity, loss of Imp2 also severely compromised bipolar cell growth (Figs. 4-7A, 4-7B, and 4-7C). In *S. cerevisiae*, the Fic1 ortholog Inn1 binds to another SH3 protein, Cyk3 (Jendretzki et al., 2009; Nishihama et al., 2009), and complexing of these two proteins with the Cdc15 homolog Hof1 has been suggested to direct septum formation and cell separation (Nishihama et al., 2009). We found that *S. pombe* Cyk3 co-immunoprecipitated with Fic1 in mitosis (Fig. 4-7G), and we also detected direct interaction between S. *pombe* Cyk3's SH3 domain and Fic1 via yeast two-hybrid (Fig. 4-7H). Accordingly, these interactions appear to be conserved. Consistent with these proteins performing a common function, loss of Cyk3 resulted in growth polarity defects similar to those seen upon loss of Fic1 or its interaction with Cdc15 or Imp2 (Figs. 4-7A, 4-7B, and 4-7C). Thus, Fic1 collaborates with associated proteins at the CR to execute

its growth polarity function, and we postulate that its C-terminus acts as an adaptor molecule for SH3 proteins to ensure integration of distinct processes during cytokinesis.

Loss of Fic1 impedes CR disassembly and leads to persistence of factors at the division site

To discern how loss of Fic1 scaffold function during cytokinesis impacts subsequent new end growth, we next defined what aspects of cytokinesis are perturbed in *fic1Δ* cells. Previous data demonstrated that *fic1Δ* was synthetically lethal with *sid2*-250 (Roberts-Galbraith et al., 2009), a temperature-sensitive allele of the SIN kinase Sid2. Consistent with Fic1 and associated factors working in parallel to the SIN, we found that *fic1Δ* and *cyk3Δ* suppressed the hyperactive SIN allele *cdc16*-116 (Fig. 4-8A), and that *fic1*Δ and *cyk3Δ* were synthetically sick or lethal with a variety of SIN alleles conferring loss of SIN function (Figs. 4-8A and 4-8B). These genetic data implied that Fic1 most likely functions during late stages of cytokinesis. In line with this idea, the percentage of *fic1Δ* cells that had undergone ingression but were still joined at their division sites was more than four times that of wild-type cells (Figs. 4-8C and 4-8D). When cells were arrested in G2 using the *cdc25*-22 allele, this difference increased, with the percentage of joined cells roughly 15 times greater in the absence of Fic1 (Figs. 4-8C and 4-8D). Similar to *S. cerevisiae inn1Δ* cells (Nishihama et al., 2009) and *S. pombe cdc15ΔSH3* cells (Roberts-Galbraith et al., 2009), many G2-arrested *fic1Δ* daughter cells that were still joined at division sites exhibited membranous bridges (Fig. 4-8E). These findings verified that the completion of cell division is perturbed in the absence of Fic1.

Consistent with early cytokinesis events proceeding appropriately without Fic1, time-lapse imaging of myosin regulatory light chain Rlc1-GFP (Le Goff et al., 2000;

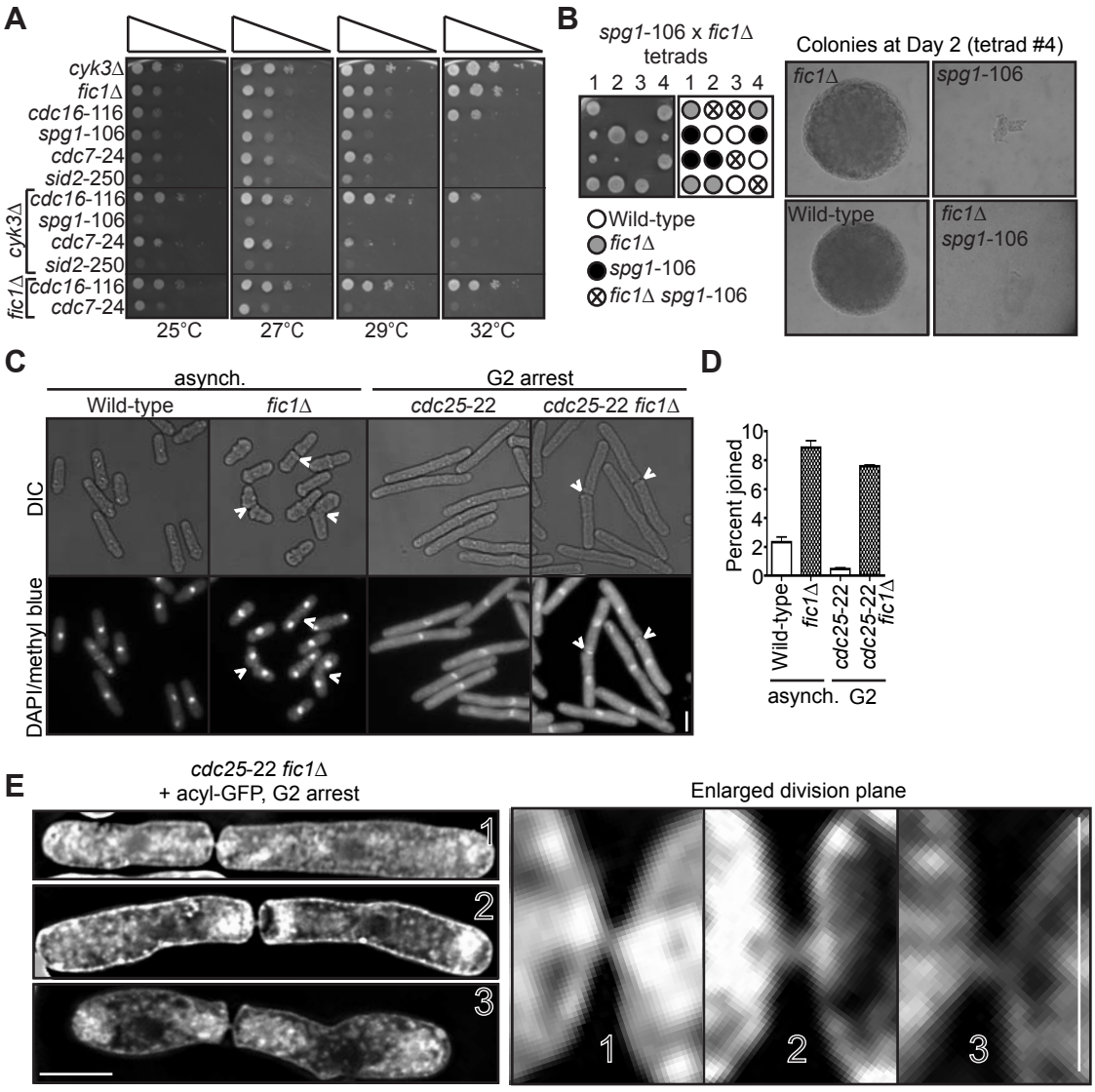

Figure 4-8

The completion of cell division is perturbed in *fic1Δ* cells.
(A) Serial 10-fold dilutions of cells of the indicated genotypes. Mutation of *cdc16* causes SIN hyperactivation, whereas mutants of *spg1*, *cdc7*, or *sid2* exhibit loss of SIN function. (B) *fic1Δ* and *spg1*-106 were mated, and tetrads were pulled on YE agar at 25°C. Genotypes were assessed by replica plating to YE agar at 36°C and to minimal medium lacking uracil. Images of colonies from a tetratype are also given. (C) Fixed-cell DIC and DAPI/methyl blue images of asynchronous and G2-arrested cells of the indicated genotypes. Arrowheads indicate cells that are still joined following ingression. (D) Quantification of (C), with four trials per genotype and n>300 for each trial. Percentages are presented as mean ± SEM. (E) Fixed-cell GFP images of G2-arrested *cdc25-22 fic1Δ* cells expressing acyl-GFP. Enlarged images of cells' division planes are also given. [Bars = 5 μm, except for enlarged regions in (E) where Bar = 2 μm]

Naqvi et al., 2000) with Sid4-GFP revealed that the CR formed and constricted normally in *fic1Δ* cells (Figs. 4-9A and 4-9B). However, at the termination of CR constriction, parts of the CR persisted at the division plane (Figs. 4-9C, 4-9D, and 4-9E). During cytokinesis, the septum closes behind the constricting CR, and septum closure can be visualized using the β-glucan synthase GFP-Cps1 (Cortes et al., 2002; Liu et al., 2002). As cytokinesis progresses, two GFP-Cps1 dots marking the leading edge of the septum can be seen getting progressively closer in the division plane, and these dots eventually join into one just as the CR completes constriction (Fig. 4-9D). We found that Rlc1-mCherry$_3$ remained at the division site following septum closure on average longer in *fic1Δ* cells compared to wild-type cells (22 min vs 8 min) (Figs. 4-9C and 4-9D). Consistent with these remnants representing the CR as a whole and not just Rlc1, phalloidin staining revealed atypical actin-rich masses, in addition to normal actin patches, flanking septa in *fic1Δ* cells (Fig. 4-9E). Thus, we concluded that the CR does not disassemble properly at the conclusion of cell division in *fic1Δ* cells.

In addition to CR-associated factors, glucanase Eng1-GFP (Martin-Cuadrado et al., 2003) persisted at ingressed division sites significantly longer in *fic1Δ* cells compared to wild-type cells (on average, 51 min vs 21 min) (Figs. 4-10A and 4-10B). Because glucanases execute septum degradation (Dekker et al., 2004; Martin-Cuadrado et al., 2003), these data suggest that cell wall turnover is inefficient at *fic1Δ* septa. We thus concluded that loss of Fic1 jeopardized the completion of cell division, stalling remodeling of new ends in the next cell cycle.

Mutants with late cytokinesis defects likewise exhibit new end growth polarity errors

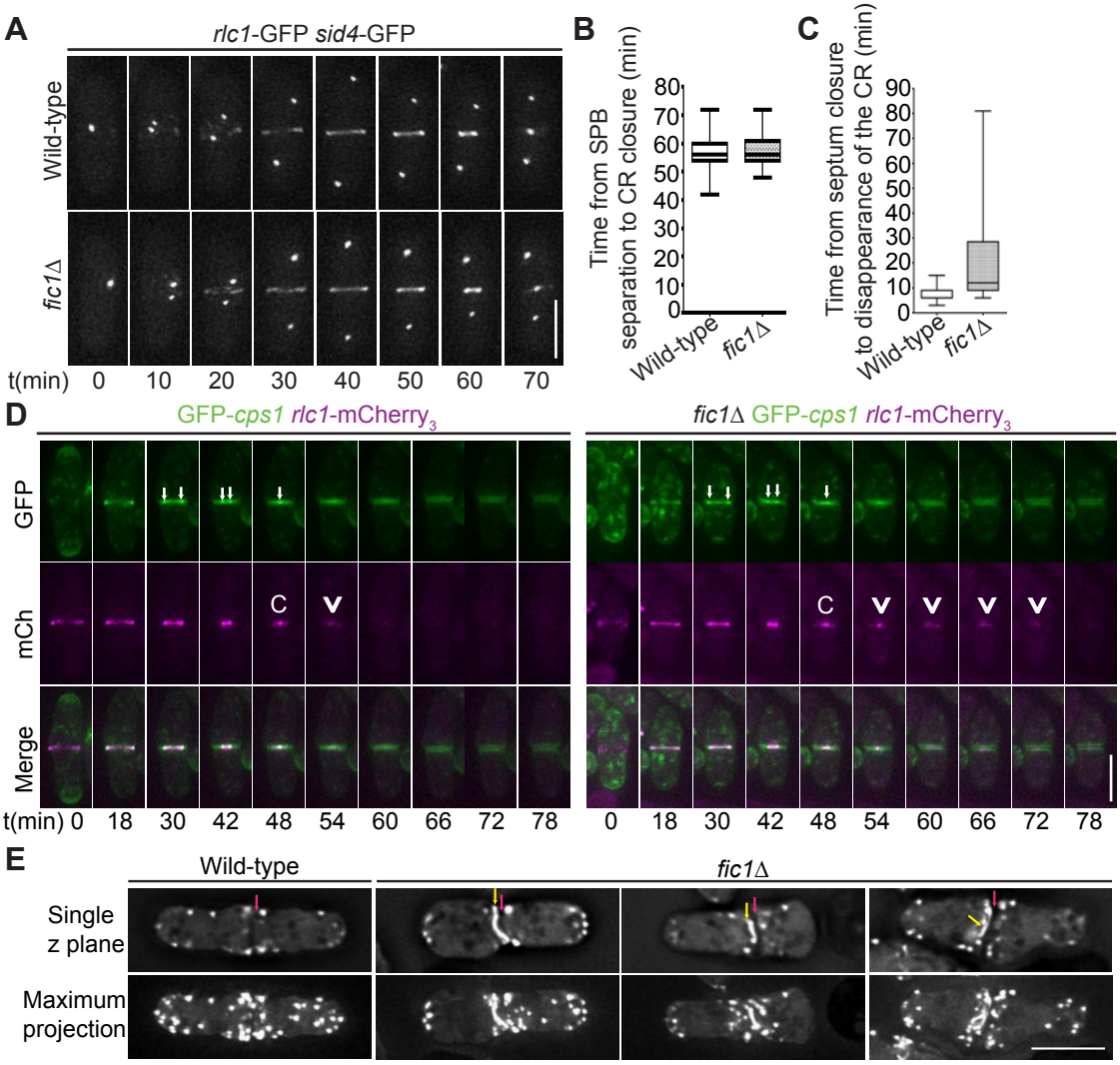

Figure 4-9

The CR does not disassemble properly following CR constriction in *fic1Δ* cells.
(A) Live-cell GFP movies of *rlc1*-GFP *sid4*-GFP and *fic1Δ rlc1*-GFP *sid4*-GFP cells. (B) Quantification of times from spindle pole body (SPB) separation to the completion of CR constriction in (A). n>20 for each genotype. Data are presented in box-and-whisker plots showing the median (line in the box), 25th-75th percentiles (box), and 5th-95th percentiles (whiskers) for each genotype. (C) Quantification of times from septum closure to disappearance of the CR at the division site for GFP-*cps1 rlc1*-mCherry$_3$ and *fic1Δ* GFP-*cps1 rlc1*-mCherry$_3$ cells. n>30 for each genotype. Data are presented in box-and-whisker plots showing the median (line in the box), 25th-75th percentiles (box), and 5th-95th percentiles (whiskers) for each genotype. (D) Live-cell GFP (green) and mCherry (mCh) (magenta) movies of GFP-*cps1 rlc1*-mCherry$_3$ and *fic1Δ* GFP-*cps1 rlc1*-mCherry$_3$ cells, with time intervals indicated and GFP/mCh images merged. White arrows in GFP images mark the septa's leading edges. The time point with only one arrow drawn marks septum closure. In the mCh images, "C" marks the point of CR closure, and arrowheads denote CR remnants persisting after this point. (E) Fixed-cell images of actin stained with Alexa Fluor 488 Phalloidin. Single z planes and maximum projections of multiple z planes are given. Red arrows indicate division planes, whereas yellow arrows indicate unusual actin masses lining the division plane. (Bars = 5 μm)

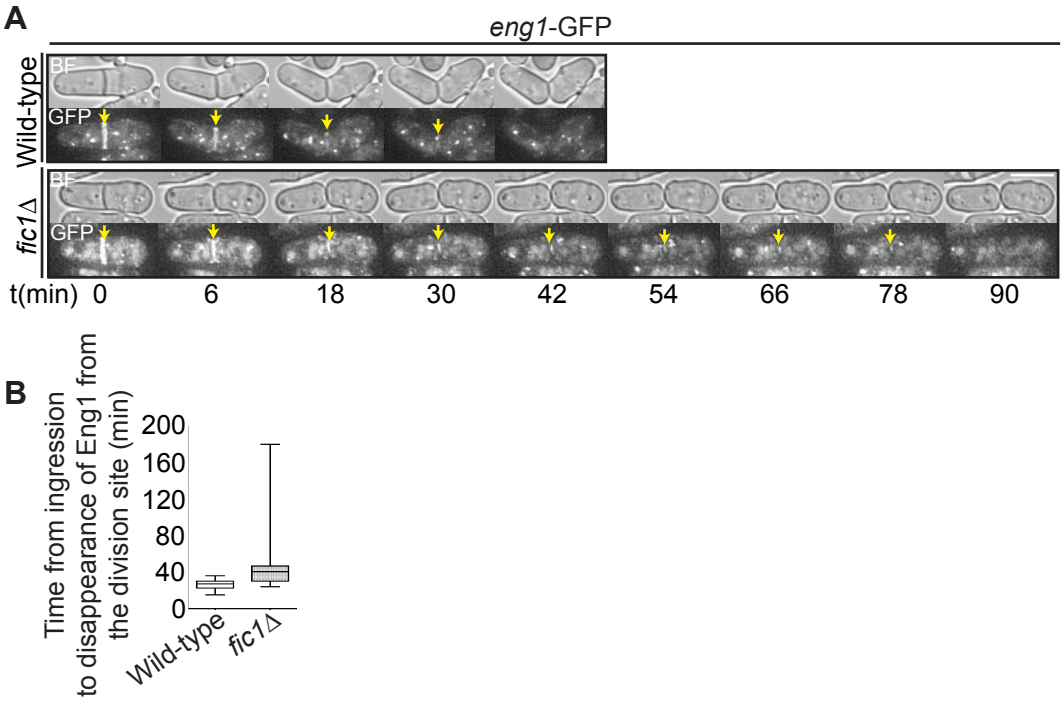

Figure 4-10

Cell wall remodeling is also delayed at the division site of *fic1Δ* cells.
(A) Live-cell bright field (BF) and GFP movies of *eng1*-GFP and *fic1Δ eng1*-GFP cells. Yellow arrows denote Eng1-GFP at the division site. (B) Quantification of times from ingression to Eng1-GFP disappearance from the division plane in movies scored in (A), with n>15 for each genotype. Data are presented in box-and-whisker plots showing the median (line in the box), 25th-75th percentiles (box), and 5th-95th percentiles (whiskers) for each genotype. (Bar = 5 μm)

Because faulty cytokinesis led to persistence of parts of the cell division machinery at *fic1Δ* division planes, we speculated that these remnants might deter subsequent polarized growth at new ends. If this were the case, one would expect other mutants with late cytokinesis defects to also show erroneous new end growth. Previous data had indicated that Fic1-associated Imp2 contributes to CR disassembly, with *imp2Δ* cells exhibiting abnormal actin structures flanking previous division sites (Demeter and Sazer, 1998). Though we had shown that *imp2Δ* cells are defective in bipolar cell growth (Figs. 4-7A, 4-7B, and 4-7C), we wanted to confirm that their growth defect was specific to new ends. Using time-lapse DIC imaging, we found that roughly 75% of *imp2Δ* cell divisions produced at least one daughter cell that failed at new end growth (Fig. 4-11A). Interestingly, both *imp2Δ* daughter cells failed at new end growth in the majority of cases (Figs. 4-11A and 4-11B). Therefore, proper disassembly of CR components correlates with new end competency for polarized growth.

In addition to showing CR disassembly defects, *fic1Δ* cells also exhibited delays in septum remodeling at the division site. We therefore tested if disruption of septum degradation could likewise impact polarized growth. Loss of Eng1 or its cooperating glucanase, Agn1 (Dekker et al., 2004), resulted in high percentages of monopolar growth (Figs. 4-11C and 4-11D). Moreover, the growth defect of *eng1Δ* daughter cells was specific to new ends (Figs. 4-11A and 4-11B). Anillin-like Mid2 and the septin ring, of which Spn1 and Spn4 form the core (An et al., 2004), target these glucanases into a ring structure around septa (Martin-Cuadrado et al., 2005). Loss of any of these proteins likewise impaired bipolar cell growth (Figs. 4-11C and 4-11D). In addition, the majority of *spn1Δ* daughter cells failed at new end growth (Figs. 4-11A and 4-11B). We therefore

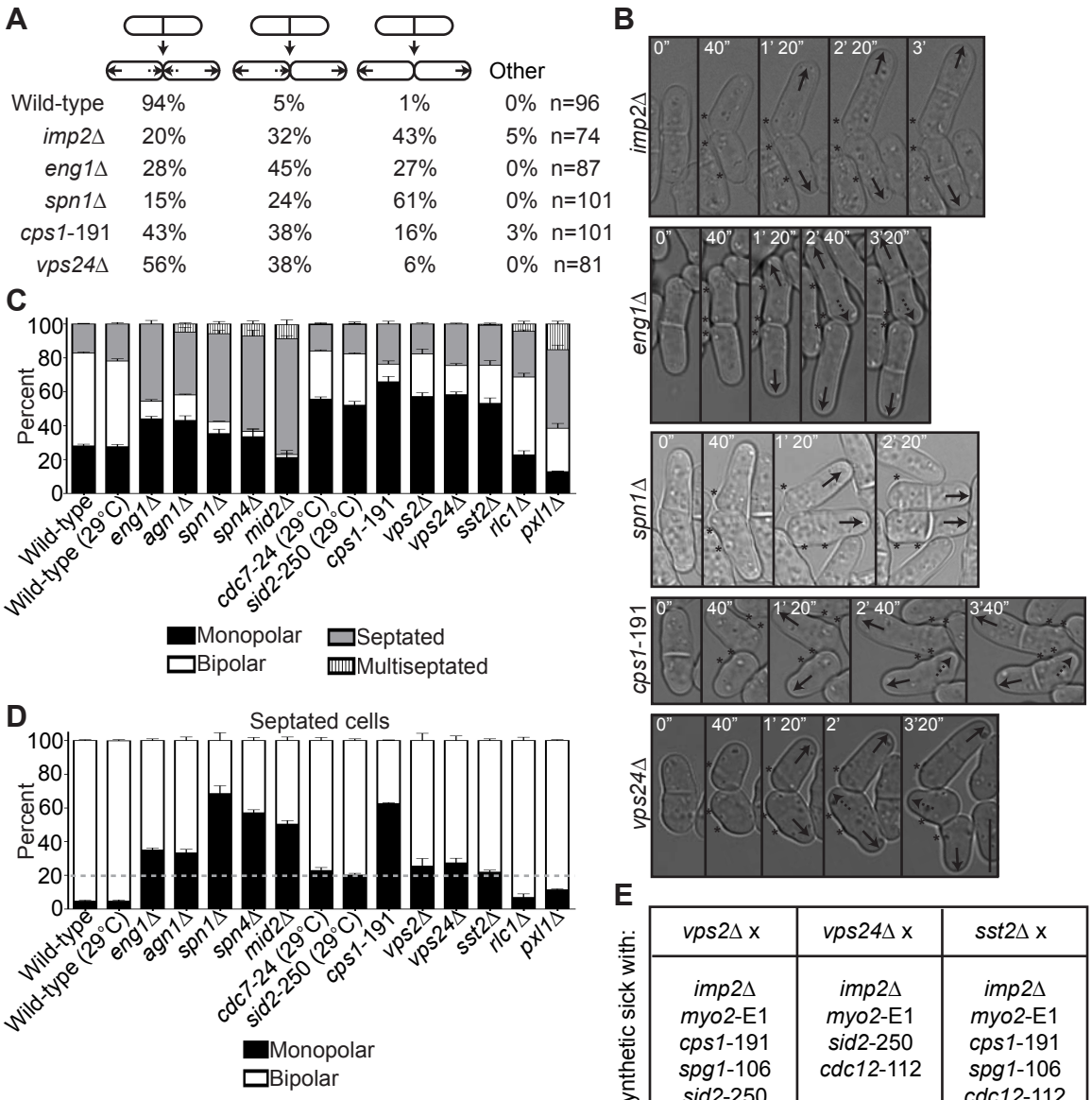

Figure 4-11

Late cytokinesis mutants phenocopy *fic1Δ*'s new end growth defect.

(A) Quantification of growth patterns for cells of the indicated genotypes. Sample size (n) is provided for each genotype. (B) Live-cell DIC movies of cells of the indicated genotypes scored in (A). The most prevalent faulty growth pattern for each genotype is pictured. Solid arrows denote old end growth, whereas dashed arrows indicate new end growth. Birth scars are marked by asterisks. Time points are noted. (C) Quantification of polarity phenotypes of calcofluor-stained cells of the indicated genotypes, with three trials per genotype and n>300 for each trial. Data are presented as mean ± SEM for each category. All cells were grown at 25°C unless otherwise noted. (D) Quantification of septated cells in (C), with three trials per genotype and n>200 for each trial. Data are presented as mean ± SEM for each category. A dashed gray line marks 20% on the y-axis. (E) Table of negative genetic interactions between deletion of genes encoding ESCRT-related proteins (ESCRT-III components Vps2 and Vps24, and ESCRT-III-associated deubiquitinase Sst2) and deletion/loss-of-function alleles of genes encoding cytokinesis factors (Imp2, myosin Myo2, β-glucan synthase Cps1, SIN GTPase Spg1, SIN kinase Sid2, and formin Cdc12). (Bar = 5 μm)

concluded that defective completion of cell wall remodeling at the division site, in addition to improper disassembly of CR components, compromises NETO efficiency.

The SIN coordinates many aspects of CR and septum regulation during late cytokinesis. Not only does SIN signaling oversee maintenance of a mature, homogenous CR (Hachet and Simanis, 2008), it mediates Cps1 targeting and accumulation at the division site (Cortes et al., 2002; Liu et al., 2002). Loss of SIN signaling during cytokinesis can thus lead to CR fragmentation (Hachet and Simanis, 2008) and abortive septation (Cortes et al., 2002). Given these phenotypes and the synthetic genetic interactions between *fic1Δ* and SIN mutants (Figs. 4-9A and 4-9B), we examined the relevance of the SIN to new end growth control. Temperature-sensitive alleles of genes encoding the SIN kinases Cdc7 and Sid2 caused mild but statistically significant growth polarity defects at semi-restrictive temperature (Figs. 4-11C and 4-11D). A temperature-sensitive allele of the gene encoding Cps1, which functions downstream of the SIN, caused dramatic defects in establishing bipolar cell growth even at permissive temperature (Figs. 4-11C and 4-11D). Additionally, a high proportion of *cps1*-191 cells failed specifically at new end growth (Figs. 4-11A and 4-11B).

Currently, the mechanism of membrane remodeling and scission at the *S. pombe* division site is unclear. In a variety of other organisms, ESCRT-III factors contribute to this process (Peel et al., 2011). ESCRT-III components have not been implicated in *S. pombe* cytokinesis regulation, though ESCRT-III-associated AMSH (*S. pombe* Sst2) localizes to the division site (Kouranti et al., 2010). We found that deletions of genes encoding ESCRT-III components Vps2 and Vps24 or ESCRT-III-associated Sst2 were synthetically sick with a variety of loss-of-function cytokinesis alleles, including *imp2Δ*

and *cps1*-191 (Fig. 4-11E). Interestingly, loss of Vps2, Vps24, or Sst2 resulted in monopolar percentages significantly greater than observed for wild-type cells (Figs. 4-11C and 4-11D), and nearly half of *vps24Δ* cell divisions resulted in one or both daughter cells that failed at new end growth prior to the next septation (Figs. 4-11A and 4-11B). Though these phenotypes were less penetrant than in other mutants, we speculate that ESCRT-III function guides membrane remodeling at the conclusion of *S. pombe* cell division to impact new end polarized growth.

Of note, deletion of *rlc1*$^{+}$ or paxillin *pxl1*$^{+}$, which function primarily in early actomyosin function at the CR (Ge and Balasubramanian, 2008; Le Goff et al., 2000; Naqvi et al., 2000; Pinar et al., 2008), did not alter growth polarity percentages as significantly as other mutations or deletions (Figs. 4-11C and 4-11D). Indeed, less than half of non-septated *rlc1Δ* and *pxl1Δ* cells were monopolar (Fig. 4-11C), and the monopolar septated percentages of these genotypes were more similar to wild-type percentages than were those of the other mutants examined (Fig 4-11D). We therefore concluded that early steps in cytokinesis do not impact subsequent polarized cell growth as much as the terminal steps in cell division.

Ineffective cytokinesis partially impedes new end tip growth even upon constitutive NETO signaling

If faithful remodeling of the division site is important for growth competency of new ends, then one would expect that prematurely triggering NETO signaling just after cell division should not fully rescue the growth polarity defects of late cytokinesis mutants. To test this, we constructed a mutant that would undergo constitutive NETO. As over-expression of a fusion protein linking cell tip-associated Tea1 with formin For3

induces NETO in G1 (Martin et al., 2005), we integrated a Tea1-For3 fusion (Fig. 4-12A) into the endogenous *tea1*$^{+}$ locus and deleted the single copy of the *for3*$^{+}$ gene. We confirmed that the Tea1-For3 fusion protein was produced *in vivo* (Fig. 4-12B) and verified that this fusion was sufficient to induce NETO in a *cdc10*-V50 G1 arrest (Figs. 4-12C and 4-12D). As previously reported (Feierbach et al., 2004), double deletion of *tea1*$^{+}$ and *for3*$^{+}$ resulted in general cell rounding (Fig. 4-12E). However, expression of the Tea1-For3 fusion protein in the absence of Tea1 and For3 individually caused cells to regain their rod-shaped appearance (Fig. 4-12E). Intriguingly, a high percentage of *tea1-for3* cells were either septated or exhibited cytokinesis defects (Figs. 4-12E and 4-12F), and *tea1-for3* cells were significantly longer at division than wild-type cells (on average, 18.3 μm vs 15.3 μm) (Figs. 4-12E and 4-12G). Thus, though the endogenous Tea1-For3 fusion protein functioned in prematurely triggering NETO, it also affected cell division.

To analyze *tea1-for3* cells in real-time, we performed time-lapse DIC imaging. As expected, most *tea1-for3* cells underwent NETO before the next cell division (Fig. 4-13A), with nearly 75% of new ends initiating growth within 50 minutes of septum splitting (Fig. 4-13B). Nonetheless, some *tea1-for3* outliers took much longer to extend at tips created by cell division (Fig. 4-13B). After grouping the times needed for tip growth to occur at previous division sites relative to the amount of time needed for the mother cell to complete cytokinesis, we found that newly-formed tips that took longer to initiate growth had been formed by more inefficient cytokinesis (Figs. 4-13C and 4-13D). As distal tip growth continued in cells undergoing division (Fig. 4-13D) and appeared unimpeded by additional factors, these findings suggested that faulty cytokinesis imposes constraints at previous division sites that counteract positive polarizing cues. We

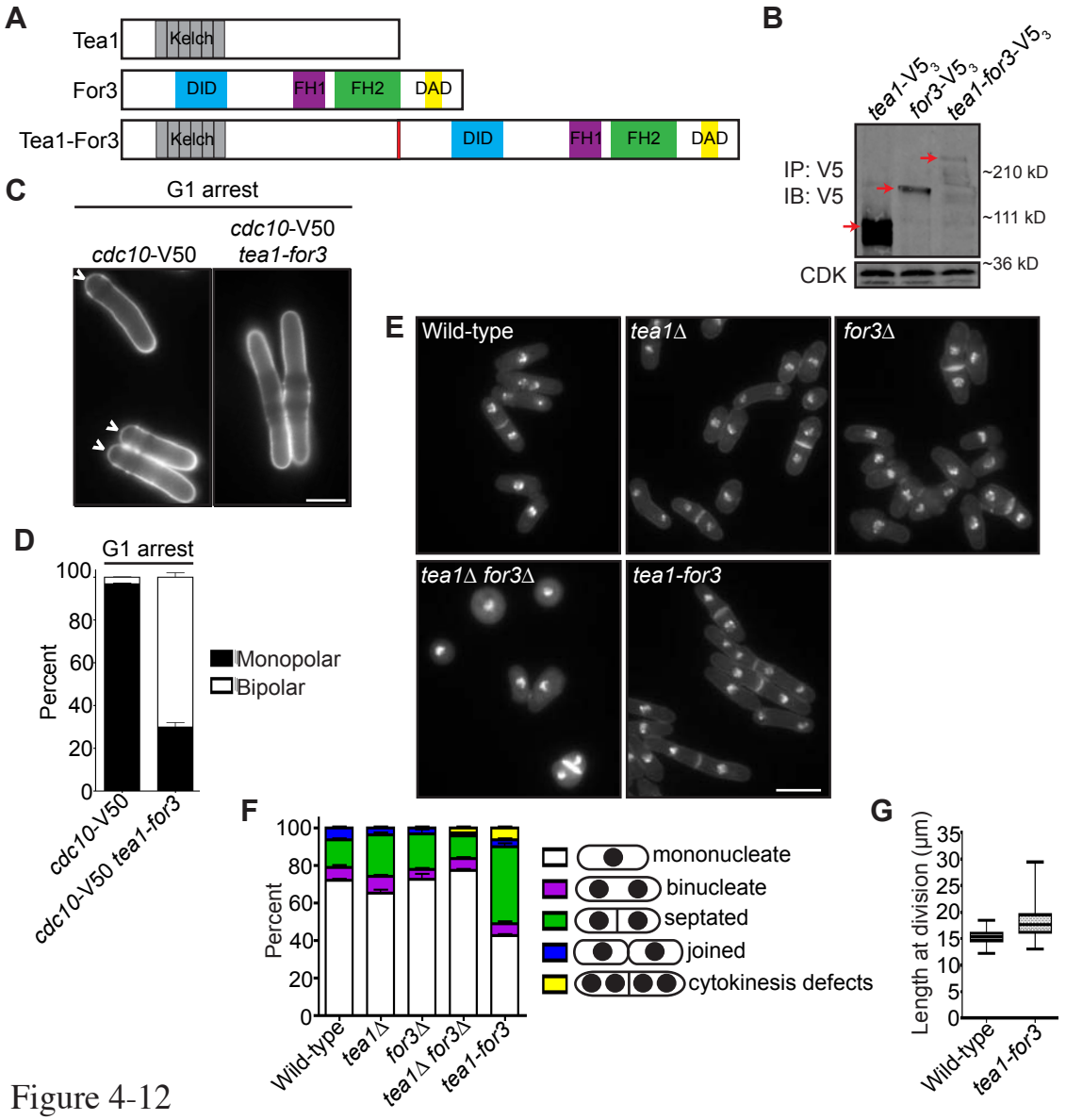

Figure 4-12

An endogenous Tea1-For3 fusion protein induces premature NETO but also impinges on cell division.

(A) Schematic of Tea1, For3, and Tea1-For3 proteins. (B) Anti-V5 immunoprecipitates from asynchronous *tea1*-V5$_3$, *for3*-V5$_3$, and *tea1-for3*-V5$_3$ cells were blotted with anti-V5 antibodies. Arrows indicate full-length proteins. Lysates were blotted with anti-CDK as a loading control. (C) Live-cell images of calcofluor-stained *cdc10*-V50 and *cdc10*-V50 *tea1-for3* cells arrested in G1. Arrowheads indicate monopolar cells. (D) Quantification of (C), with three trials per genotype and n>300 for each trial. Data are presented as mean ± SEM for each category. (E) Fixed-cell DAPI/methyl blue images of stained wild-type, *tea1Δ*, *for3Δ*, *tea1Δ for3Δ*, and *tea1-for3* cells. (F) Quantification of phenotypes of cells in (D), with three trials per genotype and n>300 for each trial. Data are presented as mean ± SEM for each category. (G) Quantification of cell lengths at cell division, with n>200 for each genotype. Data are presented as box-and-whisker plots showing the median (line in the box), 25th-75th percentiles (box), and 5th-95th percentiles (whiskers) for each genotype.(Bars = 5 μm)

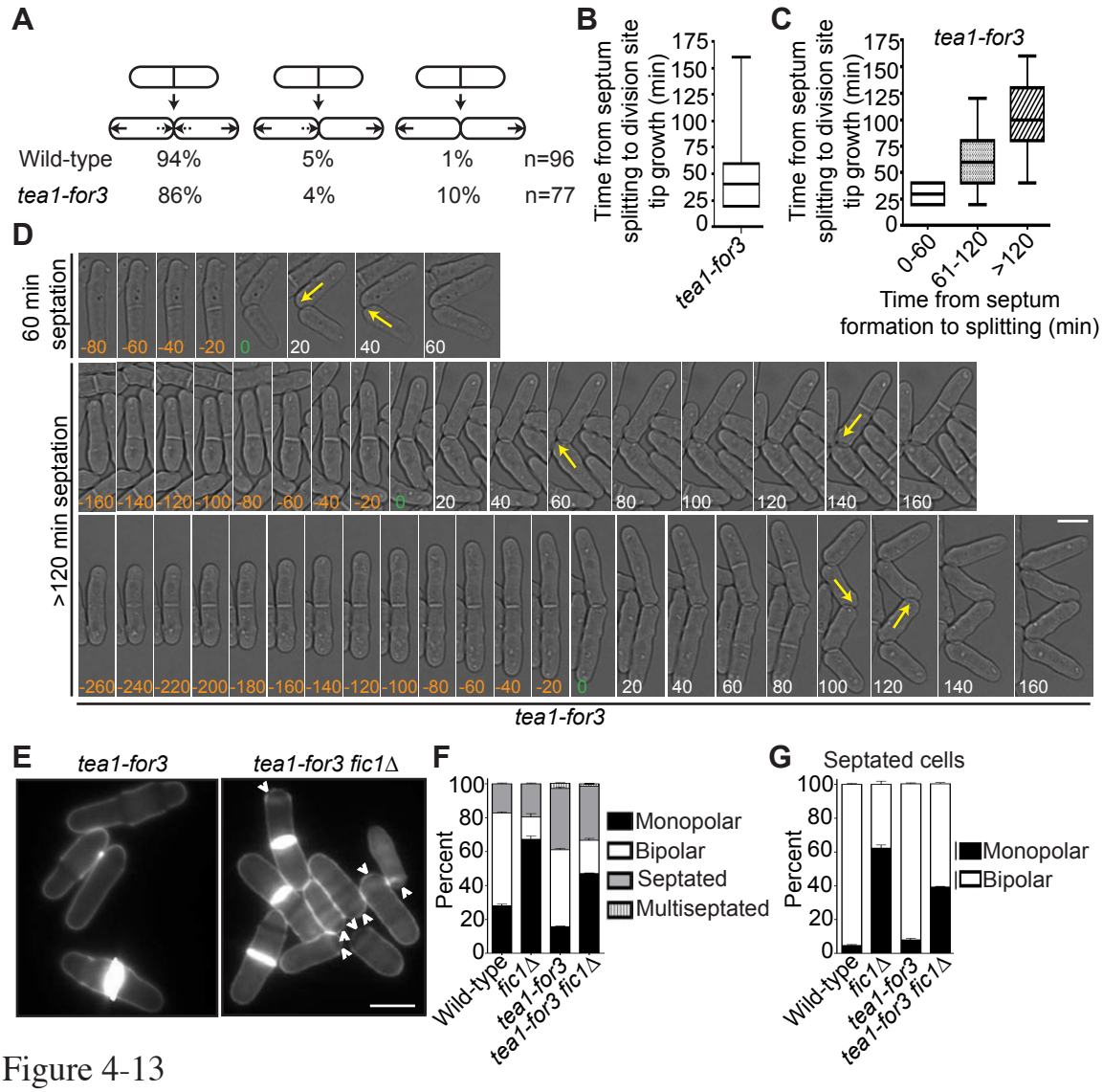

Figure 4-13

Constitutive NETO signaling does not fully rescue cytokinesis-based growth defects. (A) Quantification of growth patterns for wild-type and *tea1-for3* cells. Sample size (n) is provided for each genotype. (B) Quantification of times from septum splitting to initiation of tip growth at previous division sites for *tea1-for3* cells. Data are presented in box-and-whisker plots showing the median (line in the box), 25th-75th percentiles (box), and 5th-95th percentiles (whiskers). n>200. (C) Data for *tea1-for3* cells in (B) grouped according to the amount of time needed for the mother cell to complete septation. Data are presented in box-and-whisker plots showing the median (line in the box), 25th-75th percentiles (box), and 5th-95th percentiles (whiskers) for each category. (D) Live-cell DIC movies of *tea1-for3* cells with different times needed to complete septation. The time of septum splitting of the mother cell is marked as point zero. The initiation of tip growth at previous division sites is denoted by yellow arrows. (E) Live-cell images of calcofluor-stained *tea1-for3* and *tea1-for3 fic1Δ* cells. Arrowheads indicate monopolar cells. (F) Quantification of (E), with three trials per genotype and n>300 for each trial. Data are presented as mean ± SEM for each category. (G) Quantification of septated cells in (E) and (F), with three trials per genotype and n>200 for each trial. Data are presented as mean ± SEM for each category. (Bars = 5 μm)

corroborated this model by expressing the Tea1-For3 fusion in *fic1Δ* cells. Although *tea1-for3* cells were mostly bipolar, *tea1-for3 fic1Δ* cells showed a high percentage of monopolar growth (Figs. 4-13E, 4-13F, and 4-13G). These findings confirmed that efficient completion of cytokinesis is critical for new end growth, even when signaling networks responsible for NETO are prematurely activated.

Errors in growth polarity caused by faulty cytokinesis translate into heightened fungal invasiveness

S. pombe undergoing a dimorphic switch from single-celled to invasive form grow primarily in a monopolar fashion at old ends (Dodgson et al., 2010; Pohlmann and Fleig, 2010). Moreover, it has been postulated that cytokinesis errors might contribute to a hyphal-like transition in *S. pombe* (Bahler, 2005). We therefore considered that cytokinesis-based constraints on *S. pombe* growth polarity might facilitate invasive growth transitions. Using techniques similar to those described previously (Pohlmann and Fleig, 2010; Prevorovsky et al., 2009), we tested whether various cytokinesis mutants displaying defective bipolar growth could form pseudohyphae into 2% agar. Cells lacking Fic1 or its interacting partners Cyk3 or Imp2 were significantly more invasive than wild-type cells (Figs. 4-14A and 4-14B), and, like other invasive *S. pombe* mutants (Dodgson et al., 2010; Pohlmann and Fleig, 2010), *fic1Δ* pseudohyphae were composed of single cells oriented in filament-like projections (Fig. 4-14C). In addition to these strains, we found other cytokinesis mutants exhibiting high degrees of monopolar growth (*spn1Δ*, *cdc7*-24, and *vps24Δ*) to also be highly invasive (Figs. 4-14A and 4-14B). Of note, the *vps24Δ* strain showed drastically more invasive growth than the others, though the reasons for this are currently unclear. *rlc1Δ* and *pxl1*Δ, which possess cytokinesis

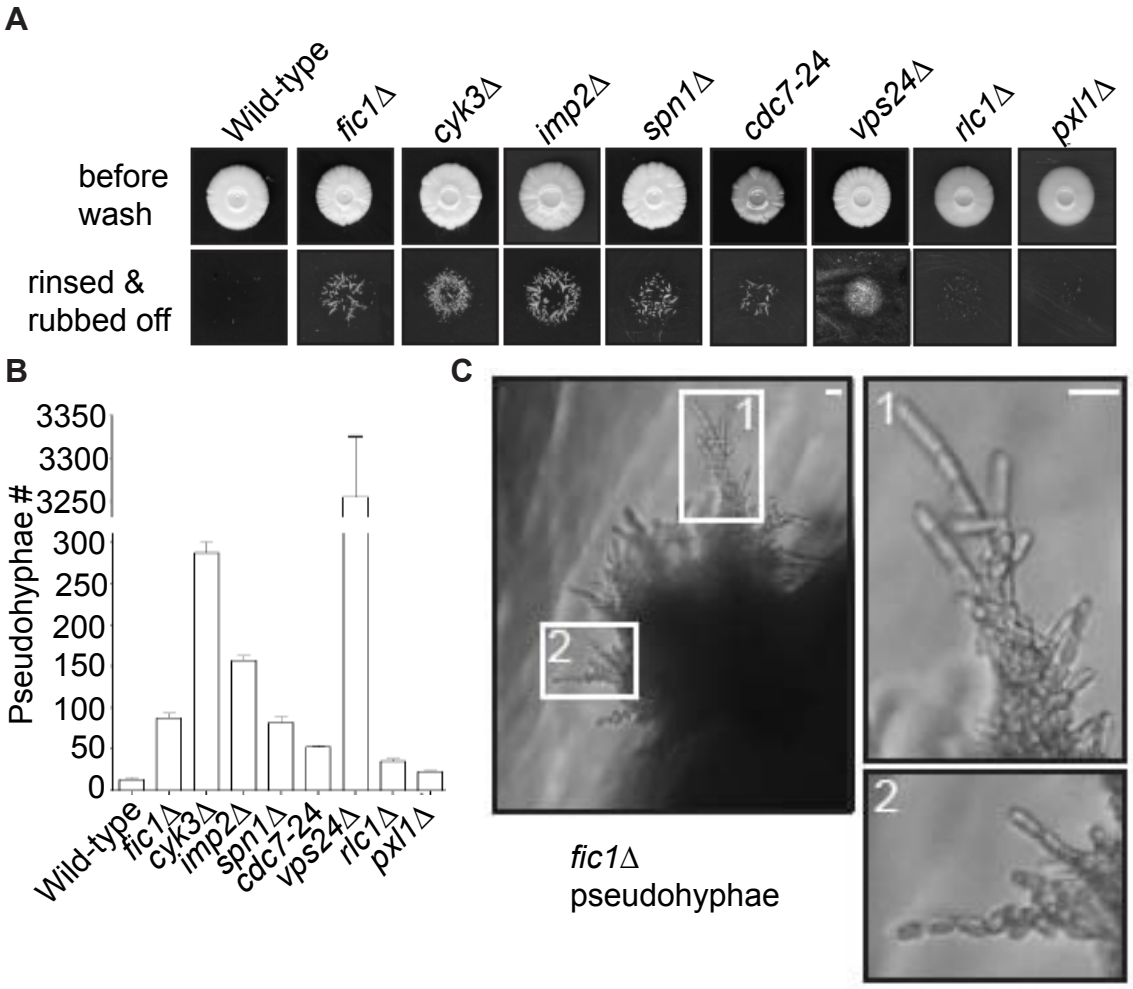

Figure 4-14

Cytokinesis-based growth defects facilitate the dimorphic switch into an invasive form. (A) Invasive growth assays for strains of the indicated genotypes on 2% agar. Cells were spotted on rich medium and incubated for 20 days at 29°C (top panel). Colonies were then rinsed under a stream of water and rubbed off (bottom panel). (B) Quantification of pseudohyphae in (A), with n≥3 for each genotype. Data are presented as mean ± SEM for each genotype. (C) Image of *fic1Δ* pseudohyphae in 2% agar, with enlarged images on the right. (Bars = 5 μm)

defects that do not considerably impact polarized cell growth (Figs. 4-11C and 4-11D), invaded less efficiently on 2% agar than cytokinesis mutants exhibiting NETO defects (Figs. 4-14A and 4-14B). This supports the notion that defective cytokinesis promotes the dimorphic switch most robustly when it results in faulty NETO.

Consistent with bipolar growth defects accompanying pseudohyphal growth, *tea1-for3* cells, which experience constitutive NETO induction, almost never extended pseudohyphae into 2% agar (Figs. 4-15A and 4-15B). Because cytokinesis-based constraints on growth polarity partially override tip-based NETO signaling, we reasoned that *tea1-for3* cells should become more invasive upon loss of Fic1. Indeed, on 2% agar *tea1-for3 fic1Δ* cells formed pseudohyphae (Fig. 4-15C), which were more numerous than those observed for wild-type and *tea1-for3* strains (Figs. 4-15A and 4-15B). Thus, perturbations in cytokinesis cause growth polarity errors that facilitate pseudohyphal growth even upon constant NETO signaling.

Lastly, we asked whether loss of polarity-relevant cytokinesis factors could partially rescue invasiveness of an *asp1Δ* strain, which is unable to undergo the dimorphic switch due to an inability to sense external cues (Pohlmann and Fleig, 2010). Previously, it was demonstrated that *asp1Δ* cells form a biofilm-like colony on 0.3% agar (Fig. 4-15D) (Pohlmann and Fleig, 2010). Growth on 0.3% agar is more sensitive for assaying invasiveness of strains that invade less efficiently, as wild-type colonies form protrusions on 0.3% agar but extend relatively few pseudohyphal projections into 2% agar (Figs. 4-14A, 4-14B, and 4-15D) (Pohlmann and Fleig, 2010). We therefore assessed the effect of cytokinesis defects on *asp1Δ* invasiveness by testing whether *asp1Δ* strains that also lacked relevant cytokinesis factors still formed biofilms on 0.3% agar.

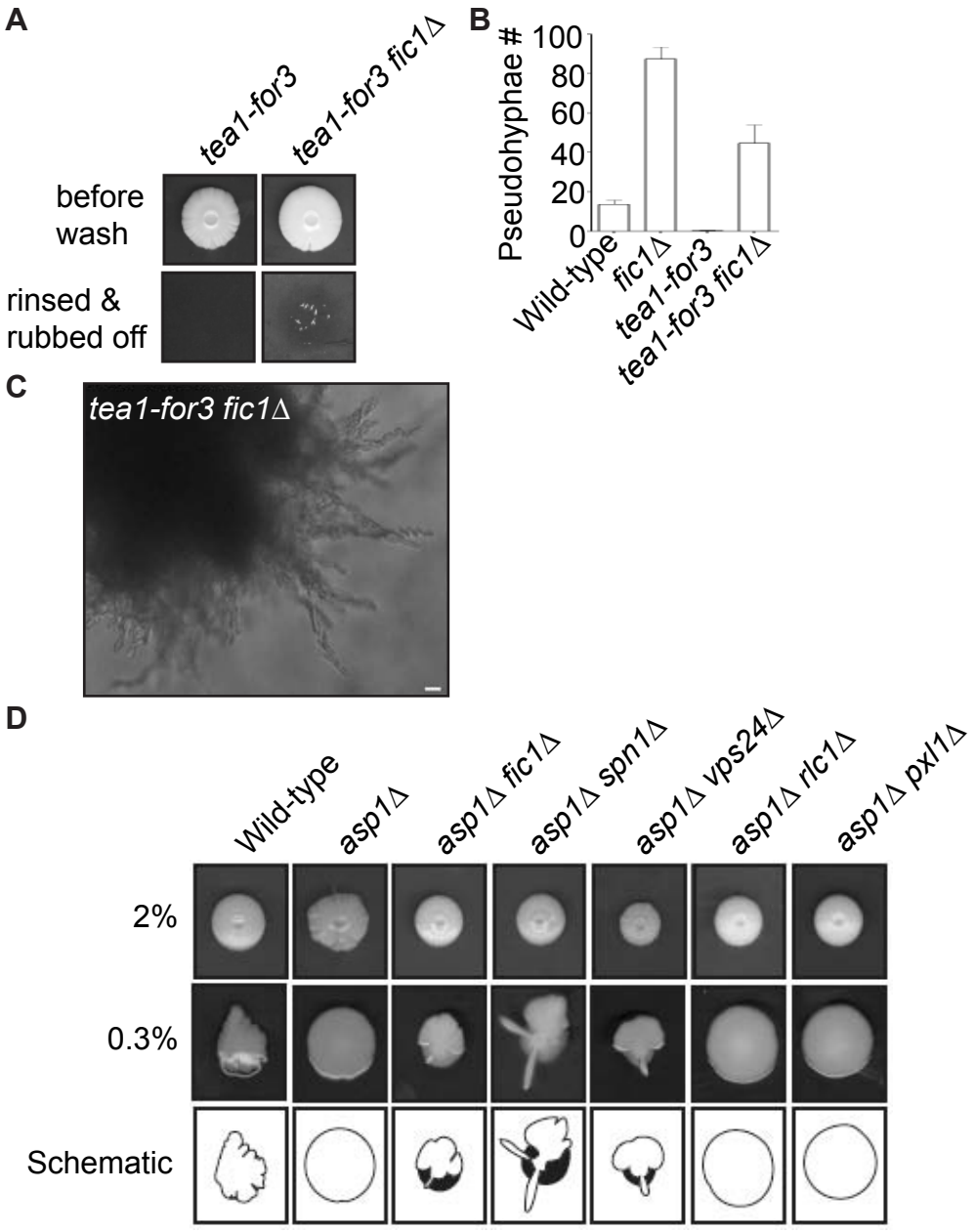

Figure 4-15

Cytokinesis-based growth defects facilitate the dimorphic switch even upon consitutive NETO induction or the loss of nutritional cues.
(A) Invasive growth assays for *tea1-for3* and *tea1-for3 fic1Δ* strains on 2% agar. Cells were spotted on rich medium and incubated for 20 days at 29°C (top panel). Colonies were then rinsed under a stream of water and rubbed off (bottom panel). (B) Quantification of pseudohyphae in (A), with n≥3 for each genotype. Data are presented as mean ± SEM for each genotype. (C) Image of *tea1-for3 fic1Δ* pseudohyphae in 2% agar. (D) Colony growth of strains of the indicated genotypes on rich medium containing 2% (top panel) or 0.3% agar (middle panel). Cells were spotted and incubated for 12 days at 29°C. Schematics of colony growth on 0.3% agar are also given (bottom panel), with white areas representing growth on the agar surface and black areas representing growth into the agar. (Bar = 5 μm)

Intriguingly, double deletion strains of *asp1Δ* with *fic1Δ*, *spn1Δ*, or *vps24Δ* did not form biofilms on 0.3% agar but instead made projections into and on the surface of the agar (Fig. 4-15D). In contrast, double deletion strains of *asp1Δ* with either *rlc1Δ* or *pxl1Δ* still formed biofilms on 0.3% agar (Fig. 4-15D). We thus concluded that cytokinesis-based constraints on polarized cell growth in *S. pombe* can foster invasiveness even in the absence of typical nutritional signals.

Discussion

In this study, we have shown how cytokinesis and cell polarity crosstalk to regulate fission yeast morphogenesis. Our data support a model (Fig. 4-16) in which Fic1 acts as an adaptor at the CR, where it guides proper completion of cytokinesis and thereby affects division site remodeling. Loss of Fic1, its interactions, or parallel pathways results in delayed growth at new ends, even upon constitutive activation of NETO signaling. Impaired bipolar cell growth resulting from defective cytokinesis in turn enhances *S. pombe* invasiveness.

Cytokinesis-based regulation of cell polarity

The majority of *S. pombe* monopolar mutants previously analyzed fail at old end growth (Huisman and Brunner, 2011). However, the cytokinesis mutants studied here were predominantly new end growth defective. As in other organisms (St Johnston and Ahringer, 2010), numerous *S. pombe* proteins known to affect growth polarity localize to the division site; this has fostered speculation that signaling at both cell tips and the division site might impact growth zones (Glynn et al., 2001). However, whether or not

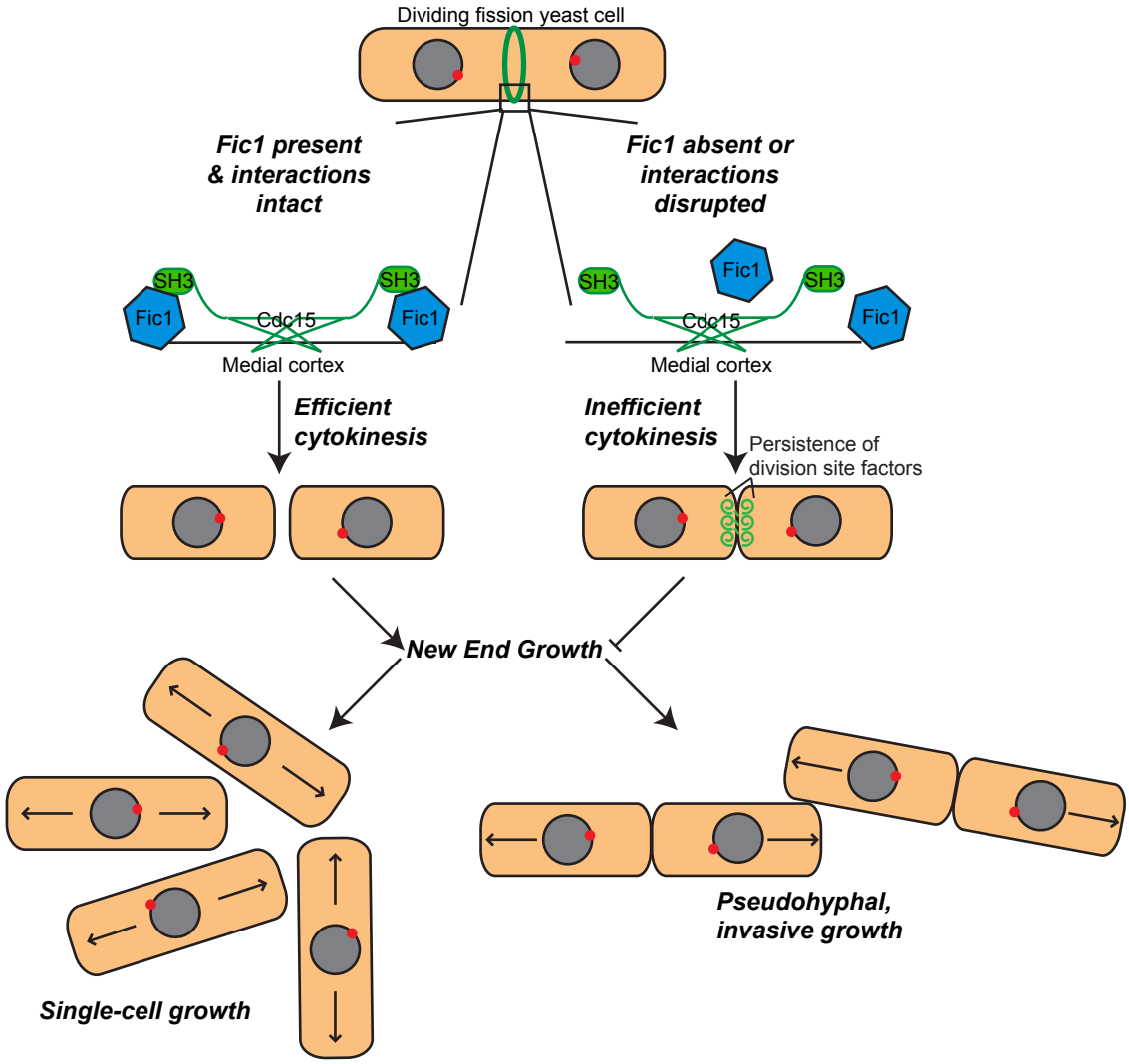

Figure 4-16

Model of Fic1's involvement in cytokinesis and the establishment of bipolar cell growth in *S. pombe*.
During cytokinesis, Fic1 serves as a scaffold for SH3 proteins, including Cdc15, at the cytokinetic ring. In the absence of Fic1, its interactions, or a parallel pathway, the completion of cell division is perturbed, and the cell division machinery persists at the previous division site. Failure to robustly complete cytokinesis impedes new end growth, even if NETO signaling is prematurely activated. Cytokinesis-based constraints on new end growth polarity aid in the transition into invasive fungal growth.

the cytokinesis functions of these proteins can specifically impact cell polarity has received little attention, especially in *S. pombe*. Our data provide evidence directly linking division site organization to *S. pombe* growth polarity. Because many factors involved in completing cell division likely also impact subsequent polarized growth, we believe our data could explain the involvement of diverse proteins in this process.

In other organisms, cytokinesis proteins appoint local regions of the cell cortex for growth following cell division (Flescher et al., 1993; Pollarolo et al., 2011; Snyder et al., 1991). For example, several budding yeast proteins, which remain at the cell cortex following cell division, have been reported to convey a cortical "tag" that marks the position of the next bud site (Flescher et al., 1993; Snyder et al., 1991). Similarly, during *Drosophila melanogaster* neurogenesis, cytokinetic furrow components mark the site from which the first dendrite will sprout (Pollarolo et al., 2011). In these cases, cytokinesis factors confer a positive polarizing cue adjacent to previous division sites, which contrasts with our findings in *S. pombe* where the cell division machinery impedes polarization and growth at new ends created by cell division.

The fact that *S. pombe* grow at old but not new ends after cell division is somewhat counterintuitive (Huisman and Brunner, 2011), especially because the cell growth machinery concentrates at the division site. Upon the completion of cytokinesis, the *S. pombe* growth machinery mysteriously shuttles to old ends rather than remaining at new ends. Why does the growth machinery relocate from the division site to old ends? One explanation is that new end cortices must be re-structured to become competent for tip growth. Indeed, specific lipid and cell wall variants contribute to *S. pombe* cytokinesis (Luo et al., 2009; Streiblova et al., 1966), and local rearrangements of these

may be required for growth activation. Moreover, the persistence of CR factors at new ends might create physical barriers to cytoskeletal elements, such as actin cables, required for tip growth. An inhibitory role for cell division in polarization is supported by studies of mutants that undergo multiple rounds of cytokinesis without physically separating, because internal cells in these structures do not grow into septa but branch adjacently. In a single-celled context, we speculate that when late cytokinetic events are perturbed, inherent delays in cortical re-structuring are exacerbated, causing growth polarity defects at new ends. In cases in which one daughter cell fails at NETO while the other is successful, we suspect these arise due to unequal partitioning of cytokinesis remnants and/or differences in cell cycle stages or life histories of daughter cells.

Consistent with furrow remodeling affecting polarization in other organisms, initial cellular protrusions of dividing mammalian cells orient away from the midbody linking daughter cells during abscission (Mullins and Biesele, 1973). Only after the completion of cell division does polarization also occur near the latent division site (Mullins and Biesele, 1973). Moreover, forced entry of HeLa cells with monopolar spindles into cytokinesis results in anucleate daughter cells that, similar to their nucleated counterparts, exhibit membrane protrusions only distal to cleavage furrows (Hu et al., 2008). Thus, similar to our model in *S. pombe*, some factor at the division site cortex, and not a cell's cytosolic constituents, requires remodeling for post-cytokinetic polarization. Recent evidence indicates that mechanosensory pathways can direct cell polarization away from points of tension (Weber et al., 2012). As modeling predicts that cortical tension peaks at the division plane during cytokinesis (White and Borisy, 1983),

it will likewise be important to assess the relevance of mechanical cues to cytokinesis-based polarization events.

Interplay within NETO and relevance of new end growth control

Previous work has implied that association of microtubule-associated protein Tea1 with formin For3 at new ends is sufficient for NETO (Martin et al., 2005). In our study, we expressed an endogenous Tea1-For3 fusion that could induce premature NETO. However, when cytokinesis was perturbed in *tea1-for3* mutants, NETO was delayed. We posit that local cortical abnormalities in cell wall, membrane, or associated factors can partially override typical growth cues in *S. pombe*, as has been observed in some plants (Panteris and Galatis, 2005). Upon defective cytokinesis, such abnormalities at the division site may physically inhibit cell growth at new ends. These defects can lead to the formation of T-shaped cells when old end growth is also blocked, as in *tea1Δ fic1Δ* mutants. Our data underscore robust completion of cytokinesis as a major determinant of *S. pombe* NETO.

Is it beneficial for a cell to halt new end growth until well after cytokinesis completion? As mentioned previously, human cells undergoing division initially move away from each other, creating a pulling force that could contribute to abscission (Mullins and Biesele, 1973). Highly adherent mammalian cells can actually complete cytokinesis, with some defects, in the absence of cortical myosin from the cleavage furrow (O'Connell et al., 1999). Constriction-independent cytokinesis was first observed in the amoeba *Dictyostelium discoideum* (Neujahr et al., 1997), which accomplishes this task by likewise polarizing and growing distally to the division site (King et al., 2010).

One could imagine that in cases where *S. pombe* cell separation is delayed, tip growth at old ends might contribute similar forces to aid in abscission. Premature new end growth signaling might unbalance these forces, leading to exacerbated cytokinesis delays as in some *tea1-for3* cells. Premature new end growth might also interfere with remodeling during cytokinesis and thereby result in cell division defects. These findings highlight interdependence between the cell polarization and division machineries in *S. pombe*.

Fic1 scaffold function during cytokinesis

Our data indicate that Fic1's C-terminus, and not its C2 domain, represents its major cytokinetic functional domain, contrasting with data reported for *S. cerevisiae* Inn1 (Nishihama et al., 2009; Sanchez-Diaz et al., 2008). Why is Fic1's C2 domain dispensable for Fic1's cytokinesis, and thus polarity, functions? Sequence alignment indicates that there is in fact very low sequence identity between Fic1 and Inn1 C2 domains (Sanchez-Diaz et al., 2008). If Fic1's C2 domain is unable to perform functions or mediate interactions that Inn1's C2 domain can, it seems reasonable that Fic1-interacting proteins may be able to compensate. Consistent with this idea, over-expression of *S. cerevisiae* Cyk3 suppresses cytokinesis defects of *inn1Δ* mutants, suggesting Cyk3 function overlaps with Inn1 (Nishihama et al., 2009). These data support that Fic1's C-terminus is an efficient signaling platform, which scaffolds SH3 domain proteins through its PxxP motifs to ensure coherent integration of late cytokinesis signals.

What is the specific function of the Fic1 scaffold during cytokinesis? Our data indicate that loss of Fic1 leads to faulty CR disassembly and prolonged persistence of

factors at the division site. CR disassembly defects were also observed in *inn1Δ S. cerevisiae* mutants, leading to speculation that Inn1 might stabilize the constricting CR by physically linking it to the ingressing membrane (Sanchez-Diaz et al., 2008). Subsequent findings countered that Inn1's C2 domain cannot bind phospholipids, and it was postulated instead that Inn1 cooperates with Cyk3 to coordinate cell wall deposition (Nishihama et al., 2009). As in *fic1Δ* cells, septation and CR disassembly defects commonly accompany one another (Demeter and Sazer, 1998; Tully et al., 2009). Because these processes are inextricably linked, it is currently difficult to tease apart which defect precedes the other in *fic1Δ* cells. Moreover, completion of cytokinesis also requires lipid rearrangements in both animal cells and *S. pombe* (Emoto and Umeda, 2000; Luo et al., 2009), and membrane bridges were observed in *fic1Δ* cells. We thus envision that Fic1's C-terminus links signaling pathways that guide completion of multiple tasks during late cytokinesis and thereby affect new end remodeling. Of note, we believe that defects in early cytokinesis do not significantly alter bipolar growth establishment, as later defects more directly impinge on division site remodeling and have less time to be remedied before the next cell division. Our data furthermore support the notion that CR constriction and disassembly occur independently (Tully et al., 2009), as CR constriction but not disassembly proceeded appropriately in *fic1Δ* cells.

Defective cytokinesis in invasive fungal growth

As fungal hyphae consist of long chains of cells, the transition into hyphal growth requires strict inhibition of cytokinesis. In some yeasts, Cdc14 phosphatase activates the Ace2 transcriptional program (Brace et al., 2011), which triggers expression of cell

separation enzymes (Colman-Lerner et al., 2001). Upon the hyphal transition in *Candida albicans*, this signaling cascade is disrupted (Gonzalez-Novo et al., 2008), and other transcription factors suppress expression of Ace2 targets (Wang et al., 2009). Therefore, cytokinetic inhibition in hyphae is believed to operate largely on a transcriptional level, and reactivation of the Ace2 transcriptional program is thought to be responsible for the evolution of single-celled yeast growth (Bahler, 2005).

In this study, we showed that fission yeast cells that undergo defective, yet not wholly abortive, cytokinesis exhibit enhanced invasive capacity. We believe cytokinesis-based constraints on growth polarity assist the transition into pseudohyphal growth because they force *S. pombe* to orient outwards and grow predominantly from old ends, a pattern commonly observed in *S. pombe* pseudohyphal growth (Dodgson et al., 2010; Pohlmann and Fleig, 2010). However, as demonstrated by *tea1Δ* cells, other changes in polarity can also enhance *S. pombe* invasiveness. Though not specifically defective at new end growth, *tea1Δ* cells grow predominantly in the direction of the mother cell, and these alterations in polarity might likewise favor growth orientations that are more conducive than bipolar growth to the invasive process.

We believe our data suggest that manipulation of cytokinesis proteins, and not necessarily signaling cascades that feed into downstream transcriptional pathways, can directly modulate the dimorphic switch. We thus speculate that the cytokinetic machinery might represent a direct target of the pseudohyphal developmental program. Intriguingly, loss of cytokinesis proteins that affect NETO rescued invasiveness of an *asp1Δ* mutant, which lacks the ability to detect nutritional cues (Pohlmann and Fleig, 2010) deemed important for the *S. pombe* dimorphic switch (Amoah-Buahin et al., 2005).

Because various environmental cues also regulate hyphal morphogenesis in pathogenic fungi (Ernst, 2000), it will be important to assess the relative significance of cytokinesis-based controls on polarized growth for invasiveness in these species.

CHAPTER V

PHOSPHOREGULATION OF CYTOKINETIC PROTEIN FIC1 CONTRIBUTES TO FISSION YEAST GROWTH POLARITY ESTABLISHMENT

Introduction

Cellular polarization underlies many facets of cell behavior, including cell growth. The rod-shaped fission yeast *S. pombe* represents a genetically tractable system for studying growth polarity regulation. Wild-type *S. pombe* cells elongate at their two cells tips in a cell cycle-controlled manner, transitioning from monopolar to bipolar growth in interphase when new ends established by cell division begin to extend. Previously, we identified the process of cytokinesis as a critical regulator of new end growth. Here, we demonstrate that Fic1, a cytokinetic factor required for typical polarized growth at new ends, is a phosphoprotein. Phosphorylation of Fic1 occurs on two C-terminal residues, which flank PxxP motifs important for protein-protein interactions at the division site. Importantly, endogenously-expressed Fic1 phosphomutants cannot support proper bipolar growth, and the resultant growth defects facilitate the switch into an invasive pseudohyphal state. Additionally, we find that CDK and casein kinase II (CK2) participate in phosphorylation of relevant Fic1 residues *in vitro*. These findings broaden the scope of signaling events that contribute to *S. pombe* growth polarity regulation, underscoring that cytokinetic factors constitute relevant targets of kinases affecting new end growth.

Results

Multiple pools of Fic1 exist in a phosphorylated state during the cell cycle

As was observed in previous studies (Bohnert and Gould, 2012; Roberts-Galbraith et al., 2009), Western blotting of Fic1-FLAG$_3$ from asynchronous wild-type cells revealed multiple bands with different gel mobilities (Fig. 5-1A). We therefore considered that Fic1 is targeted by post-translational modifications, though genome-wide screens have previously not detected such modifications on Fic1. When immunoprecipitated from asynchronous wild-type cells and treated with lambda phosphatase to eliminate all phosphorylations, Fic1-FLAG$_3$ was detected via Western blotting as only a single band (Fig. 5-1A). Thus, we concluded that Fic1 is a phosphoprotein, and, given the multiple slower migrating Fic1-FLAG$_3$ species, that Fic1 can be phosphorylated at more than one residue.

To assess whether Fic1 phosphostatus changes during the cell cycle, we first analyzed Fic1-FLAG$_3$ gel mobility in different cell cycle arrests. These arrests were achieved either through inactivation of temperature-sensitive alleles (*cdc10*-V50 G1 arrest, *cdc25*-22 G2 arrest, *nda3*-KM311 prometaphase arrest, or *cps1*-191 cytokinesis arrest) or by addition of a drug (hydroxyurea-induced S phase arrest). In all tested cell cycle arrests, Fic1-FLAG$_3$ gel mobility shifts were identical (Fig. 5-1A), indicating that various pools of phosphorylated Fic1 are present at all stages of the cell cycle. We corroborated this using a G2 block-and-release experiment, in which samples were taken at various time points following release from this arrest. As expected, all Fic1-FLAG$_3$ phosphorylated species were detected at each of the time points (Fig. 5-1B), verifying that multiple pools of phosphorylated Fic1 exist throughout cell division.

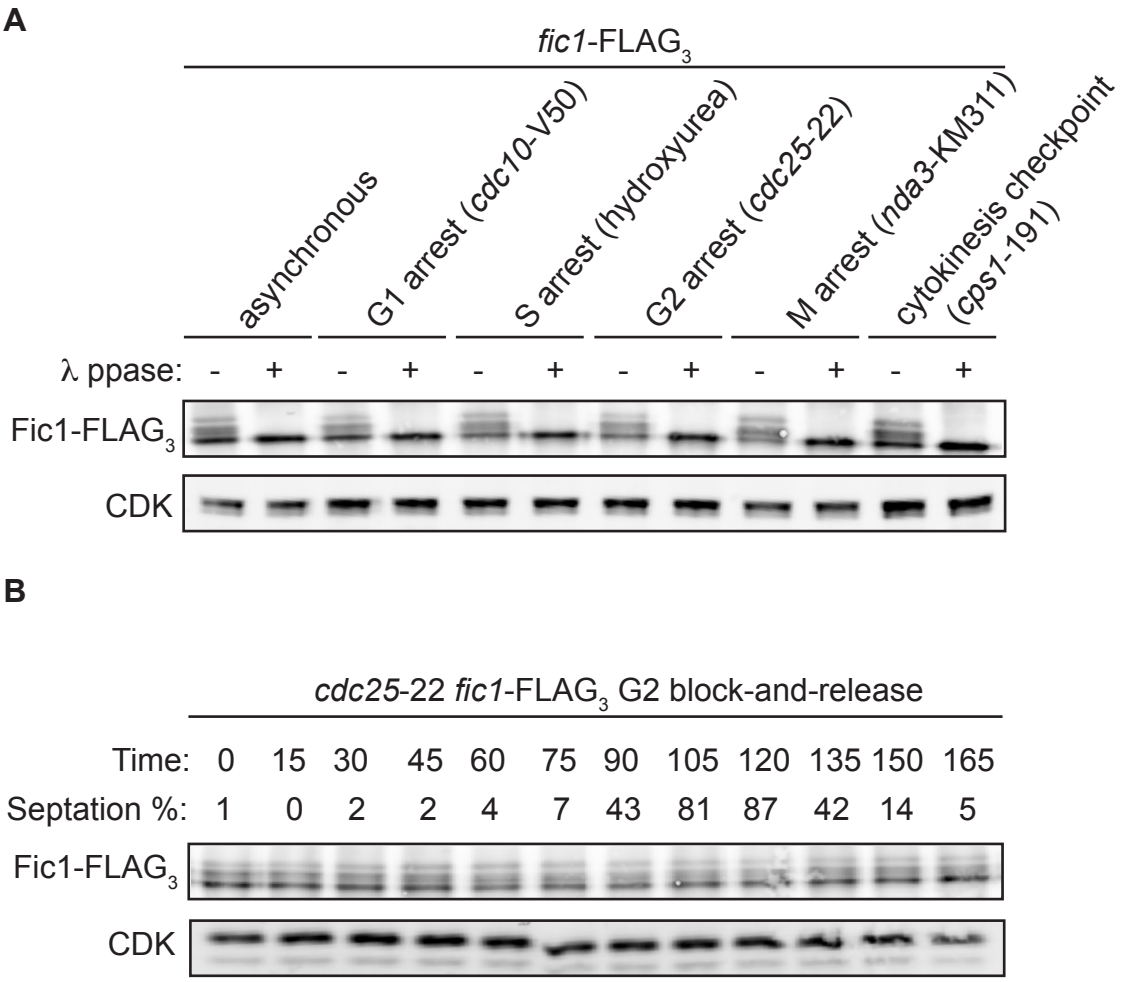

Figure 5-1

Cytokinetic protein Fic1 is phosphorylated *in vivo*.
(A) Anti-FLAG immunoprecipitates from asynchronous or cell cycle-arrested cells were either treated with lambda phosphatase or left untreated and subsequently blotted with an anti-FLAG antibody. CDK is a loading control. (B) Block-and-release of G2-arrested *cdc25*-22 *fic1*-FLAG$_3$ cells. Anti-FLAG immunoprecipitates were blotted with an anti-FLAG antibody. Time points and septation indices are noted. CDK is a loading control.

Phosphorylation correlates with domains and subpopulations of Fic1 sufficient for bipolar cell growth

We recently demonstrated that Fic1 affects the establishment of bipolar cell growth in *S. pombe* by influencing the robustness of late cytokinesis (Bohnert and Gould, 2012). Since kinases represent the broadest category of proteins affecting fission yeast morphogenesis (Martin and Chang, 2005), we wondered whether phosphorylation of Fic1 might contribute to bipolar cell growth in *S. pombe*. As an initial assessment, we investigated phosphorylation of endogenous truncations of Fic1 that differentially affect bipolar cell growth. Fic1's C-terminus [amino acids 127-end, "Fic1C" (Fig. 5-2A)], which is comprised of several PxxP motifs, localizes to the cell division site but not to cell tips, and is necessary and sufficient for bipolar cell growth. Its N-terminal C2 domain [amino acids 1-126, "Fic1N" (Fig. 5-2A)], on the other hand, neither localizes to the cell division site nor contributes to bipolar growth establishment (Bohnert and Gould, 2012). Notably, whereas Fic1N-GFP was not phosphorylated *in vivo* (Fig. 5-2B), Fic1C-$FLAG_3$ was (Figure Fig. 5-2C). Thus, we suspected that phosphorylation could potentially influence Fic1 function in cellular morphogenesis.

If this were the case, we expected that full-length Fic1 should retain the capacity to be fully phosphorylated even if it lost the ability to anchor at cell tips. We reasoned this because Fic1, unlike other characterized growth polarity factors, performs its polarity function at the cell division site and not at interphase cell tips (Bohnert and Gould, 2012). Intriguingly, when two C2 domain lysines (K22 and K27) (Fig. 5-3A), which are predicted based on homology to *S. cerevisiae* Inn1 to mediate membrane binding (Sanchez-Diaz et al., 2008), were mutated to alanine, mutant Fic1-K22,27A-GFP, unlike

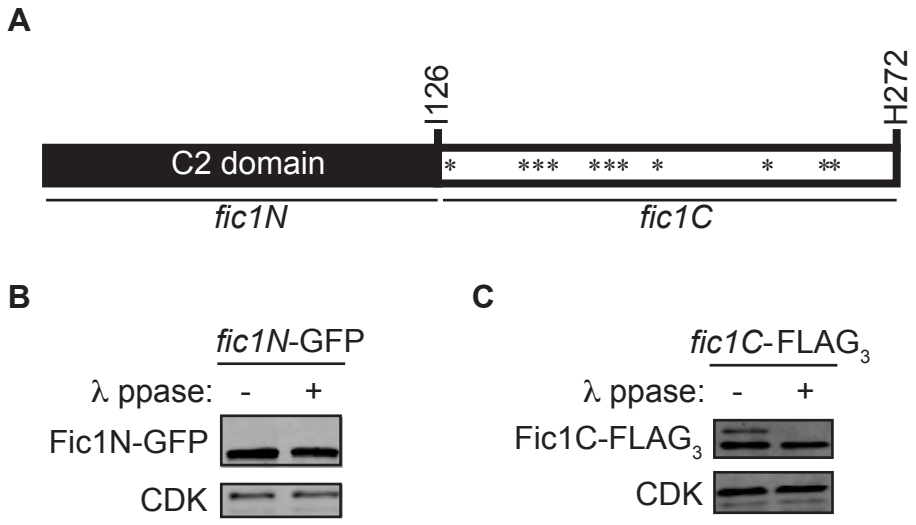

Figure 5-2

Fic1's C-terminus, which is sufficient for its polarity function, is phosphorylated *in vivo*. (A) Schematic of Fic1 domain organization, with residues of interest, fragments, and PxxP motifs (*) indicated. (B) Anti-GFP immunoprecipitates from *fic1N*-GFP cells were either treated with lambda phosphatase or left untreated and subsequently blotted with an anti-GFP antibody. CDK is a loading control. (C) Anti-FLAG immunoprecipitates from *fic1C*-$FLAG_3$ cells were either treated with lambda phosphatase or left untreated and subsequently blotted with an anti-FLAG antibody. CDK is a loading control.

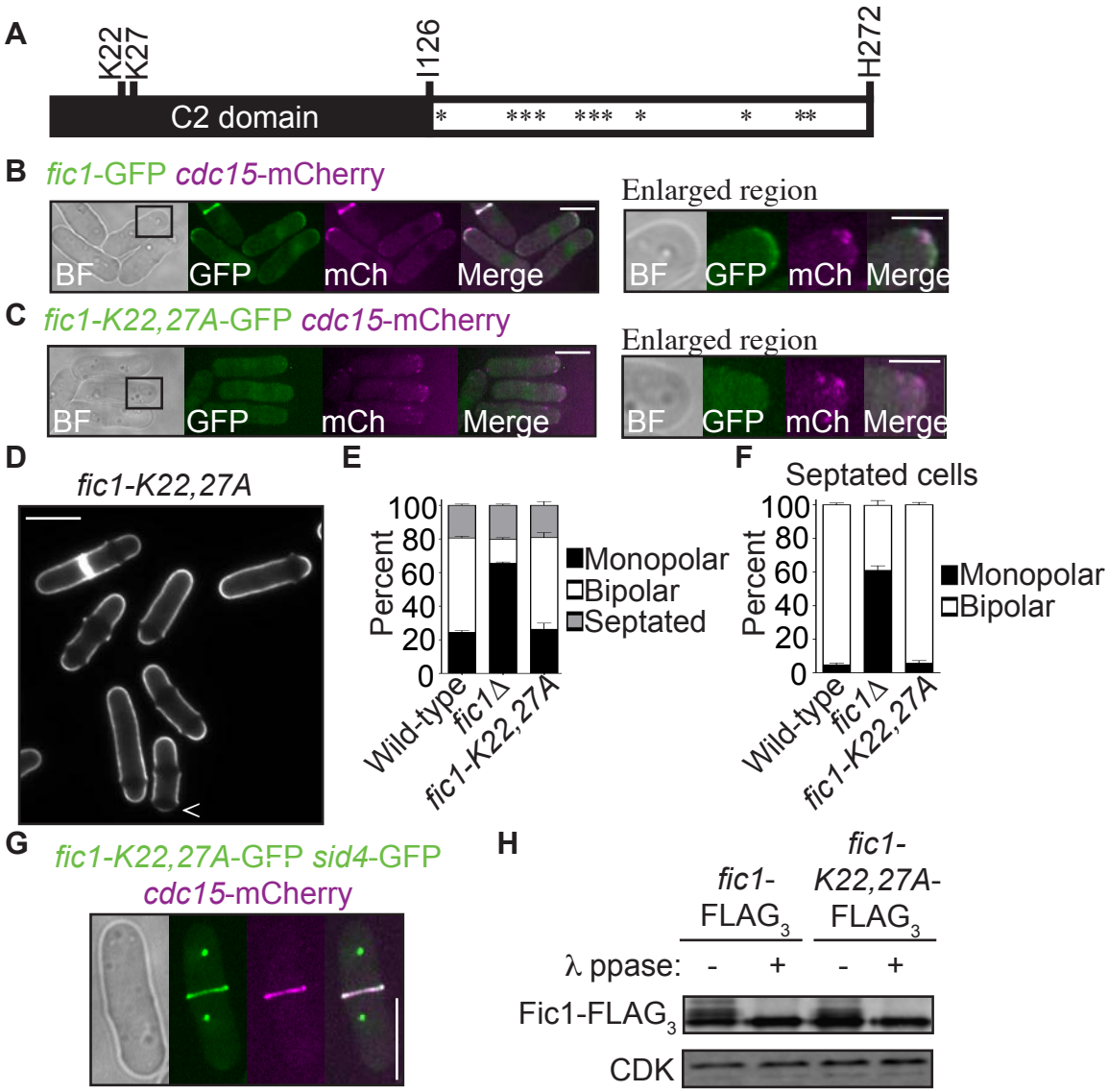

Figure 5-3

Fic1 phosphorylation does not require cell tip anchoring.
(A) Schematic of Fic1 domain organization, with residues of interest and PxxP motifs (*) indicated. (B and C) Live-cell bright field (BF), GFP, mCherry (mCh), and merged GFP/mCh images of *fic1*-GFP *cdc15*-mCherry and *fic1-K22,27A*-GFP *cdc15*-mCherry cells. A region of interest is enlarged on the right. (D) Live-cell image of calcofluor-stained *fic1-K22,27A* cells. Arrowheads indicate monopolar cells. (E) Quantification of growth polarity phenotypes for cells of the indicated genotypes. Data from three trials are presented as mean ± SEM for each category. (F) Quantification of growth polarity phenotypes for septated cells of the indicated genotypes. Data from three trials are presented as mean ± SEM for each category. (G) Live-cell BF, GFP, mCh, and merged GFP/mCh images of a *fic1-K22,27A*-GFP *sid4*-GFP *cdc15*-mCherry cell during cytokinesis. (H) Anti-FLAG immunoprecipitates from *fic1*-FLAG$_3$ or *fic1-K22,27A*-FLAG$_3$ cells were either treated with lambda phosphatase or left untreated and subsequently blotted with an anti-FLAG antibody. CDK is a loading control. [Bars = 5 μm, except for enlarged regions in (B) and (C) where Bars = 2 μm]

wild-type Fic1-GFP (Fig. 5-3B), did not properly anchor at interphase cell tips (Fig. 5-3C). Despite not localizing to cell tips, Fic1-K22,27A promoted proper bipolar growth (Figs. 5-3D, 5-3E, and 5-3F), and Fic1-K22,27A-GFP still targeted to the CR (Fig. 5-3G). Importantly, Fic1-K22,27A-FLAG$_3$ could be fully phosphorylated even though it did not accumulate at cell tips (Fig. 5-3H), consistent with phosphorylation targeting subpopulations of Fic1 involved in growth polarity establishment.

Fic1 is phosphorylated at two major sites, T178 and S241

To further explore the possibility that phosphorylation influences Fic1 function in bipolar growth establishment, we next sought to identify specific phosphorylated residues on Fic1. Mass spectrometric analyses of tandem affinity-purified Fic1-TAP samples identified only two residues, threonine 178 and serine 241, having >95% probability for phosphorylation (Figs. 5-4A, 5-4B, and 5-4C). Both phosphorylated residues were located on Fic1's C-terminus (Fig. 5-4A), consistent with phosphorylation also occurring on a Fic1C-FLAG$_3$ fragment (Fig. 5-2C).

We then integrated mutants at the endogenous *fic1* locus to test whether alteration of these sites would influence Fic1-FLAG$_3$ gel mobility shifts. Alanine mutations of T178 or S241 individually led to the elimination of the slowest migrating band, and only one phosphorylated Fic1 species remained for each mutant (Fig. 5-4D). Importantly, alanine mutations of T178 and S241 in combination resulted in a complete elimination of gel mobility shifts (Fig. 5-4D), confirming that these two residues represent major phosphosites on Fic1. When these sites were mutated to aspartate to mimic phosphorylation, similar gel mobility patterns were observed, except that all bands were

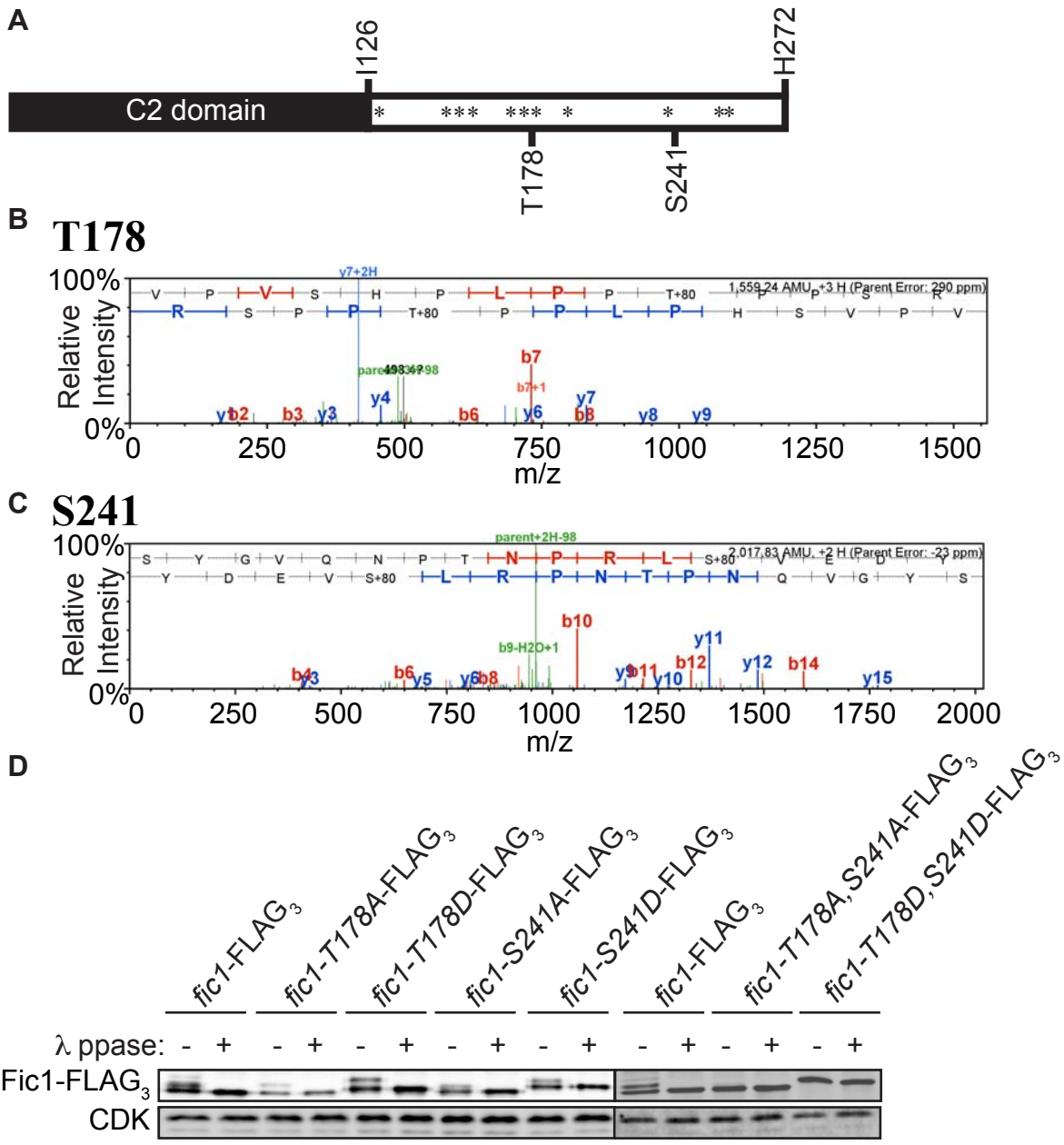

Figure 5-4

Fic1 residues T178 and S241 are phosphorylated *in vivo*.
(A) Schematic of Fic1 domain organization, with residues of interest, PxxP motifs (*), and phosphosites (labeled underneath) indicated. (B and C) Representative MS2 spectra of peptides with phosphorylated T178 or S241, respectively, identified from *fic1*-TAP samples. The peptide sequence ladder depicts Y (colored blue) and B (colored red) ions of the peptide. Green peaks indicate mass to charge (m/z) ratios of parent ions before fragmentation. Black peaks represent unidentified ions. (D) Anti-FLAG immunoprecipitates from cells of the indicated genotypes were either treated with lambda phosphatase or left untreated and subsequently blotted with an anti-FLAG antibody. CDK is a loading control.

slightly retarded in gel mobility due to constitutive charge at these positions (Fig. 5-4D). We therefore concluded that phosphorylation occurs at T178 and S241 *in vivo*, and that these sites can be phosphorylated individually or in combination.

Disruption of Fic1 phosphorylation jeopardizes bipolar cell growth and promotes the dimorphic switch

To assess the relevance of Fic1 phosphorylations to NETO, we analyzed growth polarity of phosphomutants by calcofluor staining. Individual phosphosite mutants (*fic1-T178A, fic1-T178D, fic1-S241A, fic1-S241D*), like wild-type cells, grew in a mostly bipolar fashion (Figs. 5-5A, 5-5B, and 5-5C). But, similar to *fic1Δ* cells, asynchronous *fic1-T178A,S241A* and *fic1-T178D,S241D* cells were predominantly monopolar (Figs. 5-6A, 5-6B, and 5-6C). Focusing on these mutants, we examined the relation of their growth polarity defects to cell cycle progression. As expected given that wild-type cells commonly initiate NETO by late interphase (Mitchison and Nurse, 1985), nearly all *fic1*$^{+}$ cells arrested in late G2 using the temperature-sensitive *cdc25*-22 allele initiated bipolar growth (Figs. 5-7A and 5-7B). In contrast, *cdc25*-22 *fic1-T178A,S241A* and *cdc25*-22 *fic1-T178D,S241D* cells arrested in late G2 were still largely monopolar (Figs. 5-7A an 5-7B). Such growth polarity defects mirrored those observed for *cdc25*-22 *fic1Δ* cells (Figs. 5-7A and 5-7B) (Bohnert and Gould, 2012), confirming that deregulation of Fic1 phosphorylations delays the establishment of bipolar cell growth during the cell cycle. In *fic1Δ* cells, these polarized growth defects are specific to new ends (Figs. 5-8A and 5-8B) (Bohnert and Gould, 2012). Using time-lapse DIC imaging, we confirmed that polarized growth in *fic1-T178A,S241A* and *fic1-T178D,S241D* cells was likewise faulty at new ends (Figs. 5-8A and 5-8B). Collectively, these data underscore that disruption of Fic1

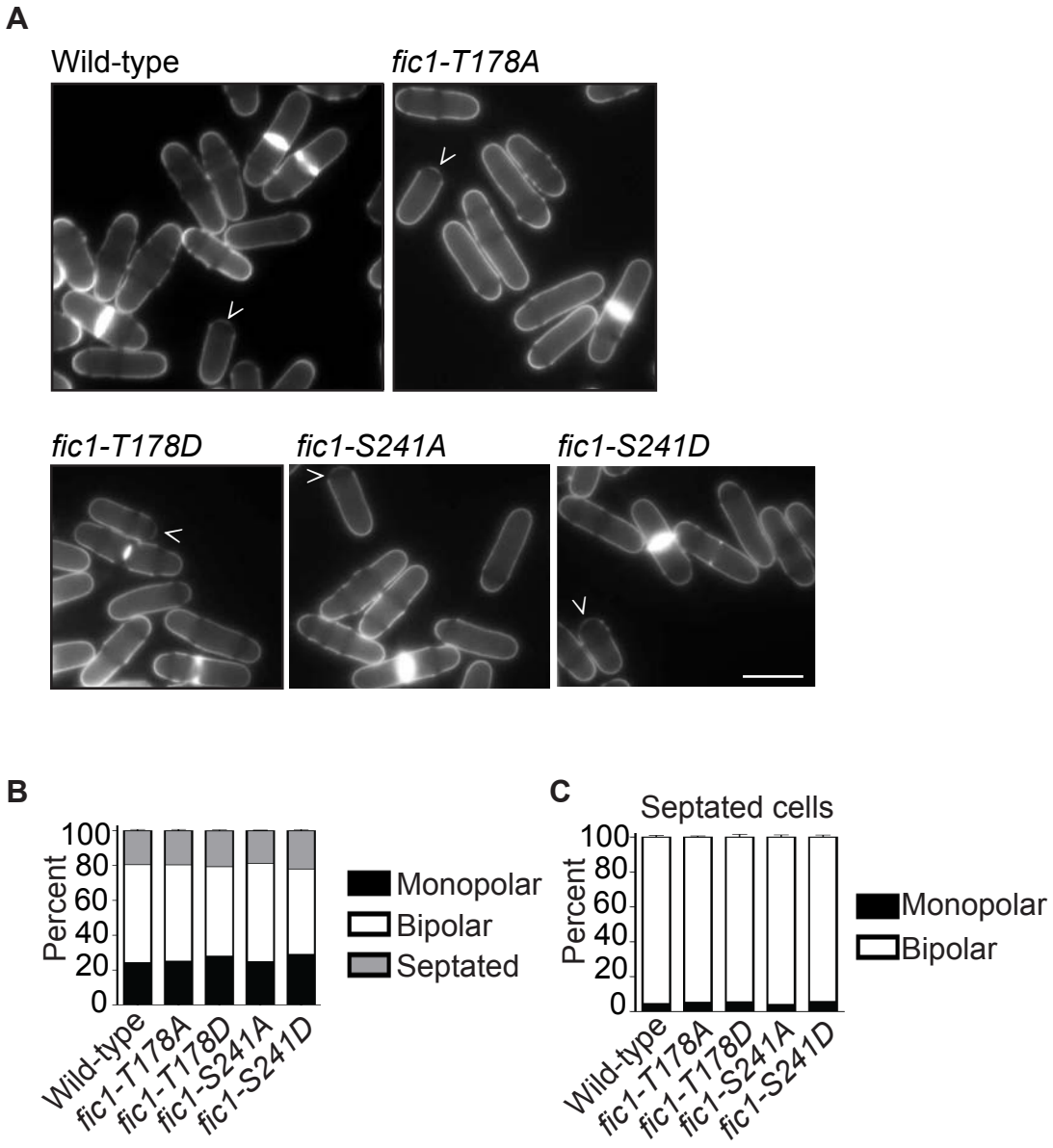

Figure 5-5

Mutation of individual Fic1 phosphosites does not affect NETO.
(A) Live-cell images of calcofluor-stained cells of the indicated genotypes. Arrowheads indicate monopolar cells. (B) Quantification of growth polarity phenotypes for cells of the indicated genotypes. Data from three trials are presented as mean ± SEM for each category. (C) Quantification of growth polarity phenotypes for septated cells of the indicated genotypes. Data from three trials are presented as mean ± SEM for each category. (Bar = 5 μm)

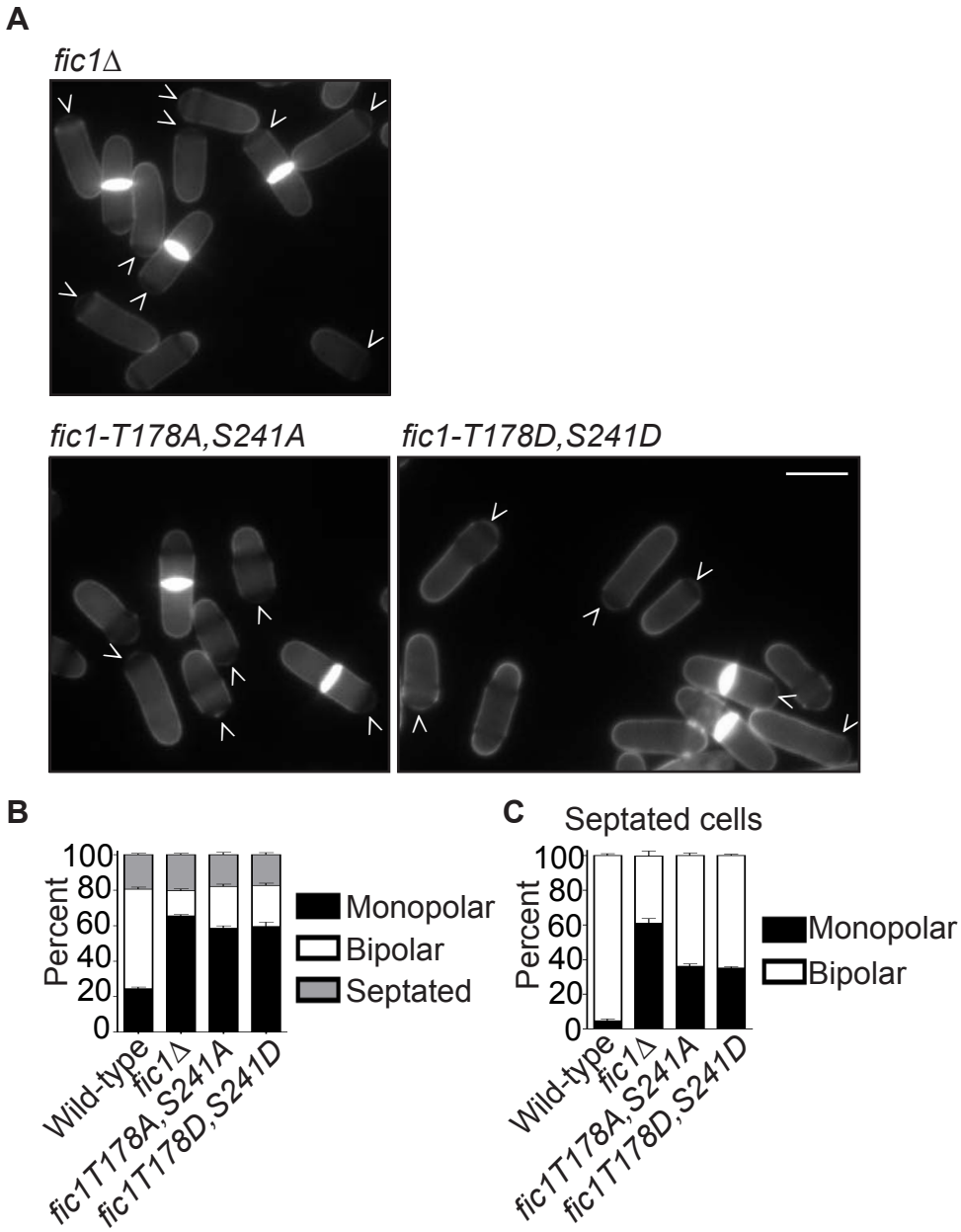

Figure 5-6

Mutation of both Fic1 phosphosites jeopardizes bipolar cell growth.
(A) Live-cell images of calcofluor-stained cells of the indicated genotypes. Arrowheads indicate monopolar cells. (B) Quantification of growth polarity phenotypes for cells of the indicated genotypes. Data from three trials are presented as mean ± SEM for each category. (C) Quantification of growth polarity phenotypes for septated cells of the indicated genotypes. Data from three trials are presented as mean ± SEM for each category. (Bar = 5 μm)

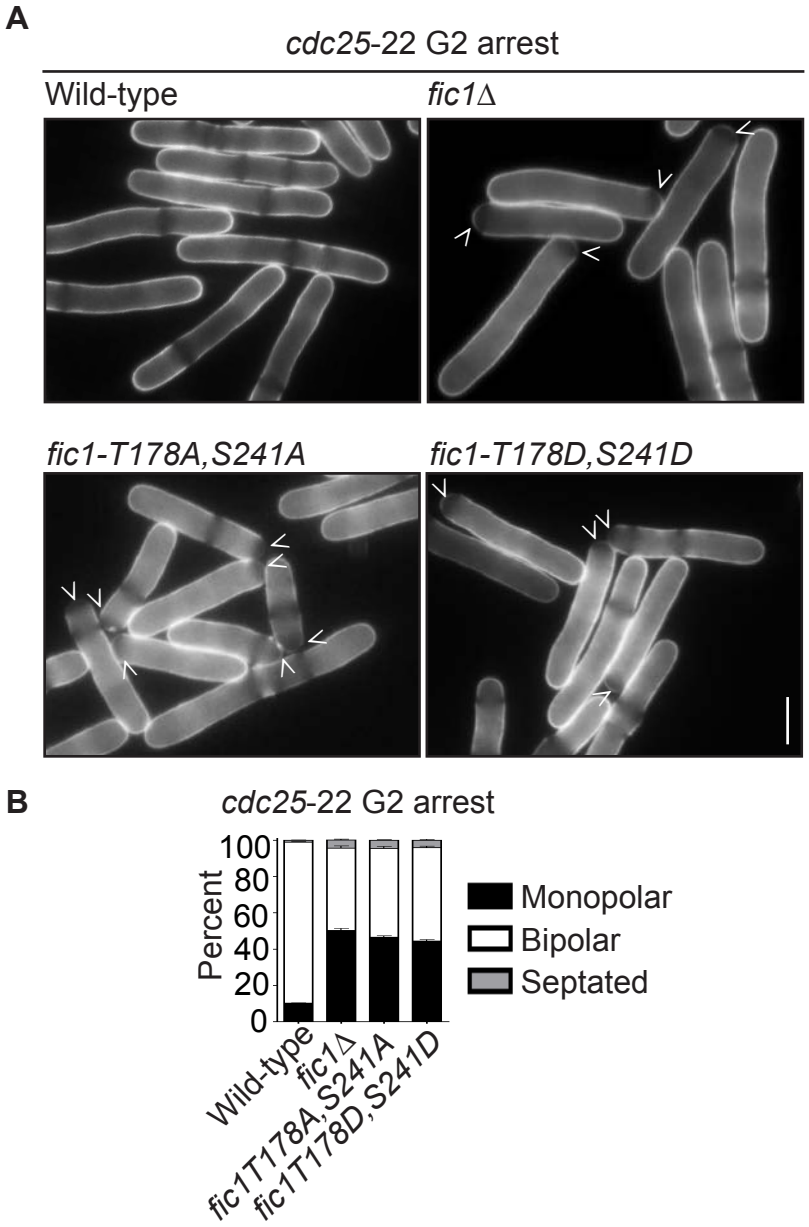

Figure 5-7

Deregulation of Fic1 phosphorylation delays bipolar growth irrespective of S phase completion.

(A) Live-cell images of G2-arrested, calcofluor-stained cells of the indicated genotypes. Arrowheads indicate monopolar cells. (B) Quantification of growth polarity phenotypes for G2-arrested cells of the indicated genotypes. Data from three trials are presented as mean ± SEM for each category. (Bar = 5 μm)

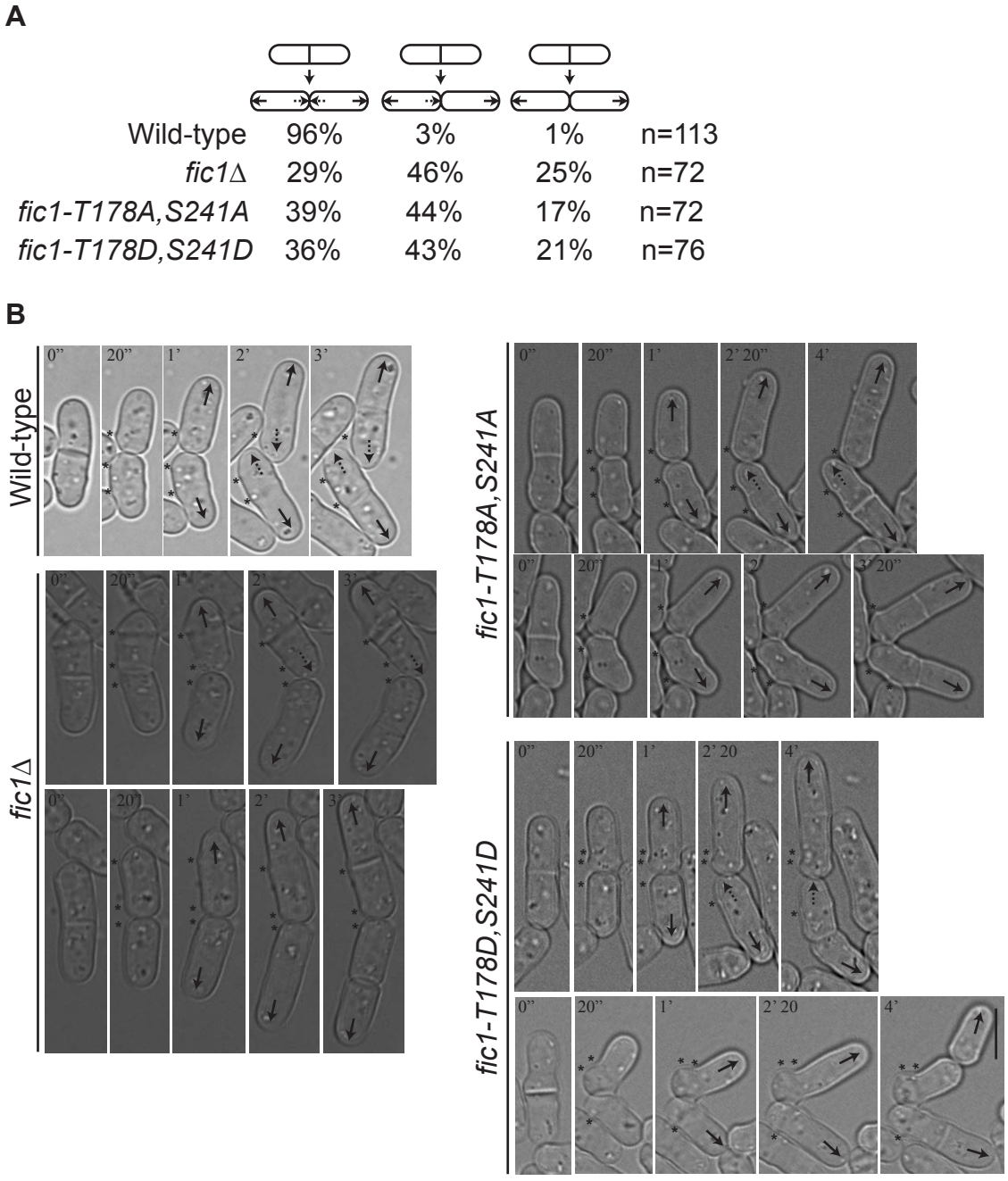

Figure 5-8

Fic1 phosphomutants fail specifically at new ends.
(A) Quantification of growth patterns for cells of the indicated genotypes. Sample size (n) is provided. (B) Live-cell DIC movies of cells of the indicated genotypes. Solid arrows denote old end growth, whereas dashed arrows indicate new end growth. Birth scars are marked by asterisks. Time points are noted. (Bar = 5 μm)

phosphorylation results in loss-of-function *fic1* alleles that are unable to facilitate proper NETO.

Cytokinesis-based constraints on *S. pombe* growth polarity support the transition into an invasive fungal form (Bohnert and Gould, 2012). Indeed, *fic1Δ* cells extend more pseudohyphae into 2% agar than do wild-type cells (Figs. 5-9A and 5-9B) (Bohnert and Gould, 2012). Consistent with *fic1* phosphomutants possessing growth polarity defects akin to *fic1Δ* cells, *fic1-T178A,S241A* and *fic1-T178D,S241D* cells similarly formed pseudohyphal structures (Figs. 5-9A and 5-9C), which were nearly as numerous as those observed for a *fic1Δ* strain (Figs. 5-9A and 5-9B). Accordingly, we concluded that the dimorphic switch from single-celled to pseudohyphal forms may be a phosphoregulated process.

CDK and CK2 participate in polarity-relevant Fic1 phosphorylation

Because kinases constitute the largest subgroup of polarity factors (Martin and Chang, 2005), we aimed to identify which catalyze Fic1 phosphorylations at T178 and S241. Unfortunately, screening of Fic1-$FLAG_3$ gel mobility shifts in a genome-wide kinase deletion library as well as in available temperature-sensitive mutants did not reveal any loss of phosphorylation. We thus imagine that redundant kinases likely target Fic1 *in vivo*.

Given this complication, we undertook a targeted *in vitro* approach to identify potential kinases involved in Fic1 phosphorylation. As CDK targets a minimal consensus of S/T-P (Ubersax and Ferrell, 2007), we considered that CDK phosphorylates T178, which fits this consensus (Fig. 5-10A). *In vitro*, CDK phosphorylated serine and

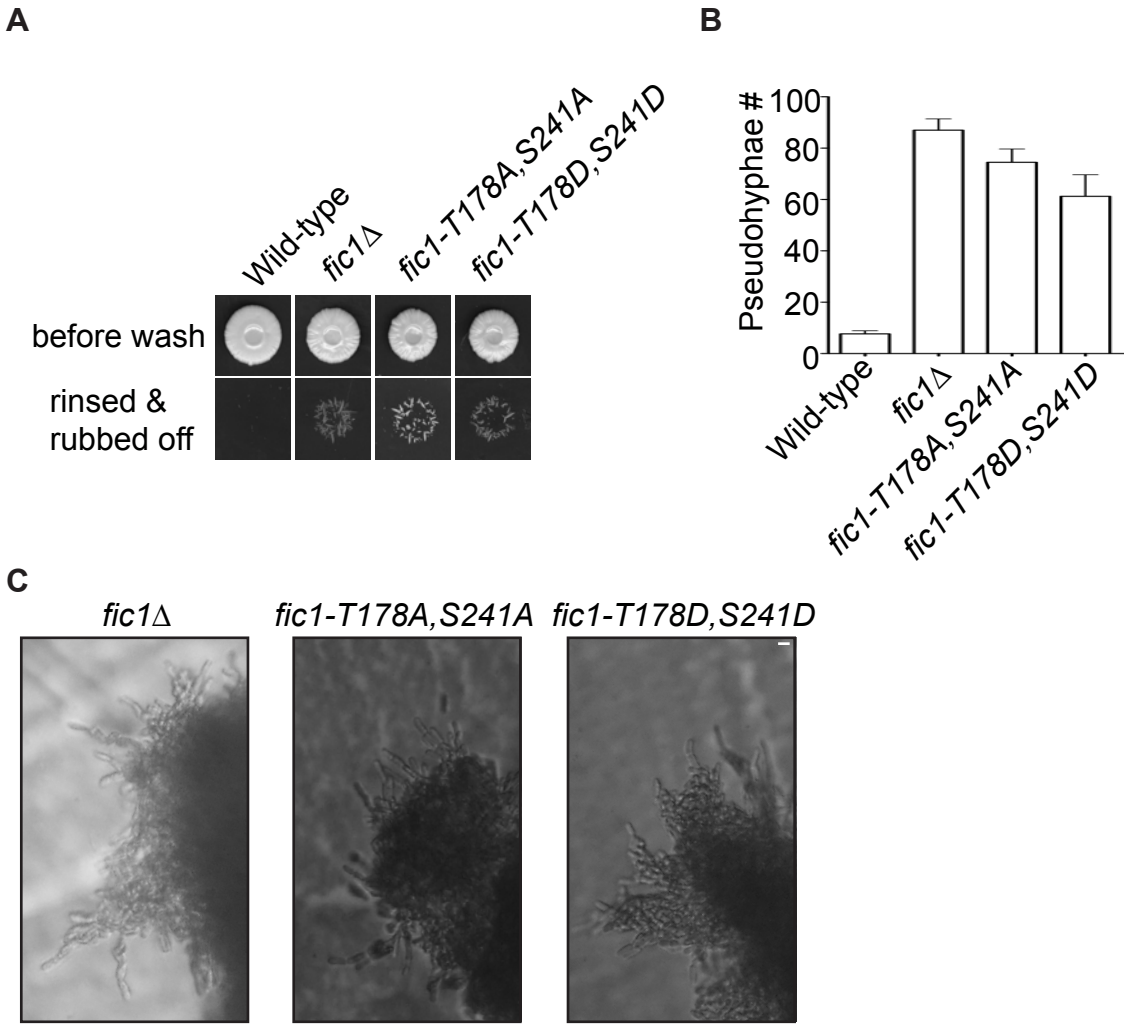

Figure 5-9

Deregulation of Fic1 phosphorylation facilitates an invasive growth transition.
(A) Invasive growth assays for strains of the indicated genotypes on 2% agar. Cells were spotted on rich medium and incubated for 20 days at 29°C (top panel). Colonies were then rinsed under a stream of water and rubbed off (bottom panel). (B) Quantification of pseudohyphae for cells of the indicated genotypes, with n≥3 for each genotype. Data are presented as mean ± SEM for each genotype. (C) Images of pseudohyphae for cells of the indicated genotypes in 2% agar. (Bar = 5 μm)

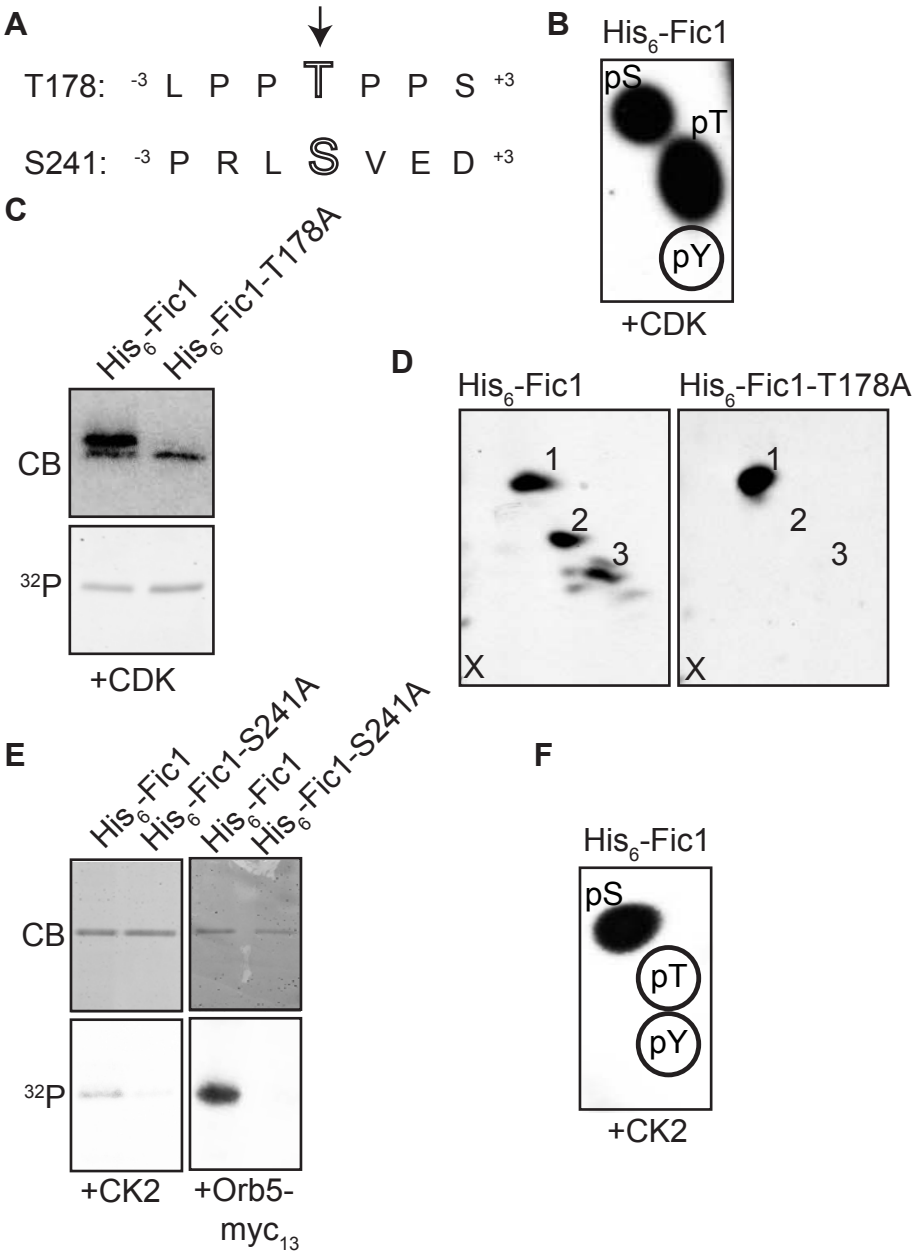

Figure 5-10

CDK and CK2 target relevant Fic1 residues *in vitro*.
(A) Schematic of residues flanking Fic1 phosphosites. The phosphorylated residues are central and are marked by an arrow. (B) Phosphoamino acid analysis of His_6-Fic1 phosphorylated by CDK. The positions of phospho-serine, phospho-threonine, and phospho-tyrosine standards are indicated. (C) CDK *in vitro* kinase assay using His_6-Fic1 or His_6-Fic1-T178A. Protein labeled by γ-^{32}P was detected by exposure to film, and the gel was stained with Coomassie Blue (CB) as a loading control. (D) Phospho-tryptic peptide analysis of His_6-Fic1 or His_6-Fic1-T178A phosphorylated by CDK. The position of the origin is indicated by an "x". The anode is on the left. (E) CK2 and Orb5-myc_{13} *in vitro* kinase assays using His_6-Fic1 or His_6-Fic1-S241A. Protein labeled by γ-^{32}P was detected by exposure to film, and the gel was stained with CB as a loading control. (F) Phosphoamino acid analysis of His_6-Fic1 phosphorylated by CK2. The positions of phospho-serine, phospho-threonine, and phospho-tyrosine standards are indicated.

threonine residues on wild-type His_6-Fic1 (Fig. 5-10B). CDK also phosphorylated His_6-Fic1-T178A *in vitro*, though phosphorylated wild-type His_6-Fic1 exhibited an additional slower migrating species (Fig. 5-10C). This suggested that His_6-Fic1-T178A cannot be fully phosphorylated by CDK *in vitro*. Tryptic peptide mapping confirmed this idea, as His_6-Fic1-T178A lacked a phosphorylated peptide observed for wild-type His_6-Fic1 (Fig. 5-10D). We therefore concluded that CDK can phosphorylate Fic1 at T178.

Although S241 does not match a CDK consensus, it fits a consensus for CK2 (S-x-x-E/D) (Fig. 5-10A) (Meggio and Pinna, 2003). We accordingly tested whether CK2 can phosphorylate S241 *in vitro*. We found that CK2 indeed phosphorylates His_6-Fic1 *in vitro* (Fig. 5-10E), and that such phosphorylation, as expected, was limited to serines (Fig. 5-10F). Of note, alanine mutation of S241 abrogated CK2-mediated phosphorylation of Fic1 (Fig. 5-10E). We also performed kinase reactions using immunoprecipitated Orb5-myc_{13}, the *S. pombe* CK2 homolog (Snell and Nurse, 1994). Importantly, Orb5-myc_{13} also phosphorylated recombinant His_6-Fic1, and alanine mutation of S241 eliminated this phosphorylation (Fig. 5-10E). Thus, we concluded that S241 is a *bona fide* CK2-targeted site.

Discussion

Though phosphorylation serves diverse roles during eukaryotic cytokinesis (Bohnert and Gould, 2011), it has been unclear whether CR protein phosphorylation impacts cellular processes other than cell separation. In this study, we demonstrate that CDK- and CK2-mediated phosphoregulation of Fic1, a scaffold for SH3 domain proteins at the CR, modulates single-celled polarized growth and the developmental transition into

an invasive, pseudohyphal state. These findings reveal a previously unanticipated role for cytokinetic phosphosignaling in cellular morphogenesis, highlighting new facets of kinase-based growth control.

Relation of Fic1 phosphorylation to domains and localization patterns

We envision that C-terminal Fic1 phosphorylation influences interactions with SH3 domain proteins, because (1) phosphosites flank PxxP motifs mediating these interactions; and (2) deregulation of phosphorylation, similar to loss of PxxP-based protein-protein interactions (Bohnert and Gould, 2011), compromises bipolar cell growth. Intriguingly, differently phosphorylated pools of Fic1 exist throughout the cell cycle. This is somewhat confounding, as Fic1 localizes to one cellular site at each cell cycle stage (Bohnert and Gould, 2012; Roberts-Galbraith et al., 2009). This implies that multiple Fic1 subpopulations exist at the same location. How can this be explained? Perhaps some Fic1-based protein-protein interactions require dynamic regulation, which involves a rapid phosphorylation/dephosphorylation cycle. In support of dynamic phosphoregulation impacting Fic1's polarity function, phospho-abolishing and phospho-mimicking mutations both jeopardize NETO. Identification of phosphoregulated interactions, as well as detailed analysis of the mechanisms underlying such control, should clarify this dynamical complexity.

Interestingly, mutation of either phosphosite alone did not compromise growth polarity; only upon mutation of both phosphosites was a phenotype observed. Because the structure of Fic1's C-terminus is unknown, it is impossible to say whether T178 and S241 are close three-dimensionally. If so, perhaps phosphorylation at both sites is

required to modulate a specific protein-protein interaction. If not, maybe these phosphorylation events regulate binding of distinct proteins, which cumulatively affect Fic1-based CR signaling. Regardless, some coordination must be achieved at the kinase level, for the two phosphosites fit dissimilar consensuses and are phosphorylated by different kinases.

Given the previous finding that Fic1's C-terminus functions as this protein's major functional domain (Bohnert and Gould, 2012), it makes sense that polarity-relevant phosphorylation would occur in this region. In contrast, mutation or loss of Fic1's N-terminal C2 domain affects neither phosphorylation nor polarity. Apparently, Fic1's N-terminus solely mediates cell tip anchoring. Though we currently lack evidence suggesting Fic1-K22,27A fails at cell tip anchoring due to impaired lipid binding, this seems the most likely explanation, given that charged interactions facilitate C2 domain-lipid associations (Cho and Stahelin, 2006). Whether Fic1's C2 domain influences CR-membrane binding during cytokinesis is also unknown, though other membrane binders, including F-BAR proteins Cdc15 and Imp2, would likely compenate for loss of this interaction. Why does Fic1 localize to cell tips if it does not perform a polarity function at this site? One possibility is that Fic1 piggybacks with another CR protein to cell tips following cell division. Consistent with Fic1 simply relocating with its binding partners during the cell cycle, Fic1 acts as a 'molecular glue,' and its protein levels do no fluctuate during the cell cycle. Thus, Fic1's scaffolding function likely dictates its localization pattern, though these associations appear functionally most relevant during cytokinesis.

Kinases involved in Fic1-based polarity regulation

CDKs are well-documented regulators of polarized cell growth in fungi. Much of this phosphoregulation centers on Cdc42, a Rho-family GTPase key in fungal cell polarity (Adams et al., 1990). Cdc42 GEFs positively regulate Cdc42 function, and, in *S. cerevisiae*, CDK-mediated phosphorylation of GEF-binding proteins facilitates this activation (McCusker et al., 2007; Shimada et al., 2000). GEFs of other polarity-relevant GTPases are directly phosphorylated and activated by CDK (Kono et al., 2008), suggesting similar mechanisms may also control Cdc42 GEFs. Cdc42 activation is enhanced via CDK-mediated inhibitory phosphorylation of Cdc42 GAPs (Knaus et al., 2007; Sopko et al., 2007), which otherwise negatively regulate Cdc42. Our findings indicate that CDK-based control of polarized cell growth extends beyond phosphoregulation of the Rho-family GTPase cycle, and that CDK-mediated phosphoregulation of the CR can impact growth zones. It will be important to determine whether CDK-mediated phosphorylation of other CR proteins, including Cdc15 (Roberts-Galbraith et al., 2010), likewise influences morphogenesis.

Though a hyphal-specific cyclin-CDK complex can restrict Cdc42 GAP function to promote *C. albicans* invasiveness (Zheng et al., 2007), other findings suggest some forms of CDK activity negatively regulate the dimorphic switch. Indeed, loss of canonical cell cycle cyclins enhances filament-like growth (Bachewich and Whiteway, 2005; Bensen et al., 2005; Chapa y Lazo et al., 2005), whereas loss of *C. albicans* Cdc14-family phosphatase, which reverses CDK-mediated phosphorylation, has the opposite effect (Clemente-Blanco et al., 2006). Thus, it will be important to further dissect mechanisms of CDK-mediated Fic1 phosphorylation to assess how this event modulates the *S. pombe* dimorphic switch.

We note that MAP kinases, which are proline-directed kinases similar to CDK (Lu et al., 2002), represent likely candidates for redundant kinases targeting Fic1 T178. MAP kinases in *S. cerevisiae* have been postulated to work in parallel to Cdc42 in directing cell polarization (Mazzoni et al., 1993), and deregulation of MAP kinase signaling can enhance invasive growth (Cook et al., 1996). Accordingly, it seems likely that MAP kinases perform a conserved polarity function in *S. pombe*, though this presumably occurs in part through phosphoregulation at the CR.

Similar to CDK, CK2 governs cellular polarization in both budding and fission yeasts (Rethinaswamy et al., 1998; Snell and Nurse, 1994). In a striking parallel to *fic1* phosphomutants, loss of CK2 function in *S. pombe* impedes the re-initiation of bipolar cell growth after cell division (Snell and Nurse, 1994). Because CK2 deregulation causes errors in both cell growth and cytokinesis (Roussou and Draetta, 1994), it is possible that CK2 influences growth polarity partly via its cytokinetic functions, which include phosphoregulation of Fic1. Not surprisingly, CK2 also impacts fungal virulence (Chiang et al., 2007), although individual CK2-mediated phosphorylation events impacting invasiveness were relatively unknown. Our identification of CK2-mediated Fic1 phosphorylation thus presents a novel facet of this signaling.

Phosphoregulation of the dimorphic switch

In *S. pombe*, Sep1 and Ace2 induce mitotic transcriptional waves (Rustici et al., 2004), which are important for expression of genes required for daughter cell separation (Martin-Cuadrado et al., 2003; Sipiczki et al., 1993). Though it has been postulated that inhibition of these transcriptional waves could trigger the dimorphic switch (Bahler,

2005), we previously noted that cytokinesis-based constraints on polarized growth in *S. pombe* may provide a more direct signaling route for this developmental program (Bohnert and Gould, 2012). In this study, we have shown that Fic1 phosphorylation regulates this protein's polarity function, and that deregulation of Fic1 phosphorylation induces hyphal-like growth. Thus, we believe our findings support the ideas that (1) phosphoregulation of the CR can directly activate the dimorphic switch; and (2) modulation of kinase and/or phosphatase signaling may be sufficient for this switch. As extensive phosphosignaling occurs during hyphal growth (Sudbery, 2011), integration of multiple cues likely guarantees the robustness of this transition.

CHAPTER VI

CONCLUSIONS

Though an extensive 'parts list' of cytokinesis factors has been defined in multiple organisms [for reviews, see (Balasubramanian et al., 2012; Pollard and Wu, 2010)], our understanding of how these proteins interact and signal during cell division is still in its infancy. In this work, I have examined mechanisms by which kinase pathways influence CR composition and function, and I have also investigated the consequences that inefficient cytokinesis exert on cellular growth.

In chapter II, I characterized a new member of the *S. pombe* CPC, contradicting previous reports (Vader et al., 2006) that Borealin does not exist in yeasts. *S. pombe* Borealin controls the activity and localization of other CPC components, including Aurora B kinase. I found that *S. pombe* Borealin, together with the rest of the CPC, influences targeting of Cdc14-family phosphatase to the CR, and thereby affects *S. pombe* cytokinesis.

In chapter III, I identified the first core CR protein targeted by the fission yeast SIN. I demonstrated that Sid2-mediated phosphorylation of formin Cdc12 is required for SIN-dependent cytokinesis. Such phosphorylation reverses multimerization of a novel formin domain, which also participates in F-actin bundling at the CR. This oligomeric switch enables CR maintenance during cytokinesis, because CRs collapse into spot-like structures upon loss of Sid2-mediated Cdc12 phosphorylation.

In chapter IV, I investigated the possibility that inefficient cytokinesis impacts subsequent polarized growth. Through structure-function analysis of Fic1, I found that CR signaling, based on Fic1 scaffolding of SH3 domain proteins, is required for NETO. Disruption of CR, cell wall, or membrane remodeling at the division site specifically impedes NETO and triggers an invasive growth transition favoring a pseudohyphal form. CR-based constraints on polarized growth partially override other growth controls, suggesting these cues are primary determinants of *S. pombe* growth polarity.

In chapter V, I analyzed the contribution of phosphosignaling to cytokinesis-based growth controls. Focusing on Fic1, I found that Fic1 is phosphorylated on two C-terminal sites, which flank SH3-binding PxxP motifs, and that deregulation of this phosphorylation jeopardizes NETO. Using a candidate approach, I identified CDK and CK2 as two kinases involved in such phosphoregulation.

Altogether, these studies reveal unexpected functions for well known cell cycle regulators, broaden our knowledge of complex phosphosignaling during cytokinesis, and describe novel links between cytokinesis and other cell cycle events. These findings thus address many facets of cell cycle control and pose many exciting questions for future research.

Aurora B-mediated regulation of *S. pombe* cytokinesis

In contrast to previous reports (Petersen and Hagan, 2003), my findings suggest that *S. pombe* Aurora B kinase, similar to Aurora B in other organisms (Ruchaud et al., 2007), controls cytokinesis. This is intriguing, because the *S. pombe* CPC is never exported out of the nucleus during the cell cycle, and *S. pombe* undergoes a closed

mitosis, in which the nuclear nevelope does not break down. How does Aurora B thus affect the CR, which lines the cell cortex? One possibility is that Aurora B phosphorylates nuclear proteins that subsequently re-localize to the division site. Cdc14-family phosphatase Clp1, for one, behaves in this manner (Trautmann et al., 2001). I have demonstrated that the *S. pombe* CPC is required for Clp1 accumulation at the CR during cytokinesis, and a research specialist in the laboratory, Jun-Song Chen, has shown that *S. pombe* Aurora B phosphorylates Clp1 *in vitro*. As Clp1 possesses multiple Aurora B consensus sites, it seems possible that Aurora B-mediated phosphorylation of Clp1 participates in such regulation. Consistent with this interpretation, some Aurora B consensus sites on Clp1 are also phosphorylated by Sid2, and these phosphorylations facilitate Clp1 cytoplasmic retention during cytokinesis (Chen et al., 2008). If Aurora B phosphorylation of Clp1 functions similarly, it will be interesting to explore how Aurora B, which is activated in early mitosis, cooperates with Sid2, which is activated later, to ensure proper targeting of Clp1 during cytokinesis. In addition, recent genome-wide analysis of Aurora B substrates in *S. pombe* uncovered other putative cytokinesis targets (Koch et al., 2011), and future validation of these substrates should clarify the extent of CPC-mediated phosphoregulation during cytokinesis.

Phosphoregulation of formin Cdc12

My data have established that Cdc12 is a phosphoprotein, and that the SIN kinase Sid2 participates in Cdc12 phosphorylation. Nonetheless, additional kinases besides Sid2 likely contribute to Cdc12 phosphoregulation, because (1) Cdc12 is phosphorylated in both late interphase and early mitosis, when the SIN is largely inactive; and (2) the

Cdc12-4A phosphomutant is still phosphorylated, though to a lesser extent than wild-type Cdc12, during cytokinesis. Unfortunately, the low abundance of Cdc12 (Wu and Pollard, 2005) has prevented large-scale purification of Cdc12 and mass spectrometric analysis of Cdc12 phosphosites. Using *in vitro* strategies similar to those used in identifying Sid2-mediated Cdc12 phosphorylation, I have also shown that *S. pombe* CDK phosphorylates Cdc12. Intriguingly, this phosphorylation is limited to N-terminal and C-terminal patches. Though canonical autoinhibition has not been demonstrated for Cdc12 (Yonetani et al., 2008), it is an attractive model that CDK-mediated phosphorylation at the formin ends may control Cdc12 activation at mitotic onset. Whether or not this involves relief of autoinhibition, similar to that observed for other formin phosphorylation events (Takeya et al., 2008; Wang et al., 2009), will be important to address in the future.

Of note, two of the N-terminal CDK phosphosites occur within a region that is conserved throughout the *Schizosaccharomyces* genus. When this region is deleted from an N-terminal fragment, CR localization no longer occurs (Yonetani et al., 2008), suggesting this stretch provides a key protein-protein binding interface. As F-BAR Cdc15 binds the Cdc12 N-terminus (Carnahan and Gould, 2003), it will be important to address whether the Cdc12-Cdc15 interaction occurs through this conserved N-terminal Cdc12 stretch, and whether CDK-mediated phosphorylation in this region also contributes to regulation of this binding.

Contribution of the Cdc12 C-terminus to formin activities

The identification of a novel C-terminal domain, which multimerizes, could potentially be paradigm-shifting in terms of how we view formin oligomerization. Though dimeric FH2 associations enhance formin-mediated actin polymerization (Chesarone et al., 2010), higher-ordered oligomers relevant *in vivo* have not been previously described. To understand in more detail the oligomerization domain identified in this work, it will be necessary to crystallize the recombinant fragment and to obtain structural information about revelant folds and/or residues. Structural data could inform future mutagenesis of this domain *in vivo* and provide insight into the conservation of such a domain among formins and other cytoskeletal factors.

My analysis indicated that Cdc12's C-terminal oligomerization domain functions in linear F-actin bundling. Accordingly, structural analyses may hint at the spatial parameters set by this oligomerization event, which guide the linearity of bundling. Still, I have shown that the oligomerization domain on its own cannot bundle F-actin; thus, outside F-actin binding sites in the C-terminus also contribute to this activity. It will therefore be important truncate the C-terminus into smaller C-terminal fragments and to test which are sufficient for F-actin binding and/or bundling *in vitro*. Importantly, the Cdc12 C-terminus appears to enhance other activities in addition to F-actin bundling. In collaboration with Dr. David Kovar's laboratory at the University of Chicago, I have shown by TIRF microscopy that the Cdc12 C-terminus stimulates FH1FH2-based actin assembly *in vitro*. In the future, it will be crucial to describe participating domains and to determine the kinetics by which the Cdc12 C-terminus also accelerates F-actin nucleation and/or polymerization.

Are the activities of the Cdc12 C-terminus regulated by mechanisms other than phosphorylation? Though canonical DID and DAD interactions are thought not to operate for Cdc12 (Yonetani et al., 2008), I have found that the Cdc12 N-terminus inhibits F-actin bundling by the Cdc12 C-terminus. Perhaps, N- and C-terminal *cis* interactions may occlude the F-actin bundling domain. Whether such interactions exist and how they contribute to autoregulation of formin activities *in vivo* should be of significant future interest.

Coordinating cell growth and division cycles

What is the advantage of *S. pombe* growing in a single-celled state? Some have postulated that single-celled growth is metabolically more efficient in nutrient-rich conditions (Bahler, 2005; Madhani and Fink, 1998); however, during starvation, invasiveness would facilitate nutrient foraging. If this is true, one would expect that in appropriate contexts nutritional cues might induce cytokinetic errors, thereby inhibiting new end growth and inducing the dimorphic switch. My studies suggest that one mechanism by which this could occur is through tweaking of Fic1 phosphoregulation. Presumably, other CR phosphoproteins that impact cell polarity could likewise be regulated upon activation of this morphogenetic program. Expression profiling of relevant kinases and phosphatases during this transition will likely provide insight into whether such alterations in signaling indeed occur. Moreover, it will be interesting to further explore whether intrinsically invasive fungal species lack phosphosignaling important for single-celled polarization and growth. It is an intriguing possibility that

new phosphosignaling events, which drove efficient cell separation, contributed to the evolution of the single-celled fungal state (Bahler, 2005).

Additionally mysterious is why polarized tip growth ceases during *S. pombe* mitosis. In an intriguing parallel, cellular polarization is also lost during animal cell mitosis, as cells round up. Clearly, these changes must involve alterations in the cellular cytoskeleton. Upon mitotic onset in *S. pombe*, interphase microtubules depolymerize as the mitotic spindle forms, and actin disappears from cell tips and concentrates at the medial CR (Chang and Martin, 2009). Currently, it is unclear how alterations in the cytoskeleton accommodate this growth switch. For example, do depolymerizing interphase microtubules provide a tubulin pool for the developing mitotic spindle, or can a cell still efficiently form a mitotic spindle if interphase microtubules persist? Whatever the nature of the signal stalling *S. pombe* mitotic tip growth, the *tea1-for3* strain created in my studies bypasses this signal and continues to grow at cell tips throughout mitosis. Thus, this strain provides a powerful tool for investigating growth regulation during mitosis. Time-lapse imaging of actin and microtubules in *tea1-for3* cells should clarify which is/are most relevant to this switch and could provide insight into the mechanisms and consequences of this coordination.

SH3 domain-based protein-protein interactions at the CR

Structure-function analysis of *S. pombe* Fic1 indicated that its C-terminus, which is composed of little other than PxxP motifs, serves as its major functional domain at the CR. Thus, we concluded that Fic1 acts as a 'molecular glue,' bridging SH3 domain proteins to expedite and direct signaling. To our knowledge, our studies define the first

specific SH3 ligand for *S. pombe* PCH proteins. Specifically, we showed that Fic1's terminal PxxP motif is responsible for binding the PCH protein Cdc15. The amino acids flanking this PxxP motif indicate it fits the binding consensus for class II SH3 domains [ϕPXϕPX+, where ϕ and + indicate hydrophobic and basic residues respectively (Mayer, 2001)]. Our laboratory has recently found that other Cdc15-binding partners, including Spa2, a GTPase involved in cytokinesis, interact with Cdc15's SH3 domain through PxxP motifs with similar residues. Thus, my identification of the Cdc15 SH3 as a class II domain could potentially be helpful in predicting other Cdc15-interacting sites. Similar analyses could also be used to characterize SH3 domains of other cytokinesis proteins, including Imp2 and Cyk3. As the Cdc15 and Imp2 SH3 domains are functionally redundant (Roberts-Galbraith et al., 2009), one might assume they bind a similar sequence. However, proteins like Fic1, which contain numerous PxxP motifs of varying consensuses, can likely accommodate interactors of differing classes. Addressing similarities and/or differences among relevant SH3 domains may therefore elucidate how they collaborate during cytokinesis.

Evidently, Fic1 binds additional SH3 proteins besides Cdc15, Imp2, and Cyk3 at the CR, because Fic1 still localizes to this site when interactions with all of these proteins are lost. In total, 21 *S. pombe* proteins possess SH3 domains, and multiple of these localize to the division site. Identification of additional Fic1-binding SH3 proteins will provide a more complete understanding of protein-protein interaction networks at the CR and will likely uncover novel cytokinetic factors impacting growth polarity.

Conclusion

As a whole, my thesis highlights the complexity of cytokinesis; indeed, multiple molecular cues govern the robustness of this final cell cycle stage and consequently influence other cell cycle events. Using fission yeast, I have uncovered novel proteins, interactions, and signaling events, which I expect will inform cytokinesis studies in other organisms. As this inventory grows with future experiments, including those proposed in this chapter, I am confident our understanding of the molecular mechanisms and consequences of CR regulation will continue to improve, providing new, useful insight into the cellular life cycle.

APPENDIX A

MATERIALS AND METHODS

Strains and general yeast methods

The *S. pombe* strains used in these studies were grown in either yeast extract (YE) media or Edinburgh minimal media (EMM) with relevant supplements. Proteins of interest were tagged endogenously at the 3' end with kan^R-, hyg^R-, or nat^R-based cassettes as previously described (Bahler et al., 1998). A lithium acetate method was used in *S. pombe* tagging transformations (Keeney and Boeke, 1994), and integration of tags was verified using whole-cell PCR and/or fluorescence microscopy. Introduction of tagged loci into other strains was accomplished using standard *S. pombe* mating, sporulation, and tetrad dissection techniques.

Cell cycle arrests were achieved as follows: (1) *cdc10*-V50 cells were arrested in G1 by shifting cultures grown at 25°C to 36°C for 4 h; (2) *cdc25*-22 cells were arrested in G2 by shifting cultures grown at 25°C to 36°C for 3 h; (3) *nda3*-KM311 cells were arrested in prometaphase by shifting cultures grown at 32°C to 18°C for 6.5 h; (4) *cps1*-191 cells were arrested in cytokinesis by shifting cultures grown at 25°C to 36°C for 3 h; (5) cells were arrested in S phase by growth in 12 mM hydroxyurea (Sigma) for 3.5 h at 32°C. For release from the *cdc25*-22 G2 arrest, cultures were cooled immediately to 25°C on ice and then grown at 25°C. For release from the hydroxyurea-induced S phase arrest, yeast were filtered, washed in yeast extract medium, and then grown at 32°C. For

release from the *nda3*-KM311 arrest, cells were shifted to 32°C for synchronous progression into anaphase.

SIN hyperactivation in *cdc16*-116 strains was induced by shifting cultures grown at 25°C to 36°C for 3-4 h. When necessary, cells were first synchronized in interphase by centrifugal elutriation using an Avanti J-26 XPI centrifuge (Beckman Coulter).

For Lat A treatment, either DMSO or DMSO containing Lat A was added to log phase cultures. The final Lat A concentration was 0.2 μM. Cultures were kept at 32°C for 8 h before fixation and staining.

For spot assays, cells were grown to log phase at 25°C, 10 million cells were resuspended in 1 mL water, and 1 mL serial dilutions were made. 2.5 μL of each dilution were plated on agar. Plates were incubated at various temperatures.

Over-expression of *nbl1(1-95)*, acyl-GFP, LifeAct-GFP, *cdc12*$^{+}$, and *cdc12* truncations was controlled by thiamine-repressible *nmt* promoters. Expression was kept off by addition of 5 μg/mL thiamine to the medium, and expression was induced by washing and culturing in medium lacking thiamine.

For spore germination experiments, sporulating diploids were digested with glusalase at 32°C, allowed to recover in YE at 32°C for 1 hr, and then grown in EMM plus supplements overnight at 25°C.

Construction of mutants

Disruption of *nbl1*$^{+}$ was achieved by PCR-based one-step homologous recombination (Bahler et al., 1998). Specifically, the *nbl1(1-95)* fragment was targeted for deletion using *ura4*$^{+}$ as the selectable marker. Following transformation of an *ade6*-

M210/*ade6*-M216 *ura4*-D18/*ura4*-D18 *leu1*-32/*leu1*-32 h-/h+ diploid with the relevant amplified fragment, stable integrants were selected and the *nbl1(1-95)* deletion was confirmed by PCR.

To create the *nbl1*-shutoff strain, a pZERO-2 vector with *nbl1(1-95)* cDNA was also generated by Integrated DNA Technologies. *nbl1(1-95)* cDNA was excised from this vector and cloned into pREP41, placing *nbl1(1-95)* expression under control of pREP41's thiamine-repressible *nmt41* promoter (Basi et al., 1993). The *nmt41-nbl1(1-95)* fragment was subcloned into a pJK148 vector, linearized within the *leu1* gene with NruI, transformed into a wild-type strain, and an integrant at the *leu1* locus was identified. In addition, a pSK vector with *nbl1(1-95)* cDNA and flanking sequences was constructed, and *nbl1(1-95)* cDNA and flanking sequences were excised from this vector and inserted into a pIRT2 vector. A diploid heterozygous for *nbl1* disruption was then transformed with this plasmid, and transformed diploids were sporulated in nitrogen-lacking EMM. Spores were subsequently isolated using glusalase, and *nbl1*-disrupted cells covered by the plasmid were selected on EMM plus adenine. These cells were then crossed to those cells having *nmt41-nbl1(1-95)* integrated, and a *nbl1*-shutoff strain, which can grow on EMM plus adenine but not on EMM plus adenine and thiamine, was selected.

The *nbl1-T91A* mutation was introduced by site-directed mutagenesis into the pIRT2 vector containing *nbl1(1-95)* cDNA and flanking sequences. A diploid heterozygous for the *nbl1* disruption was then transformed with this plasmid, and haploid *nbl1*-disrupted cells covered by the plasmid were selected. This strain was then grown to

midlog phase in YE, and 10 million cells were plated on YE plus 5-FOA to select for the appropriate replacement strain, which was confirmed by PCR and sequence analysis.

The *nbl1(1-69)* truncation was established in a wildtype diploid strain through the introduction of a stop codon and kan^R cassette after proline 69 via tagging.

Mutants and truncations of *fic1* were expressed from the endogenous $fic1^+$ locus. To make these strains, a pIRT2 vector was originally constructed in which $fic1^+$ gDNA with 5' and 3' flanks was inserted between BamHI and PstI sites of pIRT2. Mutations were then introduced via site-directed mutagenesis. The *fic1N* construct was made by inserting a stop codon after residue 126. The *fic1C* construct was created by inserting XhoI sites before both the start codon and residue 127, digesting with XhoI to release the internal fragment, re-ligating the plasmid, and adding a start codon after the remaining XhoI site. *fic1Δ* was then covered by these pIRT2-*fic1* constructs, and stable integrants resistant to 5-FOA were isolated and confirmed by whole-cell PCR and Western blotting.

To make the *tea1-for3* fusion, a pIRT2 vector was originally constructed in which $tea1^+$ gDNA with 5' and 3' flanks was inserted between SacI and SphI sites of pIRT2. Site-directed mutagenesis was performed to replace the $tea1^+$ stop codon with a SmaI/SalI/PstI multiple cloning site. $for3^+$ gDNA was amplified with a small N-terminal linker sequence and inserted between SmaI and PstI in this multiple cloning site (linker residues are Pro-Gly-Ade-Gly-Ade-Gly-Ade accounting for restriction site and added residues). *tea1Δ* was then covered by this pIRT2-*tea1-for3* construct, and stable integrants resistant to 5-FOA were isolated and confirmed by whole-cell PCR and Western blotting. An integrant was subsequently mated with *for3Δ*, such that we could isolate *tea1-for3* strains in which $tea1^+$ and $for3^+$ were lacking.

To create the endogenous *cdc12-4A* and *cdc12Δ1451-1538* alleles, a pSK vector was constructed that contained the following in order: 5' *cdc12* flank, full-length *cdc12*$^{+}$, kan^{R} cassette, and 3' *cdc12* flank. Phosphorylation site mutations were created using a QuikChange Multi-site Site-directed Mutagenesis kit (Agilent Technologies) and confirmed by sequencing. For the internal deletion, Not1 restriction sites were inserted before and after residues 1451 and 1538, respectively. After removal of residues 1451-1538 and re-ligation, the Not1 site was eliminated via mutagenesis, and the construct was re-sequenced. *cdc12-4A* and *cdc12Δ1451-1538* constructs were then cut from the vectors and transformed into wild-type *S. pombe* cells using a lithium acetate method. Kan-resistant cells were selected and sequenced to identify transformants containing appropriate mutations.

In vivo truncations of *cdc12* were generated by PCR-mediated insertions of $V5_3$ or GFP_3 after relevant amino acids.

General protein methods

Cell pellets were snap frozen in dry ice-ethanol baths. Lysates were prepared by bead disruption, using a touch vortexer or a Fastprep cell homogenizer (MP Biomedicals). Immunoprecipitations were performed in either NP40 buffer for native lysates, or in NP40 buffer containing SDS for denatured lysates as previously described (Gould et al., 1991). Protein samples were resolved by SDS-PAGE and transferred to PVDF membrane (Immobilon P; EMD Millipore). Anti-HA (12CA5), anti-Myc (9E10), anti-V5 (Invitrogen), anti-FLAG (M2; Sigma), anti-GFP (Roche), anti-Cdc15 (Roberts-Galbraith et al., 2009), or anti-Cdc2 (Sigma) were used in immunoprecipitations and/or

as primary antibodies in immunoblotting. Secondary antibodies were conjugated to Alexa Fluor 680 (Invitrogen), IRDye680LT (LI-COR Biosciences), or IRDye800 (LI-COR Biosciences). Blotted proteins were detected via an Odyssey machine (LI-COR Biosciences). For gel shifts, denatured lysates were treated with lambda phosphatase (New England Biolabs) in 25 mM HEPES-NaOH (pH 7.4), 150 mM NaCl, and 1 mM $MnCl_2$ and incubated at 30°C for 30 min with shaking. Where indicated, samples were resolved by SDS-PAGE in the presence of 10 μM Phos-tag acrylamide per the manufacturer's protocol (Wako Chemical USA).

Purification of TAP samples and identification of interacting proteins and/or phosphorylation sites were performed as previously described (Gould et al., 2004; Lu et al., 2012; Roberts-Galbraith et al., 2009).

Recombinant proteins were produced in competent BL21 cells and purified on amylose beads (New England Biolabs, Inc.) or His-Bind resin (EMD Millipore) according to the manufacturers' protocols. When necessary, recombinant proteins were concentrated using Amicon Ultra centrifugal filter units (EMD Millipore). PD-10 columns (GE Healthcare) were used for buffer exchange of eluted recombinant proteins used in F-actin assays; the final buffer for these proteins was 50 mM HEPES (pH 7.5). Native gel analysis of recombinant proteins was performed in the absence of SDS.

For *in vitro* binding assays, recombinant proteins were incubated together or with cellular immunoprecipitates for 1 h at 4°C. Following washing, samples were resolved by SDS-PAGE for Coomassie-blue staining or Western blot analysis.

In vitro kinase assays

The Ark1 kinase assay was performed as previously described (Ohi et al., 2004; Petersen et al., 2001) with minor modifications. Briefly, anti-GFP immunoprecipitates were washed three times in 1 mL NP40 buffer and three times in 1 mL 1X kinase buffer (20 mM K-HEPES, pH7.8, 5 mM $MgCl_2$, 1 mM EGTA, and 1 mM DTT). After washes, liquid was aspirated and 4 μL 5X kinase buffer was added to resuspend the beads. 5 μg purified Histone H3.2 (New England Biolabs), 50 μM cold ATP, and 5 μCi of [γ-^{32}P] ATP (Amersham Biosciences) were added. After incubation with shaking at 30°C for 30 min, reactions were terminated by addition of 5 μl of 5X SDS-PAGE loading buffer, and proteins were resolved on a 4-12% Bis-Tris gel (Invitrogen). The gel was cut in half and the upper portion (30-90 kDa) was transferred to a PVDF membrane and blotted with anti-GFP antibodies to detect Ark1-GFP. The lower part (10-30 kDa) of the same gel was stained by Coomassie blue dye to visualize Histone H3.2, and, following drying of the gel, autoradiography was used to check incorporation of ^{32}P.

For CDK kinase assays, approximately 50 ng of recombinant Cdc2 kinase complex, purified from baculovirus-infected insect cells as previously described (Yoon et al., 2002), was incubated with recombinant protein in a reaction buffer containing 50 mM Tris pH 7.4, 10 mM $MgCl_2$, 2 µM DTT, 10 µM unlabeled ATP, and 5 μCi of [γ-^{32}P] ATP. After incubation with shaking at 30°C for 30 min, reactions were terminated with 5X sample buffer, and samples were boiled and separated by SDS-PAGE. Where appropriate, phosphoamino acid analysis was performed as described in (McCollum et al., 1999).

For Sid2 kinase assays, the Sid2-Mob1 kinase complex was immunoprecipitated from SIN-activated *sid2-Myc*$_{13}$ *cdc16-116* cells. [γ^{32}P]ATP kinase assays, phosphoamino

acid analysis, and tryptic peptide mapping were performed as described in (Feoktistova et al., 2012; McCollum et al., 1999; Sparks et al., 1999) and references therein. *In vitro* phosphorylation of recombinant proteins used in *in vitro* binding assays was performed via identical kinase assays, except that radioactive [γ^{32}P]ATP was eliminated and the final concentration of unlabeled ATP in reactions was increased to 2 mM.

For CK2 kinase assays, CK2 (New England Biolabs) or Orb5-Myc_{13}, immunoprecipitated from *orb5*-Myc_{13} cells and washed in CK2 buffer (20 mM Tris-HCl, 50 mM KCl, 10 mM $MgCl_2$, pH 7.5; New England Biolabs), was incubated with recombinant protein and 5 μCi of [γ-^{32}P] ATP in CK2 buffer. After incubation with shaking at 30°C for 30 min, reactions were terminated with 5X sample buffer, and samples were boiled and separated by SDS-PAGE. Where appropriate, phosphoamino acid analysis and tryptic peptide mapping were performed as described in (McCollum et al., 1999).

F-actin binding and bundling assays

To analyze F-actin binding and bundling, rabbit skeletal muscle actin (Cytoskeleton Inc.) was resuspended in General Actin Buffer (5 mM Tris HCl (pH8), 0.2 mM $CaCl_2$, 0.2 mM ATP, 0.5 mM DTT) to a concentration of 24 µM. This was kept on ice for 1 h. 10X polymerization buffer (500 mM KCl, 20 mM $MgCl_2$, 10mM ATP) was then added to a final concentration of 1X, and tubes were nutated at room temperature for 1 h. 3 µM F-actin was subsequently incubated with recombinant proteins at room temperature for 30 min, and samples were either centrifuged or diluted 1:100 in 70 nM rhodamine-phalloidin (Cytoskeleton Inc.) for imaging. High-speed centrifugation at

100,000g and low-speed centrifugation at 15,000g were performed at room temperature for 30 min using a TLA-100 rotor (Beckman Coulter). Following centrifugation, pellets and supernatants were separated, and equal portions of pellets and supernatants were resolved by SDS-PAGE for Coomassie blue staining. The affinity (K_D) of MBP-Cdc12C for F-actin was calculated by fitting a quadratic equation to the high-speed binding data.

Yeast two-hybrid analysis

Yeast two-hybrid analysis was performed as previously described (Rosenberg et al., 2006), except that the bait and prey plasmids were either empty or encoded Cdc15 SH3 (aa843-927) (Roberts-Galbraith et al., 2009), Cyk3 SH3 (aa1-59), wild-type (Roberts-Galbraith et al., 2009) or mutant Fic1(aa190-269) fragments, or full-length Fic1.

Invasive growth assays

To assay pseudohyphal invasion into 2% agar, 5 µl containing a total of 10^5 cells were spotted on 2% YE agar and incubated at 29°C for 20 days. Colonies were subsequently placed under a steady stream of water and surface growth was wiped off using a paper towel. These methods were established in previous studies (Pohlmann and Fleig, 2010; Prevorovsky et al., 2009).

To assay whether specific mutants rescued invasiveness of an *asp1Δ* strain on 0.3% agar (Pohlmann and Fleig, 2010), 1 µl containing 10^6 cells was spotted on 0.3% YE agar as well as onto 2% agar as a control. Plates were incubated at 29°C for 12 days, at which point colony growth and/or biofilm formation were visualized.

Microscopy

Fixed- and live-cell images of *S. pombe* cells were acquired using one of the following: (1) a microscope (Axioskop II; Carl Zeiss, Inc.) equipped with a 100X NA 1.40 PlanApo oil immersion objective, a halogen lamp, and OpenLab 4.0.3 software (PerkinElmer); (2) a spinning disc confocal microscope (Ultraview LCI; PerkinElmer), which is equipped with a 100X NA 1.40 PlanApo oil immersion objective, a 488-nm argon ion laser (GFP), a 594-nm helium neon laser (RFP, mCherry), a charge-coupled device camera (Orca-ER; Hamamatsu Phototonics), and Metamorph 7.1 software (MDS Analytical Technologies; Molecular Devices); or (3) a personal DeltaVision microscope system (Applied Precision), which includes an Olympus IX71 microscope, 60X NA 1.42 PlanApo and 100X NA 1.40 UPlanSApo objectives, fixed- and live-cell filter wheels, a Photometrics CoolSnap HQ2 camera, and softWoRx imaging software.

All cells were grown to and/or arrested in log phase before fixation or live-cell imaging. Bright field images were used in determining cell lengths at division.

For nuclei and cell wall imaging, cells were fixed in 70% ethanol for at least 30 min before DAPI and methyl blue staining. For counting of cells joined at their division sites, cells were also sonicated at 3.5 W following fixation to break weak associations.

For phalloidin staining, cells were fixed in formaldehyde (Polysciences Inc.) for 5 min, and fixation was stopped by addition of PBS. Cells were washed three times in PBS and incubated with 0.1% NP40 for 1 min to permeablize cells. Cells were pelleted and washed three more times in PBS. Then, Alexa-Fluor 488 phalloidin (Molecular Probes) was added. Samples were placed on a nutator for 1 h, and then stained with DAPI if necessary.

For calcofluor staining, cells were washed in PBS and then resuspended in PBS containing 5 μg/mL calcofluor. After incubation on ice for 30 min, cells were washed three times in PBS and images were acquired using the personal DeltaVision system. Using the proximity of birth scars to cell ends, growth/morphology was scored as one of the following: monopolar (i.e., growth on one end), bipolar (i.e., growth on both ends), monopolar and septated, bipolar and septated, or multiseptated. For cells just completing division, daughter cells were scored as monopolar as long as ingression of the mother cell had progressed to such a degree that birth scars could be easily identified at new ends.

Images of yeast colonies and pseudohyphae were acquired by focusing a camera (PowerShot SD750; Canon) through a microscope (Universal; Carl Zeiss, Inc.) equipped with a 20X NA 0.32 objective.

Time-lapse imaging was performed by one of the following methods: (1) cells were secured on YE agar pads sealed with Valap (a Vaseline, lanolin, and paraffin mixture); or (2) cells were loaded into Y04C plates for 5 s at 8 psi using the ONIX microfluidics perfusion system (CellASIC), and YE liquid media flowed into the chamber at 5 psi throughout imaging. Either an objective heater system (Bioptech) or a heated chamber (Applied Precision) maintained the relevant temperature during imaging.

For time-lapse imaging of chromosomal passenger complex mutants, cells were first synchronized in G2 phase using a 7-30% lactose gradient, and then were shifted to 36°C for 2-3 h before live-cell microscopy.

For live-cell DIC movies, growth patterns were scored according to the tip growth that had occurred prior to the next septation. Relative cell ages were scored where applicable based on the number of birth scars seen on each daughter cell. Times until

NETO were only determined for cells that initiated NETO prior to the next septation, except for *tea1-for3* cells, for which tip growth at new ends was monitored until growth at these sites occurred even if this carried into the next cell cycle. During time-lapse DIC imaging, daughter cells were judged as monopolar after septum splitting when birth scars could be identified, and timing for NETO was started at this point. The point of new end growth was noted when evident elongation occurred relative to birth scars formed by cytokinesis.

Rhodamine-phalloidin-stained actin filaments and/or bundles were imaged using the DeltaVision system.

REFERENCES

Adams, A.E., D.I. Johnson, R.M. Longnecker, B.F. Sloat, and J.R. Pringle. 1990. CDC42 and CDC43, two additional genes involved in budding and the establishment of cell polarity in the yeast Saccharomyces cerevisiae. *J Cell Biol*. 111:131-142.

Almonacid, M., J.B. Moseley, J. Janvore, A. Mayeux, V. Fraisier, P. Nurse, and A. Paoletti. 2009. Spatial control of cytokinesis by Cdr2 kinase and Mid1/anillin nuclear export. *Curr Biol*. 19:961-966.

Amoah-Buahin, E., N. Bone, and J. Armstrong. 2005. Hyphal Growth in the Fission Yeast Schizosaccharomyces pombe. *Eukaryot Cell*. 4:1287-1297.

An, H., J.L. Morrell, J.L. Jennings, A.J. Link, and K.L. Gould. 2004. Requirements of fission yeast septins for complex formation, localization, and function. *Mol Biol Cell*. 15:5551-5564.

Arellano, M., A. Duran, and P. Perez. 1997. Localisation of the Schizosaccharomyces pombe rho1p GTPase and its involvement in the organisation of the actin cytoskeleton. *J Cell Sci*. 110 (Pt 20):2547-2555.

Asiedu, M., D. Wu, F. Matsumura, and Q. Wei. 2008. Phosphorylation of MyoGEF on Thr-574 by Plk1 promotes MyoGEF localization to the central spindle. *J Biol Chem*. 283:28392-28400.

Ayscough, K.R., J. Stryker, N. Pokala, M. Sanders, P. Crews, and D.G. Drubin. 1997. High rates of actin filament turnover in budding yeast and roles for actin in establishment and maintenance of cell polarity revealed using the actin inhibitor latrunculin-A. *J Cell Biol*. 137:399-416.

Bachewich, C., and M. Whiteway. 2005. Cyclin Cln3p links G1 progression to hyphal and pseudohyphal development in Candida albicans. *Eukaryot Cell*. 4:95-102.

Bahler, J. 2005. A transcriptional pathway for cell separation in fission yeast. *Cell Cycle*. 4:39-41.

Bahler, J., A.B. Steever, S. Wheatley, Y. Wang, J.R. Pringle, K.L. Gould, and D. McCollum. 1998a. Role of polo kinase and Mid1p in determining the site of cell division in fission yeast. *J Cell Biol*. 143:1603-1616.

Bahler, J., J.Q. Wu, M.S. Longtine, N.G. Shah, A. McKenzie, 3rd, A.B. Steever, A. Wach, P. Philippsen, and J.R. Pringle. 1998b. Heterologous modules for efficient and versatile PCR-based gene targeting in Schizosaccharomyces pombe. *Yeast*. 14:943-951.

Balasubramanian, M.K., D. McCollum, L. Chang, K.C. Wong, N.I. Naqvi, X. He, S. Sazer, and K.L. Gould. 1998. Isolation and characterization of new fission yeast cytokinesis mutants. *Genetics*. 149:1265-1275.

Balasubramanian, M.K., R. Srinivasan, Y. Huang, and K.H. Ng. 2012. Comparing contractile apparatus-driven cytokinesis mechanisms across kingdoms. *Cytoskeleton (Hoboken)*. 69:942-956.

Barko, S., B. Bugyi, M.F. Carlier, R. Gombos, T. Matusek, J. Mihaly, and M. Nyitrai. 2010. Characterization of the biochemical properties and biological function of the formin homology domains of Drosophila DAAM. *J Biol Chem*. 285:13154-13169.

Basi, G., E. Schmid, and K. Maundrell. 1993. TATA box mutations in the Schizosaccharomyces pombe nmt1 promoter affect transcription efficiency but not the transcription start point or thiamine repressibility. *Gene*. 123:131-136.

Beach, J.R., and T.T. Egelhoff. 2009. Myosin II recruitment during cytokinesis independent of centralspindlin-mediated phosphorylation. *J Biol Chem*. 284:27377-27383.

Behrens, R., and P. Nurse. 2002. Roles of fission yeast tea1p in the localization of polarity factors and in organizing the microtubular cytoskeleton. *J Cell Biol*. 157:783-793.

Bennett-Lovsey, R.M., A.D. Herbert, M.J. Sternberg, and L.A. Kelley. 2008. Exploring the extremes of sequence/structure space with ensemble fold recognition in the program Phyre. *Proteins*. 70:611-625.

Bensen, E.S., A. Clemente-Blanco, K.R. Finley, J. Correa-Bordes, and J. Berman. 2005. The mitotic cyclins Clb2p and Clb4p affect morphogenesis in Candida albicans. *Mol Biol Cell*. 16:3387-3400.

Bicho, C.C., D.A. Kelly, H.A. Snaith, A.B. Goryachev, and K.E. Sawin. 2010. A catalytic role for Mod5 in the formation of the Tea1 cell polarity landmark. *Curr Biol*. 20:1752-1757.

Birkenfeld, J., P. Nalbant, B.P. Bohl, O. Pertz, K.M. Hahn, and G.M. Bokoch. 2007. GEF-H1 modulates localized RhoA activation during cytokinesis under the control of mitotic kinases. *Dev Cell*. 12:699-712.

Bohnert, K.A., and K.L. Gould. 2011. On the cutting edge: post-translational modifications in cytokinesis. *Trends Cell Biol*. 21:283-292.

Bohnert, K.A., and K.L. Gould. 2012. Cytokinesis-based constraints on polarized cell growth in fission yeast. *PLoS Genet*. 8:e1003004.

Bosgraaf, L., and P.J. van Haastert. 2006. The regulation of myosin II in Dictyostelium. *Eur J Cell Biol*. 85:969-979.

Bothos, J., R.L. Tuttle, M. Ottey, F.C. Luca, and T.D. Halazonetis. 2005. Human LATS1 is a mitotic exit network kinase. *Cancer Res*. 65:6568-6575.

Boucher, L., C.A. Ouzounis, A.J. Enright, and B.J. Blencowe. 2001. A genome-wide survey of RS domain proteins. *RNA*. 7:1693-1701.

Bourhis, E., S.G. Hymowitz, and A.G. Cochran. 2007. The mitotic regulator Survivin binds as a monomer to its functional interactor Borealin. *J Biol Chem*. 282:35018-35023.

Brace, J., J. Hsu, and E.L. Weiss. 2011. Mitotic exit control of the Saccharomyces cerevisiae Ndr/LATS kinase Cbk1 regulates daughter cell separation after cytokinesis. *Mol Cell Biol*. 31:721-735.

Brand, A. 2012. Hyphal growth in human fungal pathogens and its role in virulence. *Int J Microbiol*. 2012:517529.

Burkard, M.E., J. Maciejowski, V. Rodriguez-Bravo, M. Repka, D.M. Lowery, K.R. Clauser, C. Zhang, K.M. Shokat, S.A. Carr, M.B. Yaffe, and P.V. Jallepalli. 2009. Plk1 self-organization and priming phosphorylation of HsCYK-4 at the spindle midzone regulate the onset of division in human cells. *PLoS Biol*. 7:e1000111.

Cabrera, R., J. Suo, E. Young, and E.C. Chang. 2011. Schizosaccharomyces pombe Arc3 is a conserved subunit of the Arp2/3 complex required for polarity, actin organization, and endocytosis. *Yeast*. 28:495-503.

Carmena, M. 2008. Cytokinesis: the final stop for the chromosomal passengers. *Biochem Soc Trans*. 36:367-370.

Carnahan, R.H., and K.L. Gould. 2003. The PCH family protein, Cdc15p, recruits two F-actin nucleation pathways to coordinate cytokinetic actin ring formation in Schizosaccharomyces pombe. *J Cell Biol*. 162:851-862.

Castagnetti, S., R. Behrens, and P. Nurse. 2005. End4/Sla2 is involved in establishment of a new growth zone in Schizosaccharomyces pombe. *J Cell Sci*. 118:1843-1850.

Chang, F. 1999. Movement of a cytokinesis factor cdc12p to the site of cell division. *Curr Biol*. 9:849-852.

Chang, F., D. Drubin, and P. Nurse. 1997. cdc12p, a protein required for cytokinesis in fission yeast, is a component of the cell division ring and interacts with profilin. *J Cell Biol*. 137:169-182.

Chang, F., and S.G. Martin. 2009. Shaping fission yeast with microtubules. *Cold Spring Harb Perspect Biol*. 1:a001347.

Chang, L., and K.L. Gould. 2000. Sid4p is required to localize components of the septation initiation pathway to the spindle pole body in fission yeast. *Proc Natl Acad Sci U S A*. 97:5249-5254.

Chapa y Lazo, B., S. Bates, and P. Sudbery. 2005. The G1 cyclin Cln3 regulates morphogenesis in Candida albicans. *Eukaryot Cell*. 4:90-94.

Chen, C.T., A. Feoktistova, J.S. Chen, Y.S. Shim, D.M. Clifford, K.L. Gould, and D. McCollum. 2008. The SIN kinase Sid2 regulates cytoplasmic retention of the S. pombe Cdc14-like phosphatase Clp1. *Curr Biol*. 18:1594-1599.

Chesarone, M.A., A.G. DuPage, and B.L. Goode. 2010. Unleashing formins to remodel the actin and microtubule cytoskeletons. *Nat Rev Mol Cell Biol*. 11:62-74.

Chew, T.L., W.A. Wolf, P.J. Gallagher, F. Matsumura, and R.L. Chisholm. 2002. A fluorescent resonant energy transfer-based biosensor reveals transient and regional myosin light chain kinase activation in lamella and cleavage furrows. *J Cell Biol*. 156:543-553.

Chhabra, E.S., and H.N. Higgs. 2006. INF2 Is a WASP homology 2 motif-containing formin that severs actin filaments and accelerates both polymerization and depolymerization. *J Biol Chem*. 281:26754-26767.

Chiang, L.Y., D.C. Sheppard, V.M. Bruno, A.P. Mitchell, J.E. Edwards, Jr., and S.G. Filler. 2007. Candida albicans protein kinase CK2 governs virulence during oropharyngeal candidiasis. *Cell Microbiol*. 9:233-245.

Cho, W., and R.V. Stahelin. 2006. Membrane binding and subcellular targeting of C2 domains. *Biochim Biophys Acta*. 1761:838-849.

Clark, A.G., and E. Paluch. 2011. Mechanics and regulation of cell shape during the cell cycle. *Results Probl Cell Differ*. 53:31-73.

Clemente-Blanco, A., A. Gonzalez-Novo, F. Machin, D. Caballero-Lima, L. Aragon, M. Sanchez, C.R. de Aldana, J. Jimenez, and J. Correa-Bordes. 2006. The Cdc14p phosphatase affects late cell-cycle events and morphogenesis in Candida albicans. *J Cell Sci*. 119:1130-1143.

Clifford, D.M., B.A. Wolfe, R.H. Roberts-Galbraith, W.H. McDonald, J.R. Yates, 3rd, and K.L. Gould. 2008. The Clp1/Cdc14 phosphatase contributes to the robustness of cytokinesis by association with anillin-related Mid1. *J Cell Biol*. 181:79-88.

Coffman, V.C., A.H. Nile, I.J. Lee, H. Liu, and J.Q. Wu. 2009. Roles of formin nodes and myosin motor activity in Mid1p-dependent contractile-ring assembly during fission yeast cytokinesis. *Mol Biol Cell*. 20:5195-5210.

Cole, C., J.D. Barber, and G.J. Barton. 2008. The Jpred 3 secondary structure prediction server. *Nucleic Acids Res*. 36:W197-201.

Colman-Lerner, A., T.E. Chin, and R. Brent. 2001. Yeast Cbk1 and Mob2 activate daughter-specific genetic programs to induce asymmetric cell fates. *Cell*. 107:739-750.

Cook, J.G., L. Bardwell, S.J. Kron, and J. Thorner. 1996. Two novel targets of the MAP kinase Kss1 are negative regulators of invasive growth in the yeast Saccharomyces cerevisiae. *Genes Dev*. 10:2831-2848.

Cortes, J.C., J. Ishiguro, A. Duran, and J.C. Ribas. 2002. Localization of the (1,3)beta-D-glucan synthase catalytic subunit homologue Bgs1p/Cps1p from fission yeast suggests that it is involved in septation, polarized growth, mating, spore wall formation and spore germination. *J Cell Sci*. 115:4081-4096.

Cueille, N., E. Salimova, V. Esteban, M. Blanco, S. Moreno, A. Bueno, and V. Simanis. 2001. Flp1, a fission yeast orthologue of the s. cerevisiae CDC14 gene, is not required for cyclin degradation or rum1p stabilisation at the end of mitosis. *J Cell Sci*. 114:2649-2664.

Dekker, N., D. Speijer, C.H. Grun, M. van den Berg, A. de Haan, and F. Hochstenbach. 2004. Role of the alpha-glucanase Agn1p in fission-yeast cell separation. *Mol Biol Cell*. 15:3903-3914.

Demeter, J., and S. Sazer. 1998. imp2, a new component of the actin ring in the fission yeast Schizosaccharomyces pombe. *J Cell Biol*. 143:415-427.

Dodgson, J., W. Brown, C.A. Rosa, and J. Armstrong. 2010. Reorganization of the growth pattern of Schizosaccharomyces pombe in invasive filament formation. *Eukaryot Cell*. 9:1788-1797.

Douglas, M.E., T. Davies, N. Joseph, and M. Mishima. 2010. Aurora B and 14-3-3 coordinately regulate clustering of centralspindlin during cytokinesis. *Curr Biol*. 20:927-933.

Earnshaw, W.C., and R.L. Bernat. 1991. Chromosomal passengers: toward an integrated view of mitosis. *Chromosoma*. 100:139-146.

Echard, A. 2008. Membrane traffic and polarization of lipid domains during cytokinesis. *Biochem Soc Trans*. 36:395-399.

Emoto, K., H. Inadome, Y. Kanaho, S. Narumiya, and M. Umeda. 2005. Local change in phospholipid composition at the cleavage furrow is essential for completion of cytokinesis. *J Biol Chem*. 280:37901-37907.

Emoto, K., and M. Umeda. 2000. An essential role for a membrane lipid in cytokinesis. Regulation of contractile ring disassembly by redistribution of phosphatidylethanolamine. *J Cell Biol*. 149:1215-1224.

Eng, K., N.I. Naqvi, K.C. Wong, and M.K. Balasubramanian. 1998. Rng2p, a protein required for cytokinesis in fission yeast, is a component of the actomyosin ring and the spindle pole body. *Curr Biol*. 8:611-621.

Ernst, J.F. 2000. Regulation of dimorphism in Candida albicans. *Contrib Microbiol*. 5:98-111.

Esteban, V., M. Blanco, N. Cueille, V. Simanis, S. Moreno, and A. Bueno. 2004. A role for the Cdc14-family phosphatase Flp1p at the end of the cell cycle in controlling the rapid degradation of the mitotic inducer Cdc25p in fission yeast. *J Cell Sci*. 117:2461-2468.

Esue, O., E.S. Harris, H.N. Higgs, and D. Wirtz. 2008. The filamentous actin cross-linking/bundling activity of mammalian formins. *J Mol Biol*. 384:324-334.

Feierbach, B., and F. Chang. 2001. Roles of the fission yeast formin for3p in cell polarity, actin cable formation and symmetric cell division. *Curr Biol*. 11:1656-1665.

Feierbach, B., F. Verde, and F. Chang. 2004. Regulation of a formin complex by the microtubule plus end protein tea1p. *J Cell Biol*. 165:697-707.

Feoktistova, A., J. Morrell-Falvey, J.S. Chen, N.S. Singh, M.K. Balasubramanian, and K.L. Gould. 2012. The fission yeast septation initiation network (SIN) kinase, Sid2, is required for SIN asymmetry and regulates the SIN scaffold, Cdc11. *Mol Biol Cell*. 23:1636-1645.

Field, S.J., N. Madson, M.L. Kerr, K.A. Galbraith, C.E. Kennedy, M. Tahiliani, A. Wilkins, and L.C. Cantley. 2005. PtdIns(4,5)P2 functions at the cleavage furrow during cytokinesis. *Curr Biol*. 15:1407-1412.

Fielding, A.B., E. Schonteich, J. Matheson, G. Wilson, X. Yu, G.R. Hickson, S. Srivastava, S.A. Baldwin, R. Prekeris, and G.W. Gould. 2005. Rab11-FIP3 and FIP4 interact with Arf6 and the exocyst to control membrane traffic in cytokinesis. *EMBO J*. 24:3389-3399.

Flescher, E.G., K. Madden, and M. Snyder. 1993. Components required for cytokinesis are important for bud site selection in yeast. *J Cell Biol*. 122:373-386.

Fu, C., J.J. Ward, I. Loiodice, G. Velve-Casquillas, F.J. Nedelec, and P.T. Tran. 2009. Phospho-regulated interaction between kinesin-6 Klp9p and microtubule bundler Ase1p promotes spindle elongation. *Dev Cell*. 17:257-267.

Gachet, Y., and J.S. Hyams. 2005. Endocytosis in fission yeast is spatially associated with the actin cytoskeleton during polarised cell growth and cytokinesis. *J Cell Sci*. 118:4231-4242.

Gagiano, M., F.F. Bauer, and I.S. Pretorius. 2002. The sensing of nutritional status and the relationship to filamentous growth in Saccharomyces cerevisiae. *FEMS Yeast Res*. 2:433-470.

Garcia, P., V. Tajadura, I. Garcia, and Y. Sanchez. 2006. Rgf1p is a specific Rho1-GEF that coordinates cell polarization with cell wall biogenesis in fission yeast. *Mol Biol Cell*. 17:1620-1631.

Gassmann, R., A. Carvalho, A.J. Henzing, S. Ruchaud, D.F. Hudson, R. Honda, E.A. Nigg, D.L. Gerloff, and W.C. Earnshaw. 2004. Borealin: a novel chromosomal passenger required for stability of the bipolar mitotic spindle. *J Cell Biol*. 166:179-191.

Ge, W., and M.K. Balasubramanian. 2008. Pxl1p, a paxillin-related protein, stabilizes the actomyosin ring during cytokinesis in fission yeast. *Mol Biol Cell*. 19:1680-1692.

Gillis, A.N., S. Thomas, S.D. Hansen, and K.B. Kaplan. 2005. A novel role for the CBF3 kinetochore-scaffold complex in regulating septin dynamics and cytokinesis. *J Cell Biol*. 171:773-784.

Glynn, J.M., R.J. Lustig, A. Berlin, and F. Chang. 2001. Role of bud6p and tea1p in the interaction between actin and microtubules for the establishment of cell polarity in fission yeast. *Curr Biol*. 11:836-845.

Gonzalez-Novo, A., J. Correa-Bordes, L. Labrador, M. Sanchez, C.R. Vazquez de Aldana, and J. Jimenez. 2008. Sep7 is essential to modify septin ring dynamics and inhibit cell separation during Candida albicans hyphal growth. *Mol Biol Cell*. 19:1509-1518.

Gordon, D.J., B. Resio, and D. Pellman. 2012. Causes and consequences of aneuploidy in cancer. *Nat Rev Genet*. 13:189-203.

Gould, C.J., S. Maiti, A. Michelot, B.R. Graziano, L. Blanchoin, and B.L. Goode. 2011. The formin DAD domain plays dual roles in autoinhibition and actin nucleation. *Curr Biol*. 21:384-390.

Gould, K.L., S. Moreno, D.J. Owen, S. Sazer, and P. Nurse. 1991. Phosphorylation at Thr167 is required for Schizosaccharomyces pombe p34cdc2 function. *EMBO J*. 10:3297-3309.

Gould, K.L., L. Ren, A.S. Feoktistova, J.L. Jennings, and A.J. Link. 2004. Tandem affinity purification and identification of protein complex components. *Methods*. 33:239-244.

Grallert, A., Y. Connolly, D.L. Smith, V. Simanis, and I.M. Hagan. 2012. The S. pombe cytokinesis NDR kinase Sid2 activates Fin1 NIMA kinase to control mitotic commitment through Pom1/Wee1. *Nat Cell Biol*. 14:738-745.

Gruneberg, U., R. Neef, X. Li, E.H. Chan, R.B. Chalamalasetty, E.A. Nigg, and F.A. Barr. 2006. KIF14 and citron kinase act together to promote efficient cytokinesis. *J Cell Biol*. 172:363-372.

Gupta, S., S. Mana-Capelli, J.R. McLean, C.T. Chen, S. Ray, K.L. Gould, and D. McCollum. 2013. Identification of SIN pathway targets reveals mechanisms of crosstalk between NDR kinase pathways. *Curr Biol*. 23:333-338.

Guzman-Vendrell, M., S. Baldissard, M. Almonacid, A. Mayeux, A. Paoletti, and J.B. Moseley. 2013. Blt1 and Mid1 provide overlapping membrane anchors to position the division plane in fission yeast. *Mol Cell Biol*. 33:418-428.

Hachet, O., and V. Simanis. 2008. Mid1p/anillin and the septation initiation network orchestrate contractile ring assembly for cytokinesis. *Genes Dev*. 22:3205-3216.

Hanson, P.I., R. Roth, Y. Lin, and J.E. Heuser. 2008. Plasma membrane deformation by circular arrays of ESCRT-III protein filaments. *J Cell Biol*. 180:389-402.

Harris, E.S., I. Rouiller, D. Hanein, and H.N. Higgs. 2006. Mechanistic differences in actin bundling activity of two mammalian formins, FRL1 and mDia2. *J Biol Chem*. 281:14383-14392.

Heimsath, E.G., Jr., and H.N. Higgs. 2012. The C terminus of formin FMNL3 accelerates actin polymerization and contains a WH2 domain-like sequence that binds both monomers and filament barbed ends. *J Biol Chem*. 287:3087-3098.

Honda, R., R. Korner, and E.A. Nigg. 2003. Exploring the functional interactions between Aurora B, INCENP, and survivin in mitosis. *Mol Biol Cell*. 14:3325-3341.

Howell, A.S., and D.J. Lew. 2012. Morphogenesis and the cell cycle. *Genetics*. 190:51-77.

Hu, C.K., M. Coughlin, C.M. Field, and T.J. Mitchison. 2008. Cell polarization during monopolar cytokinesis. *J Cell Biol*. 181:195-202.

Huang, H.K., J.M. Bailis, J.D. Leverson, E.B. Gomez, S.L. Forsburg, and T. Hunter. 2005. Suppressors of Bir1p (Survivin) identify roles for the chromosomal passenger protein Pic1p (INCENP) and the replication initiation factor Psf2p in chromosome segregation. *Mol Cell Biol*. 25:9000-9015.

Huang, J., Y. Huang, H. Yu, D. Subramanian, A. Padmanabhan, R. Thadani, Y. Tao, X. Tang, R. Wedlich-Soldner, and M.K. Balasubramanian. 2012. Nonmedially assembled F-actin cables incorporate into the actomyosin ring in fission yeast. *J Cell Biol*. 199:831-847.

Huang, Y., T.G. Chew, W. Ge, and M.K. Balasubramanian. 2007. Polarity determinants Tea1p, Tea4p, and Pom1p inhibit division-septum assembly at cell ends in fission yeast. *Dev Cell*. 12:987-996.

Huang, Y., H. Yan, and M.K. Balasubramanian. 2008. Assembly of normal actomyosin rings in the absence of Mid1p and cortical nodes in fission yeast. *J Cell Biol*. 183:979-988.

Huisman, S.M., and D. Brunner. 2011. Cell polarity in fission yeast: a matter of confining, positioning, and switching growth zones. *Semin Cell Dev Biol*. 22:799-805.

Hummer, S., and T.U. Mayer. 2009. Cdk1 negatively regulates midzone localization of the mitotic kinesin Mklp2 and the chromosomal passenger complex. *Curr Biol*. 19:607-612.

Hunter, T. 1987. A thousand and one protein kinases. *Cell*. 50:823-829.

Iwaki, T., N. Tanaka, H. Takagi, Y. Giga-Hama, and K. Takegawa. 2004. Characterization of end4+, a gene required for endocytosis in Schizosaccharomyces pombe. *Yeast*. 21:867-881.

Janetopoulos, C., J. Borleis, F. Vazquez, M. Iijima, and P. Devreotes. 2005. Temporal and spatial regulation of phosphoinositide signaling mediates cytokinesis. *Dev Cell*. 8:467-477.

Jelluma, N., A.B. Brenkman, N.J. van den Broek, C.W. Cruijsen, M.H. van Osch, S.M. Lens, R.H. Medema, and G.J. Kops. 2008. Mps1 phosphorylates Borealin to control Aurora B activity and chromosome alignment. *Cell*. 132:233-246.

Jendretzki, A., I. Ciklic, R. Rodicio, H.P. Schmitz, and J.J. Heinisch. 2009. Cyk3 acts in actomyosin ring independent cytokinesis by recruiting Inn1 to the yeast bud neck. *Mol Genet Genomics*. 282:437-451.

Jensen, S., M. Segal, D.J. Clarke, and S.I. Reed. 2001. A novel role of the budding yeast separin Esp1 in anaphase spindle elongation: evidence that proper spindle association of Esp1 is regulated by Pds1. *J Cell Biol*. 152:27-40.

Jeyaprakash, A.A., U.R. Klein, D. Lindner, J. Ebert, E.A. Nigg, and E. Conti. 2007. Structure of a Survivin-Borealin-INCENP core complex reveals how chromosomal passengers travel together. *Cell*. 131:271-285.

Johnson, A.E., D. McCollum, and K.L. Gould. 2012. Polar opposites: Fine-tuning cytokinesis through SIN asymmetry. *Cytoskeleton (Hoboken)*. 69:686-699.

Johnson, B.F., B.Y. Yoo, G.B. Calleja, and C.P. Kozela. 2005. Second thoughts on septation by the fission yeast, Schizosaccharomyces pombe: pull vs. push mechanisms with an appendix--dimensional modelling of the flat and variable septa. *Antonie Van Leeuwenhoek*. 88:1-12.

Joo, E., M.C. Surka, and W.S. Trimble. 2007. Mammalian SEPT2 is required for scaffolding nonmuscle myosin II and its kinases. *Dev Cell*. 13:677-690.

Kamasaki, T., M. Osumi, and I. Mabuchi. 2007. Three-dimensional arrangement of F-actin in the contractile ring of fission yeast. *J Cell Biol*. 178:765-771.

Keeney, J.B., and J.D. Boeke. 1994. Efficient targeted integration at leu1-32 and ura4-294 in Schizosaccharomyces pombe. *Genetics*. 136:849-856.

Khmelinskii, A., C. Lawrence, J. Roostalu, and E. Schiebel. 2007. Cdc14-regulated midzone assembly controls anaphase B. *J Cell Biol*. 177:981-993.

Kim, H., P. Yang, P. Catanuto, F. Verde, H. Lai, H. Du, F. Chang, and S. Marcus. 2003. The kelch repeat protein, Tea1, is a potential substrate target of the p21-activated kinase, Shk1, in the fission yeast, Schizosaccharomyces pombe. *J Biol Chem*. 278:30074-30082.

King, J.S., D.M. Veltman, M. Georgiou, B. Baum, and R.H. Insall. 2010. SCAR/WAVE is activated at mitosis and drives myosin-independent cytokinesis. *J Cell Sci*. 123:2246-2255.

King, R.W., R.J. Deshaies, J.M. Peters, and M.W. Kirschner. 1996. How proteolysis drives the cell cycle. *Science*. 274:1652-1659.

Klein, U.R., E.A. Nigg, and U. Gruneberg. 2006. Centromere targeting of the chromosomal passenger complex requires a ternary subcomplex of Borealin, Survivin, and the N-terminal domain of INCENP. *Mol Biol Cell*. 17:2547-2558.

Knaus, M., M.P. Pelli-Gulli, F. van Drogen, S. Springer, M. Jaquenoud, and M. Peter. 2007. Phosphorylation of Bem2p and Bem3p may contribute to local activation of Cdc42p at bud emergence. *EMBO J*. 26:4501-4513.

Koch, A., K. Krug, S. Pengelley, B. Macek, and S. Hauf. 2011. Mitotic substrates of the kinase aurora with roles in chromatin regulation identified through quantitative phosphoproteomics of fission yeast. *Sci Signal*. 4:rs6.

Kono, K., S. Nogami, M. Abe, M. Nishizawa, S. Morishita, D. Pellman, and Y. Ohya. 2008. G1/S cyclin-dependent kinase regulates small GTPase Rho1p through phosphorylation of RhoGEF Tus1p in Saccharomyces cerevisiae. *Mol Biol Cell*. 19:1763-1771.

Kouranti, I., J.R. McLean, A. Feoktistova, P. Liang, A.E. Johnson, R.H. Roberts-Galbraith, and K.L. Gould. 2010. A global census of fission yeast deubiquitinating enzyme localization and interaction networks reveals distinct compartmentalization profiles and overlapping functions in endocytosis and polarity. *PLoS Biol*. 8.

Kouranti, I., M. Sachse, N. Arouche, B. Goud, and A. Echard. 2006. Rab35 regulates an endocytic recycling pathway essential for the terminal steps of cytokinesis. *Curr Biol*. 16:1719-1725.

Kovar, D.R., J.R. Kuhn, A.L. Tichy, and T.D. Pollard. 2003. The fission yeast cytokinesis formin Cdc12p is a barbed end actin filament capping protein gated by profilin. *J Cell Biol*. 161:875-887.

Krapp, A., and V. Simanis. 2008. An overview of the fission yeast septation initiation network (SIN). *Biochem Soc Trans*. 36:411-415.

Laporte, D., V.C. Coffman, I.J. Lee, and J.Q. Wu. 2011. Assembly and architecture of precursor nodes during fission yeast cytokinesis. *J Cell Biol*. 192:1005-1021.

Laporte, D., N. Ojkic, D. Vavylonis, and J.Q. Wu. 2012. alpha-Actinin and fimbrin cooperate with myosin II to organize actomyosin bundles during contractile-ring assembly. *Mol Biol Cell*. 23:3094-3110.

Le Goff, X., F. Motegi, E. Salimova, I. Mabuchi, and V. Simanis. 2000. The S. pombe rlc1 gene encodes a putative myosin regulatory light chain that binds the type II myosins myo3p and myo2p. *J Cell Sci*. 113 Pt 23:4157-4163.

Le Goff, X., A. Woollard, and V. Simanis. 1999. Analysis of the cps1 gene provides evidence for a septation checkpoint in Schizosaccharomyces pombe. *Mol Gen Genet*. 262:163-172.

Leverson, J.D., H.K. Huang, S.L. Forsburg, and T. Hunter. 2002. The Schizosaccharomyces pombe aurora-related kinase Ark1 interacts with the inner centromere protein Pic1 and mediates chromosome segregation and cytokinesis. *Mol Biol Cell*. 13:1132-1143.

Li, C.R., Y.M. Wang, and Y. Wang. 2008. The IQGAP Iqg1 is a regulatory target of CDK for cytokinesis in Candida albicans. *EMBO J*. 27:2998-3010.

Lippincott, J., and R. Li. 2000. Involvement of PCH family proteins in cytokinesis and actin distribution. *Microsc Res Tech*. 49:168-172.

Liu, J., X. Tang, H. Wang, S. Oliferenko, and M.K. Balasubramanian. 2002. The localization of the integral membrane protein Cps1p to the cell division site is dependent on the actomyosin ring and the septation-inducing network in Schizosaccharomyces pombe. *Mol Biol Cell*. 13:989-1000.

Liu, J., H. Wang, and M.K. Balasubramanian. 2000. A checkpoint that monitors cytokinesis in Schizosaccharomyces pombe. *J Cell Sci*. 113 (Pt 7):1223-1230.

Liu, J., H. Wang, D. McCollum, and M.K. Balasubramanian. 1999. Drc1p/Cps1p, a 1,3-beta-glucan synthase subunit, is essential for division septum assembly in Schizosaccharomyces pombe. *Genetics*. 153:1193-1203.

Loo, T.H., and M. Balasubramanian. 2008. Schizosaccharomyces pombe Pak-related protein, Pak1p/Orb2p, phosphorylates myosin regulatory light chain to inhibit cytokinesis. *J Cell Biol*. 183:785-793.

Lordier, L., A. Jalil, F. Aurade, F. Larbret, J. Larghero, N. Debili, W. Vainchenker, and Y. Chang. 2008. Megakaryocyte endomitosis is a failure of late cytokinesis related to defects in the contractile ring and Rho/Rock signaling. *Blood*. 112:3164-3174.

Lu, K.P., Y.C. Liou, and X.Z. Zhou. 2002. Pinning down proline-directed phosphorylation signaling. *Trends Cell Biol*. 12:164-172.

Lu, L.X., M.R. Domingo-Sananes, M. Huzarska, B. Novak, and K.L. Gould. 2012. Multisite phosphoregulation of Cdc25 activity refines the mitotic entrance and exit switches. *Proc Natl Acad Sci U S A*. 109:9899-9904.

Lucero, A., C. Stack, A.R. Bresnick, and C.B. Shuster. 2006. A global, myosin light chain kinase-dependent increase in myosin II contractility accompanies the metaphase-anaphase transition in sea urchin eggs. *Mol Biol Cell*. 17:4093-4104.

Luo, J., Y. Matsuo, G. Gulis, H. Hinz, J. Patton-Vogt, and S. Marcus. 2009. Phosphatidylethanolamine is required for normal cell morphology and cytokinesis in the fission yeast Schizosaccharomyces pombe. *Eukaryot Cell*. 8:790-799.

Machaidze, G., A. Sokoll, A. Shimada, A. Lustig, A. Mazur, A. Wittinghofer, U. Aebi, and H.G. Mannherz. 2010. Actin filament bundling and different nucleating effects of mouse Diaphanous-related formin FH2 domains on actin/ADF and actin/cofilin complexes. *J Mol Biol*. 403:529-545.

Madhani, H.D., and G.R. Fink. 1998. The control of filamentous differentiation and virulence in fungi. *Trends Cell Biol*. 8:348-353.

Mah, A.S., A.E. Elia, G. Devgan, J. Ptacek, M. Schutkowski, M. Snyder, M.B. Yaffe, and R.J. Deshaies. 2005. Substrate specificity analysis of protein kinase complex Dbf2-Mob1 by peptide library and proteome array screening. *BMC Biochem*. 6:22.

Mana-Capelli, S., J.R. McLean, C.T. Chen, K.L. Gould, and D. McCollum. 2012. The kinesin-14 Klp2 is negatively regulated by the SIN for proper spindle elongation and telophase nuclear positioning. *Mol Biol Cell*. 23:4592-4600.

Martin, S.G., and M. Berthelot-Grosjean. 2009. Polar gradients of the DYRK-family kinase Pom1 couple cell length with the cell cycle. *Nature*. 459:852-856.

Martin, S.G., and F. Chang. 2005. New end take off: regulating cell polarity during the fission yeast cell cycle. *Cell Cycle*. 4:1046-1049.

Martin, S.G., W.H. McDonald, J.R. Yates, 3rd, and F. Chang. 2005. Tea4p links microtubule plus ends with the formin for3p in the establishment of cell polarity. *Dev Cell*. 8:479-491.

Martin-Cuadrado, A.B., E. Duenas, M. Sipiczki, C.R. Vazquez de Aldana, and F. del Rey. 2003. The endo-beta-1,3-glucanase eng1p is required for dissolution of the primary septum during cell separation in Schizosaccharomyces pombe. *J Cell Sci*. 116:1689-1698.

Martin-Cuadrado, A.B., J.L. Morrell, M. Konomi, H. An, C. Petit, M. Osumi, M. Balasubramanian, K.L. Gould, F. Del Rey, and C.R. de Aldana. 2005. Role of septins and the exocyst complex in the function of hydrolytic enzymes responsible for fission yeast cell separation. *Mol Biol Cell*. 16:4867-4881.

Mata, J., R. Lyne, G. Burns, and J. Bahler. 2002. The transcriptional program of meiosis and sporulation in fission yeast. *Nat Genet*. 32:143-147.

Mata, J., and P. Nurse. 1997. tea1 and the microtubular cytoskeleton are important for generating global spatial order within the fission yeast cell. *Cell*. 89:939-949.

Matsumura, F. 2005. Regulation of myosin II during cytokinesis in higher eukaryotes. *Trends Cell Biol*. 15:371-377.

Matsuyama, A., R. Arai, Y. Yashiroda, A. Shirai, A. Kamata, S. Sekido, Y. Kobayashi, A. Hashimoto, M. Hamamoto, Y. Hiraoka, S. Horinouchi, and M. Yoshida. 2006. ORFeome cloning and global analysis of protein localization in the fission yeast Schizosaccharomyces pombe. *Nat Biotechnol*. 24:841-847.

Maundrell, K. 1990. nmt1 of fission yeast. A highly transcribed gene completely repressed by thiamine. *J Biol Chem*. 265:10857-10864.

Maundrell, K. 1993. Thiamine-repressible expression vectors pREP and pRIP for fission yeast. *Gene*. 123:127-130.

Mayer, B.J. 2001. SH3 domains: complexity in moderation. *J Cell Sci*. 114:1253-1263.

Mazzoni, C., P. Zarov, A. Rambourg, and C. Mann. 1993. The SLT2 (MPK1) MAP kinase homolog is involved in polarized cell growth in Saccharomyces cerevisiae. *J Cell Biol*. 123:1821-1833.

McCollum, D., A. Feoktistova, and K.L. Gould. 1999. Phosphorylation of the myosin-II light chain does not regulate the timing of cytokinesis in fission yeast. *J Biol Chem*. 274:17691-17695.

McCusker, D., C. Denison, S. Anderson, T.A. Egelhofer, J.R. Yates, 3rd, S.P. Gygi, and D.R. Kellogg. 2007. Cdk1 coordinates cell-surface growth with the cell cycle. *Nat Cell Biol*. 9:506-515.

Meggio, F., and L.A. Pinna. 2003. One-thousand-and-one substrates of protein kinase CK2? *FASEB J*. 17:349-368.

Mendoza, M., C. Norden, K. Durrer, H. Rauter, F. Uhlmann, and Y. Barral. 2009. A mechanism for chromosome segregation sensing by the NoCut checkpoint. *Nat Cell Biol*. 11:477-483.

Michelot, A., C. Guerin, S. Huang, M. Ingouff, S. Richard, N. Rodiuc, C.J. Staiger, and L. Blanchoin. 2005. The formin homology 1 domain modulates the actin nucleation and bundling activity of Arabidopsis FORMIN1. *Plant Cell*. 17:2296-2313.

Miller, A.L., and W.M. Bement. 2009. Regulation of cytokinesis by Rho GTPase flux. *Nat Cell Biol*. 11:71-77.

Minet, M., P. Nurse, P. Thuriaux, and J.M. Mitchison. 1979. Uncontrolled septation in a cell division cycle mutant of the fission yeast Schizosaccharomyces pombe. *J Bacteriol*. 137:440-446.

Minoshima, Y., T. Kawashima, K. Hirose, Y. Tonozuka, A. Kawajiri, Y.C. Bao, X. Deng, M. Tatsuka, S. Narumiya, W.S. May, Jr., T. Nosaka, K. Semba, T. Inoue, T. Satoh, M. Inagaki, and T. Kitamura. 2003. Phosphorylation by aurora B converts MgcRacGAP to a RhoGAP during cytokinesis. *Dev Cell*. 4:549-560.

Mishima, M., V. Pavicic, U. Gruneberg, E.A. Nigg, and M. Glotzer. 2004. Cell cycle regulation of central spindle assembly. *Nature*. 430:908-913.

Mishra, M., J. Karagiannis, S. Trautmann, H. Wang, D. McCollum, and M.K. Balasubramanian. 2004. The Clp1p/Flp1p phosphatase ensures completion of cytokinesis in response to minor perturbation of the cell division machinery in Schizosaccharomyces pombe. *J Cell Sci*. 117:3897-3910.

Mitchison, J.M., and P. Nurse. 1985. Growth in cell length in the fission yeast Schizosaccharomyces pombe. *J Cell Sci*. 75:357-376.

Mizutani, T., H. Haga, Y. Koyama, M. Takahashi, and K. Kawabata. 2006. Diphosphorylation of the myosin regulatory light chain enhances the tension acting on stress fibers in fibroblasts. *J Cell Physiol*. 209:726-731.

Mizutani, T., K. Kawabata, Y. Koyama, M. Takahashi, and H. Haga. 2009. Regulation of cellular contractile force in response to mechanical stretch by diphosphorylation of myosin regulatory light chain via RhoA signaling cascade. *Cell Motil Cytoskeleton*. 66:389-397.

Mohl, D.A., M.J. Huddleston, T.S. Collingwood, R.S. Annan, and R.J. Deshaies. 2009. Dbf2-Mob1 drives relocalization of protein phosphatase Cdc14 to the cytoplasm during exit from mitosis. *J Cell Biol*. 184:527-539.

Morishita, J., T. Matsusaka, G. Goshima, T. Nakamura, H. Tatebe, and M. Yanagida. 2001. Bir1/Cut17 moving from chromosome to spindle upon the loss of cohesion is required for condensation, spindle elongation and repair. *Genes Cells*. 6:743-763.

Moseley, J.B., and B.L. Goode. 2005. Differential activities and regulation of Saccharomyces cerevisiae formin proteins Bni1 and Bnr1 by Bud6. *J Biol Chem*. 280:28023-28033.

Moseley, J.B., A. Mayeux, A. Paoletti, and P. Nurse. 2009. A spatial gradient coordinates cell size and mitotic entry in fission yeast. *Nature*. 459:857-860.

Mullins, J.M., and J.J. Biesele. 1973. Cytokinetic activities in a human cell line: the midbody and intercellular bridge. *Tissue Cell*. 5:47-61.

Nabetani, A., T. Koujin, C. Tsutsumi, T. Haraguchi, and Y. Hiraoka. 2001. A conserved protein, Nuf2, is implicated in connecting the centromere to the spindle during chromosome segregation: a link between the kinetochore function and the spindle checkpoint. *Chromosoma*. 110:322-334.

Nakajima, Y., R.G. Tyers, C.C. Wong, J.R. Yates, 3rd, D.G. Drubin, and G. Barnes. 2009. Nbl1p: A Borealin/Dasra/CSC-1-like Protein Essential for Aurora/Ipl1 Complex Function and Integrity in Saccharomyces cerevisiae. *Mol Biol Cell*. 20:1772-1784.

Nakano, K., J. Imai, R. Arai, E.A. Toh, Y. Matsui, and I. Mabuchi. 2002. The small GTPase Rho3 and the diaphanous/formin For3 function in polarized cell growth in fission yeast. *J Cell Sci*. 115:4629-4639.

Naqvi, N.I., K.C. Wong, X. Tang, and M.K. Balasubramanian. 2000. Type II myosin regulatory light chain relieves auto-inhibition of myosin-heavy-chain function. *Nat Cell Biol*. 2:855-858.

Neujahr, R., C. Heizer, and G. Gerisch. 1997. Myosin II-independent processes in mitotic cells of Dictyostelium discoideum: redistribution of the nuclei, re-arrangement of the actin system and formation of the cleavage furrow. *J Cell Sci*. 110 (Pt 2):123-137.

Nikolakaki, E., V. Drosou, I. Sanidas, P. Peidis, T. Papamarcaki, L.M. Iakoucheva, and T. Giannakouros. 2008. RNA association or phosphorylation of the RS domain prevents aggregation of RS domain-containing proteins. *Biochim Biophys Acta*. 1780:214-225.

Nishihama, R., J.H. Schreiter, M. Onishi, E.A. Vallen, J. Hanna, K. Moravcevic, M.F. Lippincott, H. Han, M.A. Lemmon, J.R. Pringle, and E. Bi. 2009. Role of Inn1 and its interactions with Hof1 and Cyk3 in promoting cleavage furrow and septum formation in S. cerevisiae. *J Cell Biol*. 185:995-1012.

Norden, C., M. Mendoza, J. Dobbelaere, C.V. Kotwaliwale, S. Biggins, and Y. Barral. 2006. The NoCut pathway links completion of cytokinesis to spindle midzone function to prevent chromosome breakage. *Cell*. 125:85-98.

O'Connell, C.B., S.P. Wheatley, S. Ahmed, and Y.L. Wang. 1999. The small GTP-binding protein rho regulates cortical activities in cultured cells during division. *J Cell Biol*. 144:305-313.

Ohi, R., T. Sapra, J. Howard, and T.J. Mitchison. 2004. Differentiation of cytoplasmic and meiotic spindle assembly MCAK functions by Aurora B-dependent phosphorylation. *Mol Biol Cell*. 15:2895-2906.

Otomo, T., D.R. Tomchick, C. Otomo, S.C. Panchal, M. Machius, and M.K. Rosen. 2005. Structural basis of actin filament nucleation and processive capping by a formin homology 2 domain. *Nature*. 433:488-494.

Panteris, E., and B. Galatis. 2005. The morphogenesis of lobed plant cells in the mesophyll and epidermis: organization and distinct roles of cortical microtubules and actin filaments. *New Phytol*. 167:721-732.

Pardo, M., and P. Nurse. 2003. Equatorial retention of the contractile actin ring by microtubules during cytokinesis. *Science*. 300:1569-1574.

Peel, S., P. Macheboeuf, N. Martinelli, and W. Weissenhorn. 2011. Divergent pathways lead to ESCRT-III-catalyzed membrane fission. *Trends Biochem Sci*. 36:199-210.

Pelham, R.J., and F. Chang. 2002. Actin dynamics in the contractile ring during cytokinesis in fission yeast. *Nature*. 419:82-86.

Pelham, R.J., Jr., and F. Chang. 2001. Role of actin polymerization and actin cables in actin-patch movement in Schizosaccharomyces pombe. *Nat Cell Biol*. 3:235-244.

Peng, T.Y., K.R. Lee, and W.Y. Tarn. 2008. Phosphorylation of the arginine/serine dipeptide-rich motif of the severe acute respiratory syndrome coronavirus nucleocapsid protein modulates its multimerization, translation inhibitory activity and cellular localization. *FEBS J*. 275:4152-4163.

Pereira, G., and E. Schiebel. 2003. Separase regulates INCENP-Aurora B anaphase spindle function through Cdc14. *Science*. 302:2120-2124.

Petersen, J., and I.M. Hagan. 2003. S. pombe aurora kinase/survivin is required for chromosome condensation and the spindle checkpoint attachment response. *Curr Biol*. 13:590-597.

Petersen, J., O. Nielsen, R. Egel, and I.M. Hagan. 1998. FH3, a domain found in formins, targets the fission yeast formin Fus1 to the projection tip during conjugation. *J Cell Biol*. 141:1217-1228.

Petersen, J., J. Paris, M. Willer, M. Philippe, and I.M. Hagan. 2001. The S. pombe aurora-related kinase Ark1 associates with mitotic structures in a stage dependent manner and is required for chromosome segregation. *J Cell Sci*. 114:4371-4384.

Pinar, M., P.M. Coll, S.A. Rincon, and P. Perez. 2008. Schizosaccharomyces pombe Pxl1 is a paxillin homologue that modulates Rho1 activity and participates in cytokinesis. *Mol Biol Cell*. 19:1727-1738.

Pines, J., and C.L. Rieder. 2001. Re-staging mitosis: a contemporary view of mitotic progression. *Nat Cell Biol*. 3:E3-6.

Pohlmann, J., and U. Fleig. 2010. Asp1, a conserved 1/3 inositol polyphosphate kinase, regulates the dimorphic switch in Schizosaccharomyces pombe. *Mol Cell Biol*. 30:4535-4547.

Polevoy, G., H.C. Wei, R. Wong, Z. Szentpetery, Y.J. Kim, P. Goldbach, S.K. Steinbach, T. Balla, and J.A. Brill. 2009. Dual roles for the Drosophila PI 4-kinase four wheel drive in localizing Rab11 during cytokinesis. *J Cell Biol*. 187:847-858.

Pollard, T.D. 2010. Mechanics of cytokinesis in eukaryotes. *Curr Opin Cell Biol*. 22:50-56.

Pollard, T.D., and J.Q. Wu. 2010. Understanding cytokinesis: lessons from fission yeast. *Nat Rev Mol Cell Biol* 11:149-155.

Pollarolo, G., J.G. Schulz, S. Munck, and C.G. Dotti. 2011. Cytokinesis remnants define first neuronal asymmetry in vivo. *Nat Neurosci*. 14:1525-1533.

Prevorovsky, M., J. Stanurova, F. Puta, and P. Folk. 2009. High environmental iron concentrations stimulate adhesion and invasive growth of Schizosaccharomyces pombe. *FEMS Microbiol Lett*. 293:130-134.

Queralt, E., and F. Uhlmann. 2008. Cdk-counteracting phosphatases unlock mitotic exit. *Curr Opin Cell Biol*. 20:661-668.

Rajagopalan, S., and M.K. Balasubramanian. 2002. Schizosaccharomyces pombe Bir1p, a nuclear protein that localizes to kinetochores and the spindle midzone, is essential for chromosome condensation and spindle elongation during mitosis. *Genetics*. 160:445-456.

Rethinaswamy, A., M.J. Birnbaum, and C.V. Glover. 1998. Temperature-sensitive mutations of the CKA1 gene reveal a role for casein kinase II in maintenance of cell polarity in Saccharomyces cerevisiae. *J Biol Chem*. 273:5869-5877.

Roberts-Galbraith, R.H., J.S. Chen, J. Wang, and K.L. Gould. 2009. The SH3 domains of two PCH family members cooperate in assembly of the Schizosaccharomyces pombe contractile ring. *J Cell Biol*. 184:113-127.

Roberts-Galbraith, R.H., and K.L. Gould. 2008. Stepping into the ring: the SIN takes on contractile ring assembly. *Genes Dev*. 22:3082-3088.

Roberts-Galbraith, R.H., M.D. Ohi, B.A. Ballif, J.S. Chen, I. McLeod, W.H. McDonald, S.P. Gygi, J.R. Yates, 3rd, and K.L. Gould. 2010. Dephosphorylation of F-BAR protein Cdc15 modulates its conformation and stimulates its scaffolding activity at the cell division site. *Mol Cell*. 39:86-99.

Rosario, C.O., M.A. Ko, Y.Z. Haffani, R.A. Gladdy, J. Paderova, A. Pollett, J.A. Squire, J.W. Dennis, and C.J. Swallow. 2010. Plk4 is required for cytokinesis and maintenance of chromosomal stability. *Proc Natl Acad Sci U S A*. 107:6888-6893.

Rosenberg, J.A., G.C. Tomlin, W.H. McDonald, B.E. Snydsman, E.G. Muller, J.R. Yates, 3rd, and K.L. Gould. 2006. Ppc89 links multiple proteins, including the septation initiation network, to the core of the fission yeast spindle-pole body. *Mol Biol Cell*. 17:3793-3805.

Roussou, I., and G. Draetta. 1994. The Schizosaccharomyces pombe casein kinase II alpha and beta subunits: evolutionary conservation and positive role of the beta subunit. *Mol Cell Biol*. 14:576-586.

Ruchaud, S., M. Carmena, and W.C. Earnshaw. 2007. Chromosomal passengers: conducting cell division. *Nat Rev Mol Cell Biol*. 8:798-812.

Rustici, G., J. Mata, K. Kivinen, P. Lio, C.J. Penkett, G. Burns, J. Hayles, A. Brazma, P. Nurse, and J. Bahler. 2004. Periodic gene expression program of the fission yeast cell cycle. *Nat Genet*. 36:809-817.

Sagona, A.P., I.P. Nezis, N.M. Pedersen, K. Liestol, J. Poulton, T.E. Rusten, R.I. Skotheim, C. Raiborg, and H. Stenmark. 2010. PtdIns(3)P controls cytokinesis through KIF13A-mediated recruitment of FYVE-CENT to the midbody. *Nat Cell Biol*. 12:362-371.

Saha, S., and T.D. Pollard. 2012. Anillin-related protein Mid1p coordinates the assembly of the cytokinetic contractile ring in fission yeast. *Mol Biol Cell*. 23:3982-3992.

Samejima, I., T. Matsumoto, Y. Nakaseko, D. Beach, and M. Yanagida. 1993. Identification of seven new cut genes involved in Schizosaccharomyces pombe mitosis. *J Cell Sci*. 105 (Pt 1):135-143.

Sanchez-Diaz, A., V. Marchesi, S. Murray, R. Jones, G. Pereira, R. Edmondson, T. Allen, and K. Labib. 2008. Inn1 couples contraction of the actomyosin ring to membrane ingression during cytokinesis in budding yeast. *Nat Cell Biol*. 10:395-406.

Sandall, S., F. Severin, I.X. McLeod, J.R. Yates, 3rd, K. Oegema, A. Hyman, and A. Desai. 2006. A Bir1-Sli15 complex connects centromeres to microtubules and is required to sense kinetochore tension. *Cell*. 127:1179-1191.

Saurin, A.T., J. Durgan, A.J. Cameron, A. Faisal, M.S. Marber, and P.J. Parker. 2008. The regulated assembly of a PKCepsilon complex controls the completion of cytokinesis. *Nat Cell Biol*. 10:891-901.

Scott, B.J., E.M. Neidt, and D.R. Kovar. 2011. The functionally distinct fission yeast formins have specific actin-assembly properties. *Mol Biol Cell*. 22:3826-3839.

Shimada, Y., M.P. Gulli, and M. Peter. 2000. Nuclear sequestration of the exchange factor Cdc24 by Far1 regulates cell polarity during yeast mating. *Nat Cell Biol*. 2:117-124.

Sipiczki, M., B. Grallert, and I. Miklos. 1993. Mycelial and syncytial growth in Schizosaccharomyces pombe induced by novel septation mutations. *J Cell Sci*. 104 (Pt 2):485-493.

Sipiczki, M., K. Takeo, M. Yamaguchi, S. Yoshida, and I. Miklos. 1998. Environmentally controlled dimorphic cycle in a fission yeast. *Microbiology*. 144 (Pt 5):1319-1330.

Skau, C.T., D.S. Courson, A.J. Bestul, J.D. Winkelman, R.S. Rock, V. Sirotkin, and D.R. Kovar. 2011. Actin filament bundling by fimbrin is important for endocytosis, cytokinesis, and polarization in fission yeast. *J Biol Chem*. 286:26964-26977.

Skillman, K.M., W. Daher, C.I. Ma, D. Soldati-Favre, and L.D. Sibley. 2012. Toxoplasma gondii profilin acts primarily to sequester G-actin while formins efficiently nucleate actin filament formation in vitro. *Biochemistry*. 51:2486-2495.

Sladewski, T.E., M.J. Previs, and M. Lord. 2009. Regulation of fission yeast myosin-II function and contractile ring dynamics by regulatory light-chain and heavy-chain phosphorylation. *Mol Biol Cell*. 20:3941-3952.

Snaith, H.A., and K.E. Sawin. 2003. Fission yeast mod5p regulates polarized growth through anchoring of tea1p at cell tips. *Nature*. 423:647-651.

Snell, V., and P. Nurse. 1994. Genetic analysis of cell morphogenesis in fission yeast--a role for casein kinase II in the establishment of polarized growth. *EMBO J*. 13:2066-2074.

Snyder, M., S. Gehrung, and B.D. Page. 1991. Studies concerning the temporal and genetic control of cell polarity in Saccharomyces cerevisiae. *J Cell Biol*. 114:515-532.

Sohrmann, M., C. Fankhauser, C. Brodbeck, and V. Simanis. 1996. The dmf1/mid1 gene is essential for correct positioning of the division septum in fission yeast. *Genes Dev*. 10:2707-2719.

Sopko, R., D. Huang, J.C. Smith, D. Figeys, and B.J. Andrews. 2007. Activation of the Cdc42p GTPase by cyclin-dependent protein kinases in budding yeast. *EMBO J*. 26:4487-4500.

Sparks, C.A., M. Morphew, and D. McCollum. 1999. Sid2p, a spindle pole body kinase that regulates the onset of cytokinesis. *J Cell Biol*. 146:777-790.

St Johnston, D., and J. Ahringer. 2010. Cell polarity in eggs and epithelia: parallels and diversity. *Cell*. 141:757-774.

Steigemann, P., C. Wurzenberger, M.H. Schmitz, M. Held, J. Guizetti, S. Maar, and D.W. Gerlich. 2009. Aurora B-mediated abscission checkpoint protects against tetraploidization. *Cell*. 136:473-484.

Stoepel, J., M.A. Ottey, C. Kurischko, P. Hieter, and F.C. Luca. 2005. The mitotic exit network Mob1p-Dbf2p kinase complex localizes to the nucleus and regulates passenger protein localization. *Mol Biol Cell*. 16:5465-5479.

Streiblova, E., I. Malek, and K. Beran. 1966. Structural changes in the cell wall of Schizosaccharomyces pombe during cell division. *J Bacteriol*. 91:428-435.

Sudbery, P.E. 2011. Growth of Candida albicans hyphae. *Nat Rev Microbiol*. 9:737-748.

Takaine, M., O. Numata, and K. Nakano. 2009. Fission yeast IQGAP arranges actin filaments into the cytokinetic contractile ring. *EMBO J*. 28:3117-3131.

Takeya, R., K. Taniguchi, S. Narumiya, and H. Sumimoto. 2008. The mammalian formin FHOD1 is activated through phosphorylation by ROCK and mediates thrombin-induced stress fibre formation in endothelial cells. *EMBO J*. 27:618-628.

Tatebe, H., K. Shimada, S. Uzawa, S. Morigasaki, and K. Shiozaki. 2005. Wsh3/Tea4 is a novel cell-end factor essential for bipolar distribution of Tea1 and protects cell polarity under environmental stress in S. pombe. *Curr Biol*. 15:1006-1015.

Thomas, S., and K.B. Kaplan. 2007. A Bir1p Sli15p kinetochore passenger complex regulates septin organization during anaphase. *Mol Biol Cell*. 18:3820-3834.

Toure, A., R. Mzali, C. Liot, L. Seguin, L. Morin, C. Crouin, I. Chen-Yang, Y.G. Tsay, O. Dorseuil, G. Gacon, and J. Bertoglio. 2008. Phosphoregulation of MgcRacGAP in mitosis involves Aurora B and Cdk1 protein kinases and the PP2A phosphatase. *FEBS Lett*. 582:1182-1188.

Trautmann, S., and D. McCollum. 2005. Distinct nuclear and cytoplasmic functions of the S. pombe Cdc14-like phosphatase Clp1p/Flp1p and a role for nuclear shuttling in its regulation. *Curr Biol*. 15:1384-1389.

Trautmann, S., S. Rajagopalan, and D. McCollum. 2004. The S. pombe Cdc14-like phosphatase Clp1p regulates chromosome biorientation and interacts with Aurora kinase. *Dev Cell*. 7:755-762.

Trautmann, S., B.A. Wolfe, P. Jorgensen, M. Tyers, K.L. Gould, and D. McCollum. 2001. Fission yeast Clp1p phosphatase regulates G2/M transition and coordination of cytokinesis with cell cycle progression. *Curr Biol*. 11:931-940.

Tsukahara, T., Y. Tanno, and Y. Watanabe. 2010. Phosphorylation of the CPC by Cdk1 promotes chromosome bi-orientation. *Nature*. 467:719-723.

Tully, G.H., R. Nishihama, J.R. Pringle, and D.O. Morgan. 2009. The anaphase-promoting complex promotes actomyosin-ring disassembly during cytokinesis in yeast. *Mol Biol Cell*. 20:1201-1212.

Ubersax, J.A., and J.E. Ferrell, Jr. 2007. Mechanisms of specificity in protein phosphorylation. *Nat Rev Mol Cell Biol*. 8:530-541.

Uehara, R., G. Goshima, I. Mabuchi, R.D. Vale, J.A. Spudich, and E.R. Griffis. 2010. Determinants of myosin II cortical localization during cytokinesis. *Curr Biol*. 20:1080-1085.

Vader, G., R.H. Medema, and S.M. Lens. 2006. The chromosomal passenger complex: guiding Aurora-B through mitosis. *J Cell Biol*. 173:833-837.

Vagnarelli, P., and W.C. Earnshaw. 2004. Chromosomal passengers: the four-dimensional regulation of mitotic events. *Chromosoma*. 113:211-222.

Vaillant, D.C., S.J. Copeland, C. Davis, S.F. Thurston, N. Abdennur, and J.W. Copeland. 2008. Interaction of the N- and C-terminal autoregulatory domains of FRL2 does not inhibit FRL2 activity. *J Biol Chem*. 283:33750-33762.

Vanoosthuyse, V., S. Prykhozhij, and K.G. Hardwick. 2007. Shugoshin 2 regulates localization of the chromosomal passenger proteins in fission yeast mitosis. *Mol Biol Cell*. 18:1657-1669.

Vavylonis, D., J.Q. Wu, S. Hao, B. O'Shaughnessy, and T.D. Pollard. 2008. Assembly mechanism of the contractile ring for cytokinesis by fission yeast. *Science*. 319:97-100.

Wang, A., P.P. Raniga, S. Lane, Y. Lu, and H. Liu. 2009a. Hyphal chain formation in Candida albicans: Cdc28-Hgc1 phosphorylation of Efg1 represses cell separation genes. *Mol Cell Biol*. 29:4406-4416.

Wang, J., S.P. Neo, and M. Cai. 2009b. Regulation of the yeast formin Bni1p by the actin-regulating kinase Prk1p. *Traffic*. 10:528-535.

Watanabe, S., Y. Ando, S. Yasuda, H. Hosoya, N. Watanabe, T. Ishizaki, and S. Narumiya. 2008. mDia2 induces the actin scaffold for the contractile ring and stabilizes its position during cytokinesis in NIH 3T3 cells. *Mol Biol Cell*. 19:2328-2338.

Weber, G.F., M.A. Bjerke, and D.W. DeSimone. 2012. A mechanoresponsive cadherin-keratin complex directs polarized protrusive behavior and collective cell migration. *Dev Cell*. 22:104-115.

Werner, M., E. Munro, and M. Glotzer. 2007. Astral signals spatially bias cortical myosin recruitment to break symmetry and promote cytokinesis. *Curr Biol*. 17:1286-1297.

White, J.G., and G.G. Borisy. 1983. On the mechanisms of cytokinesis in animal cells. *J Theor Biol*. 101:289-316.

Widlund, P.O., J.S. Lyssand, S. Anderson, S. Niessen, J.R. Yates, 3rd, and T.N. Davis. 2006. Phosphorylation of the chromosomal passenger protein Bir1 is required for localization of Ndc10 to the spindle during anaphase and full spindle elongation. *Mol Biol Cell*. 17:1065-1074.

Wilson, G.M., A.B. Fielding, G.C. Simon, X. Yu, P.D. Andrews, R.S. Hames, A.M. Frey, A.A. Peden, G.W. Gould, and R. Prekeris. 2005. The FIP3-Rab11 protein complex regulates recycling endosome targeting to the cleavage furrow during late cytokinesis. *Mol Biol Cell*. 16:849-860.

Wolf, F., R. Sigl, and S. Geley. 2007. '... The end of the beginning': cdk1 thresholds and exit from mitosis. *Cell Cycle*. 6:1408-1411.

Wolfe, B.A., and K.L. Gould. 2004. Fission yeast Clp1p phosphatase affects G2/M transition and mitotic exit through Cdc25p inactivation. *EMBO J*. 23:919-929.

Wolfe, B.A., T. Takaki, M. Petronczki, and M. Glotzer. 2009. Polo-like kinase 1 directs assembly of the HsCyk-4 RhoGAP/Ect2 RhoGEF complex to initiate cleavage furrow formation. *PLoS Biol*. 7:e1000110.

Wu, J.Q., and T.D. Pollard. 2005. Counting cytokinesis proteins globally and locally in fission yeast. *Science*. 310:310-314.

Wu, Q., R.M. Sahasrabudhe, L.Z. Luo, D.W. Lewis, S.M. Gollin, and W.S. Saunders. 2010. Deficiency in myosin light-chain phosphorylation causes cytokinesis failure and multipolarity in cancer cells. *Oncogene*. 29:4183-4193.

Xu, Y., J.B. Moseley, I. Sagot, F. Poy, D. Pellman, B.L. Goode, and M.J. Eck. 2004. Crystal structures of a Formin Homology-2 domain reveal a tethered dimer architecture. *Cell*. 116:711-723.

Xue, X.H., C.Q. Guo, F. Du, Q.L. Lu, C.M. Zhang, and H.Y. Ren. 2011. AtFH8 is involved in root development under effect of low-dose latrunculin B in dividing cells. *Mol Plant*. 4:264-278.

Yakir-Tamang, L., and J.E. Gerst. 2009. A phosphatidylinositol-transfer protein and phosphatidylinositol-4-phosphate 5-kinase control Cdc42 to regulate the actin cytoskeleton and secretory pathway in yeast. *Mol Biol Cell*. 20:3583-3597.

Yamashita, A., M. Sato, A. Fujita, M. Yamamoto, and T. Toda. 2005. The roles of fission yeast ase1 in mitotic cell division, meiotic nuclear oscillation, and cytokinesis checkpoint signaling. *Mol Biol Cell*. 16:1378-1395.

Yanagida, M. 1998. Fission yeast cut mutations revisited: control of anaphase. *Trends Cell Biol*. 8:144-149.

Yang, W., S. Ren, X. Zhang, M. Gao, S. Ye, Y. Qi, Y. Zheng, J. Wang, L. Zeng, Q. Li, S. Huang, and Z. He. 2011. BENT UPPERMOST INTERNODE1 encodes the class II formin FH5 crucial for actin organization and rice development. *Plant Cell*. 23:661-680.

Yonetani, A., and F. Chang. 2010. Regulation of cytokinesis by the formin cdc12p. *Curr Biol*. 20:561-566.

Yonetani, A., R.J. Lustig, J.B. Moseley, T. Takeda, B.L. Goode, and F. Chang. 2008. Regulation and targeting of the fission yeast formin cdc12p in cytokinesis. *Mol Biol Cell*. 19:2208-2219.

Yoon, H.J., A. Feoktistova, B.A. Wolfe, J.L. Jennings, A.J. Link, and K.L. Gould. 2002. Proteomics analysis identifies new components of the fission and budding yeast anaphase-promoting complexes. *Curr Biol*. 12:2048-2054.

Yoshida, S., S. Bartolini, and D. Pellman. 2009. Mechanisms for concentrating Rho1 during cytokinesis. *Genes Dev*. 23:810-823.

Yoshida, S., K. Kono, D.M. Lowery, S. Bartolini, M.B. Yaffe, Y. Ohya, and D. Pellman. 2006. Polo-like kinase Cdc5 controls the local activation of Rho1 to promote cytokinesis. *Science*. 313:108-111.

Zeng, X., J.A. Kahana, P.A. Silver, M.K. Morphew, J.R. McIntosh, I.T. Fitch, J. Carbon, and W.S. Saunders. 1999. Slk19p is a centromere protein that functions to stabilize mitotic spindles. *J Cell Biol*. 146:415-425.

Zhang, Z., Y. Zhang, H. Tan, Y. Wang, G. Li, W. Liang, Z. Yuan, J. Hu, H. Ren, and D. Zhang. 2011. RICE MORPHOLOGY DETERMINANT encodes the type II formin FH5 and regulates rice morphogenesis. *Plant Cell*. 23:681-700.

Zheng, X.D., R.T. Lee, Y.M. Wang, Q.S. Lin, and Y. Wang. 2007. Phosphorylation of Rga2, a Cdc42 GAP, by CDK/Hgc1 is crucial for Candida albicans hyphal growth. *EMBO J*. 26:3760-3769.

Zhou, L., J. Li, R. George, S. Ruchaud, H.G. Zhou, J.E. Ladbury, W.C. Earnshaw, and X. Yuan. 2009. Effects of Full-Length Borealin on the Composition and Protein-Protein Interaction Activity of a Binary Chromosomal Passenger Complex. *Biochemistry*. 48:1156-1161.

Zhou, M., and Y.L. Wang. 2008. Distinct pathways for the early recruitment of myosin II and actin to the cytokinetic furrow. *Mol Biol Cell*. 19:318-326.